



UNIVERSIDAD MIGUEL HERNANDEZ DE ELCHE  
INSTITUTO DE BIOLOGIA MOLECULAR Y CELULAR



# INTERACTION BETWEEN CONJUGATED POLYELECTROLYTES AND BIOLOGICAL SYSTEMS: CHARACTERIZATION AND BIOTECHNOLOGICAL APPLICATIONS

DOCTORAL THESIS

ZEHRA KAHVECI

DIRECTOR

C. REYES MATEO MARTINEZ

ELCHE, 2016





**D. Antonio V. Ferrer Montiel**, Catedrático de Bioquímica y Biología Molecular y Director del Instituto de Biología Molecular y Celular de la Universidad Miguel Hernández de Elche, **DA SU CONFORMIDAD** a la lectura de la Tesis Doctoral titulada: **“Interaction between Conjugated Polyelectrolytes and Biological Systems: Characterization and Biotechnological Applications”** presentada por Dña. Zehra Kahveci.

Para que conste y surta los efectos oportunos, firma el presente certificado en Elche, a 4 de Octubre de 2016.

Fdo.: Prof. Dr. Antonio V. Ferrer Montiel





**Dña C. Reyes Mateo Martinez**, Profesora Titular de la Universidad Miguel Hernández de Elche, **CERTIFICA**: que la Tesis Doctoral titulada **“Interaction between Conjugated Polyelectrolytes and Biological Systems: Characterization and Biotechnological Applications”** presentada por Dña. Zehra Kahveci, ha sido realizada bajo su dirección en el Instituto de Biología Molecular y Celular de la Universidad Miguel Hernández de Elche.

Para que conste y surta los efectos oportunos, firma el presente certificado en Elche, a 4 de Octubre de 2016.

Fdo.: Prof. Dra. C. Reyes Mateo Martinez



*To my parents*

*To my brother*





# Acknowledgments

I started my thesis ambitious and thirsty of knowledge and today I am finishing it even more passionate than anyone would expect. I am grateful to people who were with me all these years, when I was away from my family and roots. They all made me feel at home and make these years bearable.

All these have begun with my parents, **Rabia** and **Huseyin**, they have made this dream come through. If it were not for them, I wouldn't be here now. They gave me everything. Their support let me get to this end. They didn't complain even a day to not make me feel uncomfortable. Also, I am so fortunate to have such a caring brother, **Muzaffer**, for thinking of me in every step of his life and being there for me anytime I needed him. I feel so proud and thankful to have such a supporting and loving family.

To my other biggest support and director of my thesis, **Reyes Mateo**, for giving me this unforgettable opportunity to be a part of her laboratory and family for all these years. She guided me professionally and personally. I am honored to be her student and to be taught by her.

To my dear **M<sup>a</sup> Jose**, who was there for me anytime I needed her with an unlimited tolerance and patience. She thought me that kindness and good is still existing in this world. I am blessed to know such a nice person.

To the only man in a women jungle, **Ricardo**, whom I would like to appreciate his existence for all these years with his patience and good humor with me.

To my colleague, my friend, my sister, **Rebeca**, I am so thankful to have her since the beginning at a close distance. Excited or nervous, upset or content, we had our moments in our conjoint laboratories. I will miss having someone so close. She and David gave me the warmth of a home in Elche.

To the people at the second floor of IBMC, whom I appreciated having by my side during every hour and day of the week. **Rocio**, **Felipe**, and **Amalia**, who were there for me to share their friendship and knowledge.

To professors in our institute, and more particularly, **Javier**, **Jesus**, and **Jose Luis** for their professional and moral support. Once again, I would like to thank **Jose Luis** for his valuable help with the English corrections.

To people who helped me with paper works and bureaucracy, especially, **Elisa**, **Javier** and **May**, you have made my life agreeable.

To the people out of the institute, my friends, that I am grateful to have their support. My lovely girl, **Lucia** and her family, who was there with me since the beginning. My wild girl, **Marina**, who gives me the joy of being alive. And my dear friend, **Charlotte**, from a long distance she was with me in every step of this journey. Also, feeling blessed to know **Clara**, **Ines**, **Maria**, and my little men **Martin** and **Jose Antonio**, during these years. I feel lucky to be surrounded by such good people.

I thank you all for being a part of my life.

*"Hayatta en hakiki mürşit, ilimdir."*

*"One true mentor in life is science."*

Mustafa Kemal Atatürk





# Prefacio

El presente trabajo doctoral se ha desarrollado en el Instituto de Biología Molecular y Celular de la Universidad Miguel Hernández de Elche, bajo la dirección de la profesora C. Reyes Mateo Martínez y con el apoyo de los proyectos del Ministerio de Economía y Competitividad MAT-2011-23007 y MAT-2014-53282-R.

Siguiendo la normativa interna de la Universidad Miguel Hernández, la memoria correspondiente a la Tesis Doctoral titulada "Interaction between Conjugated Polyelectrolytes and Biological Systems: Characterization and Biotechnological Applications", ha sido redactada en lengua inglesa con apartados seleccionados en lengua española y se ha elaborado de acuerdo a la normativa de la Universidad Miguel Hernández de Elche para la "Presentación de tesis doctorales con un conjunto de publicaciones". La Tesis se ha organizado en los siguientes capítulos:

- Resumen de la Tesis redactada en lengua inglesa y lengua española
- Introducción general
- Objetivos
- Materiales y métodos
- Resumen y discusión global de los resultados obtenidos
- Conclusiones redactadas en lengua inglesa y lengua española
- Referencias
- Anexo de las publicaciones



# Abbreviations

<b>ALP</b>	Alkaline phosphatase
<b>AQS</b>	9,10 anthraquinone-2,6-disulfonic acid
<b>Bodipy</b>	BODIPY 500/510 C4,C9
<b>CD</b>	Circular dichroism
<b>CF</b>	5 (6)-Carboxyfluorescein
<b>CPs</b>	Conjugated polymers
<b>CPEs</b>	Conjugated polyelectrolytes
<b>DLS</b>	Dynamic light scattering
<b>DNA</b>	Deoxyribonucleic acid
<b>DPH</b>	1,6-diphenyl- 1,3,5-hexatriene
<b>DSC</b>	Differential scanning calorimetry
<b>E. coli</b>	Escherichia coli
<b>FRET</b>	Förster resonance energy transfer
<b>GUVs</b>	Giant unilamellar vesicles
<b>HaCat cell</b>	Immortalised human keratinocyte cell
<b>HeLa cell</b>	Henrietta Lacks' 'Immortal' cell
<b>HSA</b>	Human serum albumin
<b>HTMA-PFP</b>	Poly-([9,9-bis(6'-N,N,N-trimethylammonium)hexyl]-fluorene-phenylene) bromide
<b>HTMA-PFNT</b>	Copoly-([9,9-bis(6'-N,N,N-trimethylammonium)hexyl]-2,7-(fluorene)-alt-1,4-(naphtho[2,3c]-1,2,5-thiadiazole)) bromide
<b>LOD</b>	Limit of detection
<b>LUVs</b>	Unilamellar large vesicles
<b>NPs</b>	Nanoparticles
<b>PF</b>	Polyfluorenes
<b>PNP</b>	P-nitrophenol
<b>PNPP</b>	P-nitrophenyl phosphate
<b>TEOS</b>	Tetraethyl orthosilicate



# Index

Acknowledgments	IX
Prefacio	XIII
Abbreviations	XV
<b>Index</b>	<b>XVII</b>
<b>1. ABSTRACT/ RESUMEN</b>	<b>1</b>
<b>2. INTRODUCTION</b>	<b>7</b>
<b>2.1. Conjugated Polyelectrolytes (CPEs)</b>	<b>9</b>
2.1.1. Polyfluorenes	11
<b>2.2. CPEs as Fluorescent Markers</b>	<b>13</b>
<b>2.3. CPEs in Biosensing</b>	<b>16</b>
<b>2.4. Solubilization and Stabilization of CPEs</b>	<b>22</b>
<b>2.5. The Cationic Polyfluorene HTMA-PFP</b>	<b>25</b>
<b>3. OBJECTIVES</b>	<b>29</b>
<b>4. MATERIALS AND METHODS</b>	<b>33</b>
<b>4.1. Materials</b>	<b>35</b>
4.1.1. Lipids	35
4.1.2. Proteins	36
4.1.3. Conjugated Polyelectrolytes	37
4.1.4. Fluorescent Probes and Quenchers	38

4.1.5.	Other Reactives	39
<b>4.2.</b>	<b>Instrumentation</b>	<b>39</b>
4.2.1.	Absorption and Steady-State Fluorescence Measurements	39
4.2.2.	Optical and Electronic Microscopy Measurements	39
4.2.3.	Dynamic Light Scattering (DLS)	40
4.2.4.	Circular Dichroism (CD)	41
4.2.5.	Differential Scanning Calorimetry (DSC)	41
<b>4.3.</b>	<b>Methodology</b>	<b>42</b>
4.3.1.	Lipid Systems	42
4.3.1.1.	Description	42
4.3.1.2.	Preparation	47
4.3.2.	Fluorescence Methodologies	49
4.3.3.	Sol-gel Immobilization	55
4.3.3.1.	Description	55
4.3.3.2.	Preparation	56
<b>5.</b>	<b>OVERALL RESULTS AND DISCUSSION</b>	<b>59</b>
<b>5.1.</b>	<b>HTMA-PFP and HTMA-PFNT in Buffer</b>	<b>61</b>
<b>5.2.</b>	<b>CPEs as Fluorescent Membrane Markers</b>	<b>64</b>
5.2.1.	HTMA-PFP in Model Membranes	64
5.2.1.1.	HTMA-PFP in Anionic Lipid Membranes	64
5.2.1.2.	HTMA-PFP in Zwitterionic Lipid Membranes	67
5.2.1.3.	Selectivity of HTMA-PFP against Anionic and Zwitterionic Membranes	69
5.2.2.	HTMA-PFNT in Model Membranes	71
5.2.2.1.	HTMA-PFNT in Anionic and Zwitterionic Membranes	71

<b>5.3.</b>	<b>CPEs for Selective Recognition and Imaging of Bacteria</b>	<b>73</b>
5.3.1.	HTMA-PFP and HTMA-PFNT in Bacterial and Mammalian Model Membranes	74
5.3.2.	Selective Imaging of Bacteria over Mammalian Cells	76
<b>5.4.</b>	<b>CPE-based Nanostructures: Characterization and Biotechnological Applications</b>	<b>77</b>
5.4.1.	Multifunctional Fluorescent Nanoparticles (NPs) as Bioimaging Tools and Drug Carriers	78
5.4.1.1.	Protein-CPE Nanostructures	78
5.4.1.2.	Lipid Vesicle-CPE Nanoparticles	81
5.4.2.	Fluorescent NPs in Biosensing	82
5.4.2.1.	Free ALP Biosensor	83
5.4.2.2.	Immobilized ALP Biosensor	84
<b>6.</b>	<b>CONCLUSIONS/ CONCLUSIONES</b>	<b>87</b>
<b>7.</b>	<b>REFERENCES</b>	<b>97</b>
<b>8.</b>	<b>ANNEXES</b>	<b>113</b>
	Publication 8.1	115
	Publication 8.2	129
	Publication 8.3	155
	Publication 8.4	179
	Publication 8.5	197



# 1. ABSTRACT/ RESUMEN





Fluorescent conjugated polyelectrolytes (CPEs) display very interesting and useful properties. They are polymers with  $\pi$ -conjugated backbones which show strong absorption and high efficiencies in both photoluminescence and electroluminescence; further they contain ionic side groups to facilitate their water solubilization. These properties have been used to study interactions with biomolecules such as proteins and DNA, allowing to develop sensing platforms and bioimaging tools. In the present Thesis, we characterized two cationic CPEs, with different emission wavelength: blue-emitting HTMA-PFP and red-emitting HTMA-PFNT, and we explored their potential use in biotechnological applications.

For biomedical applications such as bioimaging, the preliminary condition is the dispersibility of CPEs in aqueous media. Therefore, in the first part of this Thesis, the behaviour of HTMA-PFP and HTMA-PFNT in aqueous solutions was explored. Afterwards, we investigated the interaction of these CPEs with anionic and zwitterionic model membranes in order to use them as fluorescent markers. This study showed that both types of CPEs have higher affinity and selectivity towards anionic lipids, which are the dominant lipid component in bacterial membranes. Taking into account these results, a study by mimicking the mammalian and bacterial membranes with different lipid mixtures was performed and the interaction of these CPEs with both model systems was explored. This study confirmed the selectivity of CPEs, especially HTMA-PFNT, towards bacterial model membranes. Preliminary experiments with living bacteria and mammalian cells supported these results, showing that in samples containing both types of cells, HTMA-PFNT only images the

## 1. Abstract

bacterial cells. These results were a proof-of-concept of its use for selective recognition and imaging of bacteria.

Moreover, we studied the ability of HTMA-PFP and HTMA-PFNT to form stable fluorescent nanostructures, and we explored their potential applications. Firstly, we investigated the interaction of HTMA-PFNT with two biological systems which are known to be used as nanocarriers: human serum albumin and lipid vesicles. Results showed the formation of red-emitting nanoparticles, preserving the biological functionality. The ability of these nanoparticles to carry hydrophobic and polar compounds was also checked, as well as, the capacity to be used as fluorescent probes for bioimaging. Results supported the potential use of these novel structures as multifunctional platforms for therapeutic and diagnostic purposes. Secondly, the complexation of blue-emitting HTMA-PFP with lipid vesicles was explored. The obtained nanoparticles were characterized and coupled to the enzyme Alkaline Phosphatase to develop a fluorescent biosensor for enzyme inhibitor determination. The components of the biosensor (nanoparticles and enzyme) were immobilized in a sol-gel matrix to facilitate its handling, allowing its reutilization. The biosensor was optimized for the determination of phosphate ion, a competitive inhibitor of the enzyme.

Los polielectrolitos conjugados fluorescentes (CPEs) presentan propiedades muy interesantes. Se trata de polímeros que poseen esqueletos con enlaces  $\pi$ -conjugados y que muestran altos coeficientes de extinción y un elevado rendimiento cuántico de fluorescencia. Además, poseen cadenas laterales que contienen grupos cargados para facilitar su solubilidad en medios acuosos. Estas propiedades pueden ser utilizadas para estudiar interacciones con biomoléculas, tales como proteínas y ADN, con objeto de desarrollar plataformas sensoriales y nuevas herramientas de bioimagen. En la presente Tesis se han caracterizado dos CPEs catiónicos que emiten en diferentes regiones espectrales: HTMA-PFP, con emisión en el azul, y HTMA-PFNT, que emite en el rojo. Además se han explorado sus posibles aplicaciones en el campo de la biotecnología.

En aplicaciones biomédicas, como es la bioimagen, un requisito indispensable es la solubilidad del CPE en medio acuoso. Por ello, en la primera parte de esta Tesis se ha explorado el comportamiento de los dos polímeros, HTMA-PFP y HTMA-PFNT, en disolución acuosa. A continuación, se ha investigado la interacción de los CPEs con modelos de membrana formados por lípidos aniónicos y zwitteriónicos, con objeto de evaluar la capacidad de utilizar estos polielectrolitos como marcadores fluorescentes de membrana. Este estudio demostró que ambos compuestos presentan una mayor afinidad y selectividad hacia lípidos aniónicos, que son el componente mayoritario de las membranas bacterianas. Teniendo en cuenta este resultado, se llevó a cabo un estudio en el que se modelizaron membranas de mamífero y bacteriana con diferentes mezclas lipídicas y se exploró cómo interaccionan HTMA-PFP y HTMA-PFNT con estos sistemas. Dicho estudio confirmó

## 1. Resumen

la preferencia de los CPEs, especialmente HTMA-PFNT, por los modelos bacterianos. Experimentos preliminares realizados con bacterias y células de mamífero soportaron estos resultados, mostrando que en muestras donde coexisten ambos tipos de células, HTMA-PFNT únicamente marca las células bacterianas. Este experimento evidencia la posible utilización de HTMA-PFNT como una herramienta para el diagnóstico y bioimagen de contaminación bacteriana.

Además, se ha estudiado la capacidad de ambos polielectrolitos para formar nanoestructuras fluorescentes estables en medio acuoso y se han explorado sus aplicaciones. Por un lado, se investigó la interacción de HTMA-PFNT con dos sistemas biológicos utilizados frecuentemente como nanotransportadores: la proteína HSA y vesículas liposomales. Así, se obtuvieron nanopartículas que emiten en el rojo y que preservan las propiedades funcionales de los sistemas biológicos que las componen. Estas nanopartículas multifuncionales fueron capaces de transportar compuestos polares e hidrofóbicos y han podido ser utilizadas como sondas fluorescentes en bioimagen. Por otro lado, también se han obtenido nanopartículas fluorescentes que emiten en el azul, a través de la interacción del polielectrolito HTMA-PFP y vesículas liposomales aniónicas. Estas nanopartículas han sido caracterizadas en detalle y acopladas a la enzima fosfatasa alcalina, con objeto de desarrollar un biosensor para la determinación de inhibidores de esta enzima. Los componentes del biosensor (nanopartículas y enzimas) se han inmovilizado en una matriz sol-gel, para facilitar su manipulación y permitir su reutilización. El biosensor ha sido optimizado para la determinación de ion fosfato, un inhibidor competitivo de la enzima.

## 2. INTRODUCTION





### 2.1. Conjugated Polyelectrolytes (CPEs)

In 2000, The Nobel Prize in Chemistry was awarded to Alan J. Heeger, Alan G. MacDiarmid and Hideki Shirakawa for their discovery about polyacetylenes that can be made conductive almost like metals by “doping” with iodine vapour (Figure 2.1) [1,2]. Although polyacetylenes are not fluorescent polymers, this was the first step towards the development of the electroluminescent conjugated polymers (CPs) [3].

As any other organic polymer, CPs are carbon-based macromolecules which are composed of repeating monomer units forming a chain, the backbone of the polymer [4]. However, the difference in how bonding takes place among the carbon atoms of the backbone is what it makes CPs unique. Unlike traditional saturated polymers such as polyethylene or polypropylene, CPs have an alternating sequence of single and double bonds along the backbone of the polymer chain, a  $\pi$ -conjugated system where electrons are effectively delocalized over the conjugation length of the polymer [5-7]. It is precisely this alternating bond sequence that enables CPs to exhibit their unique optical and electronic properties. When a CP is illuminated at an appropriate wavelength, it can lead to the excitation of an electron to a higher energy level. This creates a bound electron-hole-pair on the polymer backbone named exciton. Also, electron delocalization facilitates rapid intra- and inter-chain exciton migration, conferring collective optical responses and amplified signals when compared to conventional fluorophores [8,9]. As a consequence, CPs show strong absorption and high efficiencies in both photoluminescence and electroluminescence and exhibit large Stokes shifts [10,11]. Due to these properties, they have received significant

## 2. Introduction

attention over the last years as versatile active components in luminescent optoelectronic devices and fluorescent sensory materials [10-16]. Figure 2.1 shows some examples of CPs' backbone structures [17], including polyacetylene (PA), poly(para-phenylene) (PPP) [18], poly(para-phenylene vinylene) (PPV) [14], poly(para-phenylene ethynylene) (PPE) [19], polythiophene (PT) [20], polypyrrole (PPy) [7], polyaniline (PANI) [21] and polyfluorene (PF) [22].

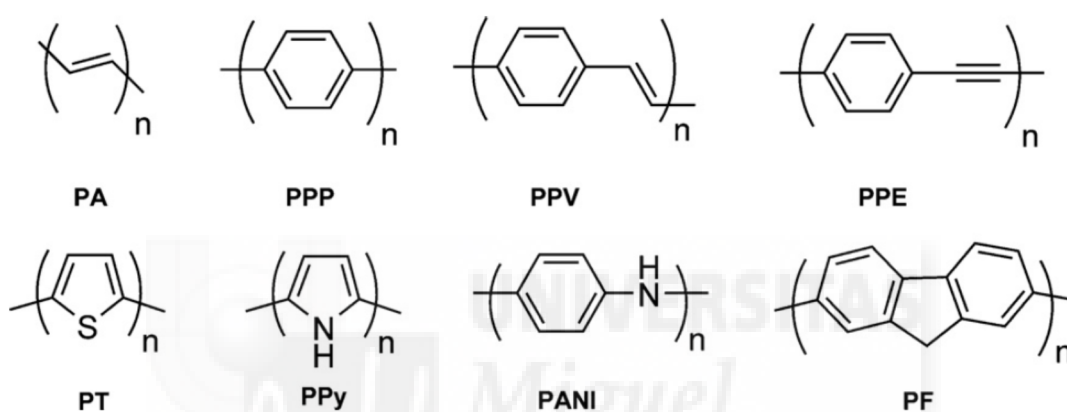


**Figure 2.1.** Molecular structures of typical conjugated polymers [17].

One of the difficulties in working with CPs is their low solubility, especially in water, which reduces luminescence yields due to the formation of large visible aggregates that precipitate from the solution. This severely limits their biological and environmental applications [23]. Consequently, many efforts are being made in this direction to develop strategies to improve the poor aqueous solubility of these macromolecules [24,25]. A common strategy employed to increase aqueous solubility of CPs is based on the enhancement of the macromolecule polarity by appending hydrophilic side chains on the main chain of polymer [26-36]. Most of water-soluble conjugated polymers, named conjugated polyelectrolytes (CPEs),

possess pendant polar groups like carbohydrates or charged moieties such as carboxylate, sulfonate, phosphonate and ammonium. These ionic side-chains facilitate polymer solubilisation, and favour electrostatic interactions with species that contain opposite charge, which is of great interest in biological and environmental applications [17,23,37-44].

### 2.1.1. Polyfluorenes

Among the CPs, those involving fluorene-based systems (Figure 2.1), named polyfluorenes (PF), offer the advantage of high fluorescence quantum yields and photostability, blue emission (suitable for energy transfer experiments), excellent thermal stability and high chemical stability against oxidants, as well as good synthetic accessibility [41,45]. Polyfluorenes are the most outstanding conjugated polymers because of their use in a variety of polymer optoelectronic devices, such as light-emitting diodes (LEDs), organic photovoltaic devices (OPVs), field-effect transistors (FETs), chemical and biosensors, lasers, memories, and light-emitting electrochemical cells (LECs) [46-48]. Polyfluorene-based CPEs consist of a rigid hydrophobic polyfluorene backbone with flexible charged side chains and have unique properties such as facile substitution at the fluorene C9 position and good chemical and thermal stability [22]. It is possible to increase the processability of these CPEs by incorporating different ionic side-chain groups and by modifying the main chain by adding some other groups. Addition of ionic side-chain groups increases the solubility in polar solvents and water [49,50]. Besides, the modification of the main chain, by functionalization of the 2,7-positions of fluorene, induces

## 2. Introduction

changes in photophysical properties of the fluorene backbone [43,51-54]. Normally, fluorene-based CPEs emit blue light, but researchers in the area are making significant efforts to shift the color to longer wavelengths. Color can be usually tuned by copolymerizing the fluorene monomers with other low-band-gap monomers or by incorporating monomers capable to conjugate with the fluorene ring to extend the conjugation length into the chain [55]. With these strategies, polyfluorenes emitting in the green and yellow region of visible spectrum have been successfully synthesized [56]. Synthesis of probes emitting in the red region is at present of great interest for *in vivo* fluorescence imaging studies because of minimum photodamage to biological samples, deep tissue penetration, and minimum interference from background autofluorescence by biomolecules in the living systems. However, despite the large amount of polyfluorenes and, in general, CPEs synthesized, bright red-emitters remain rare [57,58]. This is because the most widely used strategy to obtain these CPEs is the introduction of donor–acceptor structures in the aromatic backbone, which increases the hydrophobic character of the polymer, favouring aggregation in aqueous media and therefore reducing the fluorescence quantum yield. For example, Huang et al. have recently synthesized a red emissive polyfluorene with very low cytotoxicity and excellent photostability that is employed for cell imaging, but it is found to aggregate in the aqueous environment of cell culture medium because of the relatively hydrophobic chain structure [59]. Several strategies are being carried out to increase the quantum yield of these red-probes, such as the incorporation of bulky pendants into the backbone or side chain to avoid compact aggregation, or the introduction of small amounts of narrow-band gap moieties as energy acceptors into

the backbone to facilitate intra- and interchain energy transfer in the aggregate state [57,60].

### 2.2. CPEs as Fluorescent Markers

The design and development of new fluorescent markers having high sensitivity to image cellular and physiological processes is of great interest in applications such as clinical diagnosis, identification of cancer cells, detection of pathogenic bacterial strains, immunofluorescent techniques, catalytic pathway monitoring, and drug delivery monitoring through membrane or cytoplasm [61-63]. Ideal membrane markers should be highly fluorescent, water-soluble, biocompatible, photostable, with maximum spatial resolution, and minimal perturbation to biological systems and composed of two structural components: a group with affinity for the membrane surface and a reporter group [23]. Most of the existing membrane fluorescent markers (generally small organic fluorophores and fluorescent proteins) exhibit interesting properties. For instance they can adapt to different experimental conditions and possess tunable optical properties. However, these fluorescent materials also show important limitations such as photobleaching, self-quenching, and chemical decomposition, which restrict their applications [64,65]. The most widely known alternative to overcome these restrictions is to use semiconductor-based quantum dots (QDs), but the potential cytotoxicity risk associated with their heavy metal components, for instance cadmium, remains a major concern for the use of these nanoparticles in biological studies [66,67]. Recently, a new class of

## 2. Introduction

fluorescent carbon nanomaterials, i.e. carbon quantum dots (CQDs), has been developed (Figure 2.2) [68]. These materials, which have been used for bacterial detection, possess the attractive properties showed by QDs with the added advantage of being biocompatible as well [69]. However, complex processes of passivation and anchoring of recognition molecules using expensive and, in occasions, toxic coupling agents, are currently indispensable in the functionalization of CQDs for selective targeting [70]. In addition, long incubation times are required before cell visualization when these materials are used [68]. Therefore, the improvement of synthesis methods for the biofunctionalization and development of new fluorescent markers continues to be a significant challenge. More recently, conjugated polyelectrolytes appear as alternative to fluorescent markers used in bioimaging as they overcome most of the limitations associated with these fluorescent materials, such as the photobleaching of organic dyes and fluorescent proteins or the cytotoxicity of quantum dots [37,41,71,72].

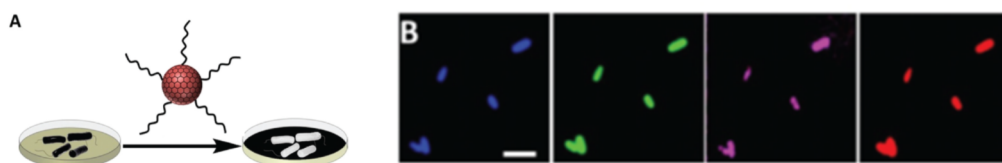


**Figure 2.2.** A. Illustration of the assay used to label the bacteria with amphiphilic carbon dots; B. Multicolour fluorescence microscopy images of *E. coli* recorded at different excitation/emission pairs in blue, green, magenta and red. Scale bar corresponds to 5  $\mu\text{m}$  [68].

In general, CPEs are biocompatible and biodegradable, and have easily amenable side chains for bioconjugation. In addition, their photophysical properties can be

feasibly customized through backbone and side-chain modifications. Conjugated with appropriate recognition elements, CPEs can be used as tracers, which can selectively accumulate in specific regions of the organism (tumors, inflamed areas, etc.) without risking cellular viability [23,41,58,73,74]. For instance, Zhu and colleagues have developed a new positively charged fluorescent conjugated polymer (PPV-1) for the detection of cell apoptosis [75]. The combination of the Oligo(ethylene glycol) side chains and half percentage of positively charges imparts PPV-1 the outstanding ability to differentiate apoptotic cells from normal cells (Figure 2.3).

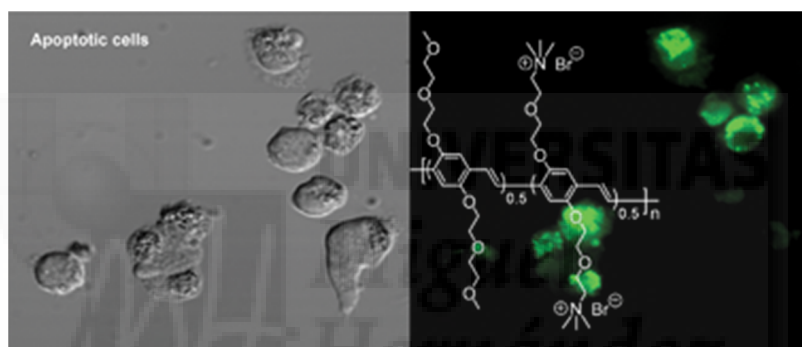


**Figure 2.3.** Microscopy images obtained for the detection of apoptosis in a simple, fluorescent label-free way by using PPV-1 [75].

Many drugs, nanoparticles, and fluorescent dyes used in cellular imaging first interact with cells through their membrane. Interaction at a molecular level, of an extracellular particle with the plasma membrane needs to be understood to evaluate its potential activity. In this regard, the use of model lipid membrane systems that imitate the complexity of natural cell membranes are useful to study the interaction of such compounds in a controlled manner for predicting their interactions with real cell membranes as well as in the development of biotechnological applications. When

## 2. Introduction

CPEs are directly added to cells for imaging analyses, they initially interact with their plasma membrane; therefore, a detailed knowing of how these polyelectrolytes insert into the membrane at a molecular level should be helpful to understand their activity, improving and expanding their applications, especially in bioimaging.

To date, very few works have been carried out aiming to this goal. The Whitten group studied the interaction of a series of antimicrobial CPEs with different model membranes to gain insight into the mechanism of their biocidal activity [76-78]. Ngo and Cosa characterized the interaction of lipid vesicles with a negatively charged CPE in order to obtain well characterized lipid/polymer complexes, with potential applications as sensing systems [79,80]. Given the objective of these works, the polymer concentration used in most of the experiments was relatively high. However, the use of CPEs as probes for bioimaging and detection of membrane processes requires minimal perturbation of the sample being studied, and requires lower polymer concentrations. In consequence, the interaction of small concentrations of CPEs with model lipid membranes, which imitate the complexity of natural cell membranes, would be explored in order to evaluate the potential use of these polyelectrolytes as fluorescent membrane markers.

### 2.3. CPEs in Biosensing

Over the past several years, the use of CPEs as sensors and biosensors has been the subject of considerable research interest. Numerous sensor systems based on these

polyelectrolytes have been developed for various analytes, including metal ions, biomolecules, proteins, enzymes and nucleic acids [17,39,81-94].

In general, CPEs-based sensing systems work either in “turn-on” or “turn-off” modes [95]. In the “turn-on” mode, initially the fluorescence of the polyelectrolyte is low and the addition of the analyte recovers its fluorescence. In contrast, in the turn-off mode, the CPE is fluorescent and upon addition of the analyte, its fluorescence decreases (Figure 2.4).

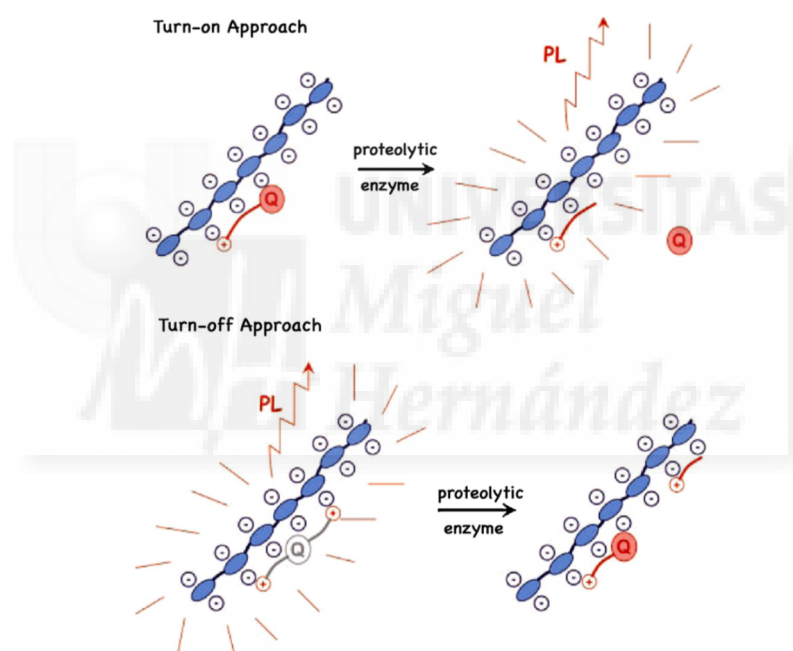


**Figure 2.4.** Illustration of the “turn-on” and “turn-off” mechanism of CPE-based sensors for protease activity [95].

Most of the CPEs-based sensors use the fluorescence quenching of the polyelectrolyte as a tool to quantify the presence of the analyte and use one of the following quenching mechanisms: photoinduced electron transfer (PET), Förster Energy Transfer (FRET) and conformational change (including analyte-induced

## 2. Introduction

aggregation quenching mechanism). Fluorescence quenching can be described as any decrease in fluorescence intensity of the fluorophore which may occur by a variety of process, including photobleaching, photo-oxidation, inner-filter effect or energy transfer [96]. The fluorescence quenching occurs mainly as either static or dynamic interaction mechanism, where the excited fluorophore returns to its ground state without emission of a photon. In static quenching, a non-fluorescent complex is formed between the quencher and fluorophore, and consequently, the quencher changes the absorption process as a perturbation of the spectrum. After excitation, the complex returns to its ground state immediately through non-radiative processes. On the other hand, dynamic quenching demands molecular contact between the quencher and excited fluorophore, and is limited by diffusion. The lifetime of the excited fluorophore is dependent on the quencher concentration. The dynamic quenching can only be observed as decrease in the intensity of the emission spectrum.

Quenching is described by the Stern-Volmer equation [96]:

$$\frac{I_0}{I} = 1 + K_{SV}[Q] \quad [2.1]$$

where  $I_0$  and  $I$  stand, respectively, for the steady-state fluorescence intensities in the absence and in presence of quencher, and  $[Q]$  is the quencher concentration. The significance of  $K_{SV}$  depends on the nature of the quenching process: it may represent the association constant for complex formation or the rate of dynamic quenching ( $K_{SV} = k_q\tau_0$ ), where  $k_q$  is the bimolecular rate constant of the quenching process, and  $\tau_0$  is the lifetime of the fluorophore. Dynamic or static quenching can be distinguished

by their unlike dependence on temperature and by the variations induced in the fluorescence lifetime or in the absorption spectrum of the fluorophore. For dynamic quenching,  $k_q$  may be as high as  $10^{10} \text{ M}^{-1}\text{s}^{-1}$  [97]. If  $k_q$  is greater than this value, it usually indicates static dynamic quenching via a complexation between the fluorophore and the quencher.

Due to the delocalized  $\pi$ -electrons, CPEs facilitate energy transfer over the polyelectrolyte chain and have special fluorescence quenching possibilities. Their repeating units turn them into long series of receptor sites which under right conditions can enhance a sensor signal (Figure 2.5). The association of an analyte to the receptor sites can totally quench the fluorescence emission, which is an advantage over small molecule based sensors, where only the interacting molecule is quenched. This phenomenon has been described by Swager and Zhou in 1995 as amplified fluorescence quenching [98,99].

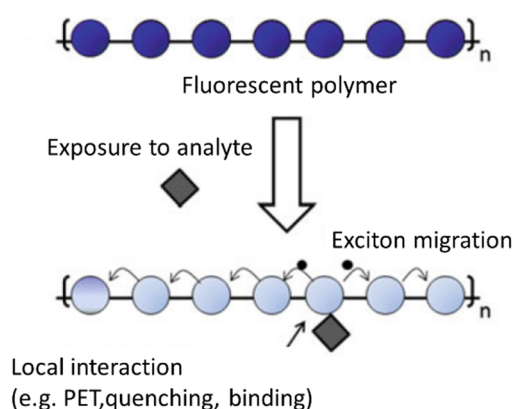


**Figure 2.5.** Schematic representation of amplified fluorescence quenching [100].

## 2. Introduction

The amplified quenching, or superquenching, of CPEs upon binding to an opposite charge molecule is frequently used in the design of CPEs-based sensors or biosensors [11,17,101,102]. Whitten's group was first to use this phenomenon for biosensing purposes [103]. They demonstrated that the fluorescence of an anionic polyelectrolyte MPS-PPV can be very efficiently quenched via photo-induced electron transfer mechanism (PET) by the positively charged acceptor methyl viologen [ $MV^{2+}$ ] (Figure 2.6). In this case, one [ $MV^{2+}$ ] molecule can quench 1000 repeat units, approximately equivalent to one whole polymer chain. The detection of a protein-binding event is done by using a biotinylated methyl viologen (B-MV). B-MV quenched the emission of MPS-PPV although with lower efficiency than [ $MV^{2+}$ ]. However, upon addition of avidin, a reversal of the B-MV quenching is seen due to the strong affinity between biotin and avidin.

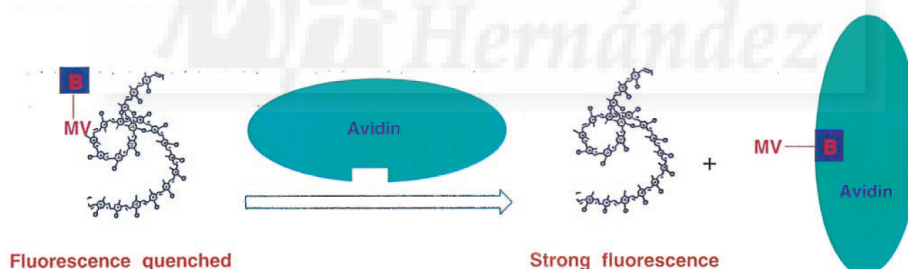


**Figure 2.6.** Illustration of the detection of avidin using a conjugated polyelectrolyte via superquenching mechanism [103].

Fluorescence can also be quenched due to Förster resonance energy transfer (FRET) between the CPEs and fluorophore with absorption spectra overlapping the polyelectrolyte emission spectrum. FRET is a well-known photophysical process whereby a donor fluorophore, initially in its electronic excited state, may transfer

energy to an acceptor fluorophore through nonradiative dipole–dipole coupling [96]. The strong distance-dependence of FRET makes it highly effective for its use in CPE-based biosensing. Changes in the distance between CPE and fluorophore can be easily correlated with the recognition events and subsequently converted into measurable fluorescence signals from both acceptor and donor emission intensities. Moreover, CPEs are natural high-performance energy donors because of their efficient light-harvesting properties and high extinction coefficients, allowing an amplified fluorescence of energy acceptors to yield high sensitivity with low signal-to-noise ratio. In 2002, for the first time, CPE-based FRET assay was applied to a specific DNA detection [13]. The assay was based on the electrostatic interaction occurring between the fluorophore labelled DNA strand and the CPE. This CPE transfers its energy to the fluorophore and detects the DNA strand with a simple and highly sensitive way.

In a recent work, Senthilkumar et al. used the FRET phenomenon to develop a fluorimetric assay for bilirubin detection [104]. Authors showed that the addition of bilirubin results in the fluorescence quenching of a water soluble polyfluorene (PF-Ph-GlcA) emission with simultaneous appearance of bilirubin emission, exhibiting visual emission color change from blue to light green. The polymer remains stable in serum even under severe basic conditions and exhibits high selectivity with visual sensitivity only towards free bilirubin in the presence of some other interferences (Figure 2.7).

## 2. Introduction

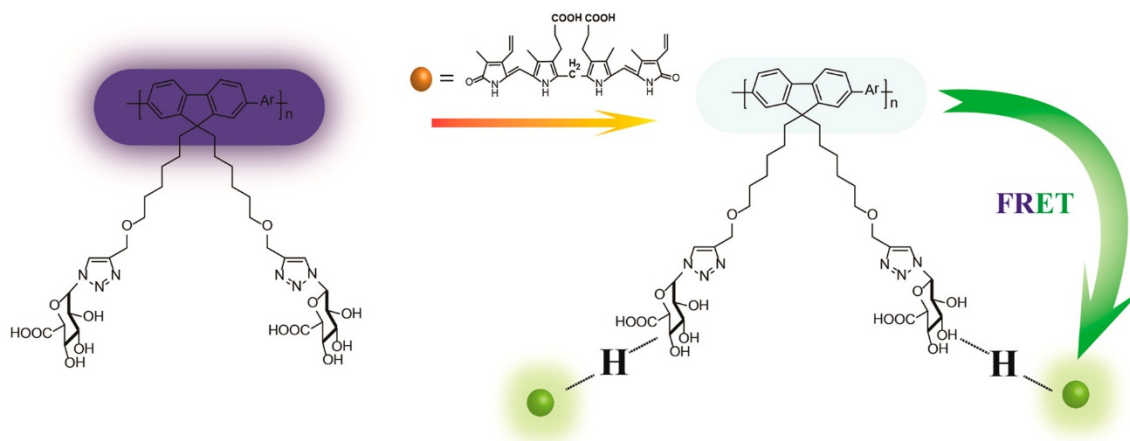


**Figure 2.7.** Schematic diagram of the mechanism used for FRET-induced sensing of bilirubin in human serum using PF-Ph-GlcA [104].

### 2.4. Solubilization and Stabilization of CPEs

As mentioned previously, in many CPEs-based applications, such as bioimaging and biosensing, a preliminary requisite is the solubility of the polymer in aqueous media. Although the incorporation of ionic side-chain groups contributes to water solubilization, many of these polyelectrolytes still have a strong tendency to aggregate. Many efforts are being addressed to develop strategies to overcome this important drawback, applicable to different type of CPEs. A strategy can be disruption of aggregates through the coupling with oppositely charged amphiphilic molecules, such as surfactants, forming stable complexes which lead to a large increase of the fluorescent quantum yields as well as to spectral changes [30,105-107]. In general, the effect of the interaction of the CPE with the surfactant is as follows: first, the surfactant induces the breaking of polymer aggregates, eliminating interchain quenching which competes with emissive intrachain exciton relaxation that reduces

the fluorescence quantum yield. Second, the surfactant induces changes to the polymer coil conformation, modifying the effective electron delocalization length, which leads to spectral shifts of the absorption and emission maxima (Figure 2.8) [107].

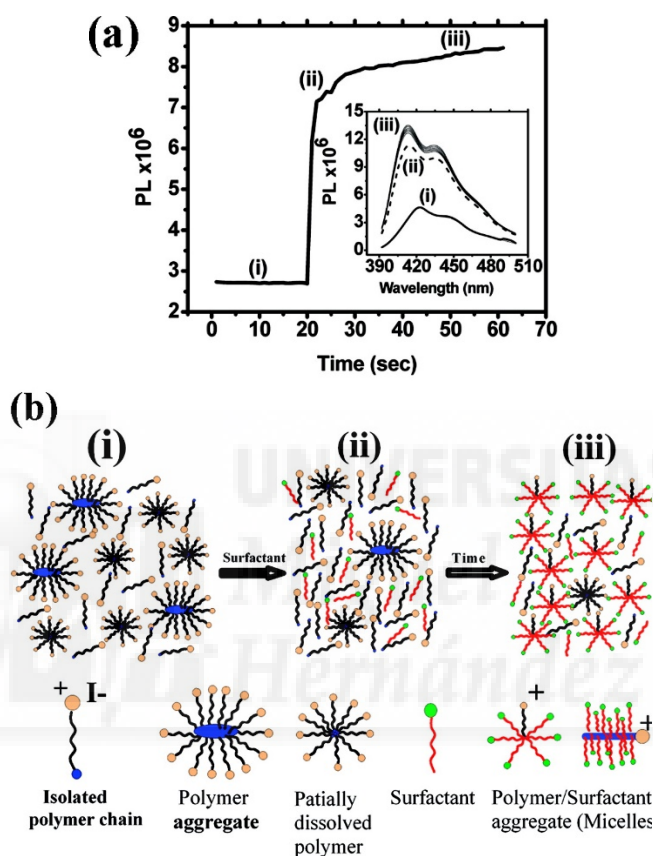


**Figure 2.8.** **a)** The dynamics of photoluminescence (PL) of CPE upon addition of surfactants. The PL level at stage **(i)** is for pure cationic conjugated polymer emission in water, and **(ii)** is the point after the addition of surfactant. **(iii)** is the region that slowly increases in PL with time. **(b)** Schematic diagram of the mechanism that represents the predicted system constituents in the three stages [107].

Another strategy is to entrap the CPEs in porous materials. Recently, Evans et al. have encapsulated CPEs in a silica matrix [108]. Within this matrix, CPEs are caged and

## 2. Introduction

retained in pores which protected them from aggregation being accessible to small molecules diffusing into the matrix. With this methodology, they obtained nanocomposites which have been used for solid-state sensors applications to detect nitroaromatic explosives. An alternative strategy to decrease the polymer intrinsic aggregation include encapsulating the hydrophobic backbone of the conjugated polymer with suitable macrocycles, such as cyclodextrins. It has been reported that the encapsulation of conjugated polymers by cyclodextrin derivatives prevents  $\pi$ - $\pi$  interactions between the polymer chains, increasing water solubility and photo and electroluminescence efficiencies [24,109,110].

Finally, another strategy may be to disrupt aggregations through the coupling with biological nanostructures with different functional properties [111-113]. The latter alternative has the advantage of not only increasing the fluorescence signal and stabilizing the polyelectrolyte in aqueous solution but also of obtaining nanoparticles which combine the properties of both constituents. Lipids have good surfactant properties, such as low toxicity and quick biodegradation, and they are also commercially available in a high state of purity [114,115]. In contact with water and under appropriate conditions, they can form cell-like structures known as liposomes, capable of solubilizing a wide variety of nonpolar compounds [116,117]. The inclusion of polymers (not the conjugated ones) in liposomes has been studied as a way to increase the long-term stability of the liposomes, increasing their applications as drug carriers [118]. However, the interaction of CPEs with liposomes as a way to disrupt aggregations has not been practically explored. This alternative could lead to

obtain multifunctional fluorescent nanoparticles that can be potentially used as drug carriers and bioimaging probes.

### 2.5. The Cationic Polyfluorene HTMA-PFP

The polyelectrolyte poly{[9,9-bis(6'-N,N,N-trimethylammonium) hexyl] fluorene-phenylene} bromide (HTMA-PFP) is a cationic polyfluorene consisting of an hydrophobic backbone which incorporates a phenyl group on the fluorene ring, and alkyl side chains with cationic charged quaternary amines (Figure 2.9) [119,120]. Its synthesis, described in Mallavia et al., is summarized as follows: firstly the neutral polyfluorene poly-(9,9-bis(6'-bromohexyl)fluorene)phenylene (P1) is obtained via Suzuki coupling reaction using 1,4-phenyldiboronic acid and 2,7-dibromo-9,9-bis(6'-bromohexyl)fluorene, with Pd(II) as a catalyst. Then, this polymer is treated with gas-phase trimethylamine to obtain the corresponding cationic polyelectrolyte, as is shown in Figure 2.9 [27].

HTMA-PFP shows interesting absorption and fluorescence properties which depend on its conformational and aggregation state. It forms very tight aggregates of low fluorescence intensity in pure water, with chains coming together and forming an inner cylindrical core. Disruption of aggregates by interaction with surfactants leads to an increase in the fluorescence signal and a blue-shift in the emission spectrum [38,45,105]. HTMA-PFP is a good energy transfer donor for acceptors over a large part of the visible spectrum because of its high fluorescent quantum yield and blue

## 2. Introduction

emission. Furthermore, it has also been shown to be an adequate energy acceptor from tryptophan residues in peptides and proteins [121,122].

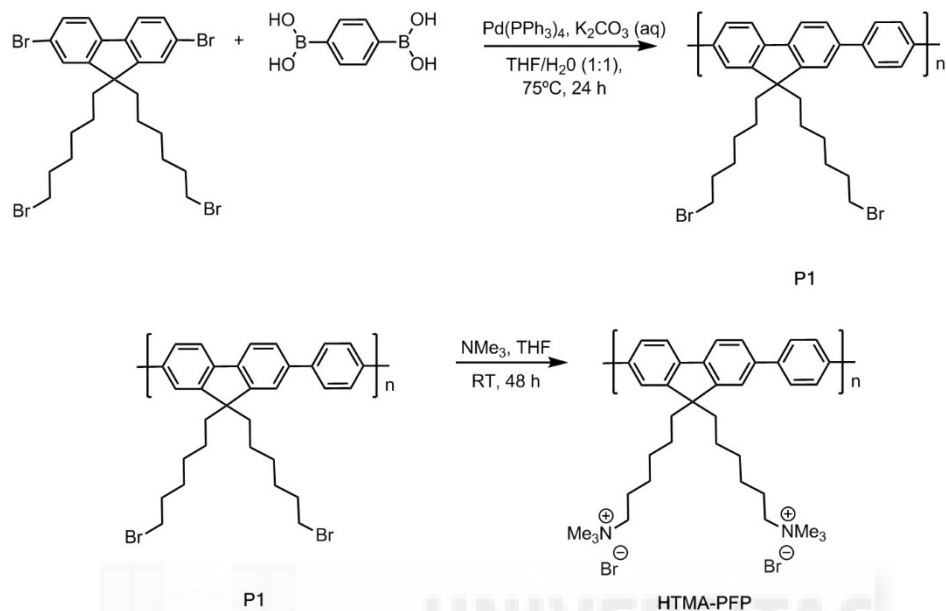


**Figure 2.9.** Schematic representation of the synthesis of HTMA-PFP.

Due to the cationic groups, HTMA-PFP has been reported to show high affinity by anionic biomolecules such as DNA and human serum albumin (HSA) [38,121,123]. Interaction of the HTMA-PFP with single and double stranded DNA, varying both the polymer and DNA molecular weights was studied by Monteserin et al. [123]. Results showed that the DNA molar concentration can be easily estimated from the changes in the physical properties of the polymer (absorption, emission, electrical conductivity, viscosity) in an aqueous solution. Moreover, Martinez-Tome et al. confirmed the interaction between HTMA-PFP and HSA in aqueous solution through alterations in the absorption and fluorescence spectra of the polyelectrolyte and the quenching of the intrinsic fluorescence of the protein, which is predominantly due to static quenching and energy transfer mechanism between protein and polymer [121].

Results suggest that polymer-protein complexes are formed with high affinity because of a combination of electrostatic interaction between the cationic side-chains of HTMA-PFP and the negatively charged surface of the protein, as well as hydrophobic interactions between the conjugated polymer backbone and the hydrophobic patches of HSA. In addition, changes in the fluorescence properties were associated to conformational changes of the protein, suggesting the use of HTMA-PFP to monitor molecular processes.

Finally, HTMA-PFP is also an electron donor and this property can be used for sensing applications. In a previous work, it was shown that p-nitrophenol (PNP), an electron acceptor that absorbs at 400 nm in its anionic form, is able to quench the fluorescence intensity of HTMA-PFP, presumably via a combination of PET and FRET mechanisms [124,125]. Cao et al. used this behaviour to develop a fluorimetric assay in buffer for the screening of  $\alpha$ -glucosidase inhibitors, taking into account that this enzyme catalyzes the hydrolysis of para-nitrophenyl- $\alpha$ -D-glucopyranoside to PNP (Figure 2.10).

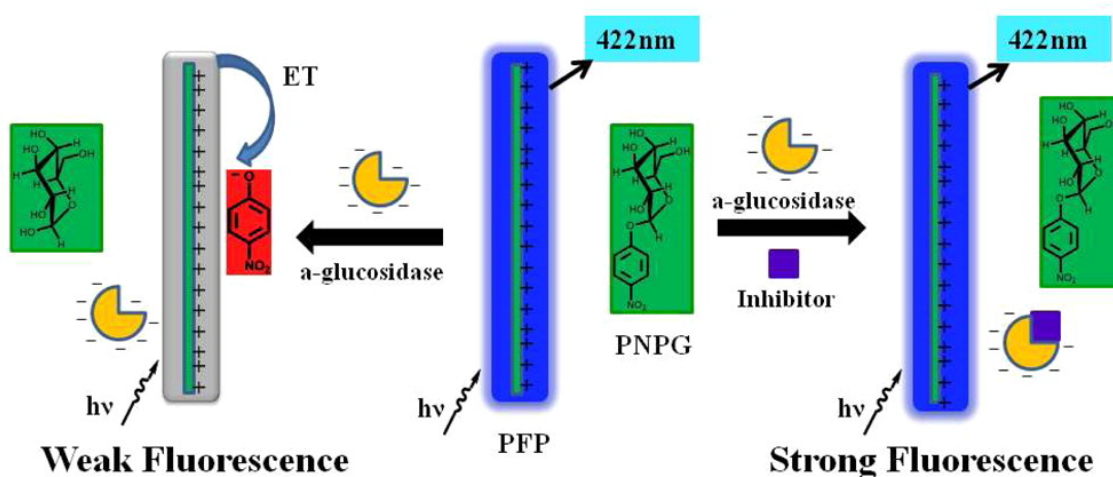


**Figure 2.10.** Illustration of the assay used to detect  $\alpha$ -glucosidase inhibitors [124].



## 3. OBJECTIVES





The main goal of this Thesis is focused on the characterization of two conjugated polyelectrolytes, blue-emitting HTMA-PFP and red-emitting HTMA-PFNT, searching their potential applications as fluorescent markers and sensing platforms. For this end, the following specific objectives are proposed:

1. Study the solubility and stability of these CPEs in aqueous media that mimic physiological conditions.
2. Analyse the interaction of HTMA-PFP and HTMA-PFNT with model lipid membrane systems that imitate natural cell membranes.
3. Explore the ability of these CPEs to form fluorescent nanoparticles through their interaction with proteins and lipid vesicles.
4. Evaluate possible biotechnological applications of HTMA-PFP, HTMA-PFNT and CPEs-based nanoparticles.
  - 4.1. CPEs as fluorescent membrane markers.
  - 4.2. CPEs for selective recognition and imaging of bacteria.
  - 4.3. CPEs-based nanoparticles in bioimaging, biosensing and as drug carriers.



## 4. MATERIALS AND METHODS



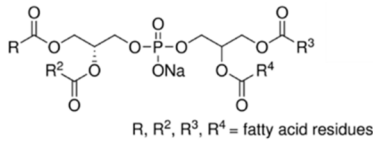


## 4.1. Materials

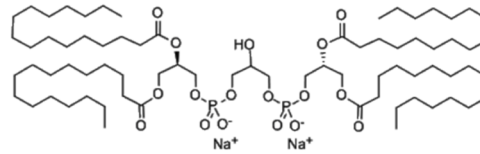
## 4.1.1. Lipids

a.

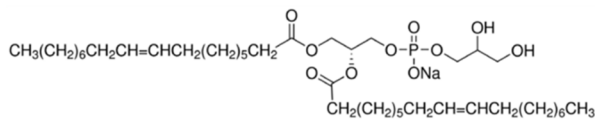
PG



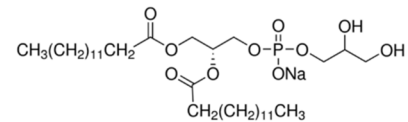
CA



DOPG

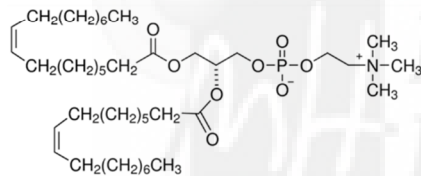


DMPG

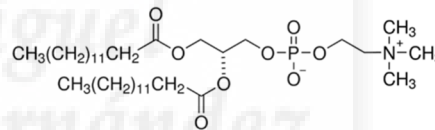


b.

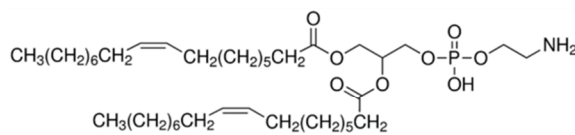
DOPC



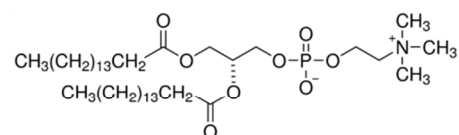
DMPC



DOPE



DPPC



c.

Cholesterol

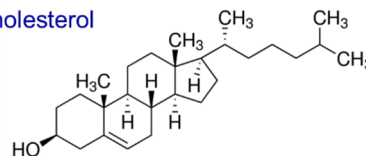


**Figure 4.1.** Chemical structures of **a)** anionic, **b)** zwitterionic phospholipids and **c)** cholesterol.

#### 4. Materials and Methods

The synthetic phospholipids 1,2-Diacyl-*sn*-glycero-3-phospho-(1-*rac*-glycerol) (PG), 1,2-dioleoyl-*sn*-glycero-3-phospho-*rac*-(1-glycerol) sodium salt (DOPG), 1,2-dimyristoyl-*sn*-glycero-3-phospho-*rac*-(1-glycerol) sodium salt (DMPG), 1,2-Dioleoyl-*sn*-glycero-3-phosphocholine (DOPC), 1,2-Dimyristoyl-*sn*-glycero-3-phosphocholine (DMPC), 1,2-Dipalmitoyl-*sn*-glycero-3-phosphocholine (DPPC), 1,2-Dioleoyl-*sn*-glycero-3-phosphoethanolamine (DOPE), Cholesterol (Chol) and Cardiolipin sodium salt from bovine heart (CA) were from Sigma-Aldrich (Spain) and used as received (Figure 4.1).

##### 4.1.2. Proteins

The Human Serum Albumin (HSA) and Bovine Alkaline Phosphatase (ALP) were from Sigma-Aldrich, and used without further purification (Figure 4.2).



**Figure 4.2.** Secondary structures of HSA ( $pI = 4.7$ ,  $M_w = 66.6$  kDa) and ALP (EC Number: 3.1.3.1,  $M_w = 160$  kDa, Optimum  $pH = 9.8$ ).

4.1.3. *Conjugated Polyelectrolytes*

The cationic CPEs HTMA-PFP ( $M_n[\text{g/mol}]=4170$ ;  $M_w[\text{g/mol}]=8340$ ) and HTMA-PFNT ( $M_n[\text{g/mol}]=4507$ ;  $M_w[\text{g/mol}]=8990$ ), were obtained and characterized in our laboratory. Briefly, stocks of the neutral polymers, poly[bis(6'-bromohexyl)fluorene-phenylene] and copoly-{9,9-bis(6-bromohexyl)-2,7-fluorene-alt-1,4-(naphto[2,3c]-1,2,5-thiadiazole)} were synthesized by Suzuki coupling reaction with Pd(II) as catalyst and treated with gas-phase trimethylamine to obtain the corresponding cationic CPEs HTMA-PFP and HTMA-PFNT, respectively [27,126,127]. Stock solutions of HTMA-PFP and HTMA-PFNT were prepared in DMSO, with final concentrations of  $3.65 \times 10^{-4}$  M (in repeat units) and stored at  $-20^\circ\text{C}$  before use (Figure 4.3).

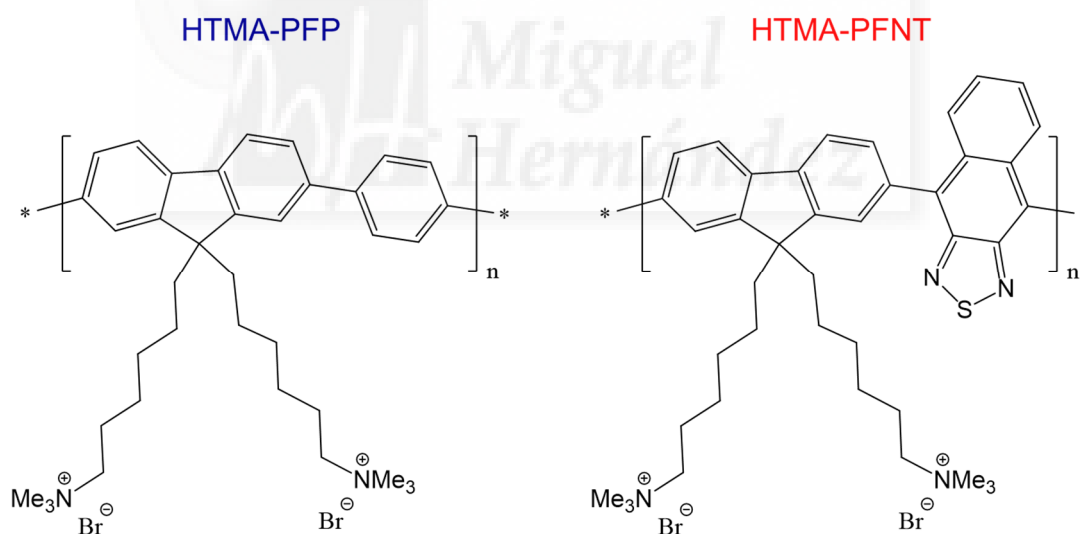


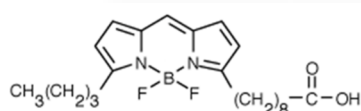
**Figure 4.3.** Chemical structures of HTMA-PFP and HTMA-PFNT.

## 4. Materials and Methods

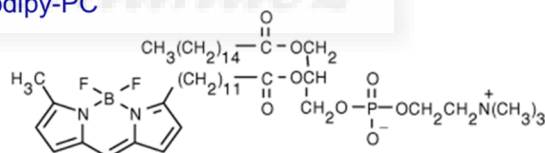
### 4.1.4. Fluorescent Probes and Quenchers

The fluorescent probes 5-butyl-4,4-difluoro-4-bora-3a,4a-diaza-s-indacene-3-nonanoic acid (BODIPY 500/510 C<sub>4</sub>,C<sub>9</sub>) and 2-(4,4-difluoro-5-methyl-4-bora-3a,4a-diaza-s-indacene-3-dodecanoyl)-1-hexadecanoyl-sn-glycero-3-phosphocholine (BODIPY-PC) were from Molecular Probes (Eugene, OR, USA). Stock solutions (1 mM) of these probes were prepared in ethanol and stored at -20 °C before use. The Rhodamine 6G was from Sigma-Aldrich, and was used without further purification. Fluorescent probes 5(6)-carboxyfluorescein (CF) and 1,6-diphenyl-1,3,5-hexatriene (DPH) and quenchers 9,10-anthraquinone-2,6-disulfonic acid (AQS) and p-nitrophenol (PNP) were obtained from Sigma-Aldrich (Spain) and dissolved in dimethyl sulfoxide (DMSO) (1.25 M), dimethylformamide (DMF) (1 mM), water (5 mM) and tris buffer 50 mM, pH 9 (5 mM), respectively, just before use (Figure 4.4).

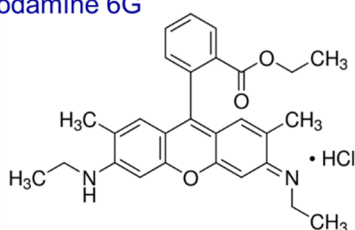
Bodipy 500/510 C<sub>4</sub>,C<sub>9</sub>



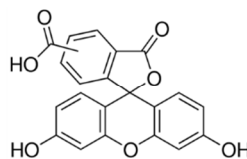
Bodipy-PC



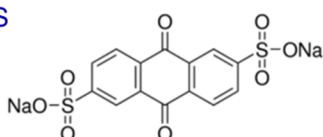
Rhodamine 6G



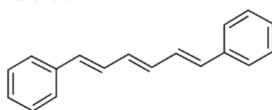
CF



AQS



DPH



PNP

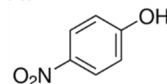


**Figure 4.4.** Chemical structures of the fluorescent probes and quenchers used.

### 4.1.5. Other Reactives

The p-nitrophenyl phosphate (PNPP) and Tetraethyl orthosilicate (TEOS) were from Sigma-Aldrich (Spain) and used as received.

All other compounds were of analytical and spectroscopic reagent grade (UVASOL, Merck). Sodium phosphate buffer (50 mM, 0.1 M NaCl, pH 7.3) and tris buffer (50 mM, pH 9.2) were prepared with Milli-Q water.

## 4.2. Instrumentation

### 4.2.1. Absorption and Steady-State Fluorescence Measurements

Absorption measurements were carried out using a UV-1603 spectrophotometer (Shimadzu, Tokyo, Japan). QuantaMaster spectrofluorometer (PTI, Birmingham, NJ, USA) interfaced with a Peltier cell was used for fluorescence spectra and fluorescence intensity measurements. The samples were placed in 10 mm × 10 mm path length quartz cuvettes. Background intensities were always subtracted from the sample. All fluorescence spectra were corrected for variations in photomultiplier response over wavelength. Steady-state fluorescence anisotropy,  $\langle r \rangle$ , was obtained using Glan-Thompson polarizers.

### 4.2.2. Optical and Electronic Microscopy Measurements

Fluorescence microscopy images of giant unilamellar vesicles, mammalian cells and bacteria were recorded using two different microscopes. First, a Nikon Eclipse

#### 4. Materials and Methods

TE2000-U inverted microscope equipped with a Nikon Digital Sight DS-1QM/H and Nikon Digital Camera DXM1200 was used. UV excitation ( $340 \text{ nm} \leq \lambda_{\text{ex}} \leq 380 \text{ nm}$ ) and blue emission ( $435 \text{ nm} \leq \lambda_{\text{em}} \leq 485 \text{ nm}$ ) was filtered using a DAPI filter cube. Data acquisition was monitored successively by manual format and data processing with NIS-Elements AR 2.30 software. And second, we used a Leica DMI 3000B inverted microscope equipped with a Leica EL6000 compact light source and a Leica digital camera DFC3000G. The imaging was performed by using a 63 $\times$  objective with 0.7 magnification and DsRed filter (Ex BP 555/25, Em BP 620/ 60). Data acquisition was monitored by manually formatting and processing with Leica Application Suite AF6000 Module Systems.

Transmission electron microscopy (TEM) measurements were performed by using a Jeol 1011 microscope (Jeol, Japan), operating at 80 kV. Samples were prepared by placing a drop of the sample on to the 300-mesh copper grid coated with carbon film, and after staining with uranyl acetate and lead citrate, they were left to air-dry before being placed under the microscope. Images were recorded with a Gatan Erlangshen ES500W camera.

##### 4.2.3. *Dynamic Light Scattering (DLS)*

The size of different nanostructures was explored by using DLS techniques with two different equipment. First, we used a Malvern Zetasizer Nano-ZS instrument, equipped with a monochromatic coherent 4mW Helium Neon laser ( $\lambda = 633 \text{ nm}$ ) as light source, with a 173 $^\circ$  scattering angle of lecture for size measurements. And

second, we used a Brookhaven 90 Plus Nanoparticle Size Analyzer instrument, equipped with a 35 mW red diode laser ( $\lambda = 640 \text{ nm}$ ) as light source, with a  $90^\circ$  scattering angle. The buffer used for the samples was previously filtered with a cellulose acetate membrane filter with a 200 nm pore size. All measurements were performed in disposable cuvettes, in triplicate.

### 4.2.4. *Circular Dichroism (CD)*

CD measurements of proteins were carried out with a Jasco spectropolarimeter, model J-815 (JASCO, Easton, MD). Spectra were collected with a scan speed of 50 nm per min, response time of 4 s, and a bandwidth of 1 nm. For each spectrum, 4 scans were accumulated and averaged to improve the signal-to-noise ratio. Spectra were recorded from 260 to 197 nm. 0.1 cm quartz cells (Hellma GmbH & Co) were used for these studies. A baseline was taken under the same conditions as those used for the sample and subtracted from each spectrum.

### 4.2.5. *Differential Scanning Calorimetry (DSC)*

DSC experiments for lipid phase transitions were performed in a high-resolution Microcal MC-2 differential scanning microcalorimeter (Malvern Instruments Ltd, England) under a constant external pressure of 30 psi in order to avoid bubble formation. The excess heat capacity functions were analyzed using Origin 7.0 (Microcal Software). Differences in the heat capacity between the sample and the reference cell were obtained by raising the temperature in the absence and presence

## 4. Materials and Methods

of the polymers. A series of three consecutive scans of the same sample were performed to ensure scan-to-scan reproducibility and reversibility.

### 4.3. Methodology

#### 4.3.1. Lipid Systems

##### 4.3.1.1. Description

Biological membranes are essential boundaries within the living cell. Plasma membranes separate the interior of the cell from the environment and participate in intercellular communication. These biomembranes are mainly composed of lipids and proteins [128-130] (Figure 4.5). Even though the lipid composition of the biomembranes is complicated, common biological membranes are primarily constructed by using phospholipids [131-134].

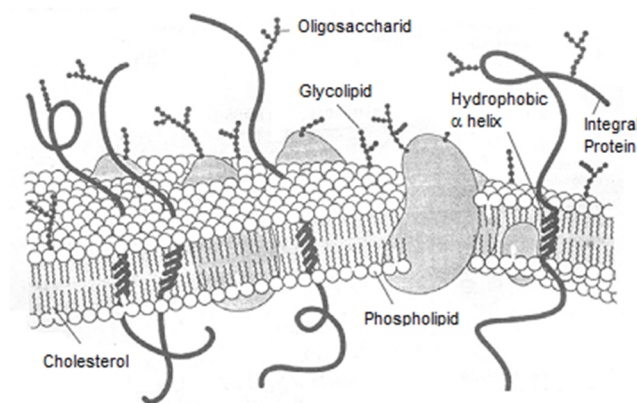


**Figure 4.5.** The fluid mosaic model of the cell membrane structure [128].

The most important property of a biological membrane is its electrical charge and the difference in potential drop between the membrane and the surrounding solution. The plasma membrane of healthy mammalian cells has an asymmetric distribution of phospholipids. The membrane outer leaflet is composed primarily of the zwitterionic phospholipids, phosphatidylcholine, and sphingomyelin, and cholesterol [135]. Therefore, the exterior membrane surface is close to a neutral charge. On the other hand, regarding the phospholipid composition of the Gram-negative bacteria membranes (using *E. coli* as a model), it has been seen that both the cytoplasmic membrane and the outer membrane are mainly composed of phosphatidylethanolamine (~70%), phosphatidylglycerol (~20%) and cardiolipin (~10%) [136]. Besides the high anionic phospholipid content of both membranes, the external face of the outer membrane also contains a high percentage of lipopolysaccharides which are negatively charged. Therefore, by varying the lipid composition, it is possible to mimic different types of cell membranes by using model membranes such as liposomes.

Liposomes, versatile tools in biology, biochemistry and medicine, are vesicles artificially prepared with phospholipids of nanometric size (although some of them can have higher sizes) and have approximately spherical shape with an internal aqueous phase surrounded by one or more lipid bilayers. They form spontaneously when lipids are in contact with water due to their amphipathic structure, with a hydrophobic tail and a polar head group (Figure 4.6) [116,117].

#### 4. Materials and Methods

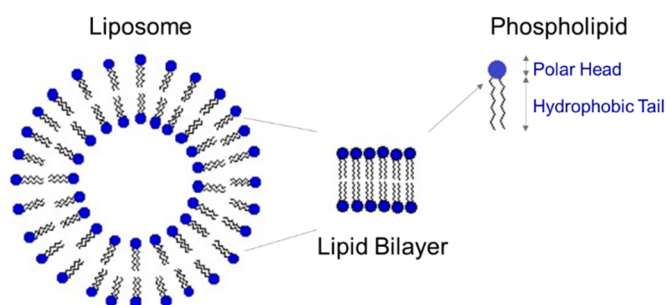


**Figure 4.6.** Schematic representation of liposomes, lipid bilayer and phospholipids.

Liposomes have been widely used as models of biological membranes or drug carriers, as their basic properties can easily be modified (for instance, by varying the lipid composition, concentration, water content and lamellarity). In these studies, one must characterize the pure liposomes as well as their mixtures with other molecules (proteins, peptides, drugs) to determine the influence of the added component on the liposome phase behavior. Lipids undergo a phase transition around a critical temperature. For homogeneous membranes, where all the lipids are identical, this temperature is known as the melting temperature,  $T_m$ , of the lipid. The phase transition temperature is defined as the temperature required to induce a change in the lipid physical state from the ordered gel phase, where the hydrocarbon chains are fully extended and closely packed to the disordered liquid crystalline phase, where the hydrocarbon chains are randomly oriented and fluid (Figure 4.7) [137,138].

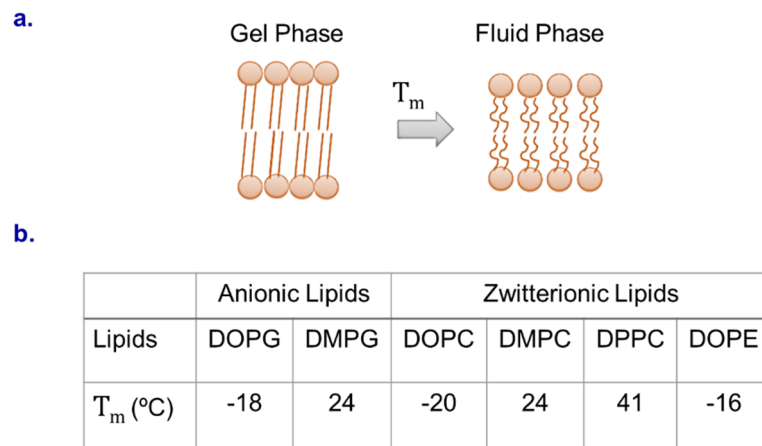


**Figure 4.7. a)** Changes observed for lipid bilayers in fluid and gel phase. **b)** Table shows lipid phase transition temperatures for the phospholipids used.

In response to the structural characteristics, in particular the number of bilayers and their size, the liposomes can be categorized as follows (Figure 4.8);

*-Multilamellar Large Vesicles (MLVs):* These structures can be formed by resuspending dried phospholipids in an aqueous solution, to the required final concentration, after agitation for several minutes [139]. MLVs are organized in concentric lipid bilayers with diameters ranging from 200 to 5000 nm and may contain 7 to 10 internal lipid bilayers. Unfortunately, their use as a model for lipid interaction with external agents is limited, since only a small percentage (10-15%) of all phospholipids are in the outermost bilayer. Also, their high turbidity limits their use in optical techniques.

#### 4. Materials and Methods

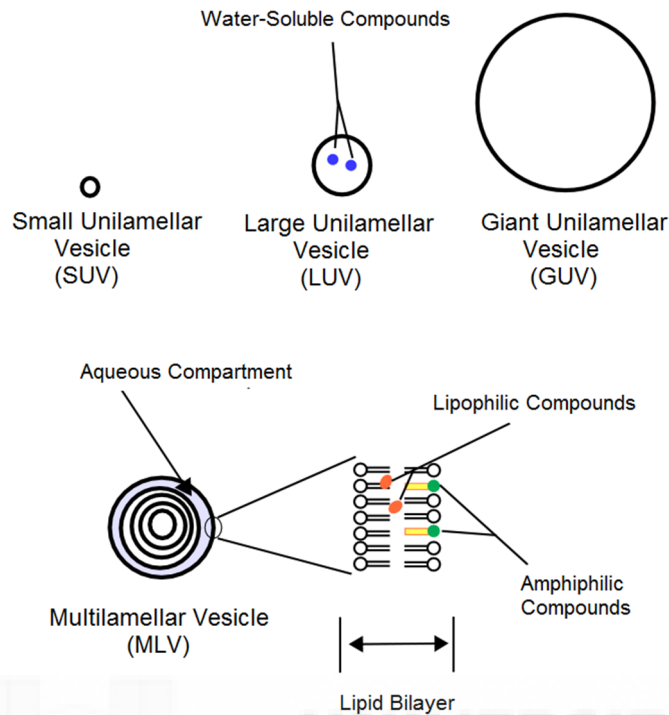


**Figure 4.8.** Schematic representation of various types of liposomes represented depending on their structural characteristics.

-*Small Unilamellar Vesicles (SUVs)*: They can be obtained by the ultrasonication of MLVs. SUVs are composed of a single lipid bilayer with diameter between 20 and 50 nm [140].

-*Large Unilamellar Vesicles (LUVs)*: They are composed of a single lipid bilayer with a diameter range of 50-500 nm. To obtain these structures, various methods may apply to suspension of phospholipids such as detergent dialysis, extrusion with French press or polycarbonate filters,  $\text{Ca}^{2+}$  induced SUVs fusion and reverse evaporation of organic solvent [141-144]. Among them, the most used

methodology is pressure extrusion through polycarbonate filters with the required pore size.

*-Giant Unilamellar Vesicles (GUVs):* These are the largest of all unilamellar vesicles, which are suitable for optical microscopy, with diameter in the range of ~10–100  $\mu\text{m}$ . They can be prepared by two different methods: electroformation and gentle hydration [145]. The electroformation with Indium Tin Oxide (ITO)-coated or titanium microscope slides gives high yield of GUVs, however the electrolysis can produce toxic by-products. Generally, this method is used for the formation of pure zwitterionic GUVs. However, the variation of the voltage and frequency may enable the GUV formation from the phospholipid mixtures containing negatively charged lipids. On the other hand, the gentle hydration method requires a few percentage of a negatively-charged lipid, and the yield of GUVs is variable and sometimes low.

### 4.3.1.2. Preparation

In the present Thesis, we used mainly LUVs and GUVs composed of different types of lipids and their preparation is described in detail, as follows;

For the preparation of the LUVs, chloroform/methanol solutions containing 3 mg of total phospholipid were dried first by evaporation under dry nitrogen gas stream and subsequently under vacuum for 3 h. MLVs were formed by resuspending the dried phospholipids in the buffer to the required final concentration. The vesicle suspension was then heated at a temperature above the phospholipid phase

#### 4. Materials and Methods

transition and vortexed several times. LUVs were prepared from these MLVs by pressure extrusion through 0.1  $\mu\text{m}$  polycarbonate filters.

For the GUVs preparation, the electroformation and the gentle hydration methods were performed. For the electroformation method, we used custom made Pt electrode-containing Teflon chambers. In summary, 1.2  $\mu\text{L}$  of a 1 mM lipid solution in chloroform was spread on each side of the Pt electrode. Removal of organic solvent traces was carried out by vacuum dehydration. Afterwards, the dried electrodes were hydrated with 450  $\mu\text{L}$  of a 200 mM sucrose solution in Milli-Q purified water. Subsequently, 7 V and 10 Hz frequency signals were applied for 2 h, followed by 1 Hz frequency signal for 30 min. After the GUV formation, the sample was collected from the chambers and transferred to the wells of a micro-slide plastic plate in which approximately 500  $\mu\text{L}$  of preparation were deposited. To better observe the GUVs under the microscope, 400  $\mu\text{L}$  of a 200 mM glucose solution was previously added to the wells in order to settle the 50  $\mu\text{L}$  of GUVs to the bottom of the chamber. Samples were preserved for 2 h at 10 °C before microscopic visualization.

For the gentle hydration method, desired phospholipids were dissolved in chloroform at 5 mM final concentration. 10  $\mu\text{L}$  of the solution was dropped on a microscope slide, which was previously washed with alcohol and dried. This sample was dried at room temperature for a few seconds and was subsequently left under vacuum for 2 h. Afterwards, the lipid film was hydrated with 15  $\mu\text{L}$  of required buffer in a humid chamber overnight. To observe the liposomes at the fluorescence microscopy, 400  $\mu\text{L}$  of buffer was added and left for 2 h to continue the hydration.

In this Thesis, vesicles having different dimensions were prepared from pure lipids as DOPC, DMPC, etc., as well as from lipid mixtures to mimic mammalian and bacterial membranes (Table 4.1).

Model System	Lipid Content	% Percentage
Mammalian Membrane	DOPC	~70
	Cholesterol	~30
<i>E.coli</i> Membrane	DOPE	~70
	DOPG	~20
	CA	~10

**Table 4.1.** Lipid content of model biomembranes (LUVs and GUVs) used in the present Thesis.

#### 4.3.2. Fluorescence Methodologies

Emission of the light from any substance is called luminescence, and occurs from electronically excited states. Depending on the nature of the excited state, luminescence is divided into two categories, fluorescence and phosphorescence (Figure 4.9). Once a molecule arrives at the lowest vibrational level of an excited singlet state, it returns to the ground state by photon emission. This process is called fluorescence. The emission rates of fluorescence are typically  $10^8 \text{ s}^{-1}$  [96]. Unlike fluorescence, a phosphorescent material does not immediately re-emit the radiation it absorbs. Phosphorescence is the emission of light from the triplet excited state, where transitions to the ground state are forbidden and the emission rates are slow ( $10^3$ - $10 \text{ s}^{-1}$ ).

#### 4. Materials and Methods

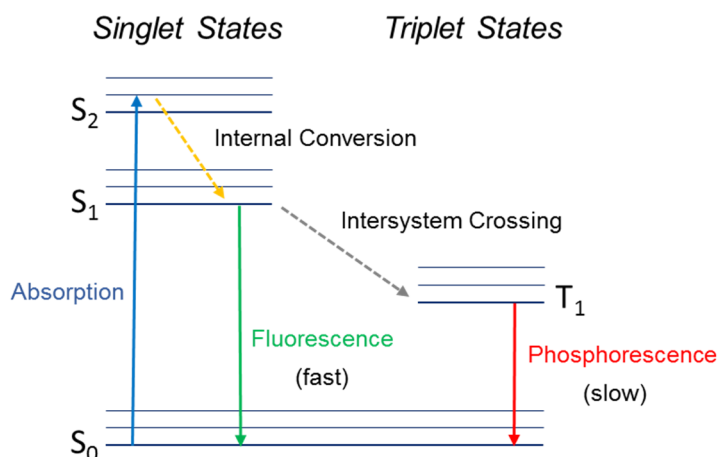


**Figure 4.9.** Jablonski diagram illustrates some possible excitation and relaxation pathways from the singlet ground state (S<sub>0</sub>) and first excited state (S<sub>1</sub>) and the triplet state (T<sub>1</sub>).

Fluorescence typically occurs from molecules with conjugated bonds, which are called fluorophores [96]. When a set of fluorophores is excited with a radiation of constant energy, they all emit photons at different frequencies. These frequencies arrange to form the fluorescence emission spectra.

Fundamental parameters commonly used in describing and comparing fluorophores are the extinction coefficient ( $\epsilon$ ) and quantum yield ( $\Phi$ ). The extinction coefficient (eq. 4.1) is the capacity for light absorption at a specific wavelength and is calculated as;

$$A = \epsilon \cdot c \cdot l \quad [4.1]$$

where, A is the absorbance at a particular wavelength, c is the concentration of the fluorophore in a cuvette and l is the path length of the cuvette. A high extinction

coefficient also indicates that a fluorophore has a high probability of fluorescence emission.

Quantum yield ( $\phi$ ) is a tool for measuring the efficiency of fluorescence emission relative to all of the possible pathways for relaxation and is generally expressed as the ratio of photons emitted to the number of photons absorbed. A high quantum yield is desirable in most imaging applications.

The  $\phi_F$  of a fluorophore (F) is determined relative to a reference compound (S). If the same excitation wavelength, gain and slit bandwidths are applied for the two samples then the  $\phi_F$  is calculated as;

$$\phi_F = \phi_S \times \frac{I_F}{I_S} \times \frac{A_S}{A_F} \times \frac{n_F^2}{n_S^2} \quad [4.2]$$

where  $\phi_S$  is the quantum yield of the reference compound;  $n$  is the refractive index of the solvent;  $I$  is the integrated fluorescence intensity; and  $A$  is the absorbance at the excitation wavelength. Absorbances at the wavelength of excitation are optimally kept in between  $A = 0.02-0.05$  in order to avoid inner filter effects and ensure linear response on the intensity.

In the present Thesis, we took advantage of the versatility of the fluorescence technique and we used it as a tool to characterize the CPEs. Below, they are summarized as follows;

*-Determination of Partition Coefficient ( $K_P$ ) between lipid and aqueous phase*

The affinity of the conjugated polyelectrolytes for the lipid membranes was estimated, at low lipid concentrations, by the following equation;

#### 4. Materials and Methods

$$\Delta I = \frac{\Delta I_{\max} [L]}{1/(K_P \gamma)^{+}[L]} \quad [4.3]$$

where  $K_P$  is the phospholipid/water partition coefficient of the polymer,  $\Delta I$  ( $\Delta I = I - I_0$ ) stands for the difference between the fluorescence intensity of the CPE measured in the presence ( $I$ ) and in the absence ( $I_0$ ) of the phospholipid vesicles,  $\Delta I_{\max} = I_{\infty} - I_0$  is the maximum value of this difference once the limiting value is reached ( $I_{\infty}$ ) upon increasing the phospholipid concentration  $[L]$ , and  $\gamma$  is the molar volume of the phospholipid (for anionic and zwitterionic phospholipids in the fluid phase, the value of  $\gamma$  is  $0.7 \text{ M}^{-1}$  and  $0.9 \text{ M}^{-1}$ , respectively) [146-148].

The  $K_P$  value can be obtained from a two parameter ( $\Delta I_{\max}$  and  $K_P$ ) fitting process. In short, the higher the  $K_P$  value, the greater the affinity of the polyelectrolyte for lipid vesicles.

##### *-Incorporation Kinetics*

Fluorene-based polymers, such as HTMA-PFP, are particularly attractive as energy donors in Förster energy transfer (FRET) because of their high fluorescent quantum yields and blue emission [122]. This property was used to explore the incorporation kinetics of HTMA-PFP into the lipid bilayer.

This kinetics was monitored as a function of time recording the increase produced in the fluorescence intensity of an acceptor chromophore previously incorporated in the membrane, after the excitation at the polymer absorption wavelength. The acceptor used was a BODIPY-PC which absorbs where the HTMA-PFP emits.

##### *-Location of the CPEs in the Lipid Membrane*

In order to study the location of the CPEs in the lipid bilayer, quenching experiments were carried out using the anionic electron acceptor 9,10-anthraquinone-2,6-disulfonic acid (AQS) as a fluorescence quencher. This molecule has been reported to be an excellent quencher for cationic conjugated polyelectrolytes and is soluble in water, but not in lipid membranes [149,150]. Stern-Volmer plots were used to determine the location of the CPEs in the different lipid systems. If the CPE is incorporated into lipid vesicles and is embedded into the lipid bilayer, AQS is not capable to quench the fluorescence of the CPE and a low value of  $K_{SV}$  is determined. On contrary, if it remains close, or at the surface of the bilayer and not within the hydrophobic core, a decrease in fluorescence intensity occurs, and a high value of  $K_{SV}$  is obtained.

##### *-Membrane Leakage Induced by CPEs*

The integrity of the membranes was confirmed by monitoring the induced release of the fluorescent probe carboxyfluorescein (CF) from lipid vesicles in the presence of the CPEs. When this fluorophore is encapsulated at high concentration in the aqueous cavity of liposomes, its fluorescence decreases by an autoquenching process [151,152]. If the vesicle membrane is perturbed by the incorporation of polyelectrolyte, the trapped CF is released and its fluorescence increases after its dilution in the buffer. To have a positive control, the total rupture of the vesicles and release of CF was performed with Triton X-100 10%.

#### 4. Materials and Methods

##### *-Phase Transition Detection*

One of the strategies to study the effect of the polyelectrolyte interaction on the physical state of a lipid bilayer is to explore how it affects to the lipid phase transition. This study can be addressed measuring the steady-state fluorescence anisotropy ( $\langle r \rangle$ ) of an extrinsic fluorescent probe in presence of the CPEs. This parameter quantifies the fluorescence polarization degree and reflects the rotational mobility of the probe and therefore, the environmental restrictions [96].

Steady state anisotropy, defined by eq 4.4

$$\langle r \rangle = \frac{I_{VV} - GI_{VH}}{I_{VV} + 2GI_{VH}} \quad [4.4]$$

was obtained by measuring the vertical and horizontal polarized components of the fluorescence emission with excitation vertical and horizontal to the emission axis. The G factor ( $G = I_{HV} / I_{HH}$ ) corrects for the transmissivity bias introduced by the detection system.

For pure phospholipids, the characteristic shape of the plot is sinusoidal with a sharp transition of anisotropy values in a short-range of temperatures, in which the average value correspond to  $T_m$ . Thus, the plot provides an accurate determination of the  $T_m$  value, which is strongly dependent on the natural dynamic motions of the bilayer and, hence, can be correlated with the structural integrity of the lipid bilayer.

### 4.3.3. *Sol-gel Immobilization*

#### 4.3.3.1. *Description*

The sol-gel process is a liquid-phase method of preparing monoliths, glasses, ceramics, fibers and powders at room temperature (Figure 4.10) [153]. This technique has been used to produce new porous nanomaterials. The main advantage of this process over other immobilization methods is its easiness to obtain materials with targeted properties, by modifying the microstructure through the process parameters, such as the choice of the precursor, its concentration, pH value, temperature and solvent. Silica sol-gel materials have been shown to form excellent media for immobilization of proteins and other biological macromolecules [154-156]. Following a reaction of hydrolysis and polycondensation of alcoxide precursors, the proteins are individually caged and retained in pores having 2 to 10 nm size. The last decade, has seen a great deal of progress in the encapsulation of these biomolecules in sol-gel matrices by modifying older conventional procedures. The entrapped biomolecule usually maintains its structural integrity and functionality, being accessible to small molecules diffusing into the matrix, all of which enable applications in biosensors and biotechnology [157].

## 4. Materials and Methods

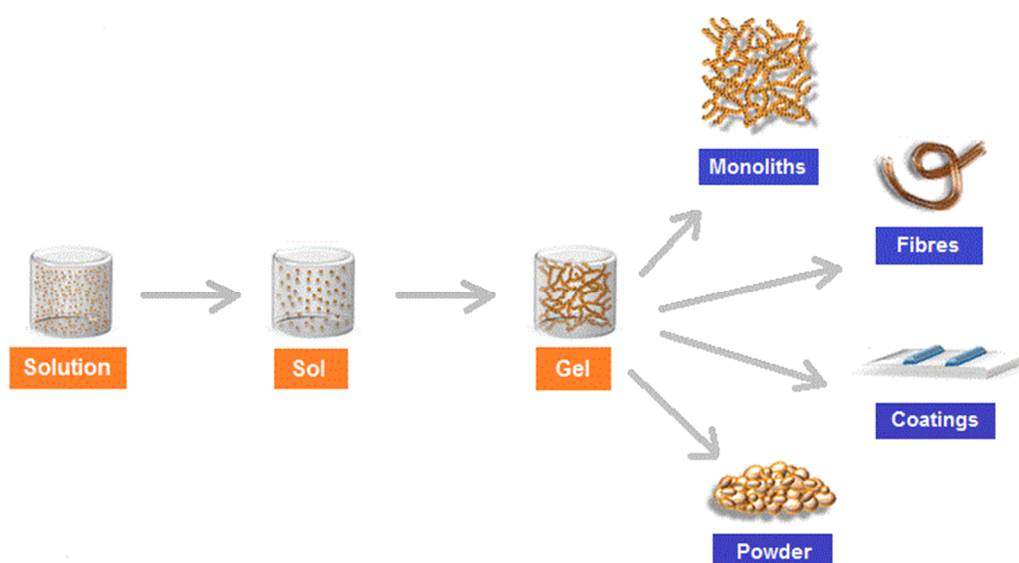


**Figure 4.10.** Schematic representation of sol-gel processing routes.

### 4.3.3.2. Preparation

In the present Thesis, we have used the sol-gel technique to immobilize the components of a novel biosensor (Alkaline Phosphatase enzyme (ALP) and fluorescent nanoparticles (NPs)) and their preparation based in the free alcohol route [158] is described, in detail, in the next paragraph:

Silica sol stock solution was prepared by mixing 4.46 mL of the precursor TEOS, 1.44 mL of H<sub>2</sub>O and 40 µL of HCl (0.62 M). The mixture was stirred regularly for 1 h in a closed vessel at room temperature (this stock can be stored at -20°C for 4 days) (Figure 4.11). Before the immobilization of the samples, silica stock solution was diluted with distilled water 1:1 (V:V). After, rotaevaporated for a weight loss of 0.62 g, which corresponds to the weight of free ethanol. Immobilized samples were prepared by mixing 700 µL of ethanol-free sol solution with 700 µL of buffered sample

which was containing the desired component to be immobilized, in an ice-cooled polystyrene cuvette. The freshly formed monoliths having a size of  $\sim 9 \times 9 \times 12$  mm were aged during 48 h, washed with buffer every 24 h, and the cuvettes were sealed with parafilm and stored in dark at 4°C.

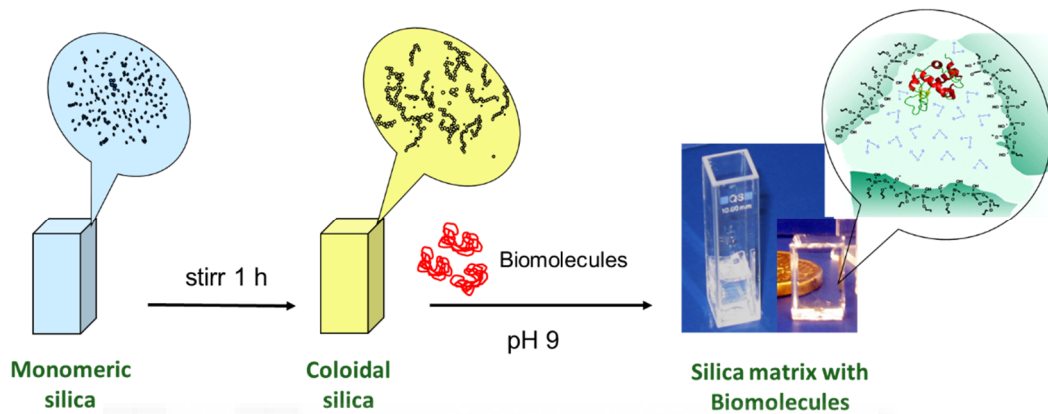


**Figure 4.11.** Schematic representation of the immobilization of biomolecules in transparent sol-gel matrices.



## 5. OVERALL RESULTS AND DISCUSSION





### 5.1. HTMA-PFP and HTMA-PFNT in Buffer

*Find below a summary of results reported in Publications 8.1 and 8.3, together with their discussion (Chapter 8).*

Our group has previously synthesized a blue-emitting cationic polyfluorene, HTMA-PFP (Chapter 4, Figure 4.3, page 37), which was discussed in section 2.5 (Chapter 2) of this Thesis. This CPE contains fluorene and phenyl units in its backbone, and side-chains with quaternary ammonium groups. Due to these cationic groups, HTMA-PFP has been reported to show high affinity by anionic biomolecules such as DNA and human serum albumin (HSA), which can be monitored from changes in its absorption and intrinsic fluorescence [38,121]. To shift the color of the polyfluorene to longer wavelengths, our group has also recently synthesized a new cationic polyfluorene, HTMA-PFNT, which emits in the red spectral region. This new polyelectrolyte incorporates the chromophore naphtha[2,3c][1,2,5] thiadiazole (NTD) on the fluorene ring, extending the conjugation length in the polymer backbone and increasing the bathochromic emission (Chapter 4, Figure 4.3, page 37). Both polyelectrolytes, HTMA-PFP and HTMA-PFNT have been carefully characterized in this Thesis to explore their potential biotechnological applications in bioimaging and biosensing.

As was mentioned previously in Chapter 2, the solubility of CPEs in aqueous media is required in biomedical applications. For this reason, we decided to study the behaviour of HTMA-PFP and HTMA-PFNT in phosphate buffer, 0.1 M NaCl (pH 7.3) in an attempt to mimic physiological conditions. Results were compared with those

## 5. Overall Results & Discussion

found in “good” solvents and are shown in Figure 5.1 and Table 5.1. Fluorescence spectra recorded in buffer were red-shifted with respect to those recorded in the organic solvents. This effect was accompanied by a slight decrease in the absorbance and a significant drop of the fluorescence quantum-yield for both polyelectrolytes, especially for HTMA-PFNT which has a higher hydrophobic character. These results suggest that, once in contact with buffer, CPEs self-assemble into aggregates. This aggregation is dominated by interchain hydrophobic interactions, which lead to lower emission intensities (self-quenching). The formation of aggregates was supported by DLS experiments (*Table 1 of Publication 8.1 and Table 2 of Publication 8.3*). Results confirm that when CPEs are added to the buffer, nanoaggregates are rapidly formed. The average size of these aggregates was time-dependent for both polyelectrolytes, by multiplying their size by 4 times, and consequently reducing their fluorescence intensity. Such effects could be explained by the existence of nonspecific electrostatic interactions between the initially formed aggregates and the anionic species contained in the buffer solution. These interactions yield neutral complexes which, upon charge neutralization, exhibit lower solubility, leading to the formation of larger aggregates.

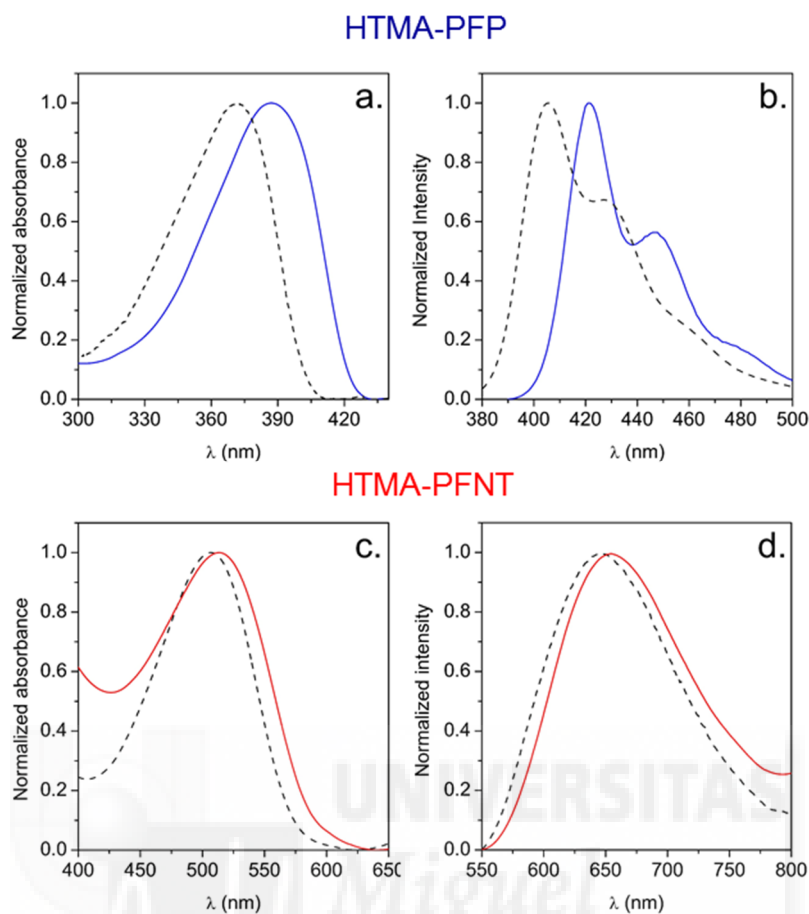


**Figure 5.1.** **a)** Normalized absorbance and **b)** fluorescence emission spectra of HTMA-PFP in buffer (blue line) and 60:40 (v/v) 2-propanol:water (dash). **c)** Normalized absorbance and **d)** fluorescence emission spectra of HTMA-PFNT in buffer (red line) and ethanol (dash).

	HTMA-PFP		HTMA-PFNT	
	Good Solvent	Buffer	Good Solvent	Buffer
$\lambda_{\max}$ (nm)	406	420	645	652
$\Phi$	0.75	0.16	0.17	0.01

**Table 5.1.** Wavelength corresponding to maximum of the emission spectrum ( $\lambda_{\max}$ ) and fluorescence quantum yield ( $\Phi$ ) of HTMA-PFP and HTMA-PFNT in buffer and good solvents (60:40 (v/v) 2-propanol:water for HTMA-PFP and ethanol for HTMA-PFNT).

## 5. Overall Results & Discussion

### 5.2. CPEs as Fluorescent Membrane Markers

Once HTMA-PFP and HTMA-PFNT were characterized in buffer, their potential use as fluorescent membrane markers was explored using model membranes of anionic and zwitterionic lipids. In the following sections, results corresponding to the different CPEs are described separately.

#### 5.2.1. HTMA-PFP in Model Membranes

*Find below a summary of results reported in Publications 8.1 and 8.2, together with their discussion (Chapter 8).*

##### 5.2.1.1. HTMA-PFP in Anionic Lipid Membranes

The interaction of HTMA-PFP with anionic vesicles was explored from changes occurring in its photophysical properties (Figure 5.2). A strong increase in the fluorescence intensity and a blue-shift of the emission spectrum was observed in the presence of low concentrations of anionic vesicles as compared to buffer. This result suggests that the interaction of HTMA-PFP with the lipid bilayer induces the breaking of aggregates, eliminating interchain quenching and increasing its fluorescence quantum yield. The partition coefficient,  $K_P$ , of HTMA-PFP between the lipid and aqueous phase was determined as was described in the section 4.3.2. of this Thesis. A value of  $K_P = 2.9 \pm 1.3 \times 10^5$  was obtained which indicates a very high affinity of the polymer for the anionic lipid bilayers, probably due to the electrostatic interaction

between the quaternary amine groups of HTMA-PFP and the negative charge of the lipid head groups.

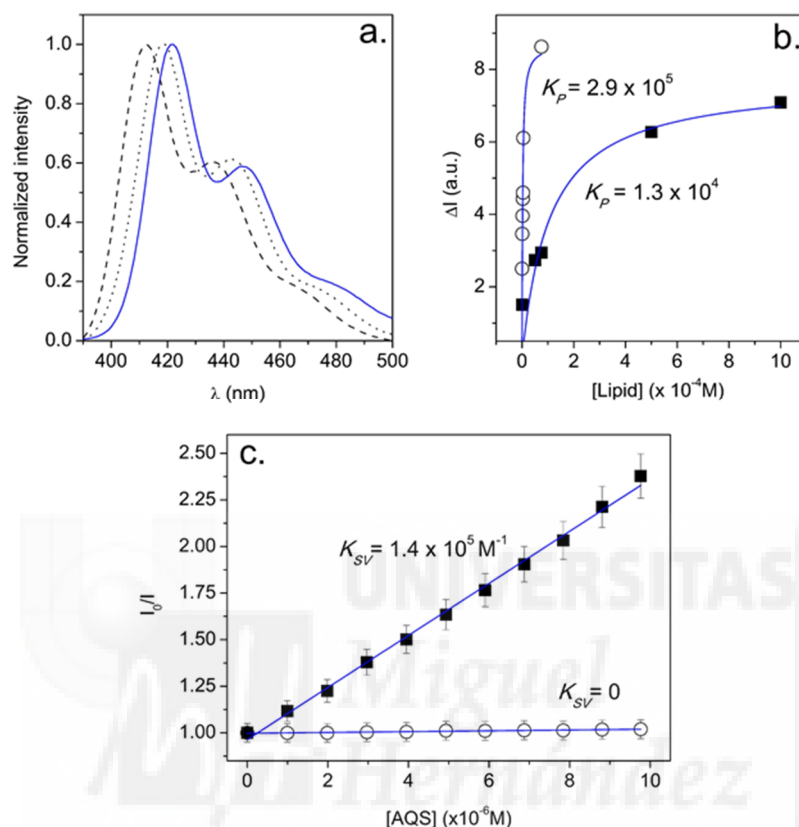
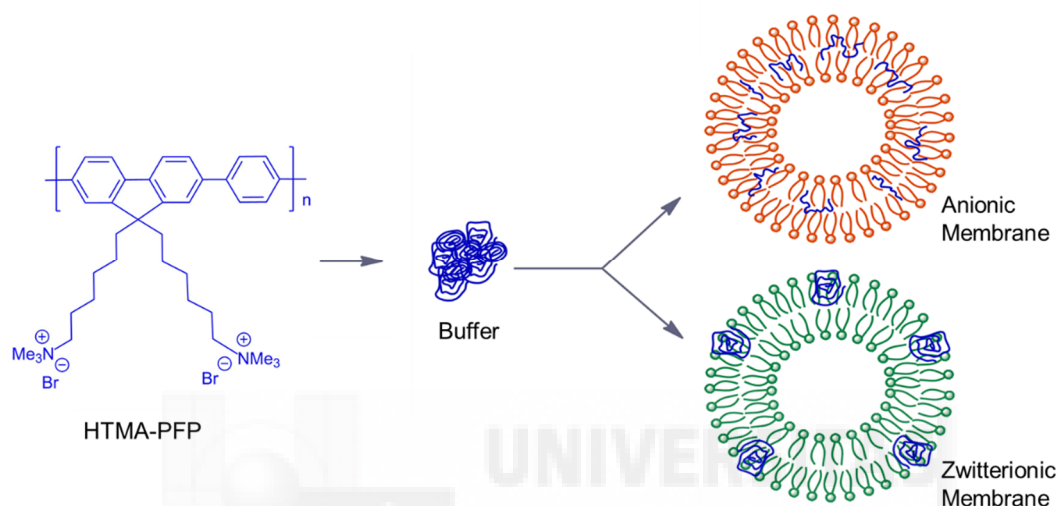


**Figure 5.2.** **a)** Normalized fluorescence emission spectra of HTMA-PFP in buffer (blue line), anionic (dash) and zwitterionic lipid vesicles (dot). **b)** Changes in fluorescence intensity ( $\Delta I$ ) at increasing concentrations of anionic (circle) and zwitterionic (solid square) lipid vesicles. **c)** Stern-Volmer plots for quenching of HTMA-PFP by AQS in anionic (circle) and zwitterionic (solid squares) lipid vesicles.

The interaction was also very fast, and was confirmed by the Förster resonance energy transfer (FRET) analysis, by using BODIPY C<sub>4</sub>C<sub>9</sub> (Bodipy) as energy acceptor (Figure 4a of Publication 8.1). Moreover, the location of the HTMA-PFP in lipid bilayer was checked from quenching experiments by using the 9,10-anthraquinone-2,6-

## 5. Overall Results & Discussion

disulfonic acid (AQS) as fluorescence quencher (Figure 5.2c). The fact that the polymer fluorescence was not quenched suggests that once HTMA-PFP interacts with the membrane, it does not remain close to the surface, but rather it is embedded in the lipid bilayer (Scheme 5.1).



**Scheme 5.1.** Schematic model, which shows the interaction between HTMA-PFP and lipid vesicles composed of anionic and zwitterionic vesicles.

The integrity of the lipid vesicles after polymer incorporation was confirmed by monitoring the induced release of the fluorescent probe carboxyfluorescein (CF) from anionic vesicles in the presence of HTMA-PFP (Figure 5a of Publication 8.1). Results show that at low concentrations of HTMA-PFP, the integrity of the vesicle is maintained (Figure 5a of Publication 8.1 and Figure 11 of Publication 8.2). Fluorescence microscopy images of giant unilamellar vesicles (GUVs) of anionic lipids also supported this result, suggesting the potential use of this polymer to label lipid membrane (Figure 5b,c of Publication 8.1). Finally, the fluorescence emission spectra of HTMA-PFP were recorded as a function of temperature for lipids with phase

transitions (Figure 5.3a). A blue-shift of the polymer fluorescence spectra was observed at the transition temperature which indicates that polyelectrolyte fluorescence is sensitive to the physical state of the lipid bilayer. All these results confirm the ability of HTMA-PFP to visualize anionic membranes and to monitor membrane processes.

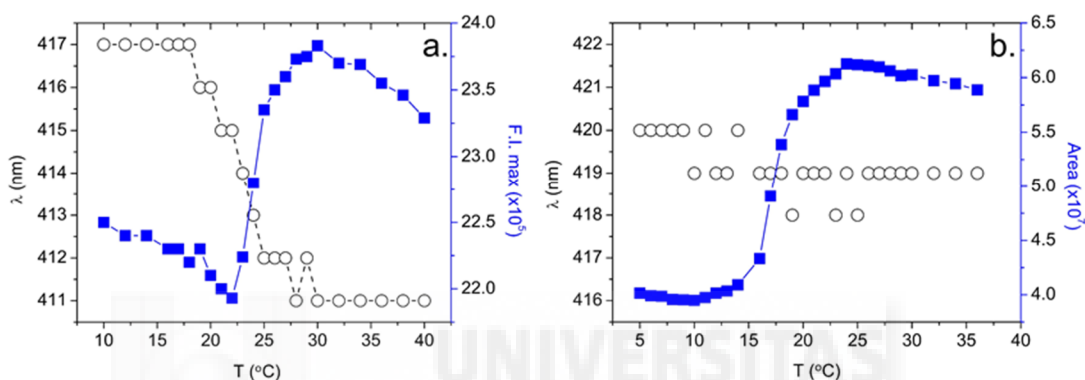


**Figure 5.3.** **a)** Temperature dependence of the fluorescence maximum position (circles) and intensity (blue squares) of HTMA-PFP in anionic lipid (DMPG). **b)** Temperature dependence of the fluorescence maximum position (circles) and fluorescence intensity measured as the integrated area under the spectrum of HTMA-PFP (blue squares) recorded in zwitterionic lipid (DMPC).

#### 5.2.1.2. HTMA-PFP in Zwitterionic Lipid Membranes

An enhancement of the fluorescence intensity and a very small blue-shift in the emission spectrum confirmed the interaction of HTMA-PFP with zwitterionic vesicles (Figure 5.2). However, the  $K_P$  value is 10 times lower than that found in the anionic vesicles, suggesting a higher affinity of HTMA-PFP for anionic vesicles than for zwitterionic ones. The kinetics of insertion of the polyelectrolyte into the zwitterionic membrane, explored by means of FRET experiments, was fast but slower than that

## 5. Overall Results & Discussion

observed for the anionic membranes (*Figure 2b of Publication 8.2*). These results indicate that the nature of the interaction between HTMA-PFP and the lipid membrane depends on the lipid headgroup charge, being mainly electrostatic for the anionic system, at least in a first step, while for the zwitterionic one it would likely be mediated by hydrophobic interactions between the conjugated backbone of the polymer and the lipid molecules. To obtain more insight into the membrane-polyelectrolyte interaction, quenching experiments were carried out by using AQS (*Figure 5.2c*). Contrary to that observed for anionic membranes, a decrease in the fluorescence signal of the polyelectrolyte was observed in the presence of the quencher. This result confirms that HTMA-PFP is incorporated into the lipid vesicle, and indicates that it remains close to the surface of the bilayer and not within the hydrophobic core (*Scheme 5.1*). This interaction does not alter the membrane integrity as was confirmed by fluorescence microscopy images, using GUVs (*Figure 6 of Publication 8.2*). Finally, for zwitterionic lipids with phase transition, HTMA-PFP was capable of detecting the transition temperature by monitoring changes in its fluorescence intensity but not in its spectral position (*Figure 5.3b*).

Comparing the interaction of HTMA-PFP with anionic and zwitterionic model membranes, we observed clear differences in  $K_P$ , location within the lipid bilayer, spectral position and fluorescence intensities, which suggest that aggregates of HTMA-PFP are better solubilized in anionic systems than in zwitterionic ones.

### 5.2.1.3. Selectivity of HTMA-PFP against Anionic and Zwitterionic Membranes

The above results confirm that the mechanism of the interaction between HTMA-PFP and lipid membranes is mediated by the lipid charge. The high affinity and rapid interaction of HTMA-PFP for anionic vesicles suggests that this CPE can be selective for this type of membranes and therefore, potentially used as a fluorescent membrane marker for systems with high anionic lipid content, such as bacterial membranes. The fact that the position of the fluorescence emission spectrum of HTMA-PFP depends on the lipid charge was used as a tool to check this hypothesis. With this end, samples containing anionic and zwitterionic vesicles together, at different proportions, were explored by monitoring the difference in spectral position (Figure 5.4a). Results show that the polymer chains are preferentially incorporated in the anionic vesicles, even though these coexist at very low proportion with the zwitterionic systems. This finding was supported by quenching experiments, which were carried out for the samples by using AQS (constant concentration) (Figure 5.4b). If effectively all the polymer chains are embedded in the anionic vesicles, then they should not be accessible to the quencher. The fact that the quenching efficiency was close to 0% for samples containing a small amount of anionic vesicles supports this hypothesis, confirming the selectivity of HTMA-PFP for anionic lipids. Microscopy fluorescence studies also support this result and show the ability of the polyelectrolyte to preferentially label and visualize populations of anionic vesicles in a mixture with zwitterionic ones (Figure 5.5).

## 5. Overall Results & Discussion

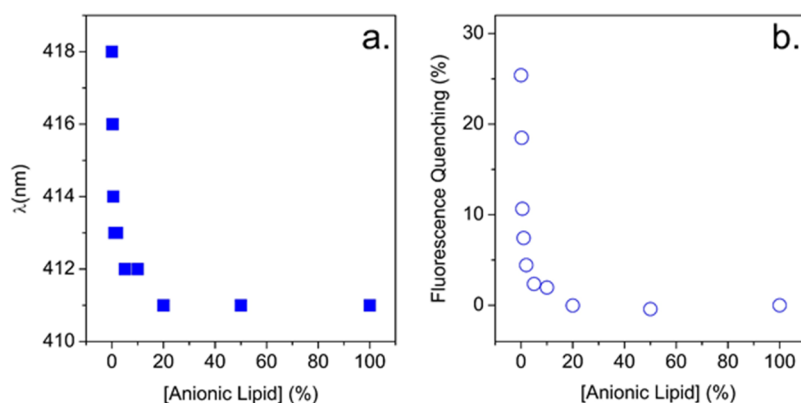


**Figure 5.4.** Membrane selectivity study of HTMA-PFP, in a mixture of anionic and zwitterionic lipid vesicles; **a)** position of the fluorescence maximum and **b)** fluorescence quenching percentage of CPE with AQS versus increased anionic vesicle.

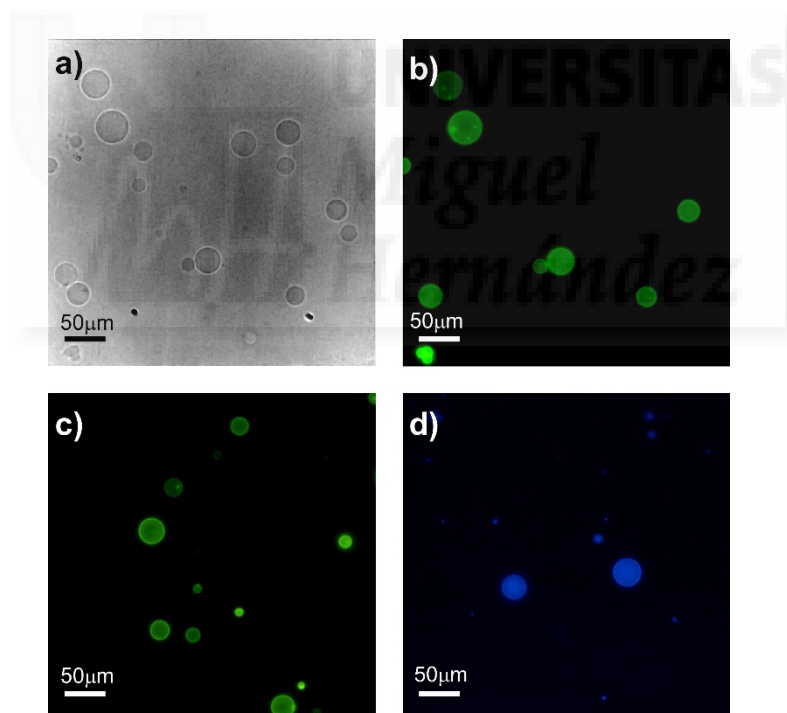


**Figure 5.5.** Microscopy images of a mixture of GUVs of Bodipy labelled-zwitterionic lipids and anionic-zwitterionic (3:1) lipids in absence of HTMA-PFP, observed by **a)** phase contrast microscopy and **b)** upon excitation with visible light. In the presence of the HTMA-PFP, upon excitation with **c)** visible light and **d)** UV-light. (a and b; c and d; correspond to the same field).

### 5.2.2. HTMA-PFNT in Model Membranes

A similar study performed for HTMA-PFP in model membranes was also carried out for the red cationic CPE.

*Find below a summary of results reported in Publications 8.3 and 8.4, together with their discussion (Chapter 8).*

#### 5.2.2.1. HTMA-PFNT in Anionic and Zwitterionic Membranes

The interaction of HTMA-PFNT with anionic and zwitterionic vesicles was confirmed with fluorescence experiments (Figure 5.6). An enhancement in fluorescence intensity compared to buffer, with several folds of amplification of the quantum-yield, was observed in a lipid concentration-dependent manner, together with a slight blue-shift of the emission maximum. These results evidence the interaction of the HTMA-PFNT with both types of membrane, as well as a clear decrease in polymer aggregation. Interpretation of results is similar to that proposed for HTMA-PFP: Probably, once HTMA-PFNT is added to the liposome suspension, self-assembled aggregates rapidly interact with the lipid membranes. This interaction should induce the disruption of aggregates through a mechanism mediated by hydrophobic interactions between the conjugated backbone of the polymer and the lipid molecules. The breakup of aggregates separates polymeric backbones, decreasing the effective conjugation length and thus reducing the self-quenching. It results in a blue shift of the emission maximum and a several-fold amplification of the fluorescence emission. From fluorescence changes recorded as a function of lipid

## 5. Overall Results & Discussion

concentration,  $K_P$  values of  $1.1 \pm 0.1 \times 10^6$  and  $1.1 \pm 0.1 \times 10^4$  were determined for anionic and zwitterionic systems, respectively, suggesting the higher affinity of HTMA-PFNT towards anionic vesicles (Figure 5.6b). Moreover, the location of HTMA-PFNT in lipid bilayers was explored using AQS (Figure 5.6c). In the zwitterionic vesicles the fluorescence was quenched, while no quenching was observed in the anionic vesicles.

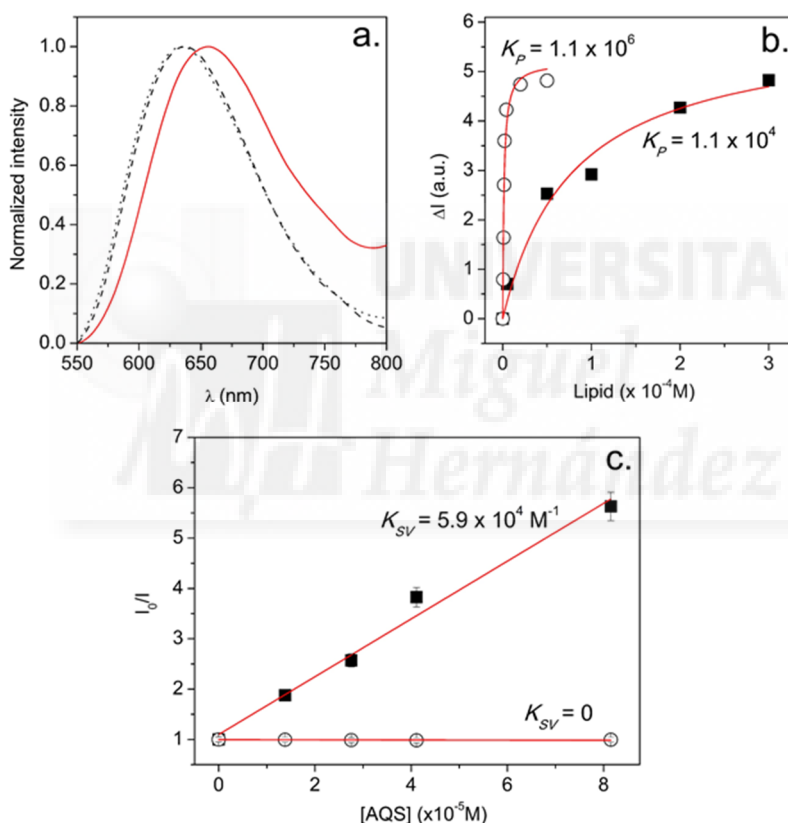


**Figure 5.6.** **a)** Normalized fluorescence emission spectra of HTMA-PFNT in buffer (red line), anionic (dash) and zwitterionic lipid vesicles (dot). **b)** Changes in fluorescence intensity ( $\Delta I$ ) at increasing concentrations of anionic (circle) and zwitterionic (solid square) lipid vesicles. **c)** Stern-Volmer plots for quenching of HTMA-PFNT by AQS in anionic (circle) and zwitterionic (solid squares) lipid vesicles.

These results indicate that HTMA-PFNT is well embedded in the bilayer of the anionic vesicles and it is located close to the membrane surface in zwitterionic system. Comparing the results obtained for HTMA-PFP and HTMA-PFNT, we assume that the nature of the interaction between these CPEs and the lipid bilayer is very similar and we can conclude that as HTMA-PFP, the red emitting HTMA-PFNT shows a preference for anionic lipids over zwitterionic ones. Finally, fluorescence studies as a function of temperature showed that the fluorescence of HTMA-PFNT was not sensitive to the physical state of the lipid bilayer, contrary to that observed for HTMA-PFP. These results evidence that both polyelectrolytes are good candidates as fluorescence membrane markers for bioimaging but that only HTMA-PFP can be used as a fluorescent probe for the detection of lipid phase changes.

### 5.3. CPEs for Selective Recognition and Imaging of Bacteria

In the light of the results obtained from the *Publications 8.1, 8.2 and 8.3*, we explored the interaction of HTMA-PFP and HTMA-PFNT, first with bacterial and mammalian model membranes, and second with bacteria *E. coli* and HeLa cells in order to evaluate the potential use of these CPEs for selective bacterial recognition.

*Find below a summary of results reported in Publications 8.4, together with their discussion.*

## 5. Overall Results & Discussion

### 5.3.1. HTMA-PFP and HTMA-PFNT in Bacterial and Mammalian Model Membranes

First, we used model membranes of different lipid compositions in order to mimic those of bacterial and mammalian membranes (Chapter 4, Table 4.1, page 49). The interaction of HTMA-PFP and HTMA-PFNT with these model systems was studied by using fluorescence emission spectra and fluorescence quenching with AQS (Figure 5.7).

Affinity studies showed that both CPEs have higher affinity for the bacterial membrane model than for the mammalian one, especially HTMA-PFNT. The high  $K_D$  value obtained for this red-emitting CPE indicates that its affinity for bacterial membrane models is 20 times higher than for mammalian ones and suggests the possibility of being more selective than the blue-emitting HTMA-PFP for bacterial membranes (Figure 5.7a,c).

Locations of both CPEs, HTMA-PFP and HTMA-PFNT, in the different lipid membrane models was explored by using AQS and related  $K_{SV}$  values were determined (Figure 5.7b,d). These values indicate that both polyelectrolytes remain close to the membrane surface in the mammalian system, and are more inserted inside the bilayer in the bacterial model. In the next study, we took advantage of this result to explore the selectivity of HTMA-PFP and HTMA-PFNT in samples where coexist both types of model membrane vesicles (Figure 5.8). Results show that when CPEs were added to samples containing a low proportion of bacterial vesicles (~20% for HTMA-PFP and ~5% for HTMA-PFNT), all the polymer chains are incorporated into the

bacterial systems and not into the mammalian ones. This study confirms the selectivity of both CPEs towards bacterial model and demonstrates that HTMA-PFNT has higher selectivity and sensitivity for this type of model membrane than HTMA-PFP.

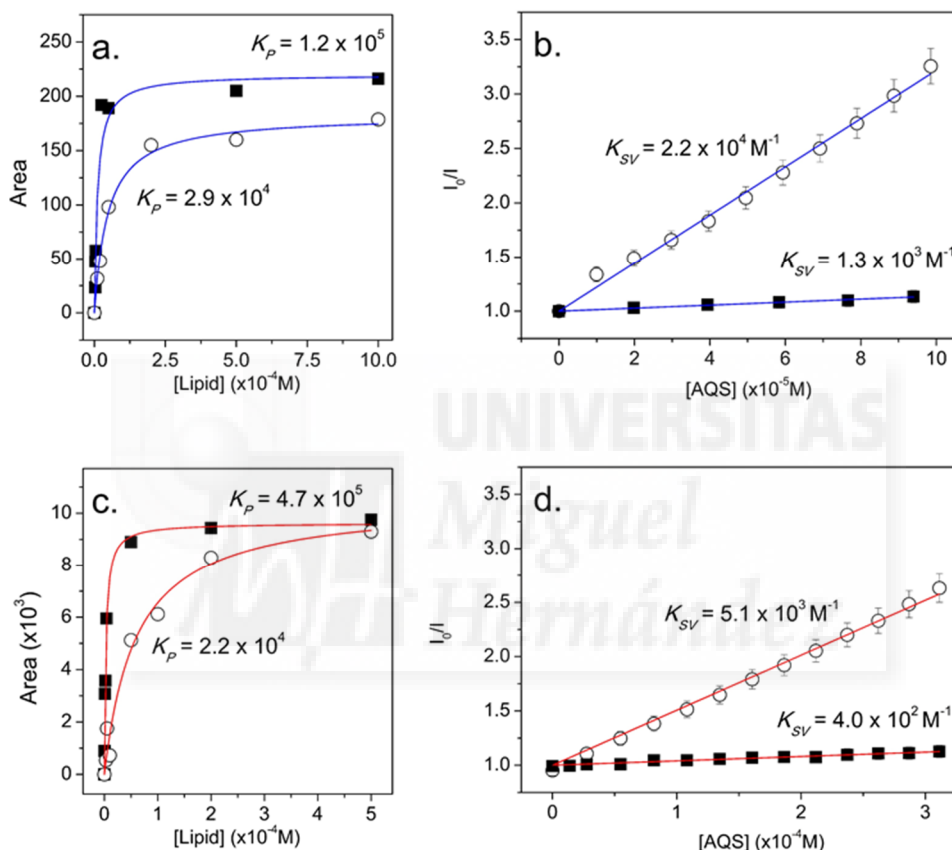


**Figure 5.7.** **a)** Area of the emission spectrum of HTMA-PFP at different concentrations of bacterial (dark squares) and mammalian (circles) model membranes. **b)** Stern-Volmer plots for quenching of HTMA-PFP by AQS in model bacterial (dark squares) and mammalian (circles) model membranes. **c)** Area of the emission spectrum of HTMA-PFNT at different concentrations of bacterial (dark squares) and mammalian (circles) model membranes. **d)** Stern-Volmer plots for quenching of HTMA-PFNT by AQS in model bacterial (dark squares) and mammalian (circles) model membranes.

## 5. Overall Results & Discussion

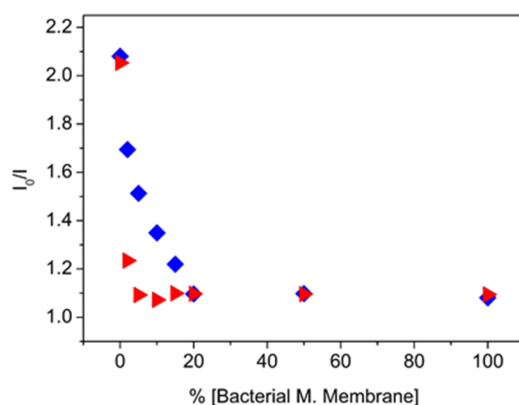


**Figure 5.8.** Quenching induced by AQS (at a constant concentration) in the fluorescence intensity of HTMA-PFP (blue diamonds) and HTMA-PFNT (red triangles), in samples containing mammalian LUVs coexisting with increasing concentrations of bacterial LUVs.

### 5.3.2. Selective Imaging of Bacteria over Mammalian Cells

Before studying the selectivity of CPEs for *E. coli* bacteria and mammalian cells, we explored the ability to label these cells separately. To this end, fluorescence microscopy studies were performed and results indicate that HTMA-PFP and HTMA-PFNT are capable of labelling *E. coli Top 10 F'* strain bacteria and HeLa cells, allowing their visualization in blue and red colors (Figure 6, Publication 8.4). Once confirmed this ability, we explored the possibility to visualize selectively the *E. coli* bacteria in a sample where coexist both populations of *E. coli* and human HeLa cells (Figure 5.9). Fluorescence images show that HTMA-PFP was capable of labelling both types of cells without, apparently, any preference for one over the other. Results obtained with the HTMA-PFNT were totally different: this CPE was only bound to the *E. coli* bacteria

without apparently labelling the human HeLa cells, thus evidencing its potential use for selective recognition and imaging of bacterial contamination.

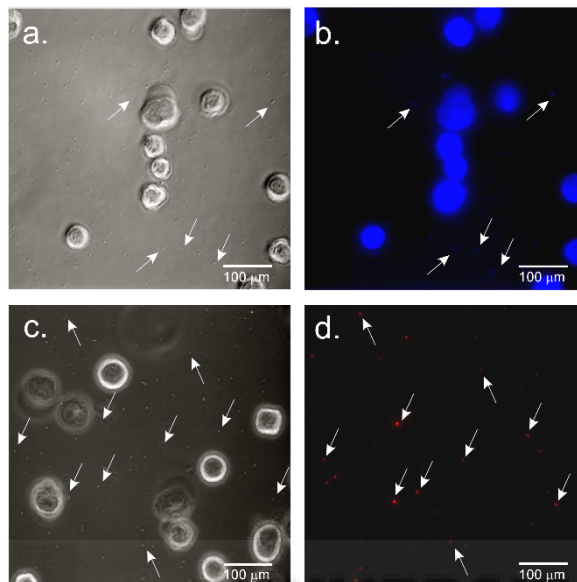


**Figure 5.9.** Microscopy images of human HeLa cells contaminated with bacteria *E. coli* after addition of HTMA-PFP in **a)** phase contrast and **b)** upon irradiation with UV-light. Microscopy images of human HeLa cells contaminated with bacteria *E. coli* after addition of HTMA-PFNT in **c)** phase contrast and **d)** upon irradiation with visible light.

#### 5.4. CPE-based Nanostructures: Characterization and Biotechnological Applications

*Find below a summary of results reported in Publications 8.3 and 8.5, together with their discussion.*

## 5. Overall Results & Discussion

### 5.4.1. Multifunctional Fluorescent Nanoparticles (NPs) as Bioimaging Tools and Drug Carriers

The previous results discussed in section 5.1 show that red-emitting HTMA-PFNT forms unstable aggregates in buffer due to its highly hydrophobic backbone, leading to detrimental emission quenching. In the following section, water solubilization and stabilization of HTMA-PFNT were improved through the formation of nanostructures by complexing the polyelectrolyte with two different biological systems: human serum albumin (HSA) and lipid vesicles. Both systems are macromolecular carriers capable of accommodating a wide variety of drugs and contain reactive functional groups (in the case of human serum albumin) or can be functionalized (in the case of liposomes) for targeting ligands [111,112]. Using both strategies, stable fluorescent nanostructures can be obtained which combine the properties of both constituents and can be potentially used as drug carriers and bioimaging probes. In *Publication 8.3*, we explored these possibilities.

#### 5.4.1.1. Protein-CPE Nanostructures

To improve the solubility and stability of HTMA-PFNT in buffer, we explored the possible formation of complexes between the polyelectrolyte and human serum albumin (HSA). Interaction was monitored from the changes observed in the fluorescence intensity of HTMA-PFNT in presence of increasing concentrations of HSA (Figure 5.10a). Association constant ( $K_A$ ) was calculated from these changes, obtaining a  $K_A = 2.2 \pm 0.2 \times 10^6 \text{ M}^{-1}$ , which indicates a strong affinity between HTMA-

PFNT and HSA. No alterations in the protein secondary structure and protein conformation were observed by using Circular Dichroism (CD) measurements (Figure 5.10b) and intrinsic fluorescence of the protein (Figure 4b of Publication 8.3).

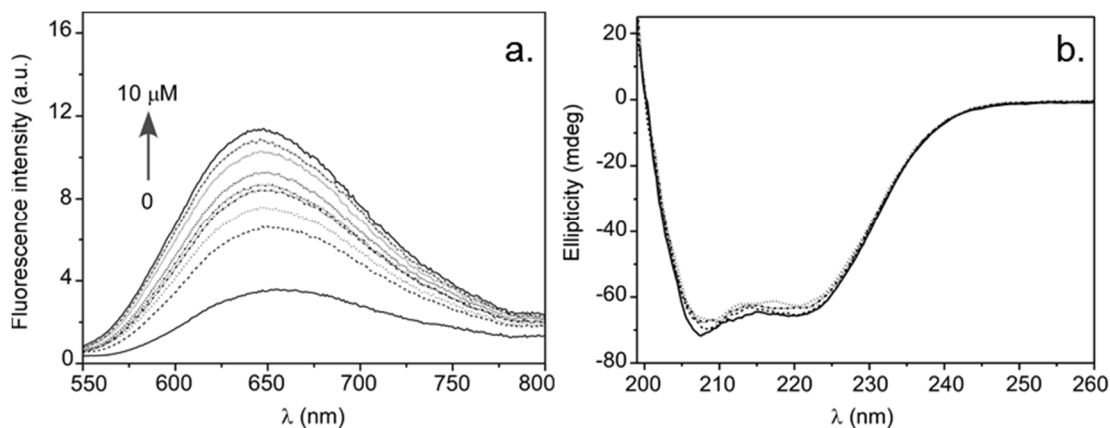
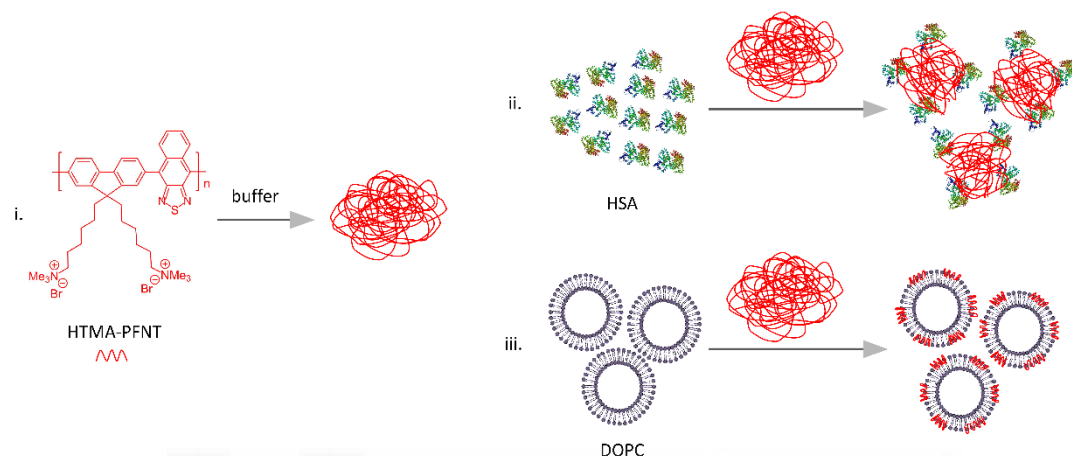


**Figure 5.10.** **a)** Fluorescence emission spectra of HTMA-PFNT in buffer with increasing concentration of HSA. **b)** Effect of HTMA-PFNT on the CD spectrum of HSA (6  $\mu$ M) in buffer. CPE concentrations were as follows: 0 (line), 6 (dash), 9 (dot), 12  $\mu$ M (dash dot).

DLS measurements were used to determine the size of these complexes. The fact that their size ( $\sim$  120 nm) was time-independent indicates that it does not correspond to a population of unstable polymeric aggregates formed in buffer, but rather it can be attributed to nanostructures composed of aggregates of polyelectrolyte coated with HSA molecules (Scheme 5.2). Probably, when the polyelectrolyte is added to the protein solution, it starts to self-assemble forming aggregates through the hydrophobic interactions of its backbone, exposing the positively charged side chains to the solvent. Simultaneously, the negatively charged HSA ( $pI=4.9$ ) interacts with these aggregates, through rapid electrostatic interaction. In addition a slower hydrophobic interaction occurs between the conjugated backbone of the polymers

## 5. Overall Results & Discussion

and the hydrophobic patches of HSA. This interaction induces conformational changes in polymer chains, disrupting backbone interactions, resulting in a blue-shift of the emission spectrum as well as an increase in fluorescence intensity.



**Scheme 5.2.** Schematic model, which shows the possible interaction between HTMA-PFNT aggregates **i)** in buffer, with **ii)** HSA and **iii)** lipid vesicles (DOPC).

Finally, we checked the ability to use these fluorescent nanoparticles as drug carriers (Table 2 of Publication 8.3). A fluorescent probe DPH, which is highly hydrophobic and non-fluorescent in water, was used as a model drug. Results showed that while DPH is non-fluorescent in the buffer containing only HTMA-PFNT, it fluoresces in the polyelectrolyte-HSA complexes. It indicates that the hydrophobic cavities of the protein are still accessible to nonpolar compounds, thus evidencing the ability of using these fluorescent nanostructures as carriers for hydrophobic drugs.

#### 5.4.1.2. Lipid Vesicle-CPE Nanoparticles

A second approach to stabilize the HTMA-PFNT in buffer was the use of liposomes. Fluorescent liposomal nanoparticles (NPs) were formed by the interaction of HTMA-PFNT with these lipid vesicles. The interaction was monitored from changes in the fluorescence intensity of the CPE (Figure 5.11a). According to DLS measurements, these nanoparticles have hydrodynamic diameter of ~ 110 nm. The ability of these fluorescent NPs to be used as carriers for hydrophobic and polar drugs was investigated by fluorescence spectroscopy. As for polymer-protein complexes, DPH was used as a model compound for hydrophobic drugs. Results indicate that the binding of HTMA-PFNT to the liposome is not affecting the insertion of the DPH in the lipid bilayer, confirming the potential use of these nanoparticles in hydrophobic drug delivery (Table 2 of Publication 8.3). Also, liposomes can be used to transport polar compounds in their inner aqueous phase. Fluorescence experiments carried out by using the polar fluorescent probe CF encapsulated in the aqueous cavity of the liposomal NPs, where its fluorescence is self-quenched, showed the ability of these nanoparticles to transport hydrophilic molecules (Figure 5.11b). Taking into account these interesting properties of fluorescent NPs, we decided to explore their stability as a function of storage time and temperature (Figure 7 of Publication 8.3). Results showed that fluorescent nanoparticles were highly stable in time and in a wide temperature range and showed high photostability. These properties suggested their potential use not only as drug carriers but also as bioimaging probes. To test this possibility, preliminary microscopy experiments were performed with the human keratinocyte cell line HaCaT. Results showed that NPs rapidly interacted with these

## 5. Overall Results & Discussion

cells, allowing their visualization under fluorescence microscopy (*Figure 8 of Publication 8.3*).

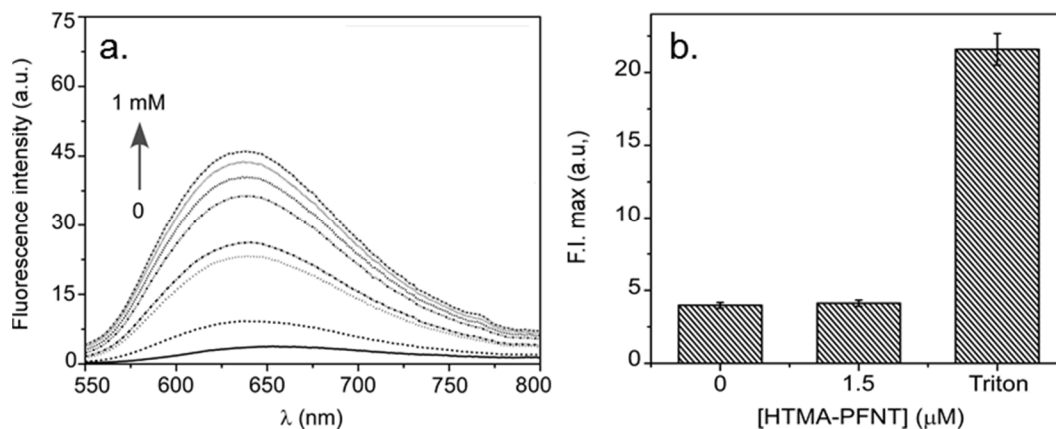


**Figure 5.11.** **a)** Fluorescence emission spectra of HTMA-PFNT in buffer with increasing concentration of lipid vesicles. **b)** Fluorescence intensity of CF encapsulated in lipid vesicles, in absence and in presence of HTMA-PFNT and after the addition of Triton (10%).

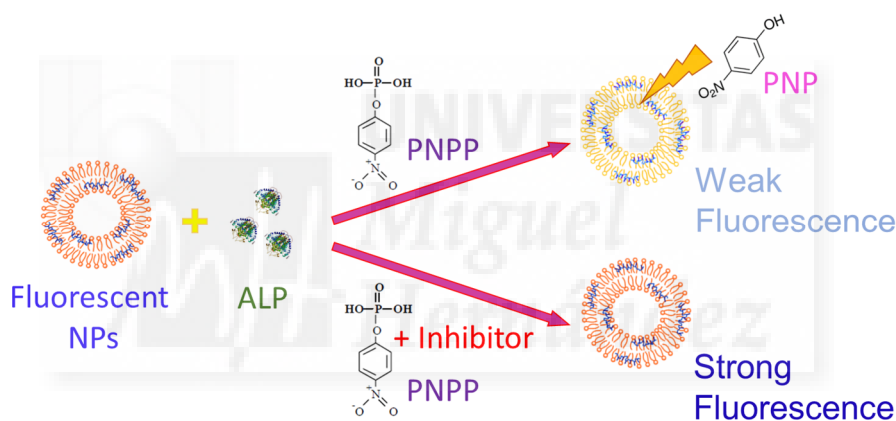
### 5.4.2. Fluorescent NPs in Biosensing

The ability of p-nitrophenol (PNP) to quench the fluorescence of HTMA-PFP was used in this work to develop a fluorescent biosensor for Alkaline Phosphate (ALP) [124]. Results of this study are reported in *Publication 8.5*. Firstly, we studied the stabilization of this CPE through its incorporation in lipid vesicles to obtain stable blue-emitting nanoparticles (NPs) (*Figure 1 of Publication 8.5*). Once the stability of the fluorescent NPs was confirmed by using fluorescence studies and DLS measurements, the ability to be quenched by PNP was explored as an essential requirement for biosensor construction (*Figure 2 of Publication 8.5*). Results indicate

that, although HTMA-PFP is incorporated into the vesicles, PNP is still capable of quench its fluorescence ( $K_{sv} = 5.08 \pm 0.07 \times 10^4 \text{ M}^{-1}$ ).

#### 5.4.2.1. Free ALP Biosensor

Once proved the quenching of the fluorescent NPs by PNP, we investigated their ability to detect ALP activity, taking into account that PNP is the final product of the hydrolysis of the substrate p-nitrophenyl phosphate (PNPP), catalysed by ALP (Scheme 5.3).



**Scheme 5.3.** Schematic model, which shows the working principle of the ALP biosensor.

To this end, increasing concentrations of PNPP were directly added to the NPs suspension, in presence of ALP. Results showed a decrease in fluorescence of NPs as the substrate concentration was increased, when the fluorescence spectra were recorded after 3 min of incubation. From this study, a value of  $K_{sv} = 4.94 \pm 0.28 \times 10^4 \text{ M}^{-1}$  was obtained, which suggests the adequate operation of the biosensor in solution

## 5. Overall Results & Discussion

(Figure 2 of Publication 8.5) and the possibility to detect ALP inhibitors. The mechanism of sensing is based on the fluorescence turn on/turn off (Scheme 5.3). The PNP produced after hydrolysis of PNPP quenches the fluorescence of NPs, leading to fluorescence turn-off, but in the presence of inhibitors, the fluorescence of the system turns on. The activity of ALP was then monitored in the presence of phosphate ion which is an inhibitor of the enzyme. Results showed that the quenching efficiency was decreased, when the inhibitor concentration was increased (Figure 4 of Publication 8.5). These studies indicate that this biosensor can be used for ALP inhibitor screening, as well as to determine the concentration of a specific inhibitor in a sample.

### 5.4.2.2. Immobilized ALP Biosensor

The practical application of the biosensor described above requires the preparation of different samples (fluorescent NPs, fresh solutions of the enzyme, etc.) each time that it is used, with the consequent economic burden. Therefore, in order to improve the performance of the biosensor, its components, ALP and NPs, were entrapped in the pores of a transparent matrix prepared by using the sol-gel process. This methodology offers many advantages such as easy handling, enhanced stability and reusability of the biosensor. Firstly, we immobilized each component separately and its properties were characterized. Results showed that, on one hand, the fluorescence properties of NPs were preserved after the immobilization, as well as the quenching of their fluorescence by PNP (Figure 6 of Publication 8.5). On the other hand, results confirmed that the activity of the enzyme was preserved, but the

kinetics was slower than in solution, probably due to the restricted diffusion of PNPP and PNP in the matrix (Figure 7 of Publication 8.5). In the light of these results, we immobilized fluorescent NPs and ALP in the same matrix to obtain the final biosensor device. The conditions of the biosensor operation were optimized in order to minimize the time of response and sensibility of the assay (Figure 8a of Publication 8.5). Finally, we explored the capacity of the biosensor to determine ion phosphate in aqueous samples. Results showed that biosensor could detect this inhibitor with a limit of detection (LOD) of 370  $\mu\text{M}$ , and that it could be reusable for, at least, seven assays (Figure 5.12).

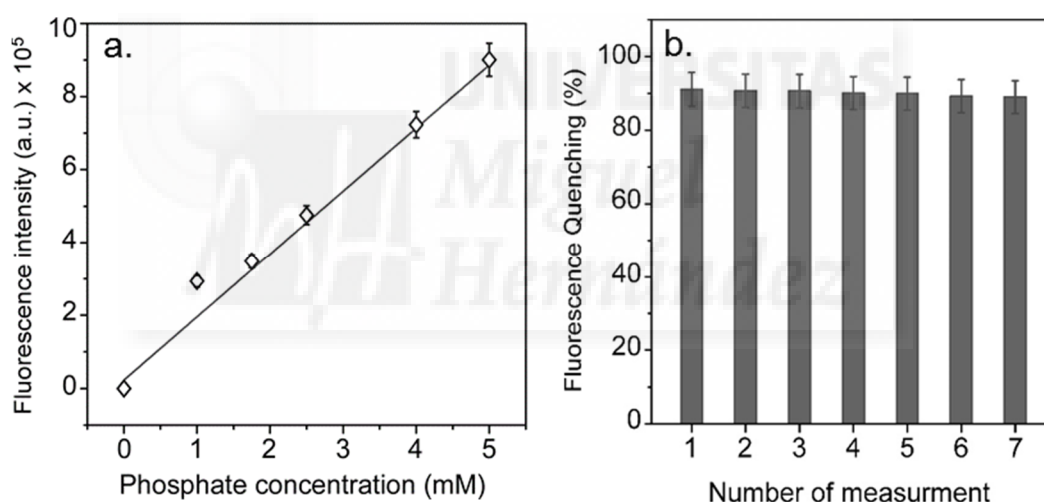


**Figure 5.12.** **a)** Fluorescence intensities recorded for immobilized ALP biosensor in the absence and presence of different concentrations of phosphate ions. **b)** Reusability study of the biosensor performed using the same monolith, for seven consecutive assays.



## 6. CONCLUSIONS/ CONCLUSIONES





- 1- The fluorescent conjugated polyelectrolytes HTMA-PFP and HTMA-PFNT, emitting in the blue and red spectral region respectively, show poor solubility in aqueous media, especially HTMA-PFNT, forming aggregates with low fluorescence efficiency, whose size increases as a function of time.
- 2- Interaction of HTMA-PFP and HTMA-PFNT with anionic model membranes induces the breaking of polymer aggregates, eliminating interchain quenching and increasing their fluorescence efficiency. CPEs rapidly incorporate into the lipid bilayer with high affinity, acting as fluorescent markers that allow the visualization of membrane structures and, in the case of HTMA-PFP, the detection of lipid phase transitions.
- 3- Both CPEs associate spontaneously with zwitterionic model membranes retaining their structural integrity without altering the spherical morphology of the lipid vesicles. These polyelectrolytes show lower affinity for zwitterionic membranes than for anionic ones, as well as a different final membrane location. While in the anionic membrane, these CPEs are embedded within the lipid bilayer, in the zwitterionic system they remain close to the surface, forming aggregates that are sensitive to the physical state of the lipid bilayer.
- 4- HTMA-PFP and HTMA-PFNT are able to label bacterial and mammalian model membranes but preferentially interact with bacterial model membranes due to their anionic character. In spite of their similar structure, HTMA-PFNT is much more selective towards bacterial model membrane than HTMA-PFP.

## 6. Conclusions

- 5- Both CPEs rapidly insert in the membrane of *E. coli* bacteria and HeLa cells allowing for their visualization in blue (with HTMA-PFP) and red (with HTMA-PFNT) colors.
- 6- In samples simultaneously containing *E. coli* bacteria and HeLa cells, HTMA-PFP is able to label both type of cells without preference, while HTMA-PFNT is apparently bound only to the *E. coli* bacteria. It indicates that HTMA-PFNT could be potentially used as a fast diagnosis tool for detecting bacterial contamination in samples.
- 7- HTMA-PFNT can be stabilized in buffer through complexation with two biological systems which are known to be used as nanocarriers: HSA and liposomal vesicles. Such interaction leads to the formation of red-emitting nanostructures that preserve the functionality of the biological systems and could be used as potential multifunctional platforms for therapeutic (drug delivery) and diagnostic (bioimaging) purposes.
- 8- The interaction of HTMA-PFP with liposomal vesicles leads to the formation of stable blue-emitting nanoparticles whose fluorescence is quenched by PNP. This property has been used to develop a fluorescent biosensor based on the inhibition of the enzyme ALP. The biosensor could be used for determination of ALP inhibitors such as phosphate ions.
- 9- Immobilization of the biosensor components (nanoparticles and ALP) in a sol-gel matrix facilitates its handling and enables its reutilization. The device has been successfully used in the determination of phosphate ions. This methodology can be extrapolated for the screening of inhibitors of other

enzymes, such as  $\alpha$ -glucosidase and  $\alpha$ -galactosidase, which catalyze reactions yielding PNP as final product.





- 1- Los polielectrolitos conjugados fluorescentes HTMA-PFP y HTMA-PFNT, que emiten en el azul y el rojo respectivamente, muestran una baja solubilidad en medio acuoso, especialmente HTMA-PFNT, formando agregados con baja eficiencia de fluorescencia cuyo tamaño aumenta en función del tiempo.
- 2- La interacción de HTMA-PFP y HTMA-PFNT con modelos de membrana aniónicos provoca la ruptura de los agregados, aumentando la intensidad de su fluorescencia al separarse las cadenas poliméricas. Estos CPEs se introducen rápidamente y con gran afinidad en el interior de la bicapa lipídica, actuando como sondas fluorescentes que permiten la visualización de las estructuras de membrana y, en el caso del HTMA-PFP, la detección de transiciones de fase lipídicas.
- 3- Ambos polielectrolitos se asocian espontáneamente con modelos de membrana zwitteriónicos, preservando su integridad estructural sin alterar la morfología esférica de las vesículas. La afinidad de los CPEs por estas vesículas lipídicas es menor que por vesículas aniónicas y, además, su localización final en la membrana es diferente. Así, en el sistema aniónico los polielectrolitos se disponen en el interior de la bicapa, mientras que en las membranas zwitteriónicas se sitúan cerca de la superficie, formando agregados cuya fluorescencia es sensible al estado físico de la membrana.
- 4- HTMA-PFP y HTMA-PFNT son capaces de marcar fluorescentemente modelos de membrana de células de mamífero y bacterianas, aunque interactúan preferentemente con los modelos bacterianos debido a su carácter aniónico.

## 6. Conclusiones

- A pesar de que poseen una estructura muy similar, el polielectrolito HTMA-PFNT es mucho más selectivo que el HTMA-PFP hacia el modelo bacteriano.
- 5- Ambos CPEs se insertan rápidamente en las membranas de bacterias *E. coli* y de células HeLa, permitiendo el marcaje y la visualización bajo el microscopio de fluorescencia de ambos sistemas en colores azul (con HTMA-PFP) o rojo (con HTMA-PFNT).
  - 6- En muestras donde coexisten bacterias *E. coli* y células HeLa, se ha observado que HTMA-PFP es capaz de marcar ambas células con la misma preferencia, mientras que HTMA-PFNT parece enlazarse únicamente a bacterias *E. coli*. Esto indica que HTMA-PFNT puede ser potencialmente utilizado como una rápida herramienta de diagnóstico de contaminación bacteriana.
  - 7- El polielectrolito HTMA-PFNT puede estabilizarse en medio acuoso a través de su interacción con sistemas biológicos utilizados como nanotransportadores, tales como la proteína HSA o vesículas liposomales. Dicha interacción da lugar a la formación de nanoestructuras que mantienen la funcionalidad del sistema biológico y que emiten en el rojo. Estas estructuras podrían ser utilizadas como plataformas multifuncionales para fines terapéuticos (transporte y liberación de fármacos) y de diagnóstico (bioimagen).
  - 8- La interacción de HTMA-PFP con vesículas liposomales da lugar a la formación de nanopartículas fluorescentes que son altamente estables en medio acuoso y cuya fluorescencia puede ser desactivada con PNP. Esta propiedad ha servido para poner a punto un biosensor fluorescente, que utiliza la enzima

ALP como elemento de reconocimiento y permite la detección de sus inhibidores, en particular del ion fosfato.

- 9- La inmovilización de los componentes del biosensor (nanopartículas y ALP) en una matriz sol-gel que facilita su manipulación y permite su reutilización. El dispositivo ha sido utilizado con éxito para determinar ion fosfato. Este mismo diseño puede ser extrapolado para la detección de inhibidores de otras enzimas, tales como la  $\alpha$ -glucosidasa y  $\alpha$ -galactosidasa, que catalizan reacciones cuyo producto final es el PNP.





## 7. REFERENCES





## References

1. Shirakawa, H.; Louis, E.J.; MacDiarmid, A.G.; Chiang, C.K.; Heeger, A.J. Synthesis of electrically conducting organic polymers: Halogen derivatives of polyacetylene, (CH)<sub>x</sub>. *Journal of the Chemical Society, Chemical Communications* **1977**, 578-580.
2. Heeger, A.J. Nobel lecture: Semiconducting and metallic polymers: The fourth generation of polymeric materials. *Rev Mod Phys* **2001**, *73*, 681-700.
3. Scott, J.C. History of Conductive Polymers. In *Nanostructured Conductive Polymers* 2010; pp. 1-17.
4. Friend, R.H.; Gymer, R.W.; Holmes, A.B.; Burroughes, J.H.; Marks, R.N.; Taliani, C.; Bradley, D.D.C.; Dos Santos, D.A.; Brédas, J.L.; Lögdlund, M.; Salaneck, W.R. Electroluminescence in conjugated polymers. *Nature* **1999**, *397*, 121-128.
5. Montilla, F.; Mateo, C.R.; Mallavia, R. Characterization of light-emitting conjugated polymers by electrochemical methods. In *Handbook of Light Emitting and Schottky Diode Research* 2009; pp. 99-132.
6. Burroughes, J.H.; Bradley, D.D.C.; Brown, A.R.; Marks, R.N.; Mackay, K.; Friend, R.H.; Burns, P.L.; Holmes, A.B. Light-emitting diodes based on conjugated polymers. *Nature* **1990**, *347*, 539-541.
7. Patil, A.O.; Heeger, A.J.; Wudl, F. Optical Properties of Conducting Polymers. *Chem Rev* **1988**, *88*, 183-200.
8. Skotheim, T.A.; Reynolds, J.R. *Handbook of Conducting Polymers* **2007**.
9. Gierschner, J.; Cornil, J.; Egelhaaf, H.J. Optical bandgaps of  $\pi$ -conjugated organic materials at the polymer limit: Experiment and theory. *Adv Mater* **2007**, *19*, 173-191.
10. Facchetti, A.  $\pi$ -Conjugated polymers for organic electronics and photovoltaic cell applications. *Chem Mater* **2011**, *23*, 733-758.
11. Thomas III, S.W.; Joly, G.D.; Swager, T.M. Chemical sensors based on amplifying fluorescent conjugated polymers. *Chem Rev* **2007**, *107*, 1339-1386.
12. Feng, F.; Liu, L.; Wang, S. Fluorescent conjugated polymer-based FRET technique for detection of DNA methylation of cancer cells. *Nat Protoc* **2010**, *5*, 1255-1264.
13. Gaylord, B.S.; Heeger, A.J.; Bazan, G.C. DNA detection using water-soluble conjugated polymers and peptide nucleic acid probes. *Proc Natl Acad Sci U S A* **2002**, *99*, 10954-10957.

## 7. References

14. Kraft, A.; Grimsdale, A.C.; Holmes, A.B. Electroluminescent Conjugated Polymers - Seeing Polymers in a New Light. *Angew Chem Int Ed* **1998**, *37*, 402-428.
15. Montali, A.; Smith, P.; Weder, C. Poly(p-phenylene ethynylene)-based light-emitting devices. *Synth Met* **1998**, *97*, 123-126.
16. Hide, F.; Díaz-García, M.A.; Schwartz, B.J.; Heeger, A.J. New Developments in the Photonic Applications of Conjugated Polymers. *Acc Chem Res* **1997**, *30*, 430-436.
17. Liu, Y.; Ogawa, K.; Schanze, K.S. Conjugated polyelectrolytes as fluorescent sensors. *J Photochem Photobiol C Photochem Rev* **2009**, *10*, 173-190.
18. Grimsdale, A.C.; Müllen, K. Polyphenylene-type emissive materials: Poly(para-phenylene)s, polyfluorenes, and ladder polymers. *Adv Polym Sci* **2006**, *199*, 1-82.
19. Bunz, U.H.F. Poly(aryleneethynylene)s: Syntheses, properties, structures, and applications. *Chem Rev* **2000**, *100*, 1605-1644.
20. Perepichka, I.F.; Perepichka, D.F.; Meng, H.; Wudl, F. Light-emitting polythiophenes. *Adv Mater* **2005**, *17*, 2281-2305.
21. MacDiarmid, A.G. "Synthetic metals": A novel role for organic polymers (Nobel lecture). *Angew Chem Int Ed* **2001**, *40*, 2581-2590.
22. Scherf, U.; List, E.J.W. Semiconducting polyfluorenes - Towards reliable structure-property relationships. *Adv Mater* **2002**, *14*, 477-487.
23. Duarte, A.; Pu, K.Y.; Liu, B.; Bazan, G.C. Recent advances in conjugated polyelectrolytes for emerging optoelectronic applications. *Chem Mater* **2011**, *23*, 501-515.
24. Van Den Boogaard, M.; Bonnet, G.; Van't Hof, P.; Wang, Y.; Brochon, C.; Van Hutten, P.; Lapp, A.; Hadziioannou, G. Synthesis of insulated single-chain semiconducting polymers based on polythiophene, polyfluorene, and  $\beta$ -cyclodextrin. *Chem Mater* **2004**, *16*, 4383-4385.
25. Burrows, H.D.; Tapia, M.J.; Fonseca, S.M.; Pradhan, S.; Scherf, U.; Silva, C.L.; Pais, A.A.C.C.; Valente, A.J.M.; Schilén, K.; Alfredsson, V.; Carnerup, A.M.; Tomšič, M.; Jamnik, A. Solubilization of poly{1,4-phenylene-[9,9-bis(4-phenoxy-butylsulfonate)] fluorene-2,7-diyl} in water by nonionic amphiphiles. *Langmuir* **2009**, *25*, 5545-5556.
26. Huang, F.; Wang, X.; Wang, D.; Yang, W.; Cao, Y. Synthesis and properties of a novel water-soluble anionic polyfluorenes for highly sensitive biosensors. *Polymer* **2005**, *46*, 12010-12015.

27. Mallavia, R.; Martinez-Peréz, D.; Chmelka, B.F.; Bazan, G.C. Blue fluorescent films based on poly-2,7-fluorene-phenylene derivatives. *Bol Soc Esp Ceram Vidr* **2004**, *43*, 327-330.
28. Liu, B.; Gaylord, B.S.; Wang, S.; Bazan, G.C. Effect of chromophore-charge distance on the energy transfer properties of water-soluble conjugated oligomers. *J Am Chem Soc* **2003**, *125*, 6705-6714.
29. Chen, Q.; Cui, Y.; Zhang, T.L.; Cao, J.; Han, B.G. Fluorescent conjugated polyfluorene with pendant lactopyranosyl ligands for studies of Ca<sup>2+</sup>-mediated carbohydrate-carbohydrate interaction. *Biomacromolecules* **2010**, *11*, 13-19.
30. Burrows, H.D.; Lobo, V.M.M.; Pina, J.; Ramos, M.L.; De Seixas Melo, J.; Valente, A.J.M.; Tapia, M.J.; Pradhan, S.; Scherf, U. Fluorescence enhancement of the water-soluble poly{1,4-phenylene-[9,9-bis-(4-phenoxybutylsulfonate)]fluorene-2,7-diyl} copolymer in n- dodecylpentaoxyethylene glycol ether micelles. *Macromolecules* **2004**, *37*, 7425-7427.
31. Jiang, H.; Taranekar, P.; Reynolds, J.R.; Schanze, K.S. Conjugated polyelectrolytes: Synthesis, photophysics, and applications. *Angew Chem Int Ed* **2009**, *48*, 4300-4316.
32. Burnell, T.; Cella, J.A.; Donahue, P.; Duggal, A.; Early, T.; Heller, C.M.; Liu, J.; Shiang, J.; Simon, D.; Slowinska, K.; Sze, M.; Williams, E. Synthesis and electrooptical properties of copolymers derived from phenol-functionalized telechelic oligofluorenes. *Macromolecules* **2005**, *38*, 10667-10677.
33. Wang, Z.Y.; Hay, A.S. Synthesis of poly(arylene ether)s based on 9,9-bis(3,5-diphenyl-4-hydroxyphenyl)fluorene. *J Polym Sci Part A* **1991**, *29*, 1045-1052.
34. Zhou, X.H.; Yan, J.C.; Pei, J. Exploiting an imidazole-functionalized polyfluorene derivative as a chemosensory material. *Macromolecules* **2004**, *37*, 7078-7080.
35. Zhou, G.; Qian, G.; Ma, L.; Cheng, Y.; Xie, Z.; Wang, L.; Jing, X.; Wang, F. Polyfluorenes with phosphonate groups in the side chains as chemosensors and electroluminescent materials. *Macromolecules* **2005**, *38*, 5416-5424.
36. Xue, C.; Donuru, V.R.R.; Liu, H. Facile, versatile prepolymerization and postpolymerization functionalization approaches for well-defined fluorescent conjugated fluorene-based glycopolymers. *Macromolecules* **2006**, *39*, 5747-5752.
37. Wang, L.; Li, H.; Cao, D. Conjugated polyelectrolytes: Synthesis and application in biomolecule detection. *Curr Org Chem* **2012**, *16*, 1468-1484.

## 7. References

38. Tapia, M.J.; Montserín, M.; Valente, A.J.M.; Burrows, H.D.; Mallavia, R. Binding of polynucleotides to conjugated polyelectrolytes and its applications in sensing. *Adv Colloid Interface Sci* **2010**, *158*, 94-107.
39. Feng, F.; Wang, H.; Han, L.; Wang, S. Fluorescent conjugated polyelectrolyte as an indicator for convenient detection of DNA methylation. *J Am Chem Soc* **2008**, *130*, 11338-11343.
40. Ambade, A.V.; Sandanaraj, B.S.; Klaikherd, A.; Thayumanavan, S. Mini Review: Fluorescent polyelectrolytes as protein sensors. *Polym Int* **2007**, *56*, 474-481.
41. Zhu, C.; Liu, L.; Yang, Q.; Lv, F.; Wang, S. Water-soluble conjugated polymers for imaging, diagnosis, and therapy. *Chem Rev* **2012**, *112*, 4687-4735.
42. Li, K.; Liu, B. Water-soluble conjugated polymers as the platform for protein sensors. *Polym Chem* **2010**, *1*, 252-259.
43. Liu, B.; Bazan, G.C. Homogeneous fluorescence-based DNA detection with water-soluble conjugated polymers. *Chem Mater* **2004**, *16*, 4467-4476.
44. Pinto, M.R.; Schanze, K.S. Conjugated polyelectrolytes: Synthesis and applications. *Synthesis* **2002**, 1293-1309.
45. Montserín, M.; Burrows, H.D.; Valente, A.J.M.; Lobo, V.M.M.; Mallavia, R.; Tapia, M.J.; García-Zubiri, I.X.; Di Paolo, R.E.; Maçanita, A.L. Modulating the emission intensity of poly-(9,9-bis(6'-N,N,N-trimethylammonium)hexyl)-fluorene phenylene bromide through interaction with sodium alkylsulfonate surfactants. *J Phys Chem B* **2007**, *111*, 13560-13569.
46. Guo, X.; Baumgarten, M.; Müllen, K. Designing  $\pi$ -conjugated polymers for organic electronics. *Prog Polym Sci* **2013**, *38*, 1832-1908.
47. Xie, L.; Yin, C.; Lai, W.; Fan, Q.; Huang, W. Polyfluorene-based semiconductors combined with various periodic table elements for organic electronics. *Progress in Polymer Science* **2012**, *37*, 1192-1264.
48. Wang, Y.; Liu, B. Cationic water-soluble polyfluorene homopolymers and copolymers: Synthesis, characterization and their applications in DNA sensing. *Curr Org Chem* **2011**, *15*, 446-464.
49. Qin, C.; Cheng, Y.; Wang, L.; Jing, X.; Wang, F. Phosphonate-functionalized polyfluorene as a highly water-soluble iron(III) chemosensor. *Macromolecules* **2008**, *41*, 7798-7804.

50. Qin, C.; Tong, H.; Wang, L. Water-soluble phosphate-functionalized polyfluorene as fluorescence biosensors toward cytochrome c. *Sci China Ser B Chem* **2009**, *52*, 833-839.
51. Dias, F.B.; King, S.; Monkman, A.P.; Perepichka, I.I.; Kryuchkov, M.A.; Perepichka, I.F.; Bryce, M.R. Dipolar stabilization of emissive singlet charge transfer excited states in polyfluorene copolymers. *J Phys Chem B* **2008**, *112*, 6557-6566.
52. Shi, H.; Sun, H.; Yang, H.; Liu, S.; Jenkins, G.; Feng, W.; Li, F.; Zhao, Q.; Liu, B.; Huang, W. Cationic polyfluorenes with phosphorescent iridium(III) complexes for time-resolved luminescent biosensing and fluorescence lifetime imaging. *Adv Funct Mater* **2013**, *23*, 3268-3276.
53. Liu, B.; Bazan, G.C. Synthesis of cationic conjugated polymers for use in label-free DNA microarrays. *Nat Protoc* **2006**, *1*, 1698-1702.
54. Pina, J.; Seixas De Melo, J.S.; Eckert, A.; Scherf, U. Unusual photophysical properties of conjugated, alternating indigo-fluorene copolymers. *J Mater Chem A* **2015**, *3*, 6373-6382.
55. Chen, L.; Tong, H.; Xie, Z.; Wang, L.; Jing, X.; Wang, F. Red electroluminescent polyfluorenes containing highly efficient 2,1,3-benzoselenadiazole- and 2,1,3-naphthothiadiazole-based red dopants in the side chain. *J Mater Chem* **2011**, *21*, 15773-15779.
56. Huang, F.; Hou, L.; Wu, H.; Wang, X.; Shen, H.; Cao, W.; Yang, W.; Cao, Y. High-efficiency, environment-friendly electroluminescent polymers with stable high work function metal as a cathode: Green- and yellow-emitting conjugated polyfluorene polyelectrolytes and their neutral precursors. *J Am Chem Soc* **2004**, *126*, 9845-9853.
57. Li, K.; Liu, B. Polymer-encapsulated organic nanoparticles for fluorescence and photoacoustic imaging. *Chem Soc Rev* **2014**, *43*, 6570-6597.
58. Kim, S.; Lim, C.K.; Na, J.; Lee, Y.D.; Kim, K.; Choi, K.; Leary, J.F.; Kwon, I.C. Conjugated polymer nanoparticles for biomedical in vivo imaging. *Chem Commun* **2010**, *46*, 1617-1619.
59. Huang, J.; Liu, Y.; Qian, C.G.; Sun, M.J.; Shen, Q.D. Multicolour fluorescence cell imaging based on conjugated polymers. *RSC Adv* **2014**, *4*, 3924-3928.
60. Liu, J.; Feng, G.; Ding, D.; Liu, B. Bright far-red/near-infrared fluorescent conjugated polymer nanoparticles for targeted imaging of HER2-positive cancer cells. *Polym Chem* **2013**, *4*, 4326-4334.

## 7. References

61. Weissleder, R.; Ntziachristos, V. Shedding light onto live molecular targets. *Nat Med* **2003**, *9*, 123-128.
62. Leevy, W.M.; Gammon, S.T.; Johnson, J.R.; Lampkins, A.J.; Jiang, H.; Marquez, M.; Piwnica-Worms, D.; Suckow, M.A.; Smith, B.D. Noninvasive optical imaging of *Staphylococcus aureus* bacterial infection in living mice using a bis-dipicolylamine-zinc(II) affinity group conjugated to a near-infrared fluorophore. *Bioconjugate Chem* **2008**, *19*, 686-692.
63. Zhou, J.; Butchosa, N.; Jayawardena, H.S.N.; Park, J.; Zhou, Q.; Yan, M.; Ramström, O. Synthesis of Multifunctional Cellulose Nanocrystals for Lectin Recognition and Bacterial Imaging. *Biomacromolecules* **2015**, *16*, 1426-1432.
64. Chen, F.; Gerion, D. Fluorescent CdSe/ZnS nanocrystal-peptide conjugates for long-term, nontoxic imaging and nuclear targeting in living cells. *Nano Lett* **2004**, *4*, 1827-1832.
65. Yang, W.; Pan, C.Y.; Liu, X.Q.; Wang, J. Multiple functional hyperbranched poly(amido amine) nanoparticles: Synthesis and application in cell imaging. *Biomacromolecules* **2011**, *12*, 1523-1531.
66. Tsoi, K.M.; Dai, Q.; Alman, B.A.; Chan, W.C.W. Are quantum dots toxic? Exploring the discrepancy between cell culture and animal studies. *Acc Chem Res* **2013**, *46*, 662-671.
67. Oh, E.; Liu, R.; Nel, A.; Gemill, K.B.; Bilal, M.; Cohen, Y.; Medintz, I.L. Meta-analysis of cellular toxicity for cadmium-containing quantum dots. *Nat Nanotechnol* **2016**, *11*, 479-486.
68. Nandi, S.; Ritenberg, M.; Jelinek, R. Bacterial detection with amphiphilic carbon dots. *Analyst* **2015**, *140*, 4232-4237.
69. Wang, Y.; Hu, A. Carbon quantum dots: Synthesis, properties and applications. *J Mater Chem C* **2014**, *2*, 6921-6939.
70. Lai, I.P.J.; Harroun, S.G.; Chen, S.Y.; Unnikrishnan, B.; Li, Y.J.; Huang, C.C. Solid-state synthesis of self-functional carbon quantum dots for detection of bacteria and tumor cells. *Sens Actuators, B Chem* **2016**, *228*, 465-470.
71. Nilsson, K.P.R.; Hammarström, P. Luminescent conjugated polymers: Illuminating the dark matters of biology and pathology. *Adv Mater* **2008**, *20*, 2639-2645.
72. An, L.; Wang, S. Conjugated polyelectrolytes as new platforms for drug screening. *Chem Asian J* **2009**, *4*, 1196-1206.

73. Pu, K.Y.; Liu, B. Fluorescent conjugated polyelectrolytes for bioimaging. *Adv Funct Mater* **2011**, *21*, 3408-3423.
74. Smith, B.A.; Smith, B.D. Biomarkers and molecular probes for cell death imaging and targeted therapeutics. *Bioconjugate Chem* **2012**, *23*, 1989-2006.
75. Zhu, C.; Yang, Q.; Liu, L.; Wang, S. A potent fluorescent probe for the detection of cell apoptosis. *Chem Commun* **2011**, *47*, 5524-5526.
76. Ding, L.; Chi, E.Y.; Schanze, K.S.; Lopez, G.P.; Whitten, D.G. Insight into the mechanism of antimicrobial conjugated polyelectrolytes: Lipid headgroup charge and membrane fluidity effects. *Langmuir* **2010**, *26*, 5544-5550.
77. Ding, L.; Chi, E.Y.; Chemburu, S.; Ji, E.; Schanze, K.S.; Lopez, G.P.; Whitten, D.G. Insight into the mechanism of antimicrobial poly(phenylene ethynylene) polyelectrolytes: Interactions with phosphatidylglycerol lipid membranes. *Langmuir* **2009**, *25*, 13742-13751.
78. Wang, Y.; Jones, E.M.; Tang, Y.; Ji, E.; Lopez, G.P.; Chi, E.Y.; Schanze, K.S.; Whitten, D.G. Effect of polymer chain length on membrane perturbation activity of cationic phenylene ethynylene oligomers and polymers. *Langmuir* **2011**, *27*, 10770-10775.
79. Ngo, A.T.; Cosa, G. Assembly of zwitterionic phospholipid/conjugated polyelectrolyte complexes: Structure and photophysical properties. *Langmuir* **2010**, *26*, 6746-6754.
80. Ngo, A.T.; Karam, P.; Cosa, G. Conjugated polyelectrolyte-lipid interactions: Opportunities in biosensing. *Pure Appl Chem* **2011**, *83*, 43-55.
81. Feng, F.; He, F.; An, L.; Wang, S.; Li, Y.; Zhu, D. Fluorescent conjugated polyelectrolytes for biomacromolecule detection. *Adv Mater* **2008**, *20*, 2959-2964.
82. Kang, M.; Nag, O.K.; Nayak, R.R.; Hwang, S.; Suh, H.; Woo, H.Y. Signal amplification by changing counterions in conjugated Polyelectrolyte-Based FRET DNA detection. *Macromolecules* **2009**, *42*, 2708-2714.
83. Kim, I.B.; Bunz, U.H.F. Modulating the sensory response of a conjugated polymer by proteins: An agglutination assay for mercury ions in water. *J Am Chem Soc* **2006**, *128*, 2818-2819.
84. Kim, I.B.; Dunkhorst, A.; Gilbert, J.; Bunz, U.H.F. Sensing of lead ions by a carboxylate-substituted PPE: Multivalency effects. *Macromolecules* **2005**, *38*, 4560-4562.

## 7. References

85. DiCesare, N.; Pinto, M.R.; Schanze, K.S.; Lakowicz, J.R. Saccharide detection based on the amplified fluorescence quenching of a water-soluble poly(phenylene ethynylene) by a boronic acid functionalized benzyl viologen derivative. *Langmuir* **2002**, *18*, 7785-7787.
86. He, F.; Tang, Y.; Yu, M.; Wang, S.; Li, Y.; Zhu, D. Fluorescence-amplifying detection of hydrogen peroxide with cationic conjugated polymers, and its application to glucose sensing. *Adv Funct Mater* **2006**, *16*, 91-94.
87. Li, C.; Numata, M.; Takeuchi, M.; Shinkai, S. A sensitive colorimetric and fluorescent probe based on a polythiophene derivative for the detection of ATP. *Angew Chem Int Ed* **2005**, *44*, 6371-6374.
88. Ho, H.A.; Leclerc, M. Optical Sensors Based on Hybrid Aptamer/Conjugated Polymer Complexes. *J Am Chem Soc* **2004**, *126*, 1384-1387.
89. Fan, C.; Plaxco, K.W.; Heeger, A.J. High-efficiency fluorescence quenching of conjugated polymers by proteins. *J Am Chem Soc* **2002**, *124*, 5642-5643.
90. Cheng, F.; Zhang, G.W.; Lu, X.M.; Huang, Y.Q.; Chen, Y.; Zhou, Y.; Fan, Q.L.; Huang, W. A cationic water-soluble poly(p-phenylenevinylene) derivative: Highly sensitive biosensor for iron-sulfur protein detection. *Macromol Rapid Commun* **2006**, *27*, 799-803.
91. Miranda, O.R.; You, C.C.; Phillips, R.; Kim, I.B.; Ghosh, P.S.; Bunz, U.H.F.; Rotello, V.M. Array-based sensing of proteins using conjugated polymers. *J Am Chem Soc* **2007**, *129*, 9856-9857.
92. Wosnick, J.H.; Mello, C.M.; Swager, T.M. Synthesis and application of poly(phenylene ethynylene)s for bioconjugation: A conjugated polymer-based fluorogenic probe for proteases. *J Am Chem Soc* **2005**, *127*, 3400-3405.
93. Liu, Y.; Schanze, K.S. Conjugated polyelectrolyte based real-time fluorescence assay for adenylate kinase. *Anal Chem* **2009**, *81*, 231-239.
94. Rininsland, F.; Xia, W.; Wittenburg, S.; Shi, X.; Stankewicz, C.; Achyuthan, K.; McBranch, D.; Whitten, D. Metal ion-mediated polymer superquenching for highly sensitive detection of kinase and phosphatase activities. *Proc Natl Acad Sci U S A* **2004**, *101*, 15295-15300.
95. Pinto, M.R.; Schanze, K.S. Amplified fluorescence sensing of protease activity with conjugated polyelectrolytes. *Proc Natl Acad Sci U S A* **2004**, *101*, 7505-7510.
96. Lakowicz, J.R. *Principles of Fluorescence Spectroscopy* **1999**.

97. Banerjee, P.; Pramanik, S.; Sarkar, A.; Bhattacharya, S.C. Deciphering the fluorescence resonance energy transfer signature of 3-pyrazolyl 2-pyrazoline in transport proteinous environment. *J Phys Chem B* **2009**, *113*, 11429-11436.
98. Zhou, Q.; Swager, T.M. Methodology for enhancing the sensitivity of fluorescent chemosensors: Energy migration in conjugated polymers. *J Am Chem Soc* **1995**, *117*, 7017-7018.
99. Zhou, Q.; Swager, T.M. Fluorescent chemosensors based on energy migration in conjugated polymers: The molecular wire approach to increased sensitivity. *J Am Chem Soc* **1995**, *117*, 12593-12602.
100. Evans, R.C.; Douglas, P. Optical sensors and probes. In *Applied Photochemistry* 2013; pp. 403-434.
101. Cumming, C.J.; Aker, C.; Fisher, M.; Fox, M.; La Grone, M.J.; Reust, D.; Rockley, M.G.; Swager, T.M.; Towers, E.; Williams, V. Using novel fluorescent polymers as sensory materials for above-ground sensing of chemical signature compounds emanating from buried landmines. *IEEE Trans Geosci Remote Sens* **2001**, *39*, 1119-1128.
102. Toal, S.J.; Trogler, W.C. Polymer sensors for nitroaromatic explosives detection. *J Mater Chem* **2006**, *16*, 2871-2883.
103. Chen, L.; McBranch, D.W.; Wang, H.-.; Helgeson, R.; Wudl, F.; Whitten, D.G. Highly sensitive biological and chemical sensors based on reversible fluorescence quenching in a conjugated polymer. *Proc Natl Acad Sci U S A* **1999**, *96*, 12287-12292.
104. Senthilkumar, T.; Asha, S.K. Selective and Sensitive Sensing of Free Bilirubin in Human Serum Using Water-Soluble Polyfluorene as Fluorescent Probe. *Macromolecules* **2015**, *48*, 3449-3461.
105. Tapia, M.J.; Monteserín, M.; Costoyas, A.; Burrows, H.D.; Marques, A.T.; Pais, A.A.C.C.; Valente, A.J.M.; Mallavia, R.; Scherf, U.; Pinazo, A.; Pérez, L.; Morán, M.C. Effects of commercial non-ionic alkyl oxyethylene and ionic biocompatible arginine-based surfactants on the photophysical behaviour of several poly(fluorene-1,4-phenylene)s. *J Mol Liq* **2010**, *156*, 18-27.
106. Tapia, M.J.; Burrows, H.D.; Knaapila, M.; Monkman, A.P.; Arroyo, A.; Pradhan, S.; Scherf, U.; Pinazo, A.; Pérez, L.; Morán, C. Interaction between the conjugated polyelectrolyte poly{[1,4-phenylene[9,9- bis(4-phenoxybutylsulfonate)]fluorene-2,7-diyl} copolymer and the lecithin mimic 1-O-(L-Arginyl)-2,3-O-dilauroyl-sn-glycerol in aqueous solution. *Langmuir* **2006**, *22*, 10170-10174.

## 7. References

107. Al Attar, H.A.; Monkman, A.P. Effect of surfactant on water-soluble conjugated polymer used in biosensor. *J Phys Chem B* **2007**, *111*, 12418-12426.
108. Evans, R.C.; Macedo, A.G.; Pradhan, S.; Scherf, U.; Carlos, L.D.; Burrows, H.D. Fluorene based conjugated polyelectrolyte/silica nanocomposites: Charge-mediated phase aggregation at the organic-inorganic interface. *Adv Mater* **2010**, *22*, 3032-3037.
109. Cacialli, F.; Wilson, J.S.; Michels, J.J.; Daniel, C.; Silva, C.; Friend, R.H.; Severin, N.; Samori, P.; Rabe, J.P.; O'connell, M.J.; Taylor, P.N.; Anderson, H.L. Cyclodextrin-threaded conjugated polyrotaxanes as insulated molecular wires with reduced interstrand interactions. *Nat Mater* **2002**, *1*, 160-164.
110. Farcas, A.; Jarroux, N.; Harabagiu, V.; Guégan, P. Synthesis and characterization of a poly[2,7-(9,9-dioctylfluorene-alt-2,7-fluorene/ $\beta$ -CD)] main chain polyrotaxane. *Eur Polym J* **2009**, *45*, 795-803.
111. Allen, T.M.; Cullis, P.R. Liposomal drug delivery systems: From concept to clinical applications. *Adv Drug Deliv Rev* **2013**, *65*, 36-48.
112. Yang, F.; Zhang, Y.; Liang, H. Interactive association of drugs binding to human serum albumin. *Int J Mol Sci* **2014**, *15*, 3580-3595.
113. Lu, X.; Jiang, R.; Yang, M.; Fan, Q.; Hu, W.; Zhang, L.; Yang, Z.; Deng, W.; Shen, Q.; Huang, Y.; Liu, X.; Huang, W. Monodispersed grafted conjugated polyelectrolyte-stabilized magnetic nanoparticles as multifunctional platform for cellular imaging and drug delivery. *J Mater Chem B* **2014**, *2*, 376-386.
114. Infante, M.R.; Pinazo, A.; Seguer, J. Non-conventional surfactants from amino acids and glycolipids: Structure, preparation and properties. *Colloids Surf A* **1997**, *123-124*, 49-70.
115. Pérez, L.; Infante, M.R.; Angelet, M.; Clapés, P.; Pinazo, A. Glycerolipid arginine-based surfactants: Synthesis and surface active properties. *Prog Colloid Polym Sci* **2004**, *123*, 210-216.
116. Bangham, A.D. Physical Structure and Behavior of Lipids and Lipid Enzymes. *Adv Lipid Res* **1963**, *64*, 65-104.
117. Bangham, A.D.; Horne, R.W. Negative staining of phospholipids and their structural modification by surface-active agents as observed in the electron microscope. *J Mol Biol* **1964**, *8*, 660-668.
118. Immordino, M.L.; Dosio, F.; Cattel, L. Stealth liposomes: Review of the basic science, rationale, and clinical applications, existing and potential. *Int J Nanomed* **2006**, *1*, 297-315.

119. Liu, B.; Wang, S.; Bazan, G.C.; Mikhailovsky, A. Shape-Adaptable Water-Soluble Conjugated Polymers. *J Am Chem Soc* **2003**, *125*, 13306-13307.
120. Liu, B.; Bazan, G.C. Optimization of the molecular orbital energies of conjugated polymers for optical amplification of fluorescent sensors. *J Am Chem Soc* **2006**, *128*, 1188-1196.
121. Martínez-Tome, M.J.; Esquembre, R.; Mallavia, R.; Mateo, C.R. Formation of complexes between the conjugated polyelectrolyte poly{[9,9-bis(6'-n,n,ntrimethylammonium) hexyl]fluorene-phenylene} bromide (HTMA-PFP) and human serum albumin. *Biomacromolecules* **2010**, *11*, 1494-1501.
122. Pinto, S.M.; Burrows, H.D.; Pereira, M.M.; Fonseca, S.M.; Dias, F.B.; Mallavia, R.; Tapia, M.J. Singlet-singlet energy transfer in self-assembled systems of the cationic poly{9,9-bis[6-N,N,N-trimethylammoniumhexyl]fluorene-co-1,4-phenylene} with oppositely charged porphyrins. *J Phys Chem B* **2009**, *113*, 16093-16100.
123. Monteserín, M.; Burrows, H.D.; Valente, A.J.M.; Mallavia, R.; Di Paolo, R.E.; Maçanita, A.L.; Tapia, M.J. Interaction between poly(9, 9-bis(6'-N, N, N-trimethylammonium)hexyl) ]fluorene phenylene) bromide and DNA as seen by spectroscopy, viscosity, and conductivity: Effect of molecular weights and DNA secondary structure. *J Phys Chem B* **2009**, *113*, 1294-1302.
124. Cao, A.; Tang, Y.; Liu, Y. Novel fluorescent biosensor for a-glucosidase inhibitor screening based on cationic conjugated polymers. *ACS Appl Mater Interfaces* **2012**, *4*, 3773-3778.
125. Naeem, A.; Khan, I.M.; Ahmad, A. Spectral investigations of multiple charge transfer complex of p-nitrophenol as an electron acceptor with donor p-dimethylaminobenzaldehyde. *Russ J Phys Chem A* **2011**, *85*, 1840-1843.
126. Molina, R.; Gómez-Ruiz, S.; Montilla, F.; Salinas-Castillo, A.; Fernández-Arroyo, S.; Del Mar Ramos, M.; Micol, V.; Mallavia, R. Progress in the synthesis of poly(2,7-fluorene-alt-1,4-phenylene), PFP, via suzuki coupling. *Macromolecules* **2009**, *42*, 5471-5477.
127. Tena, A.; Vazquez-Guilló, R.; Marcos-Fernández, A.; Hernández, A.; Mallavia, R. Polymeric films based on blends of 6FDA-6FpDA polyimide plus several copolyfluorenes for CO<sub>2</sub> separation. *RSC Adv* **2015**, *5*, 41497-41505.
128. Singer, S.J.; Nicolson, G.L. The fluid mosaic model of the structure of cell membranes. *Science* **1972**, *175*, 720-731.
129. Nicolson, G.L. The Fluid - Mosaic Model of Membrane Structure: Still relevant to understanding the structure, function and dynamics of biological membranes

## 7. References

- after more than 40 years. *Biochim Biophys Acta Biomembr* **2014**, 1838, 1451-1466.
130. Goñi, F.M. The basic structure and dynamics of cell membranes: An update of the Singer-Nicolson model. *Biochim Biophys Acta Biomembr* **2014**, 1838, 1467-1476.
131. Van Meer, G.; Voelker, D.R.; Feigenson, G.W. Membrane lipids: Where they are and how they behave. *Nat Rev Mol Cell Biol* **2008**, 9, 112-124.
132. Bangham, A.D. Lipid bilayers and biomembranes. *Annu Rev Biochem* **1972**, 41, 753-776.
133. Bangham, A.D. Membrane models with phospholipids. *Prog Biophys Mol Biol* **1968**, 18.
134. Bangham, A.D. Model membranes. *Chem Phys Lipids* **1972**, 8, 386-392.
135. Cullis, P.R.; Fenske, D.B.; Hope, M.J. Chapter 1 Physical properties and functional roles of lipids in membranes. *New Compr Biochem* **1996**, 31, 1-33.
136. Dowhan, W.; Bogdanov, M. Chapter 1 Functional roles of lipids in membranes. *New Compr Biochem* **2002**, 36, 1-35.
137. Lee, A.G. Lipid phase transitions and phase diagrams I. Lipid phase transitions. *Biochim Biophys Acta Rev Biomembr* **1977**, 472, 237-281.
138. Lewis, R.N.A.H.; McElhaney, R.N. Membrane lipid phase transitions and phase organization studied by Fourier transform infrared spectroscopy. *Biochimica et Biophysica Acta (BBA) - Biomembranes* **2013**, 1828, 2347-2358.
139. Bangham, A.D.; Standish, M.M.; Watkins, J.C. Diffusion of univalent ions across the lamellae of swollen phospholipids. *J Mol Biol* **1965**, 13, 238-252.
140. Szoka Jr., F.; Papahadjopoulos, D. Comparative properties and methods of preparation of lipid vesicles (liposomes). *Annu Rev Biophys Bioeng* **1980**, 9, 467-508.
141. Olson, F.; Hunt, C.A.; Szoka, F.C.; Vail, W.J.; Papahadjopoulos, D. Preparation of liposomes of defined size distribution by extrusion through polycarbonate membranes. *Biochim Biophys Acta Biomembr* **1979**, 557, 9-23.
142. Mayer, L.D.; Hope, M.J.; Cullis, P.R. Vesicles of variable sizes produced by a rapid extrusion procedure. *Biochim Biophys Acta Biomembr* **1986**, 858, 161-168.

143. Batzri, S.; Korn, E.D. Single bilayer liposomes prepared without sonication. *Biochim Biophys Acta Biomembr* **1973**, *298*, 1015-1019.
144. Papahadjopoulos, D.; Portis, A.; Pangborn, W. Calcium-induced lipid phase transitions and membrane fusion. *Ann New York Acad Sci* **1978**, *308*, 50-66.
145. Morales-Pennington, N.F.; Wu, J.; Farkas, E.R.; Goh, S.L.; Konyakhina, T.M.; Zheng, J.Y.; Webb, W.W.; Feigenson, G.W. GUV preparation and imaging: Minimizing artifacts. *Biochim Biophys Acta Biomembr* **2010**, *1798*, 1324-1332.
146. Coutinho, A.; Prieto, M. Self-association of the polyene antibiotic nystatin in dipalmitoylphosphatidylcholine vesicles: A time-resolved fluorescence study. *Biophys J* **1995**, *69*, 2541-2557.
147. Dwight, S.J.; Gaylord, B.S.; Hong, J.W.; Bazan, G.C. Perturbation of fluorescence by nonspecific interactions between anionic poly(phenylenevinylene)s and proteins: Implications for biosensors. *J Am Chem Soc* **2004**, *126*, 16850-16859.
148. Mateo, C.R.; Prieto, M.; Micol, V.; Shapiro, S.; Villalain, J. A fluorescence study of the interaction and location of (+)-totarol, a diterpenoid bioactive molecule, in model membranes. *Biochim Biophys Acta Biomembr* **2000**, *1509*, 167-175.
149. Chemburu, S.; Ji, E.; Casana, Y.; Wu, Y.; Buranda, T.; Schanze, K.S.; Lopez, G.P.; Whitten, D.G. Conjugated polyelectrolyte supported bead based assays for phospholipase A2 activity. *J Phys Chem B* **2008**, *112*, 14492-14499.
150. Chen, J.; Dong, W.-.; Möhwald, H.; Krastev, R. Amplified fluorescence quenching of self-assembled polyelectrolyte - Dye nanoparticles in aqueous solution. *Chem Mater* **2008**, *20*, 1664-1666.
151. Van Renswoude, J.; Hoekstra, D. Cell-induced leakage of liposome contents. *Biochemistry* **1981**, *20*, 540-546.
152. Bandyopadhyay, P.; Bandyopadhyay, P.; Regan, S.L. An ion conductor that recognizes osmotically-stressed phospholipid bilayers. *J Am Chem Soc* **2002**, *124*, 11254-11255.
153. Brinker, C.J.; Scherer, G.W. Sol-Gel Science: The Physics and Chemistry of Sol-Gel Processing. In *Sol-Gel Science: The Physics and Chemistry of Sol-Gel Processing* 2013; pp. 1-908.
154. Avnir, D.; Lev, O.; Livage, J. Recent bio-applications of sol-gel materials. *J Mater Chem* **2006**, *16*, 1013-1030.

## 7. References

155. Ellerby, L.M.; Nishida, C.R.; Nishida, F.; Yamanaka, S.A.; Dunn, B.; Valentine, J.S.; Zink, J.I. Encapsulation of proteins in transparent porous silicate glasses prepared by the sol-gel method. *Science* **1992**, *255*, 1113-1115.
156. Jin, W.; Brennan, J.D. Properties and applications of proteins encapsulated within sol-gel derived materials. *Anal Chim Acta* **2002**, *461*, 1-36.
157. Pastor, I.; Prieto, M.; Mateo, C.R. Effect of sol-gel confinement on the structural dynamics of the enzyme bovine Cu,Zn superoxide dismutase. *J Phys Chem B* **2008**, *112*, 15021-15028.
158. Ferrer, M.L.; Del Monte, F.; Levy, D. A novel and simple alcohol-free sol-gel route for encapsulation of labile proteins. *Chem Mater* **2002**, *14*, 3619-3621.



## 8. ANNEXES





## Publication 8.1





**Use of the Conjugated Polyelectrolyte Poly{[9,9-bis(6'-N,N,N-trimethylammonium)hexyl]fluorene-phenylene} Bromide (HTMA-PFP) as a Fluorescent Membrane Marker**

**Zehra Kahveci, Maria José Martínez-Tomé, Ricardo Mallavia and C. Reyes Mateo**

Instituto de Biología Molecular y Celular, Universidad Miguel Hernández, 03202

Elche, Spain

**Biomacromolecules, 2013, 14(6), 1990–1998**

**DOI: 10.1021/bm400348n**

Impact Factor: **5.583**

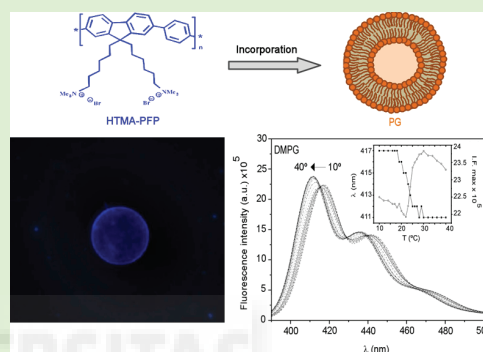


# Use of the Conjugated Polyelectrolyte Poly{[9,9-bis(6'-*N,N,N*-trimethylammonium)hexyl]fluorene-phenylene} Bromide (HTMA-PFP) as a Fluorescent Membrane Marker

Zehra Kahveci, Maria José Martínez-Tomé, Ricardo Mallavia, and C. Reyes Mateo\*

Instituto de Biología Molecular y Celular, Universidad Miguel Hernández, 03202 Elche, Spain

**ABSTRACT:** The present work explores the potential use of the conjugated cationic polyfluorene {[9,9-bis(6'-*N,N,N*-trimethylammonium)hexyl]fluorene-phenylene} bromide (HTMA-PFP) as a fluorescent membrane marker. To this end, the interaction of the polyelectrolyte with anionic model membranes has been investigated using different biophysical approaches. High affinity interaction was confirmed through alterations in the fluorescence spectrum of HTMA-PFP and by Förster resonance energy transfer (FRET) analysis. Quenching data indicate that once HTMA-PFP interacts with the membrane, it penetrates in the hydrophobic core embedded in the lipid bilayer where it presents high fluorescence quantum yield and photostability. Leakage experiments and dynamic light scattering (DLS) measurements show that the integrity of the lipid vesicles is maintained after polymer incorporation since no vesicle fusion or decomposition into small fragments is detectable. This conclusion is supported by fluorescence microscopy images, which confirm that polyelectrolyte interacts with the vesicle, labeling the lipid membrane without altering its morphology. Further experiments performed as a function of temperature indicate that the polymer is accommodated in the membrane without inducing significant loss of lipid cooperativity and without altering the packing of lipids within the bilayer. Finally, results show that polyelectrolyte fluorescence is sensitive to the large structural changes taking place in the lipid bilayer at the lipid phase transition. All these results confirm the ability of HTMA-PFP to visualize membrane structures and to monitor membrane processes.



## INTRODUCTION

The design and development of new fluorescent markers having high sensitivity to image cellular and physiological processes is of great interest in clinical diagnosis, identification of cancer cells, detection of pathogenic bacterial cells, immunofluorescent techniques, catalytic pathway monitoring, drug delivery monitoring through membrane or cytoplasm, and so on.<sup>1</sup> These materials should be highly fluorescent, water-soluble, photostable, and easy for bioconjugation, having good biocompatibility, maximum spatial resolution, and minimal perturbation to biological systems.<sup>2</sup> Most of the existing fluorescent materials designed to this end (generally, small fluorophores, fluorescent proteins, and semiconductor quantum dots) exhibit interesting properties, but also important disadvantages. For example, small fluorescent molecules and fluorescent proteins often suffer from photobleaching, and the much more stable inorganic quantum dots, generally including heavy metals such as Cd and Se, are not free from potential cytotoxicity because of the possible metals leaching from the nanoparticles.<sup>3,4</sup> Therefore, new fluorescent materials with improved properties (nontoxicity, stability, and high sensitivity) are being developed for overcoming these limitations.<sup>5,6</sup> Among them, conjugated polyelectrolytes (CPEs) seem to be interesting candidates because their unique properties. These materials are polymers with delocalized  $\pi$ -electron systems,

which show strong absorption and high efficiencies in both photoluminescence and electroluminescence,<sup>7,8</sup> containing ionic side groups to facilitate their water solubilization. In general, CPEs have high photostability and low cytotoxicity and can undergo spontaneous self-assembly through reversible, electrostatic, and/or hydrophobic interactions with some other species, generally of opposite charge, resulting in supramolecular structures with interesting optical and material properties.<sup>9</sup> In addition, these materials have easily amenable side chains for bioconjugation with various recognition elements.<sup>2,10</sup> Given these properties, CPEs have received great attention in biomedical applications, especially for developing biosensing schemes and sensing devices for biomolecules<sup>11–14</sup> and more recently have been employed as novel fluorescent probes for bioimaging.<sup>3,6,15–21</sup>

Many drugs, small molecules, nanoparticles, or fluorescent dyes used in cellular imaging first interact with cells through their membrane. Interactions, at a molecular level, of an extracellular particle with the plasma membrane need to be understood to evaluate its potential activity. In this regard, the use of model lipid membrane systems that imitate the

Received: March 7, 2013

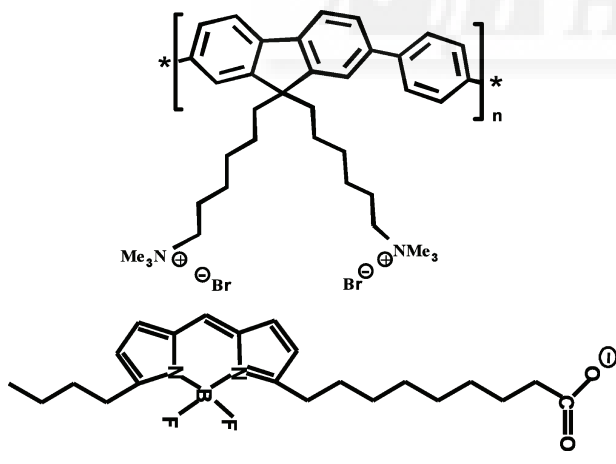
Revised: April 30, 2013

Published: May 6, 2013

complexity of natural cell membranes are useful to study the interaction of such compounds in a controlled manner, for predicting their interactions with real cell membranes as well as in the development of biotechnological applications. When CPEs are directly added to cells for imaging analyses, they initially interact with their plasma membrane; therefore, a detailed knowing of how these polyelectrolytes insert into the membrane at a molecular level should be helpful to understand their activity, improving and expanding their applications. To date, very few works have been carried out with this end in view. The Whitten group studied the interaction of a series of antimicrobial CPEs with different model membranes to gain insight into the mechanism of their biocidal activity.<sup>22–24</sup> Recently, Ngo and Cosa characterized the interaction of lipid vesicles with a negatively charged CPE in order to obtain well characterized lipid/polymer complexes, which could have applications as liposome-based sensing systems.<sup>11,25</sup> Given the objective of these works, the polymer concentration used in most of the experiments was relatively high. However, the use of CPEs as probes for bioimaging and detection of membrane processes requires minimal perturbation of the sample being studied, and consequently, low polymer concentrations.

In the present work, we have investigated the interaction of small concentrations of CPEs with model lipid membranes in order to evaluate the potential use of these polyelectrolytes as fluorescent membrane markers. To this end we have selected the CPE poly{[9,9-bis(6'-*N,N,N*-trimethylammonium)hexyl]-fluorene-phenylene} bromide (HTMA-PFP) and unilamellar vesicles composed of phosphatidylglycerol lipids (PGs) having different composition. HTMA-PFP is a water-soluble cationic poly(fluorene) (Scheme 1), being the backbone and alkyl side

**Scheme 1.** HTMA-PFP (Top) and BODIPY 500/510 C<sub>4</sub>C<sub>9</sub> (Bottom) Chemical Structures



chain hydrophobic moieties, while the cationic charged quaternary amines control electrostatic interactions.<sup>26,27</sup> Due to these cationic groups, HTMA-PFP has been reported to show high affinity by anionic biomolecules as DNA and human serum albumin (HSA)<sup>28,29</sup> and, therefore, it would have high affinity by anionic cell membranes.

## EXPERIMENTAL SECTION

**Materials.** The synthetic phospholipids 1,2-dioleoyl-*sn*-glycero-3-phospho-*rac*-(1-glycerol) sodium salt (DOPG) and 1,2-dimyristoyl-*sn*-glycero-3-phospho-*rac*-(1-glycerol) sodium salt (DMPG), were from

Sigma-Aldrich and used as received. The cationic CPE HTMA-PFP ( $M = 8340$  g/mol, repeat unit molecular weight, 694.71 g/mol;  $n' = 12$  based on polyfluorene calibration) was obtained and characterized in our laboratory as previously described.<sup>30,31</sup> In brief, a low-molecular-weight batch of the neutral polymer, poly[9,9-bis(6'-bromohexyl)-fluorene-phenylene], was synthesized by Suzuki coupling reaction with Pd(II) as catalyst and treated with gas-phase trimethylamine to obtain the corresponding cationic polyelectrolyte. Stock solutions of HTMA-PFP ( $3.65 \times 10^{-4}$  M, in repeat units) were prepared in DMSO and stored at  $-20$  °C before use. The fluorescent probe 5-butyl-4,4-difluoro-4-bora-3a,4a-diaza-*s*-indacene-3-nonanoic acid (BODIPY 500/510 C<sub>4</sub>C<sub>9</sub>) was from Molecular Probes (Eugene, OR). Stock solutions (1 mM) of this probe were prepared in ethanol and stored at  $-20$  °C before use. The fluorescent probe 5(6)-carboxyfluorescein (CF) and the quencher 9,10-anthraquinone-2,6-disulfonic acid (AQS) were obtained from Sigma-Aldrich and dissolved in ethanol (1.25 M) and water (5 mM), respectively, just before use. All other compounds were of analytical or spectroscopic reagent grade. Sodium phosphate buffer (50 mM, 0.1 M NaCl, pH 7.3) was prepared with water that was twice distilled in an all-glass apparatus and deionized using Milli-Q equipment (Millipore, Madrid).

**LUVs Formation.** Chloroform/methanol solutions containing 3 mg of total phospholipid (DOPG or DMPG) were dried first by evaporation under dry nitrogen gas stream and subsequently under vacuum for 3 h. Multilamellar vesicles (MLVs) were formed by resuspending the dried phospholipids in the buffer to a final concentration, which was 0.5 mM in most of cases. The vesicle suspension was then heated at a temperature above the phospholipid phase transition and vortexed several times. Large unilamellar vesicles (LUVs) were prepared from these MLVs by pressure extrusion through 0.1  $\mu$ m polycarbonate filters (Nucleopore, Cambridge, MA). For energy transfer experiments and anisotropy measurements, the probe BODIPY C<sub>4</sub>C<sub>9</sub> was initially added to the chloroform/methanol solutions containing DMPG, and LUVs were subsequently prepared as described below.

**Preparation of Giant Unilamellar Vesicles (GUVs).** GUVs were prepared with the gentle hydration method instead of the mostly used electroformation method because the presence of charged lipids is a limitation to the electroformation of vesicles.<sup>32</sup> Briefly, DOPG was dissolved in chloroform at 5 mM final concentration. Ten microliter of the solution was dropped on a microscope slide, which was previously washed with alcohol and dried. This sample was left to dry at the room temperature for few seconds and subsequently under vacuum for 2 h. Afterward, the lipid film was hydrated with 15  $\mu$ L of 50 mM phosphate buffer, 100 mM NaCl at pH 7.3 in a humid chamber for overnight. To observe the liposomes at the fluorescence microscopy, 400  $\mu$ L of buffer was added and left for 2 h to continue the hydration.

**Preparation of HTMA-PFP/Lipid Samples.** Aliquots of HTMA-PFP in DMSO were externally added to the lipid vesicle suspension, well above the phospholipid phase transition, to ensure that the membrane is in the fluid phase. In all cases, the proportion of DMSO in the aqueous sample was always lower than 1% (v/v). In most samples, the final concentration of HTMA-PFP was 1.5  $\mu$ M, in terms of repeat units.

**Absorption and Fluorescence Spectra.** Absorption measurements were carried out at room temperature using a Shimadzu spectrophotometer (UV-1603, Tokyo, Japan). Fluorescence spectra and fluorescence intensity measurements were performed in a PTI-QuantaMaster spectrofluorometer interfaced with a Peltier cell. The experimental samples were placed in 10  $\times$  10 mm path length quartz cuvettes. Excitation wavelength at 380 nm for HTMA-PFP was utilized. Background intensities were always checked and subtracted from the sample when it was necessary.

**Steady-State Fluorescence Anisotropy Measurements.** Steady-state anisotropy  $\langle r \rangle$ , defined by eq 1

$$\langle r \rangle = \frac{(I_{VV} - GI_{VH})}{(I_{VV} + 2GI_{VH})} \quad (1)$$

was obtained using Glan-Thompson polarizers by measuring the vertical and horizontal components of the fluorescence emission with excitation vertical and horizontal to the emission axis. The  $G$  factor ( $G = I_{HV}/I_{HH}$ ) corrects for the transmissivity bias introduced by the detection system. Measurements were carried out for samples containing DMPG labeled with BODIPY 500/510  $C_4$ ,  $C_9$ , at a 1:1000 molar ratio (probe:lipid) as a function of temperature. Lipid samples were excited at 480 nm, and the polarized emission was detected at 518 nm in the absence and presence of the HTMA-PFP. Background intensities due to the lipid vesicles in the absence of BODIPY were always taken into account.

**Fluorescence Microscopy Measurements.** Fluorescence microscopy images were recorded using a Nikon Eclipse TE2000-U inverted microscope equipped with a Nikon Digital Sight DS-1QM/H and Nikon Digital Camera DXM1200. UV excitation ( $340 \text{ nm} \leq \lambda_{\text{ex}} \leq 380 \text{ nm}$ ) and blue emission ( $435 \text{ nm} \leq \lambda_{\text{em}} \leq 485 \text{ nm}$ ) was filtered using a DAPI filter cube. We used a homemade stain-steel chamber where the over glass surface deposits approximately 500  $\mu\text{L}$  of preparation. Data acquisition was monitored successively by manual format and data processing with NIS-Elements AR 2.30 software.

**Energy Transfer Experiments.** For energy transfer experiments, the BODIPY 500/510  $C_4$ ,  $C_9$  was used as an acceptor of the HTMA-PFP excitation. The critical radius of transfer,  $R_0$ , was calculated from eq 2:<sup>14</sup>

$$R_0^6 = \frac{9000(\ln 10)\kappa^2\Phi_D J}{128\pi^5 n^4 N_{\text{AV}}} \quad (2)$$

where  $\Phi_D$  is the donor quantum yield in the absence of acceptor,  $n$  is the index of refraction of the medium,  $N_{\text{AV}}$  is Avogadro's number,  $\kappa^2$  is the orientation factor, and  $J$  corresponds to the degree of overlap between the donor emission spectrum and the acceptor absorption spectrum (overlap integral). This integral is given by eq 3:

$$J = \int_0^\infty f_D(\lambda)\epsilon_A(\lambda)\lambda^4 d\lambda \quad (3)$$

where  $\epsilon_A$  is the molar extinction coefficient of the acceptor, and  $f_D(\lambda)$  is the fluorescence spectrum of the donor normalized on the wavelength scale.

In order to determine the energy transfer efficiencies ( $E$ ), four types of spectra were recorded upon excitation at 380 nm: the spectrum of LUVs, the spectrum of LUVs doped with HTMA-PFP, the spectrum of LUVs doped with BODIPY 500/510  $C_4$ ,  $C_9$  and the spectrum of LUVs doped with HTMA-PFP and BODIPY  $C_4$ ,  $C_9$ . The first two spectra were used to correct the third and fourth spectrum, respectively, for the LUVs fluorescence and for acceptor fluorescence in the absence of the donor. The corrected spectra were used to compute the Förster resonance energy transfer (FRET) efficiency by eq 4:

$$E = 1 - I^{\text{DA}}/I^{\text{D}} \quad (4)$$

where  $I^{\text{DA}}$  and  $I^{\text{D}}$  are the fluorescence intensities in the presence and absence of acceptor, respectively.

**Quenching Experiments.** Fluorescence emission of HTMA-PFP was studied in the absence and presence of different concentration of AQS. Stern–Volmer analysis was applied to the fluorescence quenching data, according to eq 5:

$$\frac{I_0}{I} = 1 + K_{\text{SV}}[Q] \quad (5)$$

where  $I_0$  and  $I$  stand for the steady-state fluorescence intensities in the absence and in presence of quencher, respectively, and  $[Q]$  is the quencher concentration. The significance of  $K_{\text{SV}}$  depends on the nature of the quenching process: it may represent the association constant for complex formation or the rate of dynamic quenching ( $K_{\text{SV}} = k_q\tau_0$ ), where  $k_q$  is the bimolecular rate constant of the quenching process, and  $\tau_0$  is the lifetime of the biomolecule. For dynamic quenching (diffusion-controlled quenching),  $k_q$  may be as high as  $10^{10} \text{ M}^{-1} \text{ s}^{-1}$ . If  $k_q$  is greater than this value, it usually indicates static

quenching via a complexation between the fluorophore and the quencher.

**Measurements of Vesicle Leakage Induced by Polymers.** LUVs of DOPG were prepared with CF trapped in the aqueous interior at a concentration of 40 mM, in a buffer containing 50 mM phosphate and 0.1 M NaCl. The nonencapsulated CF was removed by a gel filtration column packed with Sephadex G-75 (Pharmacia, Uppsala, SW, EU) eluted with buffer containing 50 mM phosphate, 0.1 M NaCl. Self-quenching is expected at the CF packed within the vesicles. Membrane rupture (leakage) of intraliposomal CF was assayed by treating the probe-loaded vesicles with the appropriate amounts of HTMA-PFP. The total rupture of the vesicles and release of CF was performed with Triton X-100 10%.

**Dynamic Light Scattering Measurements (DLS).** The size of the polymer aggregates in buffer as well as that of the LUVs in the absence and presence of HTMA-PFP were explored by DLS techniques, using a Malvern Zetasizer Nano-ZS instrument, equipped with a monochromatic coherent 4mW Helium Neon laser ( $\lambda = 633 \text{ nm}$ ) as light source, with a  $173^\circ$  scattering angle of lecture for size measurements. The buffer previously filtered with a cellulose acetate membrane filter with a 200 nm pore size was measured at  $20^\circ \text{C}$ , before and after the addition of the polymer. The LUVs of DMPG were also explored in the absence and presence of the polymer below and above the lipid transition temperature. All measurements were performed in disposable cuvettes. Measurements were performed in triplicate.

**Calorimetry.** Differential scanning calorimetry (DSC) experiments were performed in a high-resolution Microcal MC-2 differential scanning microcalorimeter under a constant external pressure of 30 psi in order to avoid bubble formation. The excess heat capacity functions were analyzed using Origin 7.0 (Microcal Software). Differences in the heat capacity between the sample and the reference cell, which contained only buffer, were obtained by raising the temperature  $1^\circ \text{C}/\text{min}$  over the range from 15 to  $36^\circ \text{C}$  for the samples of DMPG in the absence and presence of HTMA-PFP. A series of three consecutive scans of the same sample were performed to ensure scan-to-scan reproducibility and reversibility.

## RESULTS AND DISCUSSION

**HTMA-PFP in Buffer.** The interaction of HTMA-PFP with surfactants and biomolecules other than phospholipids has been previously investigated in order to explore the potential application of this kind of polyfluorenes as sensors.<sup>33–36</sup> In those works, experiments were essentially performed in water, not buffer solution, because their goal was to characterize the interactions between the macromolecules in the absence of other substances which could interfere. However, it is known that changes in pH during the experimental measurements can give nonreliable results. For this reason, and to better simulate physiological conditions, all assays in the present work were performed in phosphate buffer, 0.1 M NaCl (pH 7.3). Consequently, before studying the interaction between HTMA-PFP and lipid membranes, we explored the behavior of the polyelectrolyte in the buffer solution, comparing the results with those found in water and good solvents. Previous works have reported that when HTMA-PFP is dissolved in water, it self-assembles into aggregates as the rest of CPEs.<sup>29,36</sup> This aggregation is dominated by interchain hydrophobic interactions, which lead to lower emission intensities and red-shift of the absorption and emission spectra, when comparing with those recorded in good solvents, due to an increase in the interchain energy transport mechanism. Figure 1 shows the normalized excitation and emission spectra of HTMA-PFP (1.5  $\mu\text{M}$  in terms of repeat units) in buffer as compared to those obtained in water and in a solvent mixture with a 60:40 (v/v) 2-propanol:water ratio (absorption spectra were very similar to

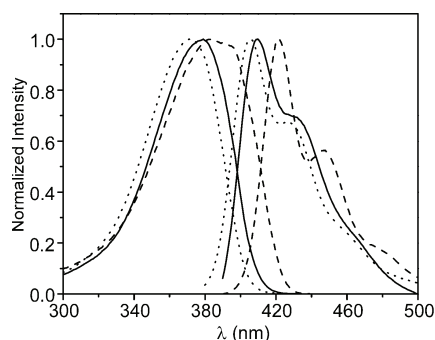


**Figure 1.** Normalized fluorescence excitation (left) and emission (right) spectra of HTMA-PFP in water (solid), phosphate buffer (dash), and 60:40 (v/v) 2-propanol:water (dot).

those of excitation, and thus they are not shown). Solvent mixtures have been proposed to be good solvents of this kind of polyelectrolyte since they allow for solvation of both components (polar and hydrophobic) of the polymer structure.<sup>37</sup> As was expected, spectra recorded in water were slightly shifted to the red with respect to those recorded in the solvent mixture, suggesting the existence of aggregates. An additional red shift of the spectra, followed by a broadness of the excitation band and a higher resolution in the vibrational structure of the emission spectrum, was observed in the buffer solution. These effects were accompanied by a slight decrease in the absorbance and a significant drop of the fluorescence quantum yield (down to  $0.16 \pm 0.03$  as compared to  $0.52 \pm 0.03$  measured in water<sup>37</sup>), as well by an increase in Rayleigh scattering of the sample (data not shown). Such effects could be explained by the existence of nonspecific electrostatic interactions between HTMA-PFP and anionic species contained in the buffer solution to yield neutral complexes which, upon charge neutralization, exhibit lower solubility, giving place to the formation of larger aggregates. To better characterize these aggregates, DLS experiments were carried out at room temperature. This technique yields information on the size distribution of macromolecules in solution in the submicrometer range. Results showed that once HTMA-PFP is added to the buffer, aggregates are rapidly formed, having hydrodynamic radius of around 110 nm (Table 1). The average size of

**Table 1. Hydrodynamic Radii, Determined by DLS Measurements, for Different Samples: HTMA-PFP in Buffer and LUVs of DMPG before and after Polymer Addition**

sample	temperature	<i>r</i> (nm)
buffer	20 °C	110 ± 40
DMPG	10 °C	56.2 ± 3.5
DMPG + HTMA-PFP	10 °C	59.2 ± 2.4
DMPG	40 °C	67.0 ± 1.5
DMPG + HTMA-PFP	40 °C	66.5 ± 0.9

aggregates largely increased through time, acquiring diameters larger than 400 nm after three hours of preparation, and consequently reducing their fluorescence intensity (it decreased for more than 60% in 1 h). Further characterization was performed by quenching experiments using the anionic electron acceptor AQS.<sup>38,39</sup> Aliquots of increasing concentration of quencher were added to a buffer solution containing HTMA-PFP (1.5 μM), and the results were compared to those obtained in water. A Stern–Volmer plot demonstrated the

highly efficient “superquenching” characteristic of this kind of polymer (Figure 2).<sup>40</sup> For water, the plot was linear in the

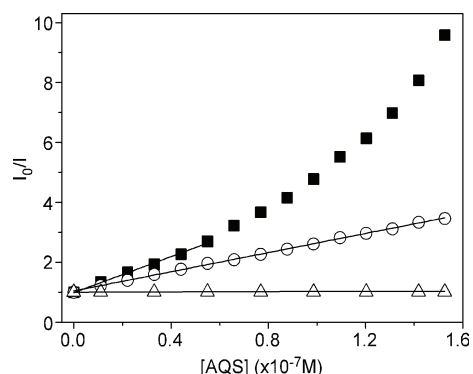


**Figure 2.** Stern–Volmer plots for quenching of HTMA-PFP (1.5 μM) by AQS in water (black squares), phosphate buffer (circles), and LUVs of DMPG (triangles).

concentration range of 0 to  $5.5 \times 10^{-8}$  M, with  $K_{SV} = 3.2 \times 10^7$  M<sup>-1</sup>, while for buffer the plot was linear within the used concentration range, with a  $K_{SV}$  value being about 50% lower than in water. When these values were used to calculate the bimolecular rate constant of the quenching process  $k_q$ , assuming  $\tau = 520$  ps,<sup>41</sup> values of  $3.08 \times 10^{16}$  M<sup>-1</sup> s<sup>-1</sup> and  $1.54 \times 10^{16}$  M<sup>-1</sup> s<sup>-1</sup> were found for water and buffer, respectively. These high values indicate, as expected, the formation of static quenching complexes via attractive electrostatic interactions between AQS and HTMA-PFP. Higher concentrations of AQS (0.5 μM) induced total quenching of the fluorescence intensity of HTMA-PFP in water, while in buffer the fluorescence signal was not completely inhibited even at 5 μM of quencher. This result is consistent with a situation in which a small fraction of polymer chains is not exposed to the solvent, probably formed by those chains being located in the core of the aggregates.

**HTMA-PFP in DMPG.** To explore the ability of HTMA-PFP to interact with lipid vesicles, different samples containing LUVs of DMPG in buffer with final lipid concentrations ranging from 0 to 1 mM were prepared, and the same concentration of HTMA-PFP (1.5 μM, in terms of repeat units) was added to all of the samples at 40 °C to ensure that the lipid bilayer was in fluid phase (DMPG presents its gel/fluid phase thermal transition around 24 °C). Note that lipid vesicles were never added to a solution previously containing HTMA-PFP in buffer, since the order of addition could affect the final result,<sup>25</sup> taking into account the high tendency of the polymer to form aggregates in buffer. Figure 3 shows the emission spectra recorded for the different samples. An enhancement of the fluorescence intensity as well as a blue-shift in the spectrum was observed up to a lipid concentration of about 0.5 mM. Higher concentrations of lipid did not modify the fluorescence spectrum. This result suggests that when HTMA-PFP is added to a vesicle suspension, it interacts with the lipid bilayer and that, as consequence of this interaction, the polymer chains become more extended than in buffer and the probability of polymer–polymer interaction (aggregation) is reduced, increasing the fluorescence quantum yield by approximately a factor of 4.2. A similar effect was observed when a cationic PPE-based CPE was added to anionic liposomes.<sup>22,23</sup> It is possible to estimate the affinity of the

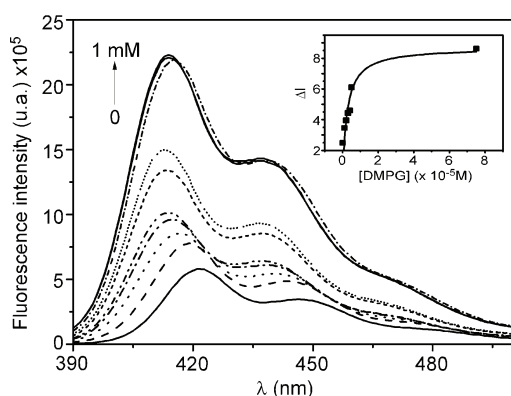


**Figure 3.** Emission spectra recorded for HTMA-PFP ( $1.5 \mu\text{M}$ ) at different DMPG concentrations 0, 0.001, 0.002, 0.003, 0.004, 0.005, 0.05, 0.1, 0.5, 1 mM in phosphate buffer. Inset: Fluorescence intensity differences at different DMPG concentrations.

polymer for the lipid membrane fitting the fluorescence intensities measured at low lipid concentrations to the following equation (see inset in Figure 3):

$$\Delta I = \frac{\Delta I_{\max}[L]}{1/(K_p\gamma) + [L]}$$

where  $K_p$  is the phospholipid/water partition coefficient of the polymer,  $\Delta I$  ( $\Delta I = I - I_0$ ) stands for the difference between the fluorescence intensity of the HTMA-PFP measured in the presence ( $I$ ) and in the absence ( $I_0$ ) of the phospholipid vesicles,  $\Delta I_{\max} = I_{\infty} - I_0$  is the maximum value of this difference once the limiting value is reached ( $I_{\infty}$ ) upon increasing the phospholipid concentration  $[L]$ , and  $\gamma$  is the molar volume of the phospholipid (for DMPG in the fluid phase, the value of  $\gamma$  is  $0.7 \text{ M}^{-1}$ <sup>42,43</sup>).

From a two-parameter ( $\Delta I_{\max}$  and  $K_p$ ) fitting procedure, a  $K_p$  value of  $(2.9 \pm 1.3) \times 10^5$  was obtained, which indicates a very high affinity of the polymer for the lipid bilayer, probably due to the electrostatic interaction between the quaternary amine

groups of HTMA-PFP and the negative charge of the lipid head groups.

The above experiments indicate that for lipid concentrations around 0.5 mM, all the polymer chains are interacting with lipids, and no aggregate remains in the buffer. This result is supported by DLS experiments of DMPG LUVs, which were performed at 40 °C (fluid phase) and 10 °C (gel phase), at the same lipid concentration. In the absence of polyelectrolyte, only a single distribution was observed centered at  $67.0 \pm 1.5 \text{ nm}$  for the lipid in the fluid phase and at  $56.2 \pm 3.5$  for the lipid in gel phase, which are compatible with the expected liposome radius (Table 1). When HTMA-PFP  $1.5 \mu\text{M}$  was added to this lipid suspension, a similar distribution was recorded centered at  $66.5 \pm 1.5 \text{ nm}$  (40 °C) and  $59.2 \pm 2.4$  (10 °C), and no additional population was detected. These results confirm that polymer aggregates are not found in the buffer, and therefore all the polymer chains are interacting with liposomes, and suggest that the integrity of the lipid vesicles is retained after HTMA-PFP interaction since no vesicle fusion or decomposition into small fragments is detectable.

To gain more insight into this interaction, we took advantage of the fact that fluorene-based polymers, such as HTMA-PFP, are particularly attractive as energy donors in FRET because of their high fluorescent quantum yields and blue emission, which allow efficient transfer to acceptors emitting over the whole visible spectrum.<sup>41</sup> Usually, donor and acceptor must be in close proximity for an efficient FRET to occur, and the efficiency of the process is dependent on the donor–acceptor distance.<sup>44</sup> Consequently, if an acceptor chromophore is embedded into the membrane, FRET from HTMA-PFP will occur only if the polymer inserts into the liposomes (on the surface or entrapped in the bilayer). BODIPY fatty acids are currently used as fluorescent probes for microscopy and spectroscopy experiments because they fluoresce in the visible with high excitation and emission spectra similar to those of the widely used xanthenes (fluorescein, rhodamine, etc.), but unlike these dyes, the BODIPY group carries no net charge and therefore the fluorophore is embedded in the membrane at a depth related to its point of attachment to the acyl chain.<sup>45</sup> Taking into account these properties, BODIPY (concretely,

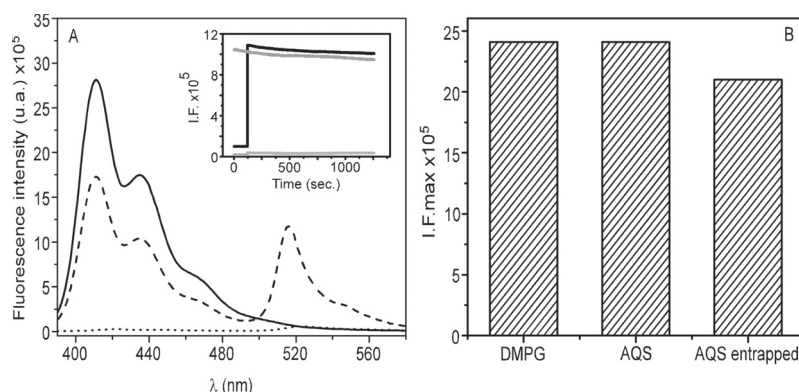


**Figure 4.** (A) Fluorescence emission spectrum of HTMA-PFP in LUVs of DMPG in the absence (solid) and in the presence (dash) of BODIPY  $\text{C}_4\text{C}_9$ , upon excitation at 380 nm. Spectra are compared with that obtained in the absence of HTMA-PFP in LUVs of DMPG labeled with BODIPY  $\text{C}_4\text{C}_9$ , excited at the same wavelength (dotted line). Inset: Kinetics of incorporation of HTMA-PFP in LUVs of DMPG at 40 °C measured by monitoring the fluorescence intensity recorded at  $\lambda_{\text{em}} = 516 \text{ nm}$  ( $\lambda_{\text{exc}} = 380 \text{ nm}$ ) in DMPG (light gray) and DMPG labeled with BODIPY (black) before and after addition ( $t = 120 \text{ s.}$ ) of HTMA-PFP. Figure also shows the photostability of HTMA-PFP upon continuous irradiation at 380 nm ( $\lambda_{\text{em}} = 450 \text{ nm}$ ) in the absence of BODIPY (dark gray). (B) Bar diagrams showing the fluorescence intensity of HTMA-PFP in LUVs of DMPG in the absence (left) and in the presence of AQS externally added (middle) or previously entrapped in the vesicles (right).

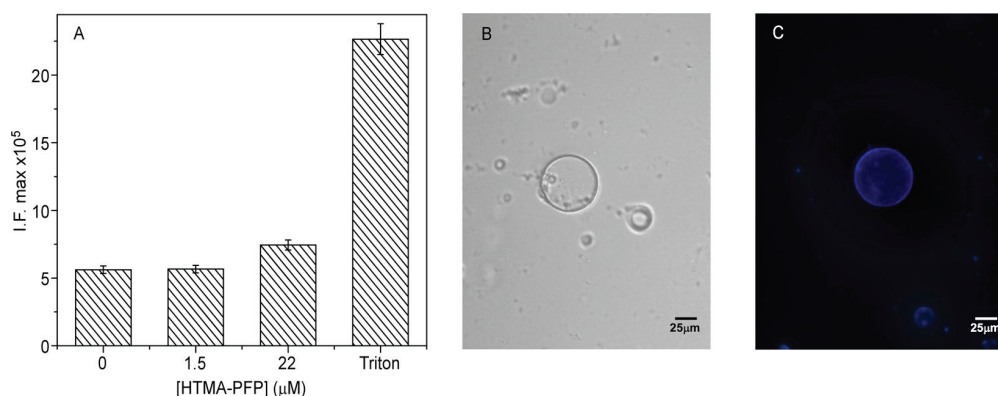


**Figure 5.** (A) Fluorescence intensity of CF encapsulated in DOPG recorded at 550 nm ( $\lambda_{\text{exc}} = 492$  nm) for increasing concentrations of HTMA-PFP (0, 1.5, 22  $\mu\text{M}$ ) and after addition of Triton-X100 (10%). Phase contrast (B) and fluorescence microscopy images (C) of GUVs of DOPG in the presence of HTMA-PFP.

BODIPY 500/510 C<sub>4</sub>,C<sub>9</sub>; Scheme 1) was used as the FRET acceptor from HTMA-PFP. From the spectral overlap between HTMA-PFP emission and BODIPY absorption spectra, a  $J = 4.97 \times 10^{14} \text{ cm}^3 \text{ M}^{-1}$  was obtained (see eq 3), considering a molar extinction coefficient of  $\epsilon = 101\,000 \text{ M}^{-1} \text{ cm}^{-1}$  at 304 nm. This value was used in eq 2 to determine  $R_0$ , considering a quantum yield for HTMA-PFP in a lipid bilayer of 0.7, as compared to  $0.52 \pm 0.03$  measured in water,<sup>37</sup> and a local refractive index of  $n = 1.425$ .<sup>46</sup> From this data, a value of  $R_0 = 42 \pm 2 \text{ \AA}$  is obtained, if an orientational factor  $\kappa^2 = 2/3$  (dynamic isotropic limit) is assumed. Given that the thickness of the DMPG bilayer in fluid phase is  $\sim 32 \text{ \AA}$ ,<sup>47</sup> it is clear that if HTMA-PFP inserts on the surface or within the bilayer, a significant energy transfer should be expected to occur. Figure 4A shows the emission spectrum of HTMA-PFP in LUVs of DMPG containing BODIPY (1:500 acceptor:lipid molar ratio) at 40 °C, together with those recorded in the absence of acceptor or polymer. The decrease of HTMA-PFP emission simultaneously with the increase of BODIPY emission upon excitation at 380 nm (where the acceptor does not absorb) is a clear evidence of FRET occurring. When different acceptor:lipid molar ratios (1:1000, 1:750, and 1:500) were explored, the same decrease in the polymer emission was observed (data not shown). From these results, an efficiency of FRET of  $\sim 40\%$  was estimated, using eq 4, after the correction procedure described in the Experimental Section, confirming that HTMA-PFP is inserted into the membranes. The existence of FRET can be also used to estimate the kinetics of incorporation of the polyelectrolyte into the membrane. This kinetics can be monitored recording the increase produced in the fluorescence intensity of BODIPY ( $\lambda_{\text{em}} = 516 \text{ nm}$ ), when it is excited at 380 nm, upon addition of HTMA-PFP. Figure 4A (inset) shows how, in the absence of polymer, the fluorescence intensity of LUVs containing BODIPY was practically negligible, while it increased abruptly after polymer addition, reaching its maximum value in the first seconds, which indicates that the incorporation of HTMA-PFP into the membrane occurs very fast. The fact that fluorescence intensity remains practically constant after membrane polymer incorporation suggests that once HTMA-PFP inserts into the bilayer it does not change its location. The slight decrease observed in the fluorescence intensity with time can be attributed to a small photobleaching of the donor occurring after continuous irradiation. To confirm this possibility, HTMA-PFP was incorporated into DMPG

vesicles in the absence of BODIPY, and the emission of polymer ( $\lambda_{\text{em}} = 450 \text{ nm}$ ) was recorded as a function of time, upon continuous excitation at 380 nm. A decrease lower than 10% was found after 20 min of irradiation, which was not observed when the sample was maintained in the dark during this time (see inset in Figure 4A).

Although FRET experiments confirm the interaction of HTMA-PFP with DMPG vesicles, they do not inform whether the polyelectrolyte remains located close of the surface or if it is embedded in the lipid bilayer. The DLS results suggest that HTMA-PFP inserts into the lipid membrane because the size of the vesicle does not change after polymer interaction. This hypothesis was checked from quenching experiments using AQS, taking advantage that this quencher is water-soluble remaining out of the lipid bilayer. When increasing concentrations of AQS as those used above in water and buffer were added to a suspension of DMPG LUVs containing HTMA-PFP, no change in the fluorescence intensity of the polymer was observed (Figure 2). The lack of quenching effect could be due to repulsions occurring between the anionic quencher and the DMPG vesicles, and therefore we considerably increased the quencher concentration up to 5  $\mu\text{M}$ , observing the same response (Figure 4B). This result indicates that once HTMA-PFP interacts with the membrane, it does not remain located close of the surface, but is embedded in the lipid bilayer, supporting the previous hypothesis. A similar experiment was performed, but this time the quencher was added to the buffer before liposomes formation, to ensure that AQS was also located in the aqueous inner cavity of the liposomes. The aim was to explore whether HTMA-PFP was able to cross the lipid bilayer. Results showed that there was  $\sim 95\%$  of polymer unquenched (Figure 4B), which suggests that HTMA-PFP can migrate to the inner monolayer but that only a small fraction of it should be located in the inner surface.

**Effect of HTMA-PFP on the Lipid Vesicle Integrity.** As was described in the Introduction, the use of CPEs as probes for bioimaging requires minimal perturbation of the sample being studied. The above experiments suggest that the integrity of the lipid vesicles is maintained after polymer incorporation. This suggestion was confirmed by monitoring the induced release of CF from DOPG vesicles in the presence of HTMA-PFP. When this fluorophore is encapsulated at high concentration in the aqueous cavity of liposomes, its fluorescence decreases by an autoquenching process;<sup>48,49</sup>

therefore, if the interaction of the polyelectrolyte with the lipid membrane produces the rupture of the lipid vesicle or the formation of pores, the trapped CF is released and fluoresces strongly after its dilution in the buffer. Figure 5A shows the fluorescence of CF encapsulated in liposomes composed of DOPG at room temperature, recorded in the absence and in the presence of increasing concentrations of HTMA-PFP and compared to that obtained after addition of Triton X-100 10% to induce lysis of vesicles. Results show that the presence of polyelectrolyte at 1.5  $\mu\text{M}$  does not modify the fluorescence intensity of CF, indicating that the integrity of the lipid vesicles is maintained at this polymer concentration. However, addition of higher amounts of HTMA-PFP produced an increase in the CF fluorescence which suggests that this polyelectrolyte, used at higher concentrations, induces alterations in lipid packing, resulting in membrane rupture or pore formation. This effect could be attributed to the quaternary amine groups of the polyelectrolyte as well as to its relatively rigid hydrophobic backbone, which have been reported to disrupt bacterial membranes (negatively charged) causing cell death.<sup>22</sup> Therefore, HTMA-PFP added at low concentrations should act as a fluorescent membrane marker, while, when used at higher concentrations, it could have some biocidal activity.

The integrity of the lipid vesicles in the presence of HTMA-PFP was also confirmed by phase contrast and fluorescence microscopy using GUVs formed by the gentle hydration method.<sup>50</sup> GUVs were composed of DOPG and microscopy images were recorded at 25  $^{\circ}\text{C}$  (Figure 5b,c). Results show that the polyelectrolyte interacts with the vesicles, labeling the lipid membrane, but its presence does not alter the morphology of the liposomes. In addition, no photobleaching was observed during the acquisition period, confirming the photostability of HTMA-PFP, which was previously shown in Figure 4 (inset), and its ability to visualize membrane structures.

**HTMA-PFP in Lipid Vesicles as a Function of Temperature.** As was previously mentioned, pure DMPG presents its gel/fluid phase thermal transition ( $T_m$ ) around 24  $^{\circ}\text{C}$ . Below this temperature, the lipids exist as a solid-like gel, the acyl chains being packed tightly against each other. Above 24  $^{\circ}\text{C}$ , the lipids are in a fluid phase where the acyl chains are disordered and rapid lateral diffusion of lipids occurs in the plane of the membrane. Taking into account this property of membrane, two types of studies were performed. First, we explored whether the presence of HTMA-PFP altered the thermotropic behavior and the structural order of the lipid bilayer and, second, we analyzed whether the fluorescence spectra of the polyelectrolyte were sensitive to the large structural changes taking place in the lipid bilayer at the lipid phase transition. For the first purpose, DSC and steady-state fluorescence anisotropy experiments were performed on LUVs of DMPG. Figure 6 (top) shows the thermograms recorded in the absence and in the presence of HTMA-PFP 1.5  $\mu\text{M}$  and 16  $\mu\text{M}$ . The fact that the position, high and width of the main peak, located near 24  $^{\circ}\text{C}$ , of the thermograms of DMPG containing polyelectrolyte were virtually identical to that of the pure lipid, even at 16  $\mu\text{M}$  of concentration, indicates that the cooperativity of the transition is preserved in the presence of the polyelectrolyte and, therefore, HTMA-PFP is not disrupting the overall structure of the lipid bilayer at the used concentrations. These results were corroborated by the anisotropy experiments carried out using the fluorescent probe BODIPY 500/510  $C_4C_9$  incorporated in DMPG (note that the traditional fluorescent probe diphenylhexatriene, DPH,

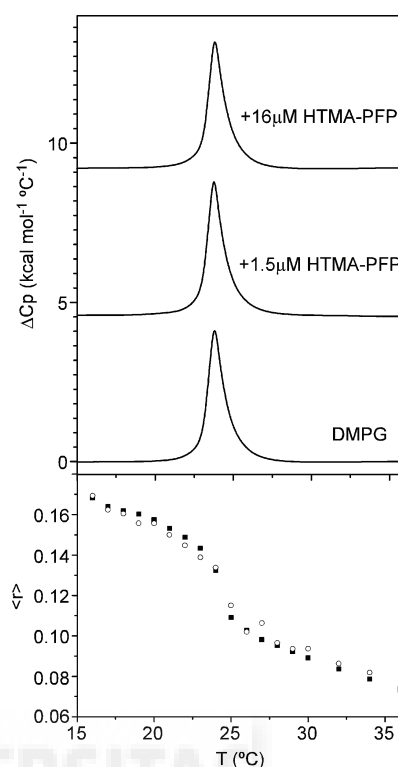


**Figure 6.** (Top) DSC thermograms of LUVs of DMPG in the absence and in the presence of 1.5  $\mu\text{M}$  and 16  $\mu\text{M}$  HTMA-PFP at temperatures between 15 and 36  $^{\circ}\text{C}$ . (Bottom) Anisotropy values,  $\langle r \rangle$ , of BODIPY  $C_4C_9$  in LUVs of DMPG in the absence (black squares) and presence (circles) of 1.5  $\mu\text{M}$  HTMA-PFP.

could not be used because it absorbs in the same region as HTMA-PFP). The plot of the steady-state fluorescent anisotropy,  $\langle r \rangle$ , of a membrane fluorescent probe versus temperature is a common tool used for liposomes characterization. For pure phospholipids, the characteristic shape of the plot is sinusoidal, with a sharp transition of anisotropy values in a short-range of temperatures in which the average value correspond to  $T_m$ . Thus, the plot provides an accurate determination of the  $T_m$  value, which is strongly dependent on the natural dynamic motions of the bilayer and, hence, can be correlated with the structural integrity of the lipid bilayer. Figure 6 (bottom) shows the changes of anisotropy,  $\langle r \rangle$ , recorded in DMPG LUVs in the absence and presence of 1.5  $\mu\text{M}$  HTMA-PFP. The anisotropy values and the shape of the curves are very similar in the two samples:  $\langle r \rangle$  slightly decreases with increasing temperature, with a sharp drop occurring at  $T_m$ , evidencing that the lipid packing of the bilayer is preserved after incorporation of HTMA-PFP.

For the second purpose, the fluorescence emission spectra of HTMA-PFP were recorded in DMPG as a function of temperature, and were compared with those obtained in DOPG, an unsaturated lipid that does not show phase transition in the observed temperature range (Figure 7 and inset). The increase in temperature, from 10 to 40  $^{\circ}\text{C}$ , induced a totally different effect in both lipid systems. In DOPG, fluorescence intensity decreased as temperature increased and the spectrum became slightly less resolved, suggesting an increase in the degree of freedom of the polymer chain with temperature. By contrast, in DMPG, a clear blue-shift in the

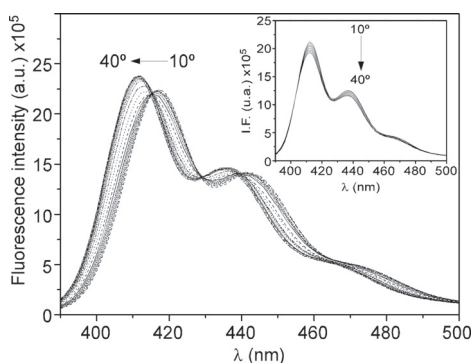


**Figure 7.** Fluorescence emission spectra of HTMA-PFP in LUVs of DMPG recorded as a function of temperature from 10 to 40 °C. Inset: Fluorescence emission spectra of HTMA-PFP in LUVs of DOPG as a function of temperature.

emission spectrum was observed when going from 10 to 40 °C, as well as a slight increase in intensity. Plots of the emission maximum wavelength peak,  $\lambda_{\text{max}}$ , and of the maximum intensity,  $I_{\text{max}}$  against temperature are shown in Figure 8A. Results show

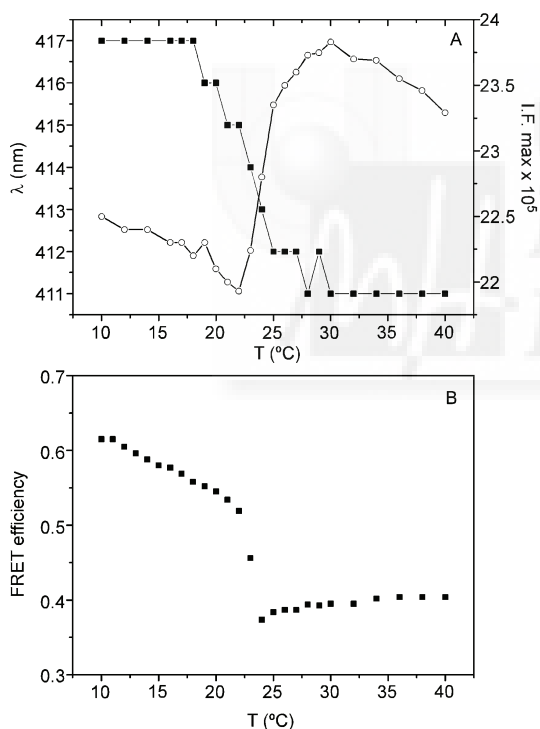


**Figure 8.** (A) Dependence with the temperature of the fluorescence maximum position (black squares) and intensity (circles) of HTMA-PFP in LUVs of DMPG. (B) Effect of temperature on the FRET efficiency between HTMA-PFP and BODIPY  $C_4C_9$  in LUVs of DMPG.

how these parameters, especially  $\lambda_{\text{max}}$ , change at the transition temperature, which indicates that polyelectrolyte fluorescence is sensitive to the physical state of the lipid bilayer. The changes observed in these experiments were reversible, and a similar spectral shift was found when the same sample was allowed to cool at 10 °C and heated again. The fact that the emission spectrum of HTMA-PFP in the gel phase is red-shifted with respect to that recorded in fluid phase and the reversibility of

the process suggest that the tight packing of lipid chains below the transition temperature forces the polymer to adopt a planarized conformation of phenyl rings extending the effective  $\pi$ -conjugation length.<sup>51</sup> In contrast, above the transition temperature, in the fluid phase, the polymer can twist to form various conformations, preventing the delocalization of  $\pi$ -electrons over the entire chain.

The lipid phase transition of DMPG was also detected by HTMA-PFP from FRET experiments performed as a function of temperature, using BODIPY  $C_4C_9$  as acceptor. The fluorescence spectra of the polymer were recorded from 10 to 40 °C in the absence and presence of acceptor, and the efficiency of the process was determined from eq 4 (Figure 8B). Results show that in gel phase the FRET efficiency is very high and decreases with increasing temperature, with a sharp drop occurring at the lipid phase transition. This behavior was reversible and could be attributed to several factors. On one hand, it is possible that the variation in the FRET efficiency was due to differences in the overlap integral,  $J$ , caused by the emission spectral shift of HTMA-PFP occurring during the phase transition. On the other hand, the fact that the average lipid–lipid distance as well as the lipid vesicle volume are higher when the bilayer is in fluid phase (see Table 1) can lead to an increase in the distance between HTMA-PFP and BODIPY, reducing the FRET efficiency with respect to that obtained in gel phase.

## CONCLUSIONS

In conclusion, this study uses different approaches to explore the interaction between the cationic CPE HTMA-PFP and anionic lipid vesicles in order to evaluate the potential use of this polyelectrolyte as a fluorescent membrane marker. Results show that HTMA-PFP rapidly incorporates into the membrane with high affinity, being embedded within the lipid bilayer where it shows high fluorescence efficiency and good stability, allowing the visualization of the membrane structures by fluorescence microscopy. This interaction perturbs neither the morphology of the vesicles nor their lipid packing, thus preserving their structural integrity. The good sensitivity of the HTMA-PFP fluorescence to the physical state of the lipid bilayer makes it an interesting tool for detecting lipid phase changes. In addition, the polyelectrolyte is a good FRET donor for acceptors emitting over the whole visible spectrum because of its high fluorescent quantum yield and blue emission and it has been also described for our group as an adequate energy acceptor from tryptophan residues in peptides and proteins.<sup>29</sup> These properties extend the potential applications of HTMA-PFP to be used for monitoring membrane–ligand interactions and liposome drug delivery. Finally, the fact that the bacterial membranes is rich in anionic lipids, principally phosphatidylglycerol, makes HTMA-PFP a suitable candidate for the study or the detection of pathogenic bacterial cells, by selectively targeting the bacterial membrane over the mostly zwitterionic membrane surfaces of healthy mammalian cells.<sup>52</sup> It could have many applications in health and environmental testing. For example, currently there is a big need to develop highly sensitive assays able to detect and visualize very small numbers of pathogenic bacterial cells in biomedical samples or in food and drinking water.<sup>53,54</sup> For that, it is necessary first to know the behavior of the polyelectrolyte in the presence of vesicles composed of zwitterionic phospholipids, as well as in samples containing both anionic and zwitterionic vesicles, which is the scope of our next study.

## ■ AUTHOR INFORMATION

## Corresponding Author

\*E-mail: rmateo@umh.es.

## Notes

The authors declare no competing financial interest.

## ■ ACKNOWLEDGMENTS

The authors thank the Spanish Ministerio de Economía y Competitividad for financial support MAT-2011-23007. We thank Rocio Esquembre and Rebeca Vázquez for their kind help and technical assistance.

## ■ REFERENCES

- (1) Weissleder, R.; Ntziachristos, V. *Nat. Med.* **2003**, *9*, 123–128.
- (2) Duarte, A.; Pu, K. Y.; Liu, B.; Bazan, G. C. *Chem. Mater.* **2011**, *23*, 501–515.
- (3) Pu, K. Y.; Liu, B. *Adv. Funct. Mater.* **2011**, *21* (18), 3408–3423.
- (4) Lee, K.; Lee, J.; Jeong, E. J.; Kronk, A.; Elenitoba-Johnson, K. S. J.; Lim, M. S.; Kim, J. *Adv. Mater.* **2012**, *24*, 2479–2984.
- (5) Herland, A.; Inganäs, O. *Macromol. Rapid Commun.* **2007**, *28*, 1703–1713.
- (6) Zhu, C.; Liu, L.; Yang, Q.; Lv, F.; Wang, S. *Chem. Rev.* **2012**, *112*, 4687–4735.
- (7) Pu, K. Y.; Cai, L.; Liu, B. *Macromolecules* **2009**, *42* (16), 5933–5940.
- (8) Thomas, S. W., III; Joly, G. D.; Swager, T. M. *Chem. Rev.* **2007**, *107*, 1339–1386.
- (9) Achyuthan, K. E.; McClain, J. L.; Zhou, Z.; Whitten, D. G.; Branch, D. W. *Anal. Sci.* **2009**, *25*, 469–474.
- (10) Wang, B.; Yuan, H.; Zhu, C.; Yang, Q.; Lv, F.; Liu, L.; Wang, S. *Sci. Rep.* **2012**, *2*, 766–774.
- (11) Ngo, A. T.; Karam, P.; Cosa, G. *Pure Appl. Chem.* **2011**, *83*, 43–55.
- (12) Liu, Y.; Ogawa, K.; Schanze, K. S. *J. Photochem. Photobiol., C* **2009**, *10*, 173–190.
- (13) Wang, L.; Li, H.; Cao, D. *Curr. Org. Chem.* **2012**, *16*, 1468–1484.
- (14) Tang, Y.; Liu, Y.; Cao, A. *Anal. Chem.* **2013**, *85*, 825–830.
- (15) Nilsson, K. P. R.; Hammarström, P. *Adv. Mater.* **2008**, *20*, 2639–2645.
- (16) Kim, I. B.; Shin, H.; Garcia, A. J.; Bunz, U. H. F. *Bioconjugate Chem.* **2007**, *18*, 815–820.
- (17) McRae, R. L.; Phillips, R. L.; Kim, I. B.; Bunz, U. H. F.; Fahrni, C. J. *J. Am. Chem. Soc.* **2008**, *130*, 7851–7853.
- (18) Zhu, C.; Yang, Q.; Liu, L.; Wang, S. *Chem. Commun.* **2011**, *47*, 5524–5526.
- (19) Feng, G.; Ding, D.; Liu, B. *Nanoscale* **2012**, *4*, 6150–6165.
- (20) Wen, Q.; Zhu, C.; Liu, L.; Yang, Q.; Wang, S.; Zhu, D. *Macromol. Chem. Phys.* **2012**, *213*, 2486–2491.
- (21) Wang, B.; Zhu, C.; Liu, L.; Lv, F.; Yang, Q.; Wang, S. *Polym. Chem.* **2013**, DOI: 10.1039/c3py00097d.
- (22) Ding, L.; Chi, E. Y.; Chemburu, S.; Ji, E.; Schanze, K. S.; Lopez, G. P.; Whitten, D. G. *Langmuir* **2009**, *25*, 13742–13751.
- (23) Ding, L.; Chi, E. Y.; Schanze, K. S.; Lopez, G. P.; Whitten, D. G. *Langmuir* **2010**, *26*, 5544–5550.
- (24) Wang, Y.; Jones, E. M.; Tang, Y.; Ji, E.; Lopez, G. P.; Chi, E. Y.; Schanze, K. S.; Whitten, D. G. *Langmuir* **2011**, *27*, 10770–10775.
- (25) Ngo, A. T.; Cosa, G. *Langmuir* **2010**, *26*, 6746–6754.
- (26) Liu, B.; Wang, S.; Bazan, G. C.; Mikhailovsky, A. J. *Am. Chem. Soc.* **2003**, *125*, 13306–13307.
- (27) Liu, B.; Bazan, G. C. *J. Am. Chem. Soc.* **2006**, *128*, 1188–1196.
- (28) Tapia, M. J.; Montserin, M.; Valente, A. J. M.; Burrows, H. D.; Mallavia, R. *Adv. Colloid Interface Sci.* **2010**, *158*, 94–107.
- (29) Martínez-Tome, M. J.; Esquembre, R.; Mallavia, R.; Mateo, C. R. *Biomacromolecules* **2010**, *11*, 1494–1501.
- (30) Mallavia, R.; Martínez-Peréz, D.; Chmelka, B. F.; Bazan, G. C. *Bol. Soc. Esp. Ceram. Vidrio* **2004**, *43*, 327–330.
- (31) Molina, R.; Gómez-Ruiz, S.; Montilla, F.; Salinas-Castillo, A.; Fernández-Arroyo, S.; Del Mar Ramos, M.; Micol, V.; Mallavia, R. *Macromolecules* **2009**, *42*, 5471–5477.
- (32) Rodríguez, N.; Pincet, F.; Cribier, S. *Colloids Surf., B* **2005**, *42*, 125–130.
- (33) Al Attar, H. A.; Monkman, A. P. *J. Phys. Chem. B* **2007**, *111*, 12418–12426.
- (34) Tapia, M. J.; Montserin, M.; Costoyas, A.; Burrows, H. D.; Marques, A. T.; Pais, A. A. C. C.; Valente, A. J. M.; Mallavia, R.; Scherf, U.; Pinazo, A.; Pérez, L.; Morán, M. C. *J. Mol. Liq.* **2010**, *156*, 18–27.
- (35) Montserin, M.; Burrows, H. D.; Valente, A. J. M.; Lobo, V. M. M.; Mallavia, R.; Tapia, M. J.; García-Zubiri, I. X.; Di Paolo, R. E.; Maçanita, A. L. *J. Phys. Chem. B* **2007**, *111*, 13560–13569.
- (36) Montserin, M.; Burrows, H. D.; Valente, A. J. M.; Mallavia, R.; Di Paolo, R. E.; Maçanita, A. L.; Tapia, M. J. *J. Phys. Chem. B* **2009**, *113*, 1294–1302.
- (37) Wang, S.; Bazan, G. C. *Chem. Commun.* **2004**, *10*, 2508–2509.
- (38) Chen, J.; Dong, W. F.; Möhwald, H.; Krastev, R. *Chem. Mater.* **2008**, *20*, 1664–1666.
- (39) Chemburu, S.; Ji, E.; Casana, Y.; Wu, Y.; Buranda, T.; Schanze, K. S.; Lopez, G. P.; Whitten, D. G. *J. Phys. Chem. B* **2008**, *112*, 14492–14499.
- (40) Fan, C.; Wang, S.; Hong, J. W.; Bazan, G. C.; Plaxco, K. W.; Heeger, A. J. *Proc. Natl. Acad. Sci. U.S.A.* **2003**, *100*, 6297–6301.
- (41) Pinto, S. M.; Burrows, H. D.; Pereira, M. M.; Fonseca, S. M.; Dias, F. B.; Mallavia, R.; Tapia, M. J. *J. Phys. Chem. B* **2009**, *113*, 16093–16100.
- (42) Dwight, S. J.; Gaylord, B. S.; Hong, J. W.; Bazan, G. C. *J. Am. Chem. Soc.* **2004**, *126*, 16850–16859.
- (43) Mateo, C. R.; Prieto, M.; Micol, V.; Shapiro, S.; Villalain, J. *Biochim. Biophys. Acta* **2000**, *1509*, 167–175.
- (44) Lakowicz, J. R. *Principles of Fluorescence Spectroscopy*; 2nd ed.; Kluwer Academic/Plenum Press: New York, 1999.
- (45) Kaiser, R. D.; London, E. *Biochim. Biophys. Acta* **1998**, *1375*, 13–22.
- (46) Toptygin, D.; Brand, L. *J. Fluoresc.* **1995**, *5*, 39–50.
- (47) Pan, J.; Heberle, F. A.; Tristram-Nagle, S.; Szymanski, M.; Koepfinger, M.; Katsaras, J.; Kucerka, N. *Biochim. Biophys. Acta* **2012**, *1818*, 2135–2148.
- (48) Van Renswoude, J.; Hoekstra, D. *Biochemistry* **1981**, *20*, 540–546.
- (49) Bandyopadhyay, P.; Bandyopadhyay, P.; Regen, S. L. *J. Am. Chem. Soc.* **2002**, *124*, 11254–11255.
- (50) Morales-Pennington, N. F.; Wu, J.; Farkas, E. R.; Goh, S. L.; Konyakhina, T. M.; Zheng, J. Y.; Webb, W. W.; Feigensohn, G. W. *Biochim. Biophys. Acta* **2010**, *1798*, 1324–1332.
- (51) Levitus, M.; Schmieder, K.; Ricks, H.; Shimizu, K. D.; Bunz, U. H. F.; Garcia-Garibay, M. A. *J. Am. Chem. Soc.* **2001**, *123*, 4259–4265.
- (52) Zhu, C.; Yang, Q.; Liu, L.; Lv, F.; Li, S.; Yang, G.; Wang, S. *Adv. Mater.* **2011**, *23*, 4805–4810.
- (53) Leevy, W. M.; Gammon, S. T.; Jiang, H.; Johnson, J. R.; Maxwell, D. J.; Jackson, E. N.; Marquez, M.; Piwnica-Worms, D.; Smith, B. D. *J. Am. Chem. Soc.* **2006**, *128*, 16476–16477.
- (54) Leevy, W. M.; Gammon, S. T.; Johnson, J. R.; Lampkins, A. J.; Jiang, H.; Marquez, M.; Piwnica-Worms, D.; Suckow, M. A.; Smith, B. D. *Bioconjugate Chem.* **2008**, *19*, 686–692.



## Publication 8.2





## **Selective Interaction of a Cationic Polyfluorene with Model Lipid Membranes: Anionic versus Zwitterionic Lipids**

**Zehra Kahveci, María José Martínez-Tomé, Rocío Esquembre, Ricardo Mallavia and C.**

**Reyes Mateo**

Instituto de Biología Molecular y Celular, Universidad Miguel Hernández, 03202

Elche, Spain

**Materials, 2014, 7(3), 2120-2140**

**DOI: 10.3390/ma7032120**

Impact Factor: **2.728**



Article

## Selective Interaction of a Cationic Polyfluorene with Model Lipid Membranes: Anionic *versus* Zwitterionic Lipids

Zehra Kahveci, María José Martínez-Tomé, Rocío Esquembre, Ricardo Mallavia and C. Reyes Mateo \*

Instituto de Biología Molecular y Celular, Universidad Miguel Hernández, Elche (Alicante) 03202, Spain; E-Mails: zkahveci@umh.es (Z.K.); mj.martinez@umh.es (M.J.M.-T.); resquembre@umh.es (R.E.); r.mallavia@umh.es (R.M.)

\* Author to whom correspondence should be addressed; E-Mail: rmateo@umh.es; Tel.: +34-966-658-469; Fax: +34-966-658-758.

Received: 2 January 2014; in revised form: 19 February 2014 / Accepted: 4 March 2014 / Published: 13 March 2014

---

**Abstract:** This paper explores the interaction mechanism between the conjugated polyelectrolyte {[9,9-bis(6'-N,N,N-trimethylammonium)hexyl]fluorene-phenylene}bromide (HTMA-PFP) and model lipid membranes. The study was carried out using different biophysical techniques, mainly fluorescence spectroscopy and microscopy. Results show that despite the preferential interaction of HTMA-PFP with anionic lipids, HTMA-PFP shows affinity for zwitterionic lipids; although the interaction mechanism is different as well as HTMA-PFP's final membrane location. Whilst the polyelectrolyte is embedded within the lipid bilayer in the anionic membrane, it remains close to the surface, forming aggregates that are sensitive to the physical state of the lipid bilayer in the zwitterionic system. The different interaction mechanism is reflected in the polyelectrolyte fluorescence spectrum, since the maximum shifts to longer wavelengths in the zwitterionic system. The intrinsic fluorescence of HTMA-PFP was used to visualize the interaction between polymer and vesicles via fluorescence microscopy, thanks to its high quantum yield and photostability. This technique allows the selectivity of the polyelectrolyte and higher affinity for anionic membranes to be observed. The results confirmed the appropriateness of using HTMA-PFP as a membrane fluorescent marker and suggest that, given its different behaviour towards anionic and zwitterionic membranes, HTMA-PFP could be used for selective recognition and imaging of bacteria over mammalian cells.

**Keywords:** polyelectrolyte; polyfluorene; fluorescent membrane marker; liposomes; bioimaging

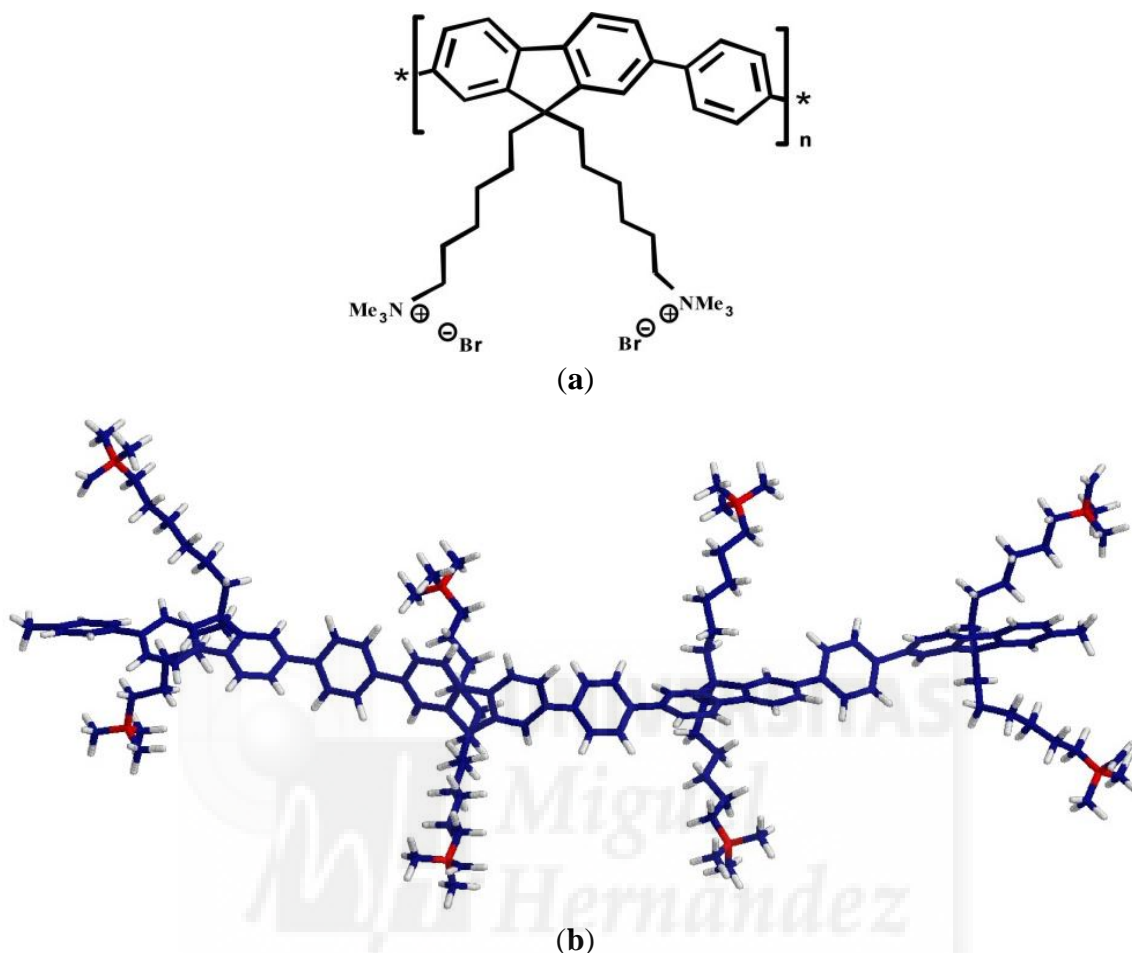
---

## 1. Introduction

Polyelectrolytes are polymers of any type and structure that carry positively or negatively charged ionizable groups. The interaction of these macromolecules with lipids or cell membranes play an important role in many biophysical applications, such as a safe and targeted delivery of genetic material to cells, stabilization of liposomes, or antimicrobial activity [1–5]. Conjugated polyelectrolytes (CPEs) are a particular type of polyelectrolytes, which have very interesting properties. They are polymers with  $\pi$ -conjugated backbones, which show strong absorption and high efficiencies in both photoluminescence and electroluminescence, and contain ionic side groups to facilitate their water solubilisation [6,7]. Over the past decades, CPEs have received a lot of attention in biomedical applications, especially for developing biosensing schemes and sensing devices for biomolecules [8–11], and more recently they have been employed as novel fluorescent probes for bioimaging [12–19]. Among CPEs, those involving fluorene-based systems offer the advantage of high fluorescence quantum yields and photostability, blue emission (suitable for energy transfer experiments), excellent thermal stability and high stability against oxidants, as well as good synthetic accessibility [19,20]. In addition, fluorene-based CPEs consist of a rigid hydrophobic polyfluorene backbone with flexible charged side chains, which induces interesting aggregation behaviour; this phenomenon directly affects their intrinsic fluorescence [21–24]. These properties have been used for studying interactions with biomolecules, such as proteins and DNA, allowing sensing platforms to be developed. However, the interaction of charged polyfluorenes with model lipid membranes, which imitate the complexity of natural cell membranes, still remains practically unexplored [25–27]. This study is of interest for predicting and understanding the mechanism of interaction with real cell membranes in order to develop new biotechnological applications.

The cationic polyelectrolyte poly{[9,9-bis(6'-N,N,N-trimethylammonium)hexyl]fluorene-phenylene} bromide (HTMA-PFP) is a water-soluble polyfluorene, consisting of a backbone and alkyl side chain hydrophobic moieties, while the cationic charged quaternary amines control electrostatic interactions (Figure 1) [28,29]. Due to this structure, the polyelectrolyte tends to establish nonspecific electrostatic interactions with species of opposite charge, such as DNA or proteins like human serum albumine (HSA), which can be monitored from changes in its absorption and intrinsic fluorescence [25,27]. In addition, the polyelectrolyte is a good energy transfer donor for acceptors over a large part of the visible spectrum because of its high fluorescent quantum yield and blue emission, and it has also been shown to be an adequate energy acceptor from tryptophan residues in peptides and proteins [25,30]. Recently, we explored the interaction of HTMA-PFP with vesicles composed of anionic phospholipids [31]. In that study, we concluded that the polyelectrolyte rapidly incorporated into the membrane with high affinity, being embedded within the lipid bilayer where it showed high fluorescence efficiency and good stability. These properties allow the visualization of the lipid vesicles with fluorescence microscopy.

**Figure 1.** (a) HTMA-PFP chemical structure; (b) the conformation of a tetramer of HTMA-PFP obtained using molecular dynamics simulations.



Fluorescent imaging of bacterial infection by selectively targeting the bacterial membrane over the membrane surfaces of healthy mammalian cells has emerged as a powerful tool with many health and environmental applications, such as visualizing small populations of bacterial cells in biological fluids or in food and drinks [32–35]. However, in spite of its advantages, to date only a small number of targeting probes have been reported for the aforementioned application. Ideal markers should be highly fluorescent, water-soluble, biocompatible, photostable, and composed of two structural components: an affinity ligand and a reporter group. The high affinity of HTMA-PFP for anionic lipids, the dominant lipid component in bacterial membranes, as well as its high fluorescence quantum yield and photostability makes HTMA-PFP a suitable candidate for this task. To explore this possibility, the selectivity of the polymer against model bacterial and mammalian membranes should be investigated. It is known that the mammalian plasma membrane is rich in zwitterionic lipids. By varying the lipid composition of the model membranes, it is possible to mimic both types of cell membranes. In this paper, we investigated the affinity and mechanism of HTMA-PFP interaction with membranes composed of zwitterionic phospholipids and the results were compared with those obtained in anionic membranes. In addition, we determined the behaviour of the polyelectrolyte in samples that simultaneously contained both anionic and zwitterionic vesicles in different ratios. Finally, it is known that molecules

having quaternary amine groups are able to disrupt bacterial membranes causing cell death [36–38], and therefore, the membrane perturbing activity of HTMA-PFP was also evaluated.

## 2. Results and Discussion

### 2.1. HTMA-PFP in Zwitterionic Membranes

In a previous paper, we investigated the behaviour of HTMA-PFP in buffer and in the presence of vesicles composed of anionic phospholipids [31]. The polyelectrolyte showed a low fluorescence quantum yield and a red-shift of the emission spectrum in buffer, which was attributed to the formation of metastable aggregates by self-assembly of the polymer hydrophobic chains and to the existence of nonspecific electrostatic interactions between these aggregates and anionic species contained in the buffer. A strong increase in the fluorescence intensity and a blue-shift of the spectrum was observed in the presence of low concentrations of anionic vesicles, indicating that HTMA-PFP interacts with the lipid bilayer with high affinity and, as a consequence of this interaction, the polymer chains become more extended than in buffer and the probability of polymer-polymer interaction (aggregation) is reduced. Additional experiments showed that the polyelectrolyte penetrates into the hydrophobic core, labelling the lipid bilayer without altering the morphology of the vesicles and allowing their visualization.

The high affinity of HTMA-PFP to anionic phospholipids is probably due to the electrostatic interaction between the quaternary amine groups of HTMA-PFP and the negative charge of the lipid head groups. Therefore, it should be of interest to know how the polymer-membrane interaction is affected by the lipid charge in order to determine the membrane selectivity of HTMA-PFP and evaluate its potential use as a fluorescent probe for bacterial imaging. To this end, we studied the interaction mechanism of the polyelectrolyte with lipid vesicles composed of zwitterionic phospholipids, comparing the results with those obtained for anionic lipid vesicles. As a first step, the affinity of HTMA-PFP to zwitterionic membranes was evaluated in samples containing large unilamellar vesicles (LUVs) of 1,2-Dimyristoyl-*sn*-glycero-3-phosphocholine (DMPC). Samples were prepared with increasing lipid concentrations (up to 1 mM) and the same concentration of HTMA-PFP (1.5  $\mu$ M, in terms of repeat units). The temperature was maintained at 40  $^{\circ}$ C to ensure that the lipid bilayer was in fluid phase (DMPC presents its main thermal phase transition around 24  $^{\circ}$ C). Figure 2a shows the emission spectra recorded for the different samples. An enhancement of the fluorescence intensity and a very small blue-shift in the spectrum was observed up to a lipid concentration of about 1 mM. Higher concentrations of lipid did not significantly modify the fluorescence signal, suggesting that, at this lipid concentration, all the polymer chains interacted with the lipids and no aggregates remained in the buffer. Changes in the fluorescence intensity were used to estimate the partition coefficient of the polyelectrolyte between the zwitterionic membrane and the aqueous phase ( $K_p$ ), which is defined in terms of molar concentrations as:

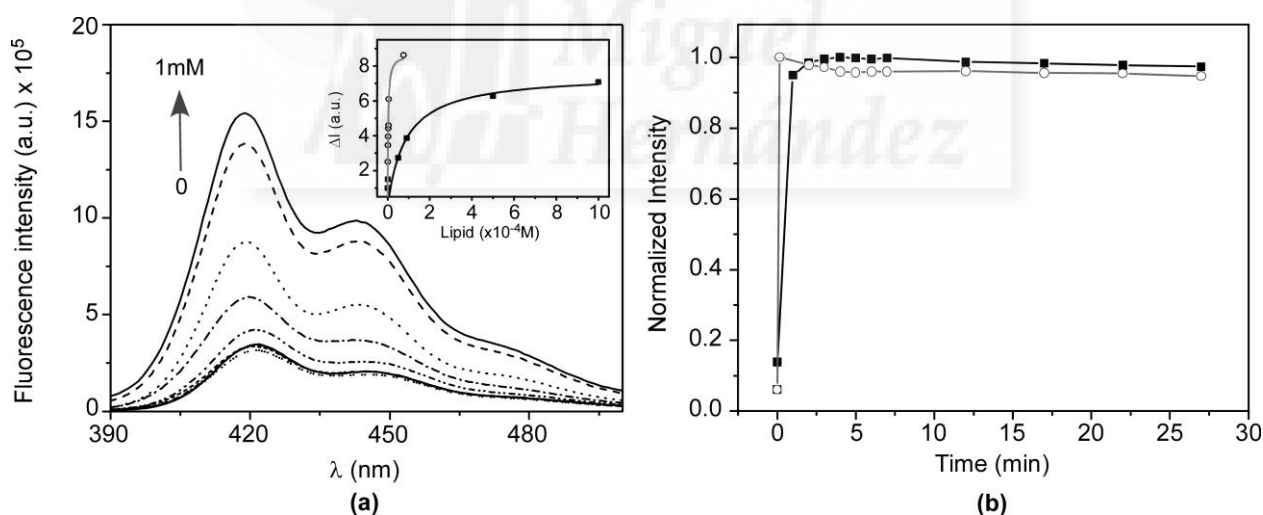
$$K_p = \frac{n_L/V_L}{n_W/V_W} \quad (1)$$

where  $n_i$  stands for moles of compound in phase  $i$  and  $V_i$  for volume of phase  $i$ . The phase is either aqueous ( $i = W$ ) or lipidic ( $i = L$ ). The quantitation of  $K_p$  was performed according to [39]:

$$\Delta I = \frac{\Delta I_{\max}[L]}{\frac{1}{K_P\gamma} + [L]} \quad (2)$$

where  $\Delta I$  ( $\Delta I = I - I_0$ ) stands for the difference between the fluorescence intensity of HTMA-PFP measured in the presence ( $I$ ) and in the absence ( $I_0$ ) of the phospholipid vesicles,  $\Delta I_{\max} = I_{\infty} - I_0$  is the maximum value of this difference once the limiting value is reached ( $I_{\infty}$ ) upon increasing the phospholipid concentration  $[L]$ , and  $\gamma$  is the molar volume of the phospholipid (for DMPC in the fluid phase the value of  $\gamma$  is  $0.9 \text{ M}^{-1}$ ) [40]. Comparing these results with those obtained for liposomes composed of the anionic phospholipid 1,2-Dimyristoyl-*sn*-glycero-3-phospho-*rac*-(1-glycerol) DMPG (see inset in Figure 2a), we conclude that HTMA-PFP shows higher affinity for anionic vesicles than for zwitterionic ones. In fact, the  $K_P$  value obtained for DMPG in the previous paper was one order of magnitude higher than that for DMPC [31].

**Figure 2.** (a) Emission spectra recorded for HTMA-PFP ( $1.5 \mu\text{M}$ ) at different DMPC concentrations 0, 0.001, 0.002, 0.003, 0.004, 0.005, 0.05, 0.085, 0.5, 1 mM. **Inset:** changes in fluorescence intensity ( $\Delta I$ ) at increasing concentrations of DMPC (black line) and DMPG (gray line); (b) incorporation kinetics of HTMA-PFP in DMPC (black line) and DMPG (gray line) labelled with BODIPY 500/510  $C_4$ ,  $C_9$  measured at  $40 \text{ }^\circ\text{C}$  by monitoring the fluorescence intensity recorded at  $\lambda_{\text{em}} = 516 \text{ nm}$  ( $\lambda_{\text{ex}} = 380 \text{ nm}$ ) after addition of polyelectrolyte.

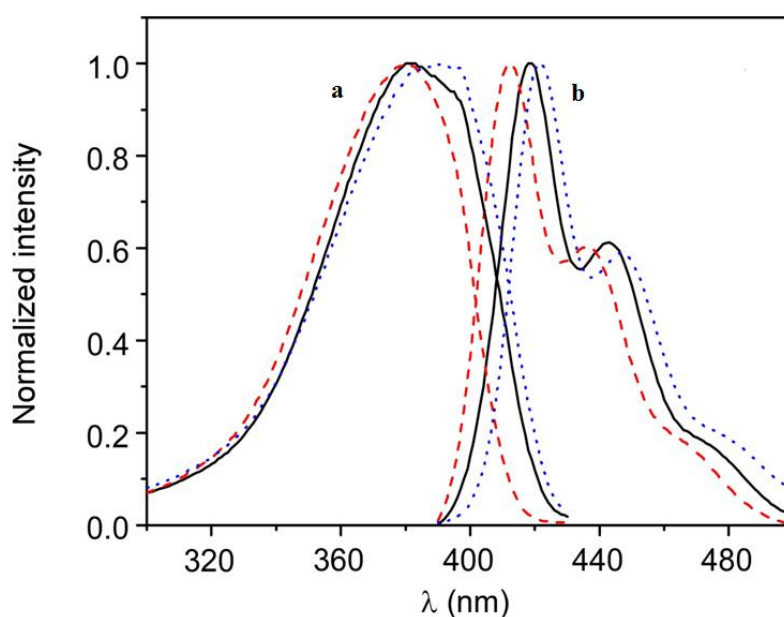


The incorporation kinetics of the polyelectrolyte into the zwitterionic membrane was explored by means of FRET experiments using BODIPY 500/510  $C_4$ ,  $C_9$ , which was previously shown to be a good energy acceptor of HTMA-PFP [31]. This BODIPY fatty acid was incorporated into the DMPC membrane before polymer addition, at a probe:lipid molar ratio of 1:500. Its fluorescence emission ( $\lambda_{\text{em}} = 516 \text{ nm}$ ) was practically negligible upon excitation at the absorption maximum wavelength of the polymer (380 nm), which was an expected result, since BODIPY does not absorb appreciably at this wavelength. HTMA-PFP's interaction with the membrane was monitored by recording the increase in the fluorescence signal as a function of time, as a consequence of the polymer-BODIPY energy transfer, and the plot was compared to that recorded for the anionic membrane under the same conditions (Figure 2b). The fluorescence intensity of BODIPY increased abruptly within a few minutes

after polymer addition, indicating that the interaction of HTMA-PFP with the zwitterionic lipid bilayer is very fast; however, it was slower than that observed for the anionic membrane, which occurred within the first few seconds.

The higher affinity of the polymer for the anionic vesicles and faster incorporation kinetics indicate that the nature of the interaction between HTMA-PFP and the lipid membrane depends on the lipid charge, which is mainly electrostatic for the anionic system, at least in a first step, while for the zwitterionic one it would likely be mediated by hydrophobic interaction between the conjugated backbone of the polymer and the lipid molecules. The differences observed in the fluorescence spectra of the polyelectrolyte in both types of lipids also point to a different interaction mode. Figure 3 shows the normalized excitation and emission spectra of HTMA-PFP in DMPC as compared to those obtained in DMPG and buffer. In DMPG, the emission maximum intensity was observed at 411 nm, while in DMPC and buffer, it was located at 418 and 422 nm, respectively. Simultaneously to the blue-shift, an increase in fluorescence intensity was observed (data not shown), which probably indicates that the metastable aggregates formed in buffer break-up upon interaction with membranes; this effect was more pronounced in the anionic bilayer than in the zwitterionic. The break-up of aggregates would decrease the conjugation length, shifting the emission spectrum to shorter wavelengths. The excitation spectra support this interpretation, since the red-shift and broadness of the band are associated with an increase in the aggregation of the polyelectrolyte [20,25,41]. All these results make evident the different interaction mechanism and suggest that aggregates of HTMA-PFP are better solubilised in the anionic membrane than in the zwitterionic.

**Figure 3.** Normalized (a) excitation and (b) emission fluorescence spectra of HTMA-PFP in buffer (blue dotted line), LUVs of DMPC (black line) and LUVs of DMPG (red dashed line) recorded at 40 °C.



To obtain more insight of the membrane-polyelectrolyte interaction, quenching experiments were carried out using the anionic electron acceptor 9,10-anthraquinone-2,6-disulfonic acid (AQS) as a fluorescence quencher. This molecule has been reported to be an excellent quencher for cationic

conjugated polyelectrolytes and is soluble in water, but not in lipid membranes [42,43]. In our previous paper, AQS was not capable of deactivating HTMA-PFP's fluorescence when HTMA-PFP was incorporated into anionic DMPG vesicles, indicating that the polyelectrolyte does not remain located close to the membrane surface, but is embedded into the lipid bilayer [31]. A similar experiment was performed in zwitterionic vesicles and the results are shown in Figure 4. Contrary to what was observed for anionic membranes, when increasing concentrations of AQS were added to a suspension of DMPC LUVs containing HTMA-PFP, a decrease in the fluorescence signal of the polyelectrolyte was observed. The corresponding Stern-Volmer plot was linear in the concentration range studied (up to 10  $\mu\text{M}$ ) and a value of  $K_{sv} = 1.4 \times 10^5 \text{ M}^{-1}$  was extracted from the slope of the plot. This value was used to calculate the bimolecular rate constant of the quenching process  $k_q$ , assuming  $\tau = 520 \text{ ps}$  [30]. A high value of  $2.7 \times 10^{14} \text{ M}^{-1}\cdot\text{s}^{-1}$  was found, which indicates, as expected, the formation of static quenching complexes between AQS and polymer. This value is, however, lower than that of  $1.5 \times 10^{16} \text{ M}^{-1}\cdot\text{s}^{-1}$  obtained in buffer [31], indicating a more reduced accessibility of the quencher to the membrane-bound polyelectrolyte as compared to the polyelectrolyte in solution. This result confirms that HTMA-PFP is incorporated into the lipid vesicle, but indicates that it remains near or at the surface of the bilayer and not in the hydrophobic core (see Figure 5).

HTMA-PFP's interaction with the zwitterionic lipid membrane was also evaluated from fluorescence microscopy images, using giant unilamellar vesicles (GUVs) prepared by the electroformation method. GUVs were composed of the zwitterionic phospholipid 1,2-Dioleoyl-*sn*-glycero-3-phosphocholine (DOPC) instead of DMPC to facilitate vesicle formation. GUVs were labelled with the fluorophore BODIPY-PC, which absorbs in the visible range without interfering with the absorption of HTMA-PFP. Images were recorded at 25  $^{\circ}\text{C}$  upon irradiation with visible- and UV-light. Figure 6 shows representative images of vesicles obtained after addition of low polymer concentrations. The results confirmed that HTMA-PFP was incorporated into the lipid vesicles, retaining their structural integrity without altering their spherical morphology. No photobleaching was observed during the acquisition period, confirming the photostability of HTMA-PFP in the zwitterionic system and its possible utilization as a fluorescent membrane marker, as was already reported in the previous paper for anionic vesicles [31].

**Figure 4.** Stern-Volmer plots for quenching of HTMA-PFP (1.5  $\mu\text{M}$ ) by AQS in LUVs of DMPC (solid squares) and in LUVs of DMPG (circles). Measurements were performed at 40  $^{\circ}\text{C}$ .

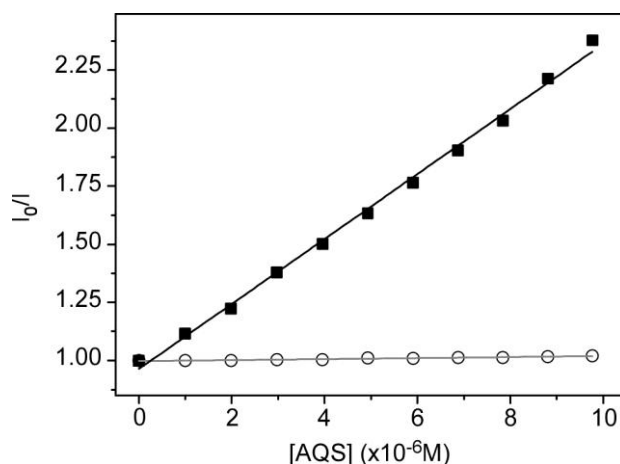


**Figure 5.** Schematic model, which shows the interaction between HTMA-PFP and lipid vesicles composed of (a) anionic and (b) zwitterionic vesicles in gel and fluid phases.

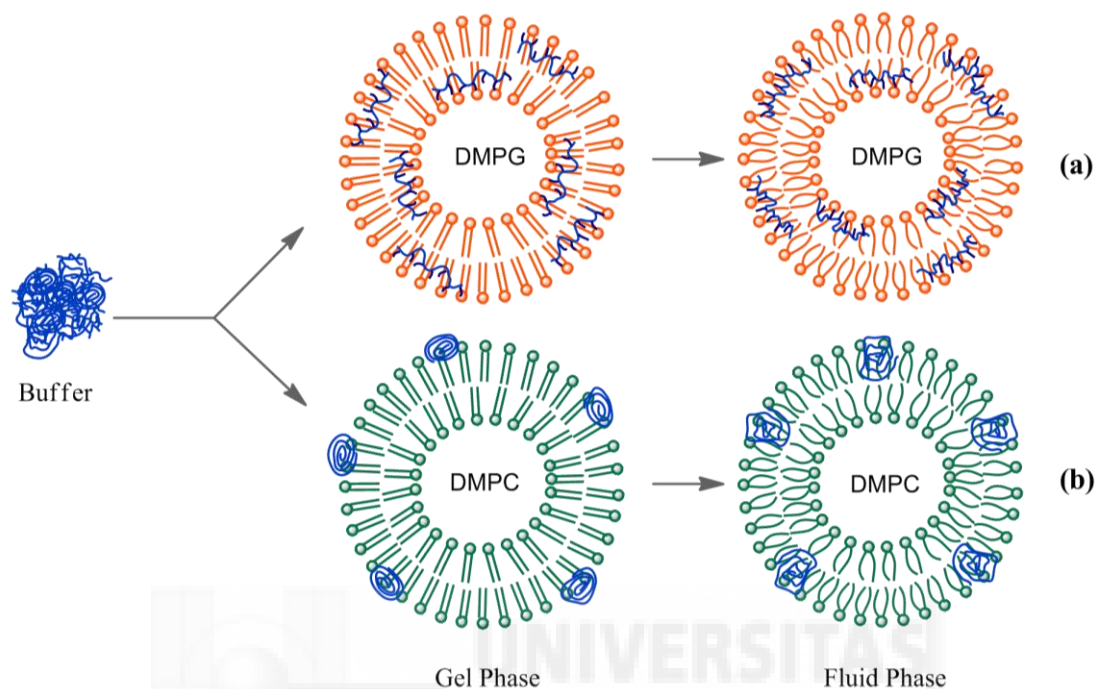
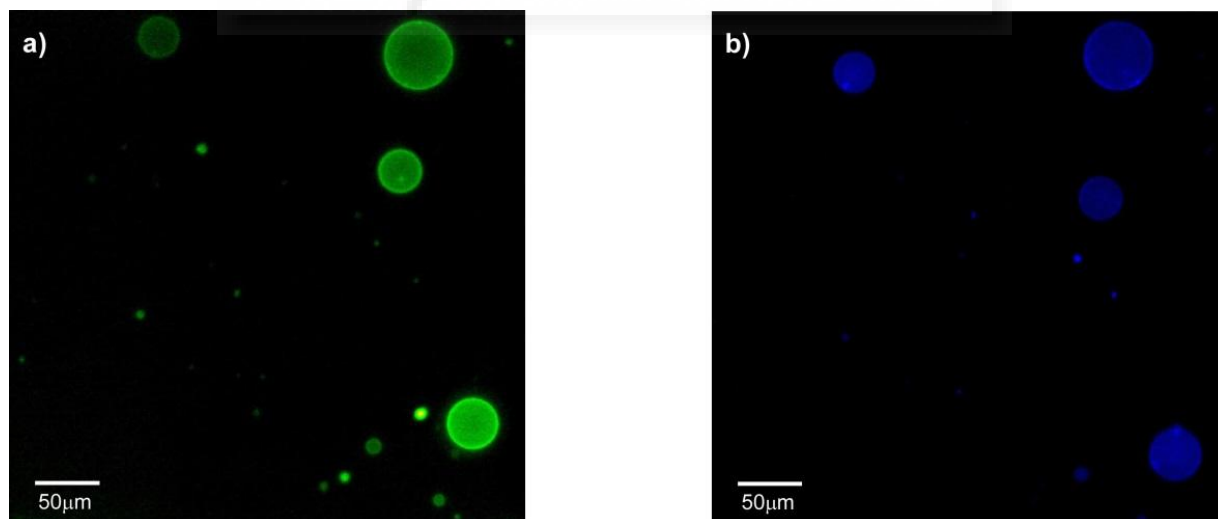


**Figure 6.** Fluorescence microscopy images of GUVs composed of DOPC labelled with BODIPY-PC, recorded upon irradiation with (a) visible- and (b) UV-light, after addition of HTMA-PFP.



### 2.2. Effect of Temperature

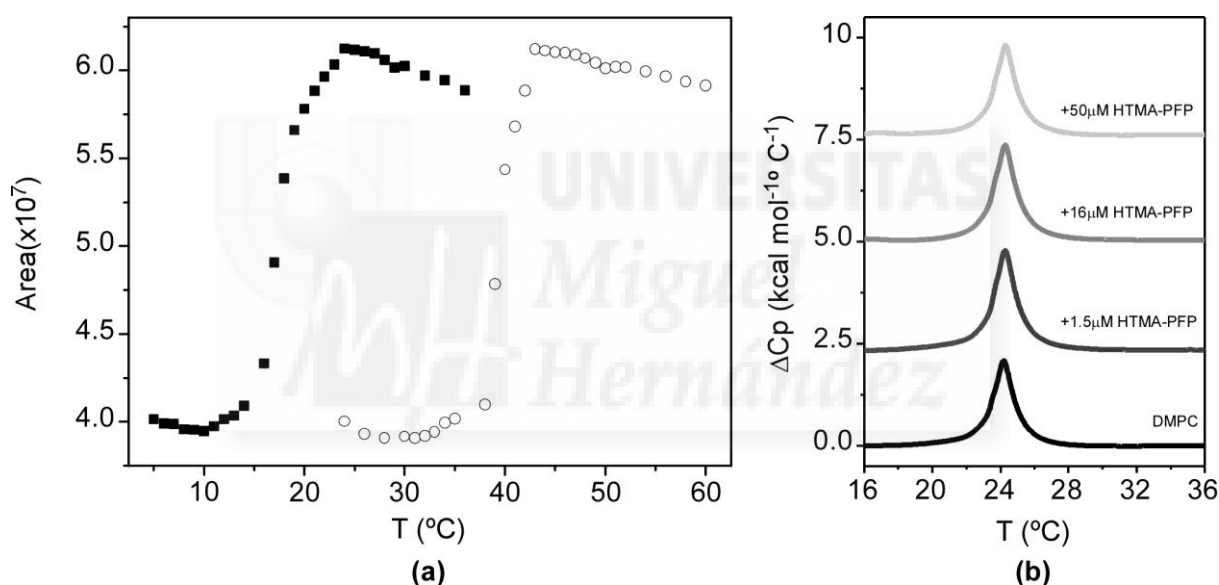
It is well known that membranes composed of a single species of lipid molecules display a thermal phase transition associated with trans-gauche isomerizations of the lipid chains, which brings the bilayer from an ordered gel to a disordered fluid state. In biological membranes, the lipids are mainly in a fluid phase, which facilitates lateral diffusion and conformational changes of membrane proteins.

Therefore, to better simulate biological membranes, all the aforementioned experiments were carried out at 40 °C to ensure that the lipid bilayer was in the fluid phase (both DMPC and DMPG present their thermal phase transition around 24 °C), with exception of the microscopy experiments which were performed at 25 °C, since the transition temperature of DOPC occurs below 0 °C. However, it is of interest to know how the large structural changes taking place in the lipid bilayer in the lipid phase transition affect polyelectrolyte behaviour. This study might lead to more insight into the polymer-membrane interaction mechanism. The effect of temperature on HTMA-PFP incorporated in DMPG was explored in the previous paper [31]. Results showed a clear red-shift in the emission spectrum when the membrane was in the gel phase and a slight decrease in fluorescence intensity accompanied by an increase in the vibrational structure. This behaviour was explained by the chemical structure of the polyelectrolyte shown in Figure 1. Probably, the tight packing of lipid chains below the transition temperature forces the polymer to adopt a planar conformation of phenyl rings, reducing its conformational flexibility and extending the effective  $\pi$ -conjugation length, shifting the emission to red [44]. In contrast, above the transition temperature, the polymer can twist to form various conformations, preventing the delocalization of  $\pi$ -electrons over the entire chain (Figure 5a).

When the effect of temperature was explored in zwitterionic vesicles, a different behaviour was observed as compared with that in anionic vesicles. In this case, the fluorescence quantum yield of HTMA-PFP decreased abruptly in the gel phase and only a very slight red shift was detected in the emission spectrum (~2 nm). Changes in fluorescence intensity were plotted as a function of temperature (Figure 7a). The results showed that from 5 to 12 °C, the fluorescence signal was practically constant. However, a significant increase was observed from 13 °C, reaching its maximum at 24 °C. One of the possible explanations for this result is that the presence of the polymer in the bilayer disrupts the van der Waals interactions between phospholipids, shifting the phase transition to lower temperatures. To explore this possibility, differential scanning calorimetry (DSC) experiments were performed on DMPC LUVs containing HTMA-PFP. Figure 7b shows the thermograms recorded in the absence or presence of increasing concentrations of polyelectrolyte (1.5, 16 and 50  $\mu$ M). From the analysis of these thermograms, transition temperatures ( $T_m$ ) and enthalpies were calculated (see legend in Figure 7b). The fact that the values obtained for DMPC containing polyelectrolyte were similar to those of the pure lipid, even at 50  $\mu$ M of concentration, indicates that the cooperativity of the transition is preserved in the presence of the polymer and, therefore, HTMA-PFP is not disrupting the overall structure of the lipid bilayer at the used concentrations. The second possibility is that the polyelectrolyte is sensitive to the lipid pretransition. The lipid pretransition is a low enthalpy transition below the main phase transition of lipid membranes in which a flat membrane in the gel phase transforms into a periodically undulated bilayer (ripple phase) with a corrugated surface profile. Generally, it is assumed that the lipids in the ripple phase are mainly in the *all-trans* configuration, as in the gel phase. However, several studies point to the existence of fluid regions coupled with the geometry of the ripples and suggest that both pretransition and main transition are caused by the same physical effect, namely chain melting [45,46]. For DMPC, this phenomenon takes place around 14 °C. Therefore, the increase in the fluorescence intensity of HTMA-PFP at 14 °C might be attributable to the conformational changes and/or to the change in location experienced by the polymer as a consequence of these structural alterations, which mainly affect the membrane surface. In order to check this possibility, we carried out a similar experiment, but incorporated the polyelectrolyte in

lipid vesicles composed of 1,2-Dipalmitoyl-*sn*-glycero-3-phosphocholine (DPPC), a zwitterionic phospholipid that presents its pretransition and main phase transition at 33.5 and 41 °C, respectively. In this case, HTMA-PFP fluorescence intensity was practically constant up to 33 °C and increased from 34 to 42 °C, coinciding with the initiation and completion of the acyl chain melting process (Figure 7a). DSC analysis was also performed for DPPC in the absence and presence of different concentrations HTMA-PFP. As was observed for DMPC, the  $T_m$  and transition enthalpies were similar to those of pure lipid (data not shown).

**Figure 7.** (a) Temperature dependence of the fluorescence intensity measured as the integrated area under the spectrum of HTMA-PFP (1.5  $\mu\text{M}$ ), recorded in DMPC (black squares) and DPPC (circles); (b) DSC thermograms of DMPC LUVs in the absence ( $T_m = 24.5$ ;  $\Delta H = 6.0$  kcal/mol) and presence of HTMA-PFP at concentrations of 1.5  $\mu\text{M}$  ( $T_m = 24.5$ ;  $\Delta H = 6.9$  kcal/mol), 16  $\mu\text{M}$  ( $T_m = 24.5$ ;  $\Delta H = 6.6$  kcal/mol) and 50  $\mu\text{M}$  ( $T_m = 24.5$ ;  $\Delta H = 6.1$  kcal/mol).



This result supports the hypothesis that HTMA-PFP aggregates are located near the bilayer surface and are, therefore, sensitive to changes occurring in this membrane region. Probably, below the pretransition, the polymer aggregates are mainly adsorbed on the surface of the vesicles instead of incorporated into the lipid bilayer (Figure 5). The beginning of pretransition allows the aggregates to solubilize better in the lipid membrane, leading to an increased fluorescence intensity. To confirm this assumption, a quenching experiment, similar to the one described before, was carried out in DMPC below the pretransition temperature at 10 °C. The quenching efficiencies were lower than those observed for the polymer in buffer, but 3-times higher than those in the fluid phase, suggesting a higher accessibility of the quencher to the polyelectrolyte (data not shown). This result indicates that, at this temperature, HTMA-PFP still interacts with the zwitterionic membrane, but remains in the lipid/water interface and is more exposed to the solvent than in the fluid phase.

### 2.3. Selectivity of HTMA-PFP against Anionic and Zwitterionic Membranes

The above results confirm that the nature of the interaction between HTMA-PFP and lipid membranes depends on the lipid charge. Although an electrostatic interaction is expected to be responsible for the high affinity of HTMA-PFP for the anionic membrane, the final location of the polyelectrolyte, which is well embedded into the bilayer core, indicates that hydrophobic forces also contribute to its solubilisation, reducing its aggregation state and increasing the fluorescence quantum yield compared to zwitterionic membranes. This behaviour suggests that HTMA-PFP is selective for anionic vesicles and can, therefore, be used as a potential bacterial membrane marker. The fact that the position of the fluorescence emission spectrum of HTMA-PFP depends on the lipid charge was used as a tool to confirm this hypothesis in this study. A series of samples containing different ratios of DMPC and DMPG LUVs (final concentration 1 mM) were prepared and the fluorescence spectrum of HTMA-PFP was recorded for each sample at 40 °C (Figure 8a). The results show a clear shift of the spectral maximum from 418 to 411 nm, when the DMPG LUVs content is increased. When the sample was composed of equal amounts of DMPC and DMPG, the spectral maximum was observed at 411 nm, indicating that all the polymer chains were incorporated into the anionic membrane and not into the zwitterionic. These results confirm the higher affinity of HTMA-PFP for the anionic membrane and can be better seen by plotting the wavelength of the maximum spectral as a function of the lipid composition (Figure 8b). The plot shows that the presence of a small amount of DMPG vesicles is sufficient to observe the position of the maximum closer to 411 than to 418 nm. This conclusion was supported by quenching experiments, which were carried out on the samples using AQS as a quencher (Figure 8c). If effectively all the polymer chains are embedded in the anionic vesicles, then they should not be accessible to the quencher. The fact that the quenching efficiency was close to 0% for samples containing a small amount of DMPG LUVs confirms this hypothesis, confirming the selectivity of HTMA-PFP for anionic lipids.

The preference of HTMA-PFP towards anionic membrane suggests, but does not prove, that the polyelectrolyte can be used to label and visualize populations of anionic vesicles over zwitterionic vesicles. To test this ability, we prepared two series of GUVs at the same lipid concentration, but with different composition. The first GUVs were composed of zwitterionic lipids of DOPC and labeled with the fluorescent probe BODIPY-PC, which could be visualized upon excitation with visible-light. The second series of GUVs also contained DOPC, but were mixed with anionic lipids of 1,2-Dioleoyl-*sn*-glycero-3-phospho-*rac*-(1-glycerol) (DOPG) in a molar ratio of 3:1 (note that GUVs of pure anionic lipids cannot be formed by the electroformation method); no fluorescent probe was added, so they could not be observed via fluorescence microscopy. Equivalent volumes of both preparations were transferred to the same well and microscopy images were recorded before and after the addition of HTMA-PFP. As expected, in the absence of the polymer both types of vesicles were visualized by phase contrast microscopy (Figure 9a), but only some of them (the zwitterionic) were fluorescent under Vis-light (Figure 9b), and no fluorescence image was detected when the sample was excited with UV-light. Fluorescence microscopy images recorded after addition of polyelectrolyte are shown in Figure 10. The pictures show that the vesicles that fluoresce in green upon irradiation with visible light (Figure 10a) are different from those fluorescing in blue with UV-light (Figure 10b). This

result is direct evidence that the polyelectrolyte selectively labels the anionic vesicles and, therefore, supports its potential use as a bacterial imaging probe.

**Figure 8.** (a) Normalized fluorescence emission spectra of HTMA-PFP (1.5  $\mu\text{M}$ ) in a mixture of DMPC and DMPG LUVs (final lipid concentration 1 mM) recorded at increasing anionic vesicle content; (b) position of the fluorescence maximum as a function of increased DMPG vesicle percentage; (c) fluorescence quenching percentage of HTMA-PFP (1.5  $\mu\text{M}$ ) with AQS (5  $\mu\text{M}$ ) versus increased DMPG vesicle percentage.

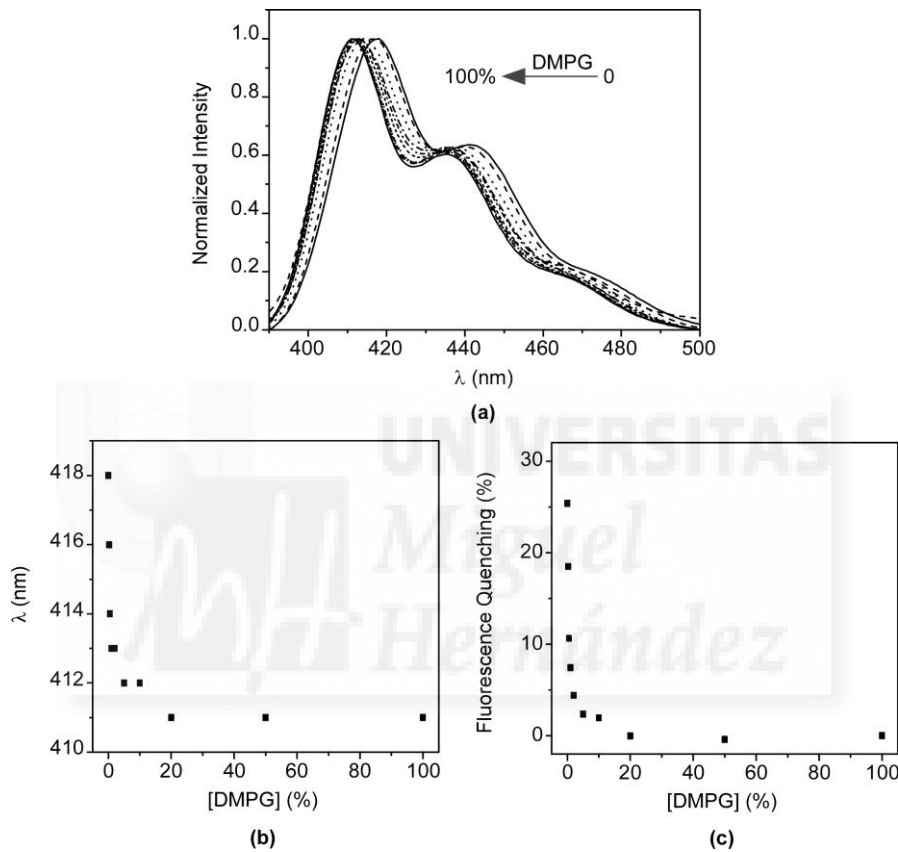


**Figure 9.** Microscopy images of a mixture of GUVs of DOPC-BODIPY and DOPC/DOPG (3:1) observed by (a) phase contrast microscopy and (b) upon excitation with Vis-light (both images correspond to the same field).

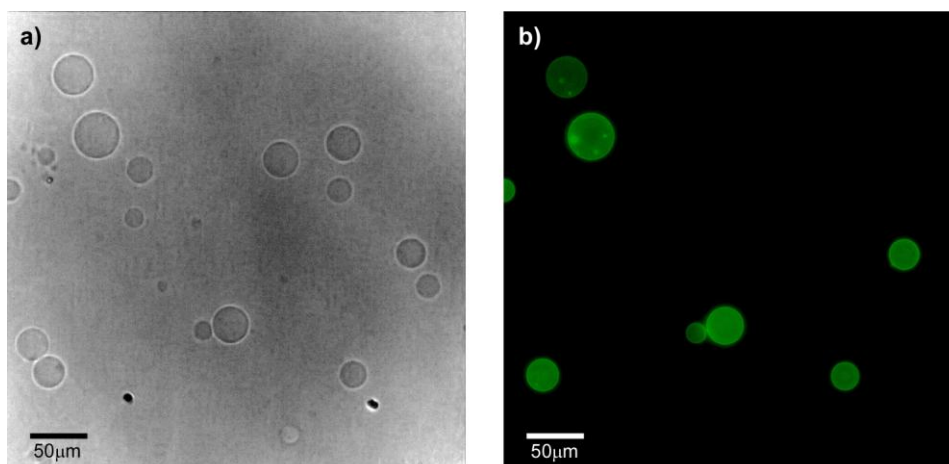
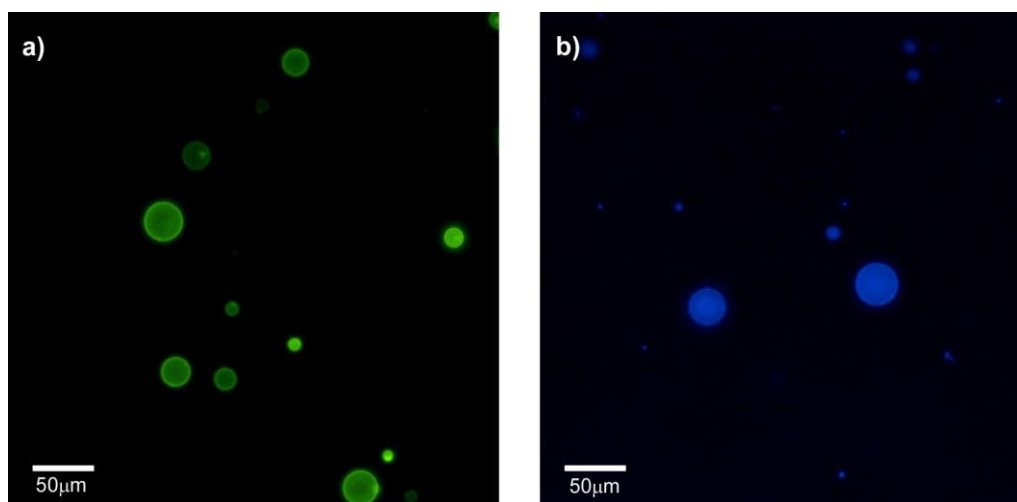


**Figure 10.** Fluorescence microscopy images of a mixture of GUVs of DOPC-BODIPY and DOPC/DOPG (3:1) observed after HTMA-PFP addition, upon excitation with (a) Vis-light and (b) UV-light (both images correspond to the same field).



#### 2.4. Ability of HTMA-PFP to Destabilize Anionic Vesicles

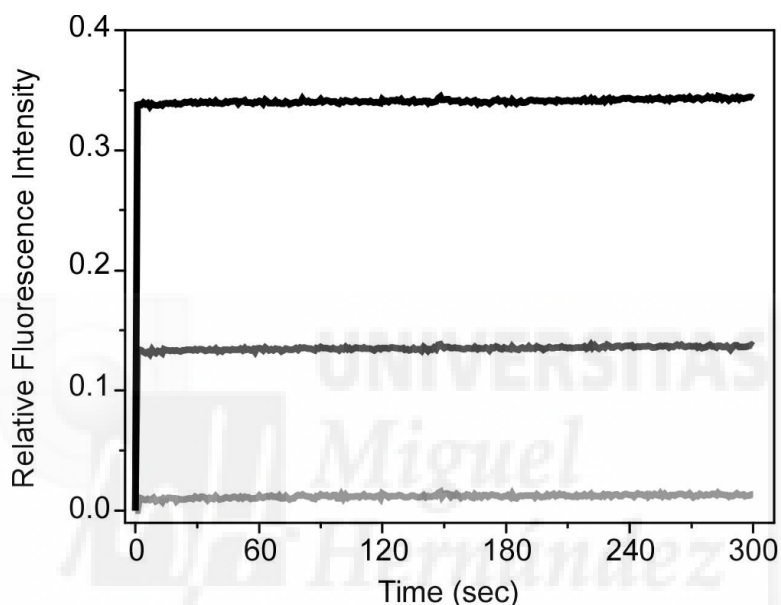
Molecules with quaternary amine groups have been reported to disrupt bacterial membranes causing cell death [36,37]. The biocide action involves perturbation of the bacterial membrane lipid bilayers through interaction of the positively charged quaternary nitrogen with the polar phospholipid head groups. The hydrophobic part of the molecule subsequently interacts and inserts into the hydrophobic membrane core, causing the rearrangement of the membrane and the subsequent leakage of intracellular constituents [38]. Recently, a series of cationic poly(phenylene ethynylene) (PPE)-based conjugated polyelectrolytes containing pendant quaternary amine groups have been described as exhibiting biocidal activity against a variety of bacterial species [47]. In order to explore if HTMA-PFP with these cationic groups could also be used to this end, we evaluated the membrane stability of anionic vesicles as a function of time in the presence of increasing concentrations of polyelectrolyte. Stability was assessed through leakage experiments using the fluorophore carboxyfluorescein (CF), whose absorption and fluorescence do not interfere with that of HTMA-PFP. CF was encapsulated at high concentrations in the aqueous cavity of LUVs composed of DOPG, as described in the Experimental Section. Under these conditions, the CF fluorescence is very low due to self-quenching [48,49]. If the vesicle membrane is perturbed by the incorporation of polyelectrolyte, then the dye is released and the fluorescence signal increases after its dilution in buffer. CF leakage was calculated from Equation (3):

$$\text{CF leakage} = \frac{F - F_0}{F_{\max} - F} \quad (3)$$

where  $F_0$  and  $F$  are the fluorescence intensities of CF in the vesicles in the absence and presence of HTMA-PFP, respectively, and  $F_{\max}$  is the maximum fluorescence intensity of the sample observed after addition of Triton-X100 (10%) that causes the complete lysis of the vesicles. Figure 11 shows the fluorescence leakage profiles from DOPG vesicles upon addition of three increasing concentrations of polyelectrolyte. Results show that at 1.5  $\mu\text{M}$  of HTMA-PFP, the fluorescence leakage was practically

zero and therefore the integrity of the anionic vesicle is maintained at this polymer concentration, as was observed in the previous study [31]. However, higher concentrations caused membrane perturbation and the dye leakage increased as a function of the polymer concentration. The leakage process was very fast, occurring within the first few seconds after the addition of the polyelectrolyte. This suggests that, at these concentrations, the polymer is able to alter the integrity of the anionic vesicles, and that, once internalized, it quickly disrupts the lipid bilayer resulting in membrane rupture.

**Figure 11.** Fluorescence leakage profiles from DOPG vesicles with the addition of HTMA-PFP (1.5  $\mu\text{M}$ ; light grey, 22  $\mu\text{M}$ ; grey, 60  $\mu\text{M}$ ; black line) to phosphate buffer at room temperature.



### 3. Experimental Section

#### 3.1. Materials

The cationic CPE HTMA-PFP ( $M = 8340$  g/mol, repeat unit molecular weight, 694.71 g/mol;  $n' = 12$  based on polyfluorene calibration) was obtained and characterized in our laboratory as previously described [50,51]. In brief, a low-molecular-weight batch of the neutral polymer, poly[9,9-bis(6'-bromohexyl)fluorene-phenylene], was synthesized by Suzuki coupling with Pd(II) as a catalyst and treated with gas-phase trimethylamine to obtain the corresponding cationic polyelectrolyte. Stock solutions of HTMA-PFP ( $3.65 \times 10^{-4}$  M, in repeat units) were prepared in DMSO and stored at  $-20$  °C before use. The fluorescent probes 5-butyl-4,4-difluoro-4-bora-3a,4a-diaza-s-indacene-3-nonanoic acid (BODIPY 500/510  $\text{C}_4, \text{C}_9$ ) and 2-(4,4-difluoro-5-methyl-4-bora-3a,4a-diaza-s-indacene-3-dodecanoyl)-1-hexadecanoyl-sn-glycero-3-phosphocholine (BODIPY-PC) were from Molecular Probes (Eugene, OR, USA). Stock solutions (1 mM) of these probes were prepared in ethanol and stored at  $-20$  °C before use. The fluorescent probe 5(6)-carboxyfluorescein (CF) and the quencher 9,10-anthraquinone-2,6-disulfonic acid (AQS) were obtained from Sigma-Aldrich (St. Louis, MO, USA) and dissolved in DMSO (1.25 M) and water (5 mM), respectively, just before use. The synthetic phospholipids 1,2-Dioleoyl-sn-glycero-3-phosphocholine

(DOPC), 1,2-Dioleoyl-sn-glycero-3-phospho-rac-(1-glycerol) sodium salt (DOPG), 1,2-Dimyristoyl-sn-glycero-3-phosphocholine (DMPC), 1,2-Dimyristoyl-sn-glycero-3-phospho-rac-(1-glycerol) sodium salt (DMPG) and 1,2-Dipalmitoyl-sn-glycero-3-phosphocholine (DPPC) were from Sigma-Aldrich and used as received. All other compounds were of analytical or spectroscopic reagent grade. Sodium phosphate buffer (50 mM, 0.1 M NaCl, pH 7.4) was prepared with water, which was twice distilled in all-glass apparatus and deionized using Milli-Q equipment (Millipore, Madrid, Spain).

### 3.2. LUVs Formation

Chloroform/methanol solutions containing 3 mg of total phospholipid (DOPC, DOPG, DMPC, DMPG, DPPC) were dried first by evaporation under dry nitrogen gas stream and subsequently under vacuum for 3 h. Multilamellar vesicles (MLVs) were formed by resuspending the dried phospholipids (0.5 mM for DOPG and DMPG, 1 mM for DOPC, DMPC and DPPC) in the buffer to the required final concentration. The vesicle suspension was then heated at a temperature above the phospholipid phase transition and vortexed several times. Large unilamellar vesicles (LUVs) were prepared from these MLVs by pressure extrusion through 0.1  $\mu\text{m}$  polycarbonate filters (Nucleopore, Cambridge, MA, USA). For energy transfer experiments, the probe BODIPY C<sub>4</sub> C<sub>9</sub> (at the adequate probe-to-lipid ratio of 1:500) was initially added to the chloroform/methanol solutions containing DMPC and DMPG and LUVs were subsequently prepared as described above.

### 3.3. Preparation of Giant Unilamellar Vesicles (GUVs)

Giant unilamellar vesicles (GUVs) composed of DOPC/DOPG (3/1) and DOPC containing fluorescent probe, BODIPY-PC at the adequate probe-to-lipid ratio (1:250), were prepared by the electroformation method [52,53] using custom made Pt electrode-containing Teflon chambers. Briefly, 1.2  $\mu\text{L}$  of a 1 mM lipid solution in chloroform containing the fluorescent probe was spread on each side of the Pt electrode. Removal of organic solvent traces was carried out by vacuum dehydration. Afterwards, the dried electrodes were hydrated with 450  $\mu\text{L}$  of a 200 mM sucrose solution in Milli-Q purified water. Subsequently, 7 V voltage and 10 Hz frequency signal were applied for 2 h, followed by 1 Hz frequency signal for 30 min. After GUV formation, the sample was collected from the chambers and transferred to the wells of a micro-slide plastic plate, which deposits approximately 500  $\mu\text{L}$  of preparation. To better observe the GUVs under the microscope, 400  $\mu\text{L}$  of a 200 mM glucose solution were previously added to the wells in order to settle the 50  $\mu\text{L}$  of GUVs to the bottom of the chamber. Samples were preserved for 2 h at 10  $^{\circ}\text{C}$  before microscopic visualization.

### 3.4. Preparation of HTMA-PFP/Lipid Samples

Aliquots of HTMA-PFP in DMSO were externally added to the lipid vesicle suspension, well above the phospholipid phase transition to ensure that the membrane was in the fluid phase. In all cases, the proportion of DMSO in the aqueous sample was always lower than 1% (V/V). In most samples, the final concentration of HTMA-PFP was 1.5  $\mu\text{M}$  in terms of repeat units.

### 3.5. Absorption and Fluorescence Spectra

Absorption measurements were carried out at room temperature using a UV-1603 spectrophotometer (Shimadzu, Tokyo, Japan). Fluorescence spectra and fluorescence intensity measurements were performed on a QuantaMaster spectrofluorometer (PTI, Birmingham, NJ, USA) interfaced with a Peltier cell. The experimental samples were placed in 10 mm × 10 mm path length quartz cuvettes. The excitation wavelength for HTMA-PFP was set to 380 nm. Background intensities were always checked and subtracted from the sample when necessary.

### 3.6. Fluorescence Microscopy Measurements

Fluorescence microscopy images were recorded using a Nikon Eclipse TE2000-U (Melville, NY, USA) inverted microscope equipped with a Nikon Digital Sight DS-1QM/H and Nikon Digital Camera DXM1200. UV excitation ( $340 \text{ nm} \leq \lambda_{\text{ex}} \leq 380 \text{ nm}$ ) and blue emission ( $435 \text{ nm} \leq \lambda_{\text{em}} \leq 485 \text{ nm}$ ) was filtered using a DAPI filter cube. Visible excitation ( $465 \text{ nm} \leq \lambda_{\text{ex}} \leq 495 \text{ nm}$ ) and green emission ( $515 \text{ nm} \leq \lambda_{\text{em}} \leq 555 \text{ nm}$ ) was filtered using a FITR filter cube. Data acquisition was monitored successively by manually formatting and data processing with NIS-Elements AR 2.30 software.

### 3.7. Quenching Experiments

Fluorescence emission of HTMA-PFP was studied in the absence and presence of different concentrations of AQS in DMPC LUVs. Stern-Volmer analysis was applied to the fluorescence quenching data according to Equation (4):

$$\frac{I_0}{I} = 1 + K_{SV}[Q] \quad (4)$$

where  $I_0$  and  $I$  stand for the steady-state fluorescence intensities in the absence and presence of quencher, respectively, and  $[Q]$  is the quencher concentration. The significance of  $K_{SV}$  depends on the nature of the quenching process: it may represent the association constant for complex formation or the rate of dynamic quenching ( $K_{SV} = k_q\tau_0$ ); where  $k_q$  is the bimolecular rate constant of the quenching process and  $\tau_0$  is the lifetime of the biomolecule. For dynamic quenching (diffusion-controlled quenching),  $k_q$  may be as high as  $10^{10} \text{ M}^{-1}\cdot\text{s}^{-1}$ . If  $k_q$  is greater than this value, it usually indicates static quenching via a complexation between the fluorophore and the quencher.

### 3.8. Measurements of Vesicle Leakage Induced by Polymers

DOPG LUVs were prepared with carboxyfluorescein (CF) trapped in the aqueous interior at a concentration of 40 mM, in a buffer containing 50 mM phosphate and 0.1 M NaCl, pH 7.4. The non-encapsulated CF was removed by gel filtration over a column packed with Sephadex G-75 (Pharmacia, Uppsala, Switzerland) eluted with buffer containing 50 mM phosphate, 0.1 M NaCl, pH 7.4. Self-quenching is expected at high concentrations of CF within the small volume of the vesicle interior. Membrane rupture (leakage) of intraliposomal CF was assayed by treating the probe-loaded vesicles with the appropriate amounts of HTMA-PFP. The total rupture of the vesicles and release of CF was performed with Triton X-100 10%.

### 3.9. Calorimetry

Differential scanning calorimetry (DSC) experiments were performed in a high-resolution Microcal MC-2 differential scanning microcalorimeter (GE Healthcare, Piscataway, NJ, USA) under a constant external pressure of 30 psi in order to avoid bubble formation. The excess heat capacity functions were analyzed using Origin 7.0 (Microcal Software). Differences in the heat capacity between the sample and the reference cell, which contained only buffer, were obtained by raising the temperature 1 °C/min over a range from 16 to 36 °C for the DMPC samples in the absence and presence of different concentrations of the HTMA-PFP. A series of three consecutive scans of the same sample were performed to ensure scan-to-scan reproducibility and reversibility.

### 3.10. Molecular Dynamics Simulations

The three-dimensional model of HTMA-PFP was first generated using ChemDraw 10.0 (CambridgeSoft), and then refined with Chem3D (CambridgeSoft) using the MM2 energy minimization procedure.

## 4. Conclusions

The interaction of the cationic polyfluorene HTMA-PFP with zwitterionic lipid bilayers was characterized and compared with the interaction reported for anionic bilayers in order to explore the possibility of using this polyelectrolyte as a bacterial imaging probe. Results indicate that HTMA-PFP at low concentrations associates spontaneously with both type of lipid vesicles, retaining their structural integrity without altering their spherical morphology. The polyelectrolyte shows higher affinity for anionic membranes than for zwitterionic membranes, as well as a different final membrane location. While in the anionic membrane, the polyelectrolyte is embedded within the lipid bilayer, in the zwitterionic system it remains close to the surface, forming aggregates that are sensitive to the physical state of the lipid bilayer. On the basis of these results, it is possible to conclude that the nature of the interaction between HTMA-PFP and lipid membranes depends on the lipid charge. Although an electrostatic interaction was expected to be responsible for the high affinity for anionic membranes, the final location of the polyelectrolyte, which is well-embedded in the bilayer core, indicates that hydrophobic forces also contribute to its solubilisation, reducing its aggregation state and increasing its fluorescence quantum yield compared to zwitterionic membranes. Fluorescence microscopy images of a mixture of anionic and zwitterionic vesicles confirm that HTMA-PFP selectively labels the anionic vesicles. In addition, leakage experiments indicate that the addition of higher amounts of polyelectrolyte destabilizes the anionic lipid bilayer, producing membrane rupture. Therefore, in conclusion, this work supports the use of HTMA-PFP as a fluorescent marker in membrane studies and indicates that, given its different behaviour towards anionic and zwitterionic membranes, the polyelectrolyte could be used for selective recognition, imaging, and killing of bacteria over mammalian cells.

## Acknowledgments

The authors thank the Spanish Ministerio de Economía y Competitividad and Generalitat Valenciana for financial support MAT-2011-23007 and PROMETEO/2013/018, respectively.

## Author Contributions

Zehra Kahveci conducted most of the experiments related to this study under the supervision of C. Reyes Mateo. The work was planned by C. Reyes Mateo and Ricardo Mallavia. The conjugated polyelectrolyte was synthesized and provided by Ricardo Mallavia. María José Martínez-Tomé collaborated in the fluorescence measurements and Rocío Esquembre in the fluorescence microscopy studies. The paper was written and edited by Zehra Kahveci and C. Reyes Mateo.

## Conflicts of Interest

The authors declare no conflict of interest.

## References

1. Kepczynski, M.; Jamroz, D.; Wyrwal, M.; Bednar, J.; Rząd, E.; Nowakowska, M. Interactions of a hydrophobically modified polycation with zwitterionic lipid membranes. *Langmuir* **2012**, *28*, 676–688.
2. Parhamifar, L.; Larsen, A.K.; Hunter, A.C.; Andresen, T.L.; Moghimi, S.M. Polycation cytotoxicity: A delicate matter for nucleic acid therapy—Focus on polyethylenimine. *Soft Matter* **2010**, *6*, 4001–4009.
3. Stadler, B.; Chandrawati, R.; Goldie, K.; Caruso, F. Capsosomes: Subcompartmentalizing polyelectrolyte capsules using liposomes. *Langmuir* **2009**, *25*, 6725–6732.
4. Ding, L.; Chi, E.Y.; Schanze, K.S.; Lopez, G.P.; Whitten, D.G. Insight into the mechanism of antimicrobial conjugated polyelectrolytes: Lipid headgroup charge and membrane fluidity effects. *Langmuir* **2010**, *26*, 5544–5550.
5. Eren, T.; Som, A.; Rennie, J.R.; Nelson, C.F.; Urgina, Y.; Nusslein, K.; Coughlin, E.B.; Tew, G.N. Antibacterial and hemolytic activities of quaternary pyridinium functionalized polynorbornenes. *Macromol. Chem. Phys.* **2008**, *209*, 516–524.
6. Thomas, S.W., III; Joly, G.D.; Swager, T.M. Chemical sensors based on amplifying fluorescent conjugated polymers. *Chem. Rev.* **2007**, *107*, 1339–1386.
7. Pu, K.Y.; Cai, L.; Liu, B. Design and synthesis of charge-transfer-based conjugated polyelectrolytes as multicolor light-up probes. *Macromolecules* **2009**, *42*, 5933–5940.
8. Liu, Y.; Ogawa, K.; Schanze, K.S. Conjugated polyelectrolytes as fluorescent sensors. *J. Photochem. Photobiol. C Photochem. Rev.* **2009**, *10*, 173–190.
9. Ngo, A.T.; Karam, P.; Cosa, G. Conjugated polyelectrolyte-lipid interactions: Opportunities in biosensing. *Pure Appl. Chem.* **2011**, *83*, 43–55.
10. Wang, B.; Yuan, H.; Zhu, C.; Yang, Q.; Lv, F.; Liu, L.; Wang, S. Polymer-drug conjugates for intracellular molecule-targeted photoinduced inactivation of protein and growth inhibition of cancer cells. *Sci. Rep.* **2012**, *2*, doi:10.1038/srep00766.

11. Wang, L.; Li, H.; Cao, D. Conjugated polyelectrolytes: Synthesis and application in biomolecule detection. *Curr. Org. Chem.* **2012**, *16*, 1468–1484.
12. Feng, G.; Ding, D.; Liu, B. Fluorescence bioimaging with conjugated polyelectrolytes. *Nanoscale* **2012**, *4*, 6150–6165.
13. Kim, I.B.; Shin, H.; Garcia, A.J.; Bunz, U.H.F. Use of a folate-PPE conjugate to image cancer cells *in vitro*. *Bioconjug. Chem.* **2007**, *18*, 815–820.
14. McRae, R.L.; Phillips, R.L.; Kim, I.B.; Bunz, U.H.F.; Fahrni, C.J. Molecular recognition based on low-affinity polyvalent interactions: Selective binding of a carboxylated polymer to fibronectin fibrils of live fibroblast cells. *J. Am. Chem. Soc.* **2008**, *130*, 7851–7853.
15. Nilsson, K.P.R.; Hammarström, P. Luminescent conjugated polymers: Illuminating the dark matters of biology and pathology. *Adv. Mater.* **2008**, *20*, 2639–2645.
16. Pu, K.Y.; Liu, B. Fluorescent conjugated polyelectrolytes for bioimaging. *Adv. Funct. Mater.* **2011**, *21*, 3408–3423.
17. Tang, Y.; Liu, Y.; Cao, A. Strategy for sensor based on fluorescence emission red shift of conjugated polymers: Applications in pH response and enzyme activity detection. *Anal. Chem.* **2013**, *85*, 825–830.
18. Zhu, C.; Yang, Q.; Liu, L.; Wang, S. A potent fluorescent probe for the detection of cell apoptosis. *Chem. Commun.* **2011**, *47*, 5524–5526.
19. Zhu, C.; Liu, L.; Yang, Q.; Lv, F.; Wang, S. Water-soluble conjugated polymers for imaging, diagnosis, and therapy. *Chem. Rev.* **2012**, *112*, 4687–4735.
20. Monteserín, M.; Burrows, H.D.; Valente, A.J.M.; Lobo, V.M.M.; Mallavia, R.; Tapia, M.J.; García-Zubiri, I.X.; di Paolo, R.E.; Maçanita, A.L. Modulating the emission intensity of poly-(9,9-bis(6'-N,N,N-trimethylammonium)hexyl)-fluorene phenylene bromide through interaction with sodium alkylsulfonate surfactants. *J. Phys. Chem. B* **2007**, *111*, 13560–13569.
21. Wang, S.; Bazan, G.C. Solvent-dependent aggregation of a water-soluble poly(fluorene) controls energy transfer to chromophore-labeled DNA. *Chem. Commun.* **2004**, *10*, 2508–2509.
22. Burrows, H.D.; Lobo, V.M.M.; Pina, J.; Ramos, M.L.; de Seixas Melo, J.; Valente, A.J.M.; Tapia, M.J.; Pradhan, S.; Scherf, U. Fluorescence enhancement of the water-soluble poly{1,4-phenylene-[9,9-bis-(4-phenoxybutyl)sulfonate]fluorene-2,7-diyl} copolymer in *n*-dodecylpentaoxyethylene glycol ether micelles. *Macromolecules* **2004**, *37*, 7425–7427.
23. Knaapila, M.; Almasy, L.; Garamus, V.M.; Pearson, C.; Pradhan, S.; Petty, M.C.; Scherf, U.; Burrows, H.D.; Monkman, A.P. Solubilization of polyelectrolytic hairy-rod polyfluorene in aqueous solutions of nonionic surfactant. *J. Phys. Chem. B* **2006**, *110*, 10248–10257.
24. Monteserín, M.; Tapia, M.J.; Ribeiro, A.C.F.; Santos, C.I.A.V.; Valente, A.J.M.; Burrows, H.D.; Mallavia, R.; Nilsson, M.; Soderman, O. Multicomponent interdiffusion and self-diffusion of the cationic poly{[9,9-bis(6'-N,N,N-trimethylammonium)hexyl]fluorene-phenylene} dibromide in a dimethyl sulfoxide + water solution. *J. Chem. Eng. Data* **2010**, *55*, 1860–1866.
25. Martínez-Tome, M.J.; Esquembre, R.; Mallavia, R.; Mateo, C.R. Formation of complexes between the conjugated polyelectrolyte poly{[9,9-bis(6'-N,N,N-trimethylammonium)hexyl]fluorene-phenylene} bromide (HTMA-PFP) and human serum albumin. *Biomacromolecules* **2010**, *11*, 1494–1501.

26. Montserrat, M.; Burrows, H.D.; Valente, A.J.M.; Mallavia, R.; di Paolo, R.E.; Maçanita, A.L.; Tapia, M.J. Interaction between poly(9,9-bis(6'-N,N,N-trimethylammonium)hexyl]fluorene phenylene) bromide and DNA as seen by spectroscopy, viscosity, and conductivity: Effect of molecular weights and DNA secondary structure. *J. Phys. Chem. B* **2009**, *113*, 1294–1302.
27. Tapia, M.J.; Montserrat, M.; Valente, A.J.M.; Burrows, H.D.; Mallavia, R. Binding of polynucleotides to conjugated polyelectrolytes and its applications in sensing. *Adv. Colloid Interface Sci.* **2010**, *158*, 94–107.
28. Liu, B.; Wang, S.; Bazan, G.C.; Mikhailovsky, A. Shape-adaptable water-soluble conjugated polymers. *J. Am. Chem. Soc.* **2003**, *125*, 13306–13307.
29. Liu, B.; Bazan, G.C. Optimization of the molecular orbital energies of conjugated polymers for optical amplification of fluorescent sensors. *J. Am. Chem. Soc.* **2006**, *128*, 1188–1196.
30. Pinto, S.M.; Burrows, H.D.; Pereira, M.M.; Fonseca, S.M.; Dias, F.B.; Mallavia, R.; Tapia, M.J. Singlet-singlet energy transfer in self-assembled systems of the cationic poly{9,9-bis[6'-N,N,N-trimethylammoniumhexyl]fluorene-co-1,4-phenylene} with oppositely charged porphyrins. *J. Phys. Chem. B* **2009**, *113*, 16093–16100.
31. Kahveci, Z.; Martınez-Tomé, M.J.; Mallavia, R.; Mateo, C.R. Use of the conjugated polyelectrolyte poly{[9,9-bis(6'-N,N,N-trimethylammonium)hexyl]fluorene-phenylene} bromide (HTMA-PFP) as a fluorescent membrane marker. *Biomacromolecules* **2013**, *14*, 1990–1998.
32. Leevy, W.M.; Gammon, S.T.; Jiang, H.; Johnson, J.R.; Maxwell, D.J.; Jackson, E.N.; Marquez, M.; Piwnica-Worms, D.; Smith, B.D. Optical imaging of bacterial infection in living mice using a fluorescent near-infrared molecular probe. *J. Am. Chem. Soc.* **2006**, *128*, 16476–16477.
33. Leevy, W.M.; Gammon, S.T.; Johnson, J.R.; Lampkins, A.J.; Jiang, H.; Marquez, M.; Piwnica-Worms, D.; Suckow, M.A.; Smith, B.D. Noninvasive optical imaging of *Staphylococcus aureus* bacterial infection in living mice using a bis-dipicolylamine-zinc(II) affinity group conjugated to a near-infrared fluorophore. *Bioconjug. Chem.* **2008**, *19*, 686–692.
34. Sasser, T.A.; van Avermaete, A.E.; White, A.; Chapman, S.; Johnson, J.R.; van Avermaete, T.; Gammon, S.T.; Leevy, W.M. Bacterial infection probes and imaging strategies in clinical nuclear medicine and preclinical molecular imaging. *Curr. Top. Med. Chem.* **2013**, *13*, 479–487.
35. Liu, C.; Gu, Y. Noninvasive optical imaging of *staphylococcus aureus* infection *in vivo* using an antimicrobial peptide fragment based near-infrared fluorescent probes. *J. Innov. Opt. Health Sci.* **2013**, *6*, doi:10.1142/S1793545813500260.
36. Laopaiboon, L.; Hall, S.J.; Smith, R.N. The effect of a quaternary ammonium biocide on the performance and characteristics of laboratory-scale rotating biological contactors. *J. Appl. Microbiol.* **2002**, *93*, 1051–1058.
37. Kenawy, E.R.; Worley, S.D.; Broughton, R. The chemistry and applications of antimicrobial polymers: A state-of-the-art review. *Biomacromolecules* **2007**, *8*, 1359–1384.
38. McBain, A.J.; Ledger, R.G.; Moore, L.E.; Catrenich, C.E.; Gilbert, P. Effects of quaternary-ammonium-based formulations on bacterial community dynamics and antimicrobial susceptibility. *Appl. Environ. Microbiol.* **2004**, *70*, 3449–3456.
39. Coutinho, A.; Prieto, M. Self-association of the polyene antibiotic nystatin in dipalmitoylphosphatidylcholine vesicles: A time-resolved fluorescence study. *Biophys. J.* **1995**, *69*, 2541–2557.

40. Davenport, L.; Dale, R.E.; Bisby, R.H.; Cundall, R.B. Transverse location of the fluorescent probe 1,6-diphenyl-1,3,5-hexatriene in model lipid bilayer membrane systems by resonance excitation energy transfer. *Biochemistry* **1985**, *24*, 4097–4108.
41. Al Attar, H.A.; Monkman, A.P. Effect of surfactant on water-soluble conjugated polymer used in biosensor. *J. Phys. Chem. B* **2007**, *111*, 12418–12426.
42. Chemburu, S.; Ji, E.; Casana, Y.; Wu, Y.; Buranda, T.; Schanze, K.S.; Lopez, G.P.; Whitten, D.G. Conjugated polyelectrolyte supported bead based assays for phospholipase A<sub>2</sub> activity. *J. Phys. Chem. B* **2008**, *112*, 14492–14499.
43. Chen, J.; Dong, W.F.; Mähwald, H.; Krastev, R. Amplified fluorescence quenching of self-assembled polyelectrolyte—Dye nanoparticles in aqueous solution. *Chem. Mater.* **2008**, *20*, 1664–1666.
44. Levitus, M.; Schmieder, K.; Ricks, H.; Shimizu, K.D.; Bunz, U.H.F.; Garcia-Garibay, M.A. Steps to demarcate the effects of chromophore aggregation and planarization in poly(phenyleneethynylene)s. 1. Rotationally interrupted conjugation in the excited states of 1,4-bis(phenylethynyl)benzene. *J. Am. Chem. Soc.* **2001**, *123*, 4259–4265.
45. Heimburg, T. A model for the lipid pretransition: Coupling of ripple formation with the chain-melting transition. *Biophys. J.* **2000**, *78*, 1154–1165.
46. Riske, K.A.; Barroso, R.P.; Vequi-Suplicy, C.C.; Germano, R.; Henriques, V.B.; Lamy, M.T. Lipid bilayer pre-transition as the beginning of the melting process. *Biochim. Biophys. Acta* **2009**, *1788*, 954–963.
47. Wang, Y.; Tang, Y.; Zhou, Z.; Ji, E.; Lopez, G.P.; Chi, E.Y.; Schanze, K.S.; Whitten, D.G. Membrane perturbation activity of cationic phenylene ethynylene oligomers and polymers: Selectivity against model bacterial and mammalian membranes. *Langmuir* **2010**, *26*, 12509–12514.
48. Bandyopadhyay, P.; Bandyopadhyay, P.; Regen, S.L. An ion conductor that recognizes osmotically-stressed phospholipid bilayers. *J. Am. Chem. Soc.* **2002**, *124*, 11254–11255.
49. Van Renswoude, J.; Hoekstra, D. Cell-induced leakage of liposome contents. *Biochemistry* **1981**, *20*, 540–546.
50. Mallavia, R.; Martínez-Peréz, D.; Chmelka, B.F.; Bazan, G.C. Blue fluorescent films based on poly-2,7-fluorene-phenylene derivatives. *Bol. Soc. Esp. Ceram. Vidrio* **2004**, *43*, 327–330.
51. Molina, R.; Gómez-Ruiz, S.; Montilla, F.; Salinas-Castillo, A.; Fernández-Arroyo, S.; del Mar Ramos, M.; Micol, V.; Mallavia, R. Progress in the synthesis of poly(2,7-fluorene-alt-1,4-phenylene), PFP, via suzuki coupling. *Macromolecules* **2009**, *42*, 5471–5477.
52. Angelova, M.I.; Dimitrov, D.S. Liposome electroformation. *Faraday Discuss. Chem. Soc.* **1986**, *81*, 303–311.
53. Esquembre, R.; Pinto, S.N.; Poveda, J.A.; Prieto, M.; Mateo, C.R. Immobilization and characterization of giant unilamellar vesicles (GUVs) within porous silica glasses. *Soft Matter* **2012**, *8*, 408–417.



## Publication 8.3





**New Red-Emitting Conjugated Polyelectrolyte: Stabilization by Interaction with Biomolecules and Potential Use as Drug Carriers and Bioimaging Probes**

**Zehra Kahveci, Rebeca Vázquez-Guilló, Maria José Martínez-Tomé, Ricardo Mallavia  
and C. Reyes Mateo**

Instituto de Biología Molecular y Celular, Universidad Miguel Hernández, 03202  
Elche, Spain

**ACS Appl. Mater. Interfaces, 2016, 8 (3), 1958–1969**

**DOI: 10.1021/acsami.5b10167**

Impact Factor: **7.145**



# New Red-Emitting Conjugated Polyelectrolyte: Stabilization by Interaction with Biomolecules and Potential Use as Drug Carriers and Bioimaging Probes

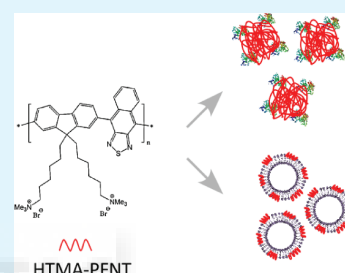
Zehra Kahveci, Rebeca Vázquez-Guilló, Maria José Martínez-Tomé, Ricardo Mallavia, and C. Reyes Mateo\*

Instituto de Biología Molecular y Celular, Universidad Miguel Hernández, 03202 Elche, Alicante, Spain

## Supporting Information

**ABSTRACT:** The design and development of fluorescent conjugated polyelectrolytes (CPEs) emitting in the red region of the visible spectrum is at present of great interest for bioimaging studies. However, despite the wide variety of CPEs available, stable bright red-emitters remain scarce due to their low solubility and instability in aqueous media, consequently limiting their applications. In this work, we have synthesized and characterized a new red-emitting cationic conjugated polyelectrolyte copoly- $\{[9,9\text{-bis}(6'\text{-}N,N,N\text{-trimethylammonium)hexyl}]-2,7\text{-}(\text{fluorene})\text{-}alt\text{-}1,4\text{-}(\text{naphtho}[2,3c]\text{-}1,2,5\text{-thiadiazole})\}$  bromide (HTMA-PFNT), based on the incorporation of naphtho[2,3c][1,2,5]thiadiazole on fluorene backbone to increase the bathochromic emission, extending the conjugation length in the polymer backbone. Water stabilization was achieved by binding the polyelectrolyte to two different biological systems which are currently used as nanocarriers: human serum albumin (HSA) and lipid vesicles. Using both systems, stable nanostructures of different composition were obtained and their properties were characterized. The properties of the protein-based nanoparticles are consistent with polyelectrolyte aggregates covered with HSA molecules, while the liposome system is composed of lipid vesicles coated with polyelectrolyte chains partially inserted in the bilayer. Both protein and vesicle structural integrity were not affected after their interaction with HTMA-PFNT, as well as the carrier properties, allowing for the binding and transport of ligands. In addition, the nanoparticles displayed the ability of labeling the cell membrane of living cells. All these results extend the potential applications of these novel multifunctional nanoparticles as therapeutic carriers and bioimaging probes.

**KEYWORDS:** conjugated polyelectrolytes, naphthothiadiazol, polyelectrolyte-protein interactions, polyelectrolyte-liposome interactions, bioimaging probes, multifunctional nanoparticles



## INTRODUCTION

Fluorescent conjugated polyelectrolytes (CPEs) are a class of conjugated polymers having backbones with  $\pi$ -delocalized electronic structures and pendant substituents with ionic functionalities. Electron delocalization facilitates rapid intra- and interchain exciton migration, conferring collective optical responses and amplified signals when comparing to conventional fluorophores.<sup>1,2</sup> In general, CPEs have high absorptivity and photostability, large Stokes shift and low cytotoxicity, and have easily amenable side chains for bioconjugation with various recognition elements. In addition, the photophysical properties of these polyelectrolytes can be feasibly customized through backbone and side-chain modifications. Given these properties, CPEs have received great attention in biomedical applications, especially for developing biosensing schemes and sensing devices for biomolecules.<sup>3–8</sup> More recently CPEs appear as an alternative to fluorescent markers used in bioimaging because they overcome most of the limitations associated with these fluorescent materials, such as the photobleaching of organic dyes and fluorescent proteins or the cytotoxicity of quantum dots.<sup>9,10</sup> Conjugated with appropriate recognition elements, CPEs can be used as tracers,

which will selectively accumulate in specific regions of the organism (tumors, inflamed areas, etc.).<sup>3,9</sup>

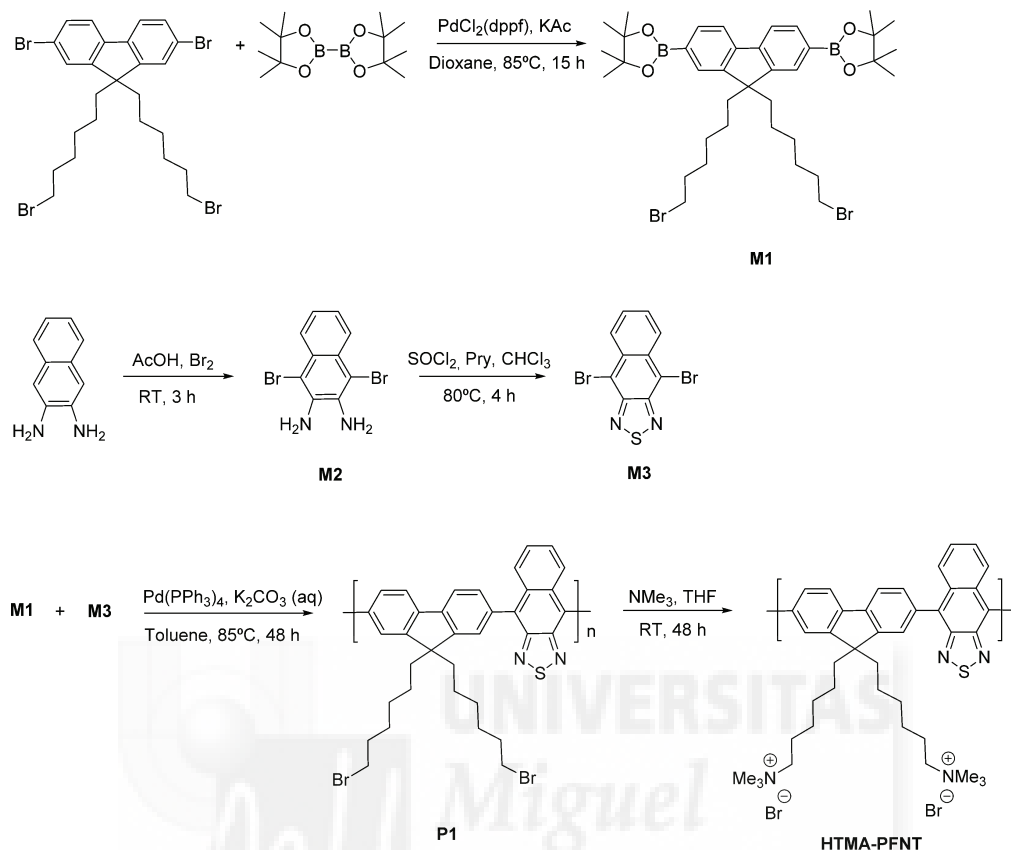
For biomedical applications such as bioimaging the prerequisite condition is the dispersibility of CPEs in aqueous media. Although the incorporation of ionic side groups contributes to water solubilization, these polyelectrolytes still have a strong tendency to aggregate in this medium due to their hydrophobic aromatic backbone, forming unstable heterogeneous nanoaggregates. It results in a reduction in the photoluminescence quantum yield as a consequence of their self-quenching, which is not desirable for many of these applications. To overcome this drawback different approaches are being carried out through the addition of ionic and nonionic surfactants, lipids, cyclodextrins, and proteins or by encapsulating the CPEs in porous silica matrix in order to reduce CPEs aggregation in water.<sup>11–14</sup> Another approach is to fabricate CPEs nanoparticles through various synthetic techniques including polymerization, emulsion, and nanoprecipitation.<sup>15</sup>

**Received:** October 23, 2015

**Accepted:** December 28, 2015

**Published:** December 28, 2015

**Scheme 1. Synthetic Approach of Copoly-[[9,9-bis(6'-*N,N,N*-trimethylammonium)hexyl]-2,7-(fluorene)-*alt*-1,4-(naphtho[2,3c]-1,2,5-thiadiazole)} Bromide (HTMA-PFNT)**



Fluorene-based CPEs consist of a rigid hydrophobic polyfluorene backbone with flexible charged side chains, which induces interesting aggregation behavior. They have unique properties such as facile substitution at the fluorene C9 position, good chemical and thermal stability, and high fluorescence quantum yield. It is possible to increase the processability of these CPEs by incorporation of different ionic side groups and/or with modification of the main chain by adding some other groups. Incorporation of the ionic side groups increases the solubility in polar solvents and water. Besides, modification of the main chain induces changes in photophysical properties of the fluorene backbone.<sup>7,16–19</sup> Normally, fluorene-based CPEs emit blue light, but researchers in the area are making significant efforts to tune color to longer wavelengths. Color can be tuned, among others, by copolymerizing the fluorene monomers with other low band gap monomers or incorporating monomers able to conjugate with the fluorene ring in order to extend the conjugation length into the chain.<sup>20</sup> With these strategies polyfluorenes emitting in the green and yellow region of visible spectrum have been successfully synthesized.<sup>21</sup> Synthesis of probes emitting in the red region is at present of great interest for *in vivo* fluorescence imaging studies because of minimum photodamage to biological samples, deep tissue penetration, and minimum interference from background autofluorescence by biomolecules in the living systems. However, despite the large amount of CPEs synthesized, bright red-emitters remain rare.<sup>15,22</sup> This is because the most widely used strategy to obtain these CPEs is the introduction of donor–acceptor structures in the

aromatic backbone, which increases the hydrophobic character of the polymer, favoring aggregation in aqueous media and therefore reducing the fluorescence quantum yield. For example, Huang et al. have recently synthesized a red emissive polyfluorene with very low cytotoxicity and excellent photostability that was employed for cell imaging, but it was found to aggregate in the aqueous environment of cell culture medium because of the relatively hydrophobic chain structure.<sup>23</sup> Several strategies have been reported to increase the quantum yield of these red-probes, such as the incorporation of bulky pendants into the backbone or side chain in order to avoid compact aggregation or the introduction of small amounts of narrow-band gap moieties as energy acceptors into the backbone to facilitate intra- and interchain energy transfer in the aggregate state.<sup>15,24</sup> Finally, one other strategy may be to disrupt aggregations through the coupling with complexing agents, as was previously mentioned, or with biological nanostructures having different functional properties. This last alternative has the advantage of not only increasing the fluorescence signal of the polyelectrolyte but also stabilizing it in aqueous solution obtaining nanoparticles which combine the properties of both constituents.<sup>25</sup>

Our group has previously synthesized a blue-emitter cationic conjugated polyelectrolyte, copoly-[[9,9-bis(6'-*N,N,N*-trimethylammonium)hexyl]-2,7-(fluorene)-*alt*-1,4-(phenylene)} bromide (HTMA-PFP), which incorporates a phenyl group on the fluorene backbone and shows interesting properties as a fluorescent marker.<sup>12,26,27</sup> Here we describe the synthesis and characterization of a new red-emitter cationic polyfluorene,

copoly- $\{[9,9\text{-bis}(6'\text{-}N,N,N\text{-trimethylammonium})\text{hexyl}]\text{-}2,7\text{-}(\text{fluorene})\text{-}alt\text{-}1,4\text{-}(\text{naphtho}[2,3c]\text{-}1,2,5\text{-thiadiazole})\}$  bromide (HTMA-PFNT), which incorporates the chromophore naphtho $[2,3c][1,2,5]$  thiadiazole (NTD) instead of the phenyl group to increase the bathochromic emission, extending the conjugation length in the polymer backbone. Water solubilization and stabilization were improved by complexing the polyelectrolyte with two different biological systems: human serum albumin (HSA) and lipid vesicles. Both systems are macromolecular carriers capable of accommodating a wide variety of drugs and contain reactive functional groups (in the case of HSA) or can be functionalized (in the case of liposomes) for targeting ligands.<sup>28,29</sup> Using both strategies, stable fluorescent nanostructures were obtained and characterized, and their functional properties were evaluated. Results show that protein structure and integrity of the vesicles as well as carrier properties were not affected after their interaction with HTMA-PFNT. Therefore, the complexation of the polyelectrolyte with the biological systems not only favors its solubility and stability in aqueous solvent but also leads to fluorescent nanoparticles which combine the properties of both constituents and can be potentially used as drug carriers and bioimaging probes.

## EXPERIMENTAL SECTION

**Materials.** For chemical reactions all solvents were at HPLC grade and used as received (Aldrich Corporation). 2,3-Diaminonaphthalene and 9,9-bis(6-bromohexyl)-2,7-dibromofluorene were provided from TCI Europe and SYNTHON Chemicals GmbH & Co, respectively. The human serum albumin (HSA) and synthetic phospholipid 1,2-dioleoyl-*sn*-glycero-3-phosphocholine (DOPC) were from Sigma-Aldrich, as well as Rhodamine 6G, and were used as received. The fluorescent probes 5(6)-carboxyfluorescein (CF) and 1,6-diphenyl-1,3,5-hexatriene (DPH) and the quencher 9,10-anthraquinone-2,6-disulfonic acid (AQS) were obtained from Sigma-Aldrich (St. Louis, MO, USA) and dissolved in dimethyl sulfoxide (DMSO) (1.25 M), dimethylformamide (DMF) (1 mM), and water (5 mM), respectively, just before use. All other solvents were of spectroscopic reagent grade (UVASOL, Merck). Sodium phosphate buffer (50 mM, 0.1 M NaCl, pH 7.4) was prepared with water, which was twice distilled in an all-glass apparatus and deionized using Milli-Q equipment (Millipore, Madrid, Spain).

**Synthesis and Characterization of Polyelectrolytes.** Monomers 2,7-(4,4,5,5-tetramethyl-[1,3,2] dioxaborolane)-9,9-bis(6'-bromohexyl)-fluorene (M1), 1,4-dibromo-2,3-diaminonaphthalene (M2), and 4,9-dibromonaphtho $\{2,3\}$ -1,2,5-thiadiazole (M3) were obtained as previously described by Bazan et al.,<sup>18</sup> Yang et al.,<sup>30</sup> and Tena et al.,<sup>31</sup> respectively (see Scheme 1).

**Synthesis of Copoly-[9,9-bis(6'-bromohexyl)-2,7-fluorene-*alt*-1,4-(naphtho[2,3c]-1,2,5-thiadiazole)] (P1).** A mixture of M3 (1.25 mmol), M1 (1.25 mmol), and  $[\text{Pd}(\text{PPh}_3)_4]$  (0.02 mmol) was dissolved in toluene (25 mL), and a water solution of  $\text{K}_2\text{CO}_3$  (15 mL, 2M) was added. The mixture was stirred at 85 °C for 48 h in an inert atmosphere. An end-capping procedure was realized using bromobenzene and phenylboronic acid. Afterward, 150 mL of methanol was added, and the precipitated product was collected by filtration and washed twice with methanol (150 mL) and acetone (75 mL). The solid was washed with brine, extracted with chloroform, dried over anhydrous magnesium sulfate, and filtered, and the solvent was evaporated. Finally, the product was reprecipitated twice with methanol, collected by filtration, and dried under vacuum to give a red solid film (yield: 85%).  $^1\text{H}$  NMR (500 MHz,  $\text{CDCl}_3$ )  $\delta$  (ppm): 8.20–8.00 (m, 4H), 7.90–7.40 (m, 6H), 3.32 (br, 4H), 2.12 (br, 4H), 1.76 (br, 4H), and 1.40–0.90 (br, 12H).  $^{13}\text{C}$  NMR (125 MHz,  $\text{CDCl}_3$ )  $\delta$  (ppm): 151.8, 151.1, 140.9, 135.7, 132.2, 130.6, 129.1, 127.4, 126.6, 122.7, 120.3, 55.4, 40.2 ( $\text{CH}_2\text{-Br}$ ), 34.1, 32.7, 29.2, 27.9, 24.1. FT-IR (pellet BrK,  $\text{cm}^{-1}$ ): 2930 (s), 2855, 1449, 1387 (s), 1267,

889, 821 (s,  $\nu\text{-}(\text{CH}_2)_n$ ), 762 (s,  $\nu\text{-Naph}$ ), 644 ( $\nu\text{-}(\text{CH}_2)\text{-Br}$ ), 562, 529 (s), and 442. GPC (PS calibration)  $M_n$  [g/mol] = 4507;  $M_w$  [g/mol] = 8990.

**Synthesis of Copoly-[9,9-bis(6'-*N,N,N*-trimethylammonium)-hexyl]-2,7-(fluorene)-*alt*-1,4-(naphtho[2,3c]-1,2,5-thiadiazole) Bromide (HTMA-PFNT).** P1 (0.6 mmol per unit) was dissolved in THF (50 mL) at  $-78$  °C (dry ice-acetone bath) in an inert atmosphere. Using a coldfinger condenser, an excess of trimethylamine (7 mL) was added drop by drop. The mixture was stirred at room temperature for 24 h. Subsequently, water (50 mL) and another 7 mL of trimethylamine were added, repeating the previous procedure for 24 h. The solvent and the surplus of trimethylamine were evaporated. Afterward, acetone was added to precipitate the polyelectrolyte, and it was finally collected by filtration. The precipitate (deep red solid) was dried at 40 °C under the vacuum overnight (yield 94%).  $^1\text{H}$  NMR (500 MHz,  $\text{DMSO-}d_6$ )  $\delta$  (ppm): 8.40–7.90 (m, 4H), 7.90–7.40 (m, 6H), 3.27 (br, 4H), 3.08 (s, 18H), 2.19 (br, 4H), 1.65 (br, 4H), and 1.37–0.80 (br, 12H).  $^{13}\text{C}$  NMR (125 MHz,  $\text{DMSO-}d_6$ )  $\delta$  (ppm): 151.0, 150.5, 140.3, 135.2, 131.3, 130.2, 127.1, 126.8, 126.5, 126.3, 120.3, 65.1 ( $\text{CH}_2\text{-N}$ ), 55.0, 52.1 ( $\text{CH}_3\text{-N}$ ), 44.2, 29.1, 25.8, 23.9, 22.2. FT-IR (pellet BrK,  $\text{cm}^{-1}$ ): 3417 (s,  $\nu\text{-}(\text{NR}_3^+)$ ), 2927 (s), 2856, 1628(s), 1478 (s), 1389 (s), 1251, 1124, 964, 899, 825 ( $\nu\text{-}(\text{CH}_2)_n$ ), 764 (s,  $\nu\text{-Naph}$ ), and 533.

**Nuclear Magnetic Resonance and Fourier Transform Infrared Spectroscopy.**  $^1\text{H}$  and  $^{13}\text{C}$  NMR spectra were recorded on a Bruker AVANCE 500 ( $^1\text{H}$ : 500 MHz,  $^{13}\text{C}$ : 125 MHz) spectrometer using chloroform-*d* ( $\text{CDCl}_3$ ) and  $\text{DMSO-}d$  as solvents. The chemical shifts for  $^1\text{H}$  and  $^{13}\text{C}$  NMR were given in  $\delta$  (ppm) with tetramethylsilane as an internal reference. Processing of spectra was done using TopSpin 3.2. FTIR spectra were obtained using a Bruker IFS 66/S spectrometer with samples prepared as KBr pellets.

**Gel Permeation Chromatography (GPC).** Size Exclusion Chromatographic (SEC) analysis was carried out on a Shimadzu LC-20AD, index refraction detector RID-10A and on an Evaporative Light Scattering Detector (ELSD 3300, Alltech Associates, Inc.). SEC analysis of 20  $\mu\text{L}$  of samples was injected in a column PLgel 5  $\mu\text{m}$  MIXED-C;  $2 \times (300 \times 7.5 \text{ mm})$  from Polymer Laboratories Ltd. Samples were around 3–5 mg/mL in THF (as eluent) and were filtered through a nylon 0.45  $\mu\text{m}$  syringe. Number-average ( $M_n$ ) and weight-average ( $M_w$ ) molecular weights were determined by using Polymer Laboratories EasiCal Polystyrene standards for calibration.

**Absorption and Fluorescence Measurements.** Absorption measurements were carried out at room temperature using a UV-1603 spectrophotometer (Shimadzu, Tokyo, Japan). Fluorescence spectra and fluorescence intensity measurements were performed on a QuantaMaster spectrofluorometer (PTI, Birmingham, NJ, USA) interfaced with a Peltier cell. The experimental samples were placed in 10 mm  $\times$  10 mm path length quartz cuvettes. Background intensities were always checked and subtracted from the sample when necessary. All fluorescence spectra were corrected for variations in photomultiplier response over wavelength. Steady-state fluorescence anisotropy,  $\langle r \rangle$ , of DPH was obtained using Glan-Thompson polarizers by measuring the vertical and horizontal components of the fluorescence emission with excitation vertical and horizontal to the emission axis. The  $G$  factor corrects for the transmissivity bias introduced by the detection system. Measurements were carried out for samples containing DPH in buffer, DOPC and HSA in the absence and the presence of HTMA-PFNT. Samples were excited at 370 nm, and the polarized emission was detected at 430 nm. Background intensities due to samples in the absence of DPH were always taken into account.

**Preparation and Characterization of Fluorescent Nanoparticles. LUVs Formation.** Chloroform/methanol solutions containing 3 mg of total phospholipid (DOPC) were dried first by evaporation under dry nitrogen gas stream and subsequently under vacuum for 3 h. Multilamellar vesicles (MLVs) were formed by resuspending the dried phospholipids in the buffer to the required final concentration. The vesicle suspension was then vortexed several times. Large unilamellar vesicles (LUVs) were prepared from these MLVs by

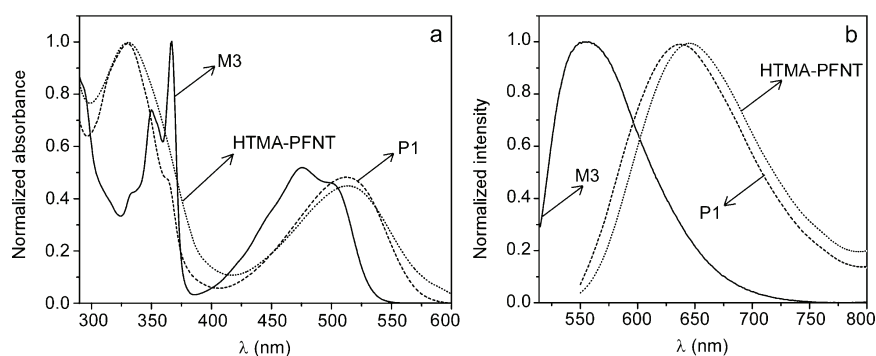


**Figure 1.** a) Normalized absorption spectra and b) fluorescence emission spectra ( $\lambda_{\text{exc}} = 510$  nm) of M3 (line), P1 (dashed), and HTMA-PFNT (dotted) in chloroform.

pressure extrusion through  $0.1 \mu\text{m}$  polycarbonate filters (Nucleopore, Cambridge, MA, USA).

**Preparation of Fluorescent Nanoparticles.** Aliquots of HTMA-PFNT, previously solubilized in DMSO ( $3.65 \times 10^{-4}$  M, in repeat units) and stored at  $-20^\circ\text{C}$ , were externally added either to the protein solution ( $6 \mu\text{M}$ ) or to the LUVs suspension ( $1 \text{ mM}$  in lipid) and incubated for 20 min at room temperature. In all cases, the proportion of DMSO in the aqueous sample was always lower than 1% (V/V). In most samples, the final concentration of HTMA-PFNT was  $1.5 \mu\text{M}$  in terms of repeat units.

**Circular Dichroism Experiments.** CD measurements of HSA and its polymer complexes were carried out with a Jasco spectropolarimeter, model J-815 (JASCO, Easton, MD). Spectra were collected at  $25^\circ\text{C}$  with a scan speed of 50 nm per min, response time of 4 s, and a bandwidth of 1 nm. For each spectrum, four scans were accumulated and averaged to improve the signal-to-noise ratio. Spectra were recorded from 260 to 197 nm using  $0.1 \text{ cm}$  quartz cells. A baseline was taken under the same conditions as those used for the sample and subtracted from each spectrum.

**Fluorescence Quenching Experiments.** Fluorescence emission of HTMA-PFNT in buffer and incorporated in DOPC LUVs was studied in the absence and the presence of different concentrations of AQS. This molecule is an electron acceptor and acts as a quencher of cationic conjugated polyelectrolytes, forming static quenching complexes via attractive electrostatic interactions.<sup>32</sup> Stern–Volmer analysis was applied to the fluorescence quenching data according to eq 1

$$\frac{I_0}{I} = 1 + K_{\text{SV}}[Q] \quad (1)$$

where  $I_0$  and  $I$  stand for the steady-state fluorescence intensities in the absence and the presence of quencher, respectively,  $[Q]$  is the quencher concentration, and  $K_{\text{SV}}$  is the Stern–volmer constant which represents the association constant for complex formation in the case of static quenching.<sup>33</sup>

**Measurements of Vesicle Leakage Induced by Polymers.** DOPC LUVs were prepared with carboxyfluorescein (CF) trapped in the aqueous interior at a concentration of 40 mM, in a buffer containing 50 mM phosphate and 0.1 M NaCl, pH 7.4. The nonencapsulated CF was removed by gel filtration over a column packed with Sephadex G-75 (Pharmacia, Uppsala, Switzerland) eluted with buffer containing 50 mM phosphate, 0.1 M NaCl, pH 7.4. Self-quenching is expected at high concentrations of CF within the small volume of the vesicle interior. Membrane rupture (leakage) of intraliposomal CF was assayed by treating the probe-loaded vesicles with the  $1.5 \mu\text{M}$  of HTMA-PFNT. The total rupture of the vesicles and release of CF was performed with Triton X-100 10%.

**Dynamic Light Scattering (DLS).** The size of the different structures, in the absence and the presence of HTMA-PFNT, was explored by DLS techniques, using a Malvern Zetasizer Nano-ZS instrument, equipped with a monochromatic coherent 4 mW Helium Neon laser ( $\lambda = 633 \text{ nm}$ ) as the light source, with a  $173^\circ$  scattering

angle of lecture for size measurements. All measurements were performed in disposable cuvettes. Measurements were performed in triplicate.

**Microscopy Measurements.** Fluorescence microscopy images were recorded using a Leica DMI 3000B inverted microscope equipped with a Leica EL6000 compact light source and a Leica digital camera DFC3000G. The imaging was performed by using a  $63\times$  objective with 0.7 magnification and filter DsRed (Ex BP 555/25, Em BP 620/60). Data acquisition was monitored by manually formatting and processing with Leica Application Suite AF6000 Module Systems. Transmission electron micrographs (TEM) were performed using a Jeol 1011 microscope (Jeol, Japan), operating at 80 kV. Samples were prepared by placing a drop of the sample on to the 300-mesh copper grid coated with carbon film, and after staining with uranyl acetate and lead citrate, they were left to air-dry before being placed under the microscope. Images were recorded with a Gatan Erlangshen ESS00W camera.

**Cell Imaging.** The human cell line HaCaT was cultured in high glucose DMEM medium (Sigma, D5671) supplemented with 2 mM L-glutamine, 10% FBS, 1 mM pyruvate, 2 mM glutamine, 50  $\mu\text{g}/\text{mL}$  gentamicin, and 2  $\mu\text{g}/\text{mL}$  fungizone, at  $37^\circ\text{C}$  in a humidified incubator in a 5%  $\text{CO}_2$  atm. For microscopy images, HaCaT cells were previously trypsinized, harvested, resuspended in phosphate-buffered saline (100,000 cells/mL), and captured as images in the absence and the presence of HTMA-PFNT.

## RESULTS AND DISCUSSION

**Synthesis and Characterization of the New Conjugated Polyelectrolyte.** The synthesis of the polyelectrolyte HTMA-PFNT is described in Scheme 1. First, the nonionic precursor P1 was synthesized by a Suzuki cross-coupling reaction from the monomers M1 and M3. In classical conditions, P1 was obtained as a red solid with 85% yield. Gel permeation chromatography (GPC) analysis showed that the weight-average molecular weight ( $M_w$ ) of P1 was 8990 with a polydispersity index ( $\text{PDI} = M_w/M_n$ ) of 1.99 (Figure S1). Afterward, P1 was derivatized by a quaternization reaction (Menschutkin reaction), by using trimethylamine condensed in a vessel reaction, in order to obtain cationic polyelectrolyte HTMA-PFNT, a deep red solid with 94% of yield. The further characterizations of these polymers (P1, HTMA-PFNT) have been done by different techniques.

The  $^1\text{H}$  and  $^{13}\text{C}$  NMR spectra of P1 and HTMA-PFNT show similar results to other analogous polyfluorenes synthesized by the same method and correspond with the assignment shown in the experimental part. In P1  $^1\text{H}$  NMR spectra (Figure S2), we can see the aromatic signals typical of this polymer, and, thanks to heteronuclear single quantum correlation (HSQC) experiments (Figure S3), it is possible to

relate these signals with the carbon peaks in  $^{13}\text{C}$  NMR spectra (Figure S4). In HTMA-PFNT  $^1\text{H}$  NMR spectra (Figure S5), the small shift of the signal at 3.32 ppm in P1 corresponding to the  $\text{CH}_2\text{-Br}$ , as well as the appearance of a new signal at 3.08 ppm that integrates for 18 H ( $\text{N-CH}_3$ ) and the ammonium specific signals (52.1 ppm) in the  $^{13}\text{C}$  experiment (Figure S6), is evidence of the quaternization reaction. Also, IR spectra of P1 and HTMA-PFNT confirm the conversion of the pendant groups due to the disappearance of the  $\text{CH}_2\text{-Br}$  tension band at  $644\text{ cm}^{-1}$  and the appearance of the ammonium band at  $3417\text{ cm}^{-1}$  (Figure S7).

The UV-vis normalized absorption of monomer M3 and polymers P1 and HTMA-PFNT in chloroform at room temperature are shown in Figure 1a.

Results show that significant changes in spectra have occurred by the conjugation of the polymer. The absorption spectrum of the monomer M3, recorded between 290 and 600 nm, is structured and shows three characteristic absorptions peaks at 350, 370, and 475 nm, with a shoulder at 500 nm. The absorption spectra of P1 and HTMA-PFNT are practically similar, as was expected, exhibiting two absorption bands in the range explored. The fact that these bands are different than those corresponding to chromophores NTD and fluorene, separately, together with the red-shift observed in the VIS absorption band, suggest that conjugation occurs between both chromophores.

Normalized emission spectra of monomer M3 and polymer P1 in chloroform are shown in Figure 1b. M3 presents the emission maxima at 555 nm, while the synthesized P1 exhibits an unstructured band with its maximum peak very red-shifted, at 637 nm, showing a large Stokes shift (around 125 nm). The shape and position of the emission spectrum was not altered upon excitation at different wavelength, both in the UV and VIS absorption bands. In the same way, excitation spectrum of P1 was similar to that of absorption, independently of the emission wavelength (data not shown). These results support the hypothesis of effective conjugation taking place between fluorene and NTD and playing an important role in the red-shift of the emission spectrum. Extension of  $\pi$ -conjugation has also been observed for NTD derivatives with the chromophore directly connected to other phenyl groups.<sup>34</sup> Authors showed that the position of the NTD emission peak significantly depends on the aryl substituent and its degree of planarity, going from yellow to pure red as the number of phenyl groups was increased, so the red-emission was obtained without any strong donor group in the molecular structure.

Derivatization of P1 to obtain the polyelectrolyte HTMA-PFNT scarcely modified the fluorescence spectra (Figure 1b), shifting the maximum wavelength from 637 to 643 nm. The small red-shift observed in HTMA-PFNT can be attributed to differences in the conformation and organization of the polymer chains in the solvent, as a consequence of the presence of the cationic trimethylammonium group. The red-emission of HTMA-PFNT suggests that it could be used in biosensing and bioimaging studies, but, as was indicated in the introduction of this work, for this kind of applications the stability in aqueous media is essential. Therefore, in a first step we have explored the behavior of HTMA-PFNT in buffer, comparing the results with those obtained in a good solvent. This study was carried out in buffer, instead of water, in order to better simulate physiological conditions.

**Characterization of HTMA-PFNT in Buffer.** The absorption and emission properties of HTMA-PFNT were

characterized in 50 mM phosphate buffer, 100 mM NaCl (pH 7.3). Previous works have reported that when fluorene-based CPEs are dissolved in aqueous solvents, they self-assemble into aggregates.<sup>35,36</sup> This aggregation is dominated by interchain hydrophobic interactions which lead to lower emission intensities and red-shift of the absorption and emission spectra, when comparing with those recorded in good solvents, due to an increase in the interchain energy transport mechanism. In this work ethanol was selected as a good solvent where HTMA-PFNT shows good fluorescence quantum yield because it allows solvation of both components (polar and hydrophobic) of the polymer structure (Table 1). Absorption spectra of the

**Table 1. Absorption and Fluorescence Characterization of HTMA-PFNT in Ethanol, Buffer, HSA, and LUVs of DOPC<sup>a</sup>**

	abs		em	
	$\lambda_{\text{max}}$ (nm)	$\lambda_{\text{max}}$ (nm)	$\Phi_{\text{F}}$	BW (nm)
ethanol	510	645	0.17	121
buffer	518	652	0.01	124
HSA	514	646	0.04	121
DOPC		635	0.14	114

<sup>a</sup>Wavelength corresponding to the maximum of the VIS absorption band and emission spectrum ( $\lambda_{\text{max}}$ ), fluorescence quantum yield ( $\Phi_{\text{F}}$ ) calculated using Rhodamine 6G as standard, and width of the emission spectrum at half height (BW).

polyelectrolyte in both media were recorded between 290 and 650 nm, although Figure 2a only includes the normalized absorption spectra recorded in the visible region to facilitate their comparison. In ethanol, a perfectly definite and clear absorption spectrum was observed, with a maximum peak around 510 nm. Studies at different concentrations showed that the absorbance at 510 nm increased linearly following the Lambert-Beer law over the repeat unit concentration range up to  $1.5 \times 10^{-5}\text{ M}$  without significant changes in spectral shape, indicating that the polymer structure is not affected by dilution for these polymer. From these results, a molar absorption coefficient of  $\epsilon = 7620\text{ M}^{-1}\text{ cm}^{-1}$  was calculated for the polyelectrolyte in ethanol at 510 nm, while it was found to be  $9590\text{ M}^{-1}\text{ cm}^{-1}$  for the UV band at 330 nm. When HTMA-PFNT was dissolved in buffer the spectrum showed a 7 nm red-shift of the absorption band (Table 1), as well as an enhancement in absorbance below 450 nm, which is indicative of an increase in the scatter of the sample. In contrast to that observed in ethanol, the absorbance at 518 nm did not increase linearly with increasing concentrations, leading to turbid samples which evidence the poor solubility of HTMA-PFNT in buffer, with the consequent formation of aggregates. Figure 2b shows the emission spectra of the polyelectrolyte recorded in both media, at the same conditions. As in absorption, the emission spectrum in buffer was slightly broader and shifted to the red than that recorded in ethanol (see the inset in Figure 2b and Table 1). This effect was accompanied by a very drastic drop of the fluorescence quantum yield (down to 0.01 as compared to 0.17 measured in ethanol), supporting the existence of aggregates. To better characterize these aggregates DLS experiments were carried out at room temperature. This technique yields information on the size distribution of macromolecules in solution in the submicrometer range. Results show that, while in ethanol the presence of self-aggregates was not detected, in buffer, polymer aggregates were rapidly formed having a hydrodynamic diameter of around 150

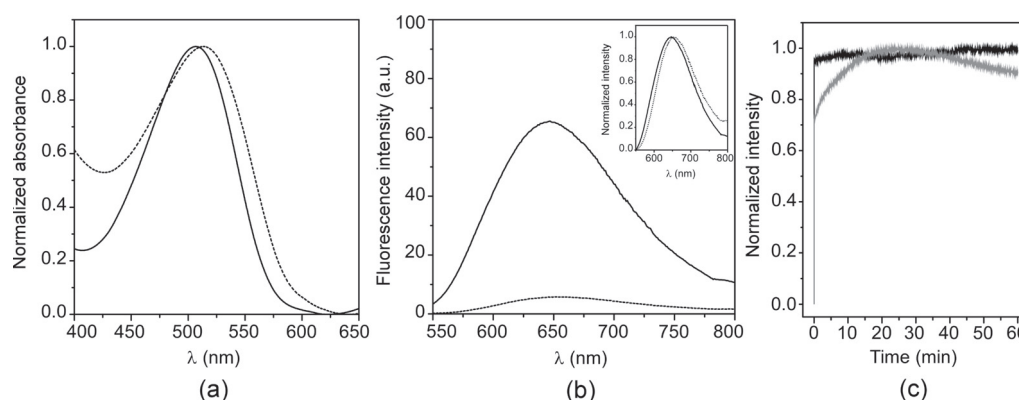


**Figure 2.** a) Normalized absorption spectra of HTMA-PFNT ( $7.3 \mu\text{M}$  in terms of repeat units) in ethanol (solid line) and buffer (dashed line). b) Fluorescence emission spectra of HTMA-PFNT in ethanol (solid line) and buffer (dashed line). **Inset:** Normalized fluorescence emission spectra of HTMA-PFNT ( $1.5 \mu\text{M}$  in terms of repeat units) in ethanol (solid) and buffer (dashed). c) Stability of the fluorescence intensity of HTMA-PFNT in ethanol (black) and buffer (gray) with time. ( $\lambda_{\text{exc}} = 510 \text{ nm}$ ;  $\lambda_{\text{em}} = 650 \text{ nm}$ ).

**Table 2.** Hydrodynamic Diameter of the Different Nanostructures, and Steady State Fluorescence Anisotropy Values,  $\langle r \rangle$ , of DPH in Ethanol, Buffer, HSA, and LUVs of DOPC in the Absence (–) and the Presence (+) of HTMA-PFNT<sup>a</sup>

	$d$ (nm)				$\langle r \rangle$	
	– HTMA-PFNT	+ HTMA-PFNT		– HTMA-PFNT	+ HTMA-PFNT	
		$t_0$	$t = t_0 + 1\text{h}$			
ethanol	not detected	not detected	not detected	0	0	
buffer	not detected	$150 \pm 48$	$374 \pm 66$			
HSA	$5.1 \pm 1.4$	$124 \pm 56$	$114 \pm 31$	$0.307 \pm 0.005$	$0.275 \pm 0.005$	
DOPC	$99 \pm 39$	$110 \pm 54$	$107 \pm 25$	$0.109 \pm 0.005$	$0.109 \pm 0.005$	

<sup>a</sup> $t_0$  was 1 min for ethanol and buffer and 20 min for HSA and DOPC.

nm (Table 2). The average size of aggregates largely increased through time, acquiring diameters larger than 370 nm after 1 h of incubation and, consequently, reducing their fluorescence intensity which, at difference of ethanol, was unstable with time (Figure 2c). A similar behavior was recently reported by our group for the cationic conjugated polyelectrolyte HTMA-PFP.<sup>26</sup> When the polyelectrolyte was added to the buffer, metastable aggregates were formed, and, as for HTMA-PFNT, this effect was accompanied by a red-shift of the emission spectrum and a decrease in fluorescence intensity. However, the fluorescence drop for HTMA-PFP was much less than for HTMA-PFNT probably because the higher hydrophobic character of the polymer backbone favors the close proximity of chains and, therefore, the self-quenching of the red-emitting conjugated polyelectrolyte.

**HTMA-PFNT/HSA Interactions.** HSA is a globular protein composed of a single polypeptide of 585 amino acids with three  $\alpha$ -helical domains I–III. This protein contains hydrophobic cavities which allow the binding and transport of a wide variety of nonpolar compounds. Its isoelectric point is 4.9;<sup>37</sup> therefore, the protein displays a negative net charge at neutral pH, favoring the interaction with cationic compounds, such as HTMA-PFNT. However, the charge distribution is not homogeneous through the three domains, being domains I and II more acidic than domain III.<sup>38</sup> In order to improve the solubility and stability of HTMA-PFNT in buffer, we have explored the possible formation of complexes between the polyelectrolyte and HSA. Interaction was monitored from the changes observed in the fluorescence intensity of HTMA-PFNT after addition to a HSA protein solution ( $6 \mu\text{M}$ ). Interaction occurred apparently in two steps (Figure S8a). In

the first seconds, the fluorescence increased abruptly, reaching  $\sim 85\%$  of its maximum value, but it took around 20 min for total stabilization. These results suggest that not only electrostatic interactions but also hydrophobic forces contribute to the polymer–protein complexes stabilization, as also occurs for the blue polymer HTMA-PFP.<sup>12</sup> In order to determine the affinity of HTMA-PFNT to HSA, the fluorescence spectra of the polyelectrolyte were recorded at increasing concentrations of HSA. The experiment was carried out preparing different samples of the protein in buffer, at concentrations from 0 to  $10 \mu\text{M}$ . The same concentration of polyelectrolyte ( $1.5 \mu\text{M}$ , in terms of repeat units) was added to all of the samples. Samples were incubated for 20 min at room temperature. An enhancement of the fluorescence intensity as well as a blue-shift in the emission spectrum was observed up to a protein concentration of about  $6 \mu\text{M}$  (Figure 3, Table 1). Higher concentrations of protein did not modify the fluorescence spectrum. The changes in the fluorescence spectrum of HTMA-PFNT in the presence of the protein were used to estimate the apparent association constant of the polymer–protein complexes ( $K_A$ ). The inset in Figure 3 represents the increase in fluorescence measured at the maximum of the spectrum ( $\Delta I = I_{\text{HTMA-PFNT-HSA}} - I_{\text{HTMA-PFNT}}$ ) versus HSA concentration. Determination of  $K_A$  was made by fitting these data to the Benesi–Hildebrand equation.<sup>39,40</sup> The solid line of the inset in Figure 3 shows this fit, which yields a value of  $K_A = 2.2 \pm 0.2 \times 10^6 \text{ M}^{-1}$ , indicative of strong affinity between both macromolecules. The value is in the same range as those determined for HTMA-PFP bound to HSA and to other negatively charged biomolecules such as DNA, confirming that

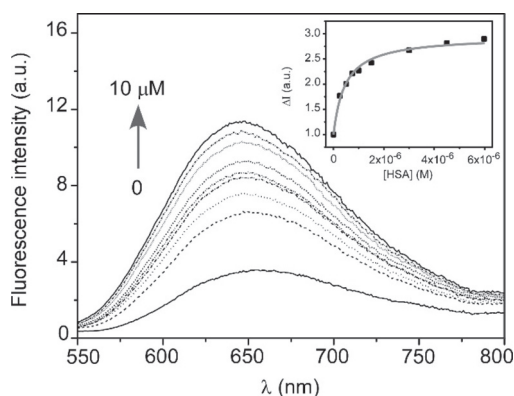


**Figure 3.** Fluorescence emission spectra of HTMA-PFNT ( $1.5 \mu\text{M}$ ) in buffer with increasing concentrations of HSA. **Inset:** Differences in fluorescence intensity by addition of HSA. ( $\lambda_{\text{exc}} = 510 \text{ nm}$ ).

electrostatic interactions are responsible for the formation of the polymer–protein complexes, at least in the first step.<sup>12,36</sup>

In order to investigate if the binding processes alter the intramolecular forces responsible for maintaining the secondary structure of HSA, resulting in a conformational change of the protein, CD spectra were recorded. Figure 4a shows the far-UV CD spectra of HSA ( $6 \mu\text{M}$ ) in the absence and in the presence of different concentrations of HTMA-PFNT (0, 6, 9, and  $12 \mu\text{M}$ ). In the absence of polyelectrolyte, the spectrum exhibited two negative bands, at 208 and 222 nm, characteristic of the  $\alpha$ -helical structure. Addition of increasing concentrations of polyelectrolyte practically did not alter the signal of HSA, suggesting that protein conformation is preserved upon polymer interaction, at least at the concentrations used. To confirm this hypothesis, the fluorescence emission spectrum of the HSA was recorded at increasing concentrations of HTMA-PFNT. HSA contains a single tryptophan, Trp-214, and 18 tyrosine residues which are responsible for its fluorescence emission. Trp-214 is located in domain II, within a hydrophobic pocket, while tyrosines are distributed along the whole polypeptide chain. Upon excitation at 280 nm, both tryptophan and tyrosine are readily excited, but most of the fluorescence comes from Trp-214, due to the efficient resonance energy transfer (RET) from tyrosine to tryptophan.<sup>41</sup> Figure 4b shows the fluorescence emission spectrum ( $\lambda_{\text{exc}} = 280 \text{ nm}$ ) of a  $6.0 \mu\text{M}$  HSA solution in buffer at different HTMA-PFNT

concentrations (up to  $13 \mu\text{M}$ ). In the absence of the polyelectrolyte, spectrum displayed a rather broad fluorescence band, characteristic of tryptophan, with a maximum at  $\sim 335 \text{ nm}$  which indicates that this residue is relatively buried inside the HSA.<sup>33</sup> Addition of HTMA-PFNT induced a decrease in the intensity of the emission maximum, while the position of the spectral maximum was preserved, supporting that the protein conformation is still essentially the same. It suggests that because of the interaction of HTMA-PFNT with HSA, the polyelectrolyte quenches the fluorescence of Trp214, probably through an energy transfer mechanism since there is an overlap between the fluorescence spectrum of HSA and the UV absorption peak of the HTMA-PFNT absorption spectrum (see Figure 1a). These results, together with the anionic character of domain II, support the idea of this protein domain being involved in the interaction HSA-polyelectrolyte.

The above results indicate that the presence of HSA helps to solubilize and stabilize the polyelectrolyte in buffer, forming polymer–protein complexes without perturbing protein conformation. However, although the fluorescence quantum yield is 4-fold higher than in buffer, it is still low as compared to that determined in ethanol (Table 1). There are several possible explanations for this result. On one hand, it could be that the polymers when interacting with the HSA are still exposed to sufficient interfacial water to reduce the fluorescence relative to in ethanol. Another explanation is that the interaction occurs between HSA and polymeric aggregates previously formed in buffer, instead of between single molecules of protein and polymer. This last hypothesis was confirmed by examining the size and shape of the polymer–protein complexes using DLS and TEM. DLS measurements were carried out at room temperature for the protein ( $6 \mu\text{M}$ ) in the absence and the presence of the polyelectrolyte ( $1.5 \mu\text{M}$ ). Results showed peaks at 5 nm, in the absence of polyelectrolyte, according to the hydrodynamic diameter of HSA. However, once HTMA-PFNT was added to the protein solution, the intensity of this peak decreased considerably, and a new peak having a higher hydrodynamic diameter was observed around 120 nm, remaining constant through time (Table 2). The fact that the peak was stable as a function of time indicates that it does not correspond to a population of unstable polymeric aggregates formed in buffer, but it could be attributed to nanostructures composed of aggregates of polyelectrolyte coated with HSA molecules, as was previously proposed. This

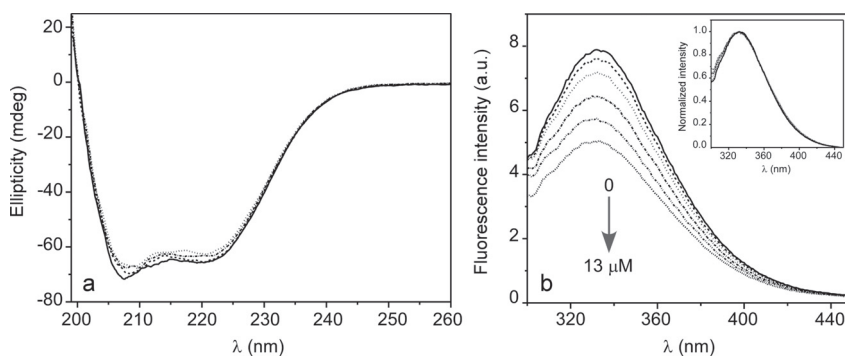
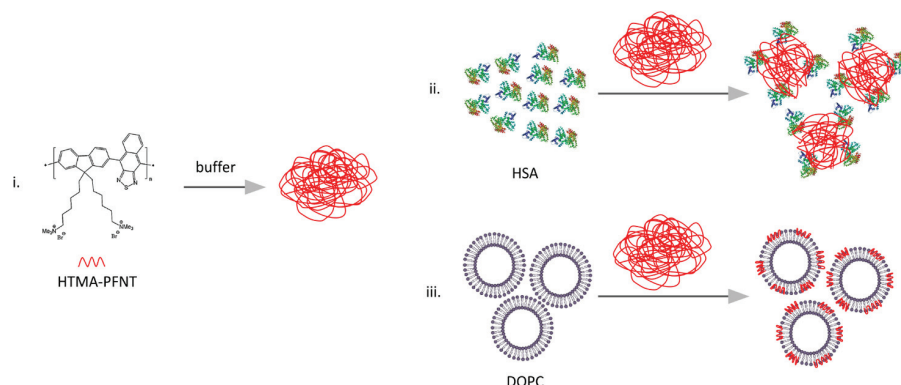


**Figure 4.** a) Effect of HTMA-PFNT on the CD spectrum of HSA ( $6 \mu\text{M}$ ) in buffer. Polyelectrolyte concentrations were as follows: 0 (line), 6 (dash), 9 (dot), and  $12 \mu\text{M}$  (dash dot). b) Fluorescence emission spectra of HSA ( $6 \mu\text{M}$ ) in buffer (line) with increasing concentrations of HTMA-PFNT. **Inset:** Normalized fluorescence emission spectra of HSA in the absence and the presence of increasing concentrations of HTMA-PFNT. ( $\lambda_{\text{exc}} = 280 \text{ nm}$ ).

**Scheme 2. Schematic Model, Which Shows the Possible Interaction between HTMA-PFNT Aggregates (i) in Buffer (ii) with HSA and (iii) Lipid Vesicles of DOPC**



conclusion is supported by the TEM images included in the Supporting Information (Figure S10) and schematized in Scheme 2. Probably, when the polyelectrolytes are added to the protein solution, they start to self-assemble forming aggregates through the hydrophobic interactions of their backbones, exposing the positively charged side chains to the solvent. Simultaneously, proteins interact with the aggregates in two steps: The initial step involves a rapid electrostatic interaction between the domains I and II of the HSA, which shows a negative net charge under the experimental conditions, and the positively charged surface of the polymer aggregates. This interaction induces desolvation of the polymer chains located in the surface, increasing the fluorescence signal with respect to that observed in buffer. The subsequent step involves a slower hydrophobic interaction between the conjugated backbone of the polymers and the hydrophobic patches of HSA domain II. This interaction induces conformational changes in the polymer chains, disrupting backbone interactions, resulting in a blue-shift of the emission spectrum as well as an additional increase in fluorescence intensity.

Finally, we have explored if the ability of HSA to bind and transport hydrophobic compounds is maintained after interaction with HTMA-PFNT, to evaluate the possibility of using these fluorescent nanostructures as drug carriers. For this end, we have selected the fluorophore DPH as a model compound for a hydrophobic drug. This molecule is nonfluorescent in aqueous media but becomes strongly fluorescent when incorporated in nonpolar environments, where it fluoresces at an emission wavelength different from that of HTMA-PFNT (430 nm). In addition, this fluorophore shows a high steady-state anisotropy,  $\langle r \rangle$ , in motionally restricted environments, such as the hydrophobic cavities of HSA.<sup>42</sup> A few microliters from the stock solution of DPH in DMF were added ( $3 \mu\text{M}$  final concentration) to buffer samples containing HSA  $3 \mu\text{M}$ , in the absence and the presence of polyelectrolyte, and to a sample containing only polyelectrolyte ( $1.5 \mu\text{M}$ ) in buffer and were allowed to stabilize for 30 min. Fluorescence spectra and anisotropy values of the different samples are shown in Figure S9 and Table 2. Results indicate that while DPH is nonfluorescent in the buffer containing only HTMA-PFNT, it fluoresces in the polyelectrolyte-HSA complexes (although with less intensity than in the protein solution), showing a high anisotropy value. It suggests that in the presence of HTMA-PFNT, a part of the hydrophobic cavities of the protein is still accessible to nonpolar compounds, thus evidencing the ability

of using these fluorescent nanostructures as carriers for hydrophobic drugs.

**HTMA-PFNT/Liposomes Interactions.** A second approach to stabilize the HTMA-PFNT in buffer was the use of liposomes, in order to obtain fluorescent nanoparticles which were capable of performing more than one function simultaneously. Polyelectrolyte-liposome interaction was explored in samples containing LUVs of the zwitterionic lipid DOPC (1 mM), monitoring the changes occurring in the polyelectrolyte fluorescence. When HTMA-PFNT was added to the sample, a strong increase in the fluorescence signal was observed, reaching  $\sim 85\%$  of its intensity maximum value in a few seconds and taking around 20 min for total stabilization (Figure S8b). To determine the affinity of HTMA-PFNT to liposomes, samples containing increasing concentrations of LUVs, with final lipid concentrations ranging from 0 to 1 mM, were prepared in buffer. The same concentration of HTMA-PFNT ( $1.5 \mu\text{M}$ , in terms of repeat units) was added to all of the samples, which were incubated for 20 min at room temperature. Figure 5 shows the emission spectra recorded for the different samples. A strong enhancement of the fluorescence intensity was observed up to a lipid concentration of about 1 mM. Higher concentrations of lipid did not modify the fluorescence signal indicating that at this lipid concentration, all the polymer chains bind to the lipid membrane from

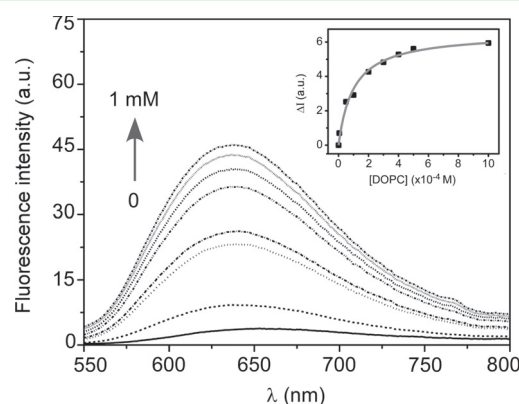


**Figure 5.** Fluorescence emission spectra of HTMA-PFNT ( $1.5 \mu\text{M}$ ) in buffer with increasing concentrations of DOPC. **Inset:** Differences in fluorescence intensity by increasing the DOPC concentration. ( $\lambda_{\text{exc}} = 510 \text{ nm}$ ).

the aqueous medium and no aggregates remain in the buffer. Changes in the fluorescence intensity were used to estimate the partition coefficient of the polyelectrolyte between the zwitterionic membrane and the aqueous phase ( $K_p$ ), fitting the fluorescence intensities measured at low lipid concentrations to the following equation (see the inset in Figure 5)<sup>43</sup>

$$\Delta I = \frac{\Delta I_{\max}[L]}{1/(K_p\gamma) + [L]} \quad (2)$$

where  $K_p$  is the phospholipid/water partition coefficient of the polymer,  $\Delta I$  ( $\Delta I = I - I_0$ ) stands for the difference between the fluorescence intensity of the HTMA-PFNT measured in the presence ( $I$ ) and in the absence ( $I_0$ ) of the phospholipid vesicles,  $\Delta I_{\max} = I_{\infty} - I_0$  is the maximum value of this difference once the limiting value is reached ( $I_{\infty}$ ) upon increasing the phospholipid concentration  $[L]$ , and  $\gamma$  is the molar volume of the phospholipid (for DOPC in the fluid phase the value of  $\gamma$  is  $0.9 \text{ M}^{-144}$ ). From a two-parameter ( $\Delta I_{\max}$  and  $K_p$ ) fitting procedure, a  $K_p$  value of  $(1.1 \pm 0.1) \times 10^4$  was obtained, which indicates high affinity of the polymer for the lipid bilayer. This value is in the same range as that determined for the blue cationic polyelectrolyte HTMA-PFP in zwitterionic liposomes but 1 order of magnitude lower than that determined in anionic liposomes,<sup>27</sup> suggesting that hydrophobic forces more than electrostatics are responsible for the interaction between polyelectrolyte and liposome. Simultaneously to the fluorescence intensity increase (the quantum yield grew to 0.14 as compared to 0.01 measured in buffer), a 17 nm blue-shift and a slight narrowing of the emission spectrum of the polyelectrolyte was observed after incorporation into the vesicles (Figure 5 and Table 1). These results evidence a clear reduction in the polymer aggregation as a consequence of membrane interaction. Probably, once HTMA-PFNT is added to the liposome suspension, self-assembled aggregates rapidly interact with the lipid membranes. This interaction should induce the disruption of aggregates through a mechanism mediated by hydrophobic interactions between the conjugated backbone of the polymer and the lipid molecules. The breakup of aggregates separates the polymeric backbones, decreasing the effective conjugation length and thus reducing self-quenching. It results in a blue-shift of the emission maximum and a several-fold amplification of the fluorescence emission. The fact that the fluorescence spectrum maximum is even more shifted to the blue than that found in ethanol (Table 1) suggests that incorporation of the polyelectrolyte into the bilayer causes a twist of the main chain, reducing the planarity of the backbone and therefore the conjugation length.

In order to explore if the polyelectrolyte-membrane interaction destabilizes the liposome bilayer structure, various types of experiments were carried out. First, DLS measurements of DOPC vesicles were performed before and after polymer addition. In the absence of polyelectrolyte, a single distribution was observed centered at  $99 \pm 39 \text{ nm}$  (Table 2). When HTMA-PFNT  $1.5 \mu\text{M}$  was added to this lipid suspension, a similar distribution was recorded centered at  $110 \pm 54 \text{ nm}$ , and no additional population was detected. These results confirm that polymer aggregates are not found in the buffer, and therefore all the polymer chains are interacting with liposomes and suggest that the integrity of the lipid vesicles is retained after HTMA-PFNT interaction since no vesicle fusion or decomposition into small fragments is detectable. This hypothesis was supported by TEM images

that were taken for DOPC samples in the absence and the presence of polyelectrolyte (Figure S10). Additionally, the effect of polyelectrolyte on the liposome integrity was explored through leakage experiments, by monitoring the induced release of the fluorophore CF from DOPC vesicles in the presence of HTMA-PFNT. When CF is encapsulated at high concentration in the aqueous cavity of lipid vesicles, its fluorescence decreases by an autoquenching process;<sup>45,46</sup> therefore, if the vesicle membrane is perturbed by the incorporation of polyelectrolyte, then the dye is released and the fluorescence signal increases after its dilution in buffer. Figure 6a shows the CF fluorescence intensity encapsulated in

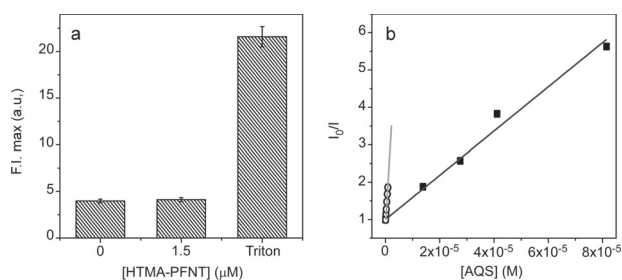


**Figure 6.** a) Fluorescence intensity of CF encapsulated in DOPC liposomes recorded at 525 nm in the absence and the presence of HTMA-PFNT ( $1.5 \mu\text{M}$ ) and after addition of Triton (10%). b) Stern–Volmer plots for quenching of HTMA-PFNT ( $1.5 \mu\text{M}$ ) by AQS in buffer (o) and vesicles of DOPC (■).

DOPC liposomes in the absence and the presence of HTMA-PFNT ( $1.5 \mu\text{M}$ ) and after addition of Triton (10%) which induces the complete lysis of the vesicles. Results show that the presence of polyelectrolyte at  $1.5 \mu\text{M}$  does not modify the fluorescence intensity of CF, confirming that the integrity of the lipid vesicles is maintained at this polymer concentration.

Although the above experiments confirm the interaction of HTMA-PFNT with the lipid vesicles, preserving their integrity to yield fluorescent nanoparticles, they do not inform if the polyelectrolyte remains located close to the surface or embedded in the lipid bilayer. To gain more insight into this subject quenching experiments of the polyelectrolyte, in the presence and in the absence of lipid vesicles, were carried out using the anionic electron acceptor AQS. This molecule has been reported to be an excellent quencher for cationic conjugated polyelectrolytes, and it is soluble in water but not in lipid bilayer.<sup>32,47</sup> When increasing concentrations of AQS were added to both samples, a decrease in the fluorescence signal was observed, being this effect higher in buffer than in the vesicle suspension (Figure 6b). The Stern–Volmer plots were linear in the range studied (up to  $10 \mu\text{M}$ ), with  $K_{sv} = 1.1 \pm 0.2 \times 10^6$  and  $K_{sv} = 5.9 \pm 0.2 \times 10^4$  for buffer and lipid vesicles, respectively (see eq 1), indicating that the polymeric chains are inserted in the lipid bilayer close to the membrane surface, relatively accessible to the quenchers, and not in the deep hydrophobic core. According to all these results (fluorescence spectra, DLS, TEM, leakage, and quenching experiments), we have proposed a model for the interaction between HTMA-PFNT and liposomes, which is shown in Scheme 2.

The ability of these fluorescent nanoparticles to be used as drug carriers was investigated, as for polymer-HSA complexes, using DPH as a model compound for a hydrophobic drug. Experiments were carried out at low lipid concentrations to be

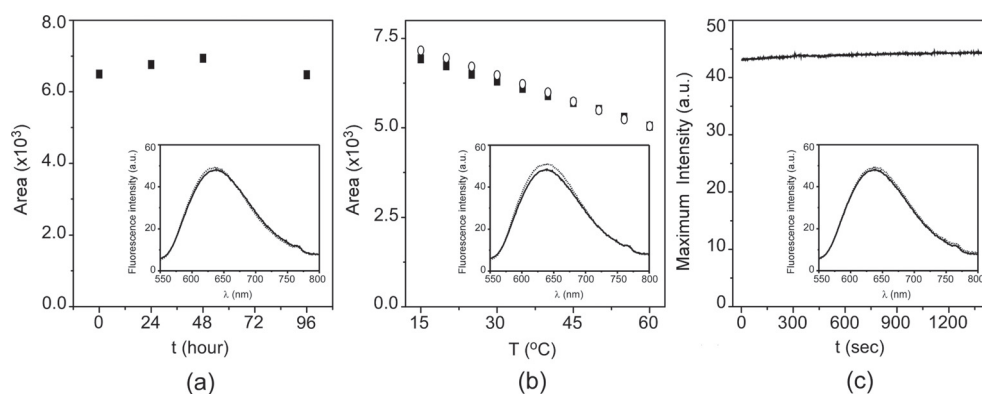


**Figure 7.** a) Effect of storage time, b) temperature, and c) continuous radiation of HTMA-PFNT incorporated in DOPC liposomes. For temperature experiments the sample was heated from 15 to 60  $^{\circ}\text{C}$  (■) and subsequently cooled to the starting temperature (○). Insets: Fluorescence emission spectra recorded at the beginning (black line) and end (dots) of each experiment. ( $\lambda_{\text{exc}} = 510 \text{ nm}$ ).

sure that all the liposomes were in contact with the polyelectrolyte. The fluorescence spectra and anisotropies of DPH were recorded in lipid vesicles in the presence and the absence of polyelectrolyte. Results are shown in Figure S9 and Table 2. The fact that the fluorescence intensity and anisotropy values were similar in both samples (with and without polyelectrolyte) indicates that HTMA-PFNT binding onto the liposome is not affecting the insertion of the DPH in the lipid bilayer, confirming the use of these fluorescent nanoparticles as nanocarriers for hydrophobic drugs. Liposomes can also be used to transport polar compounds in its inner aqueous phase. The previous leakage experiments made with CF to confirm the integrity of the liposome coated with HTMA-PFNT serve also to show their ability to carry hydrophilic molecules.

Taking into account the interesting properties of these nanoparticles we decided to explore their stability as a function of storage time and temperature, monitoring the fluorescence spectra and plotting the area of each spectrum as a function of these parameters. Results show that when samples are kept in the dark at 4  $^{\circ}\text{C}$ , the fluorescence signal and the spectrum shape were unaltered at least for 3 days after preparation, indicating that aggregation between vesicles is not taking place (Figure 7a). The absence of aggregation was verified from DLS experiments since similar distributions, centered around 110 nm, were obtained for the same sample with 2 h of difference (Table 2). Thermal stability of the nanoparticles was evaluated from 15  $^{\circ}$  to 60  $^{\circ}\text{C}$  and from 60 to 15  $^{\circ}\text{C}$  for the same sample (Figure 7b). Fluorescence intensity showed a slight decrease in the temperature range explored when temperature was increased, which have been also reported for other conjugated polyelectrolytes.<sup>48,49</sup> The fact that the initial fluorescence intensity was recovered after cooling indicates that the reduction of intensity is mainly caused by the increase of probability of nonradiative transitions at higher temperatures, and not by aggregation of nanoparticles induced by temperature, with the subsequent deposition of the aggregates formed. In addition to the storage time and temperature studies, we have explored the photostability by monitoring the fluorescence signal of the nanoparticles under continuous radiation, recording the emission spectra at the beginning and the end of the radiation (Figure 7c). No photobleaching was observed during this period indicating that the fluorescent nanoparticles are photostable and, therefore, particularly suited as bioimaging probes.

To test the above possibility, preliminary fluorescence and phase contrast microscopy experiments were performed with the human keratinocyte cell line HaCaT. The microscopy images were obtained before and after addition of the liposome-based nanoparticles. Figure 8 shows the cells in the presence of

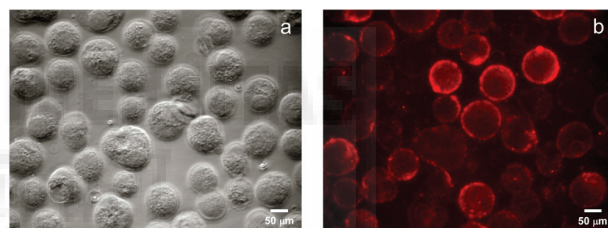


**Figure 8.** Microscopy images of HaCaT cells in the presence of liposome-based nanoparticles (0.2  $\mu\text{M}$  final polymer concentration) observed under a) phase contrast and b) visible-light using the Leica DsRed filter set containing an excitation filter at 555/25 nm band-pass and an emission filter at 620/60 nm band-pass.

the fluorescent nanoparticles (final concentration 0.2  $\mu\text{M}$  in polymer) observed by phase contrast microscopy (a) and upon excitation with Vis-light using an excitation filter at 555/25 nm band-pass and an emission filter at 620/60 nm band-pass (b). Both images correspond to the same field and were taken 5 min after nanoparticle addition. Results show that nanoparticles rapidly interact with the cells, allowing for their visualization under fluorescence microscopy. The fact that similar images were observed after 1 h of incubation indicates that nanoparticles do not affect the integrity of the cellular membrane and confirms the ability of these structures to be used as fluorescent probes for biological imaging.

## CONCLUSIONS

In conclusion, a new red-emitting fluorene-based conjugated polyelectrolyte HTMA-PFNT has been synthesized by incorporation of the chromophore naphtha[2,3c][1,2,5]thiadiazole (NTD) on fluorene backbone, extending the conjugation length in the polymer chain. The polyelectrolyte shows poor solubility in buffer, leading to aggregates of very low fluorescent quantum yield. Complexation of HTMA-PFNT with two biological systems which are known to be used as nanocarriers, HSA and lipid vesicles, allows for its stabilization in buffer without perturbing the biomolecule structure and

vesicle integrity, leading to red fluorescent nanostructures of similar size but different composition. The properties of the protein nanoparticles are consistent with polyelectrolyte aggregates covered with HSA molecules. Furthermore, the ability of the protein to bind nonpolar compounds is preserved after interaction with the polyelectrolyte, allowing for the transport of small hydrophobic drugs. The liposome-based nanoparticles consist of lipid vesicles coated with polyelectrolyte and are much more fluorescent than the previous one, showing a high stability with time, temperature, and light. Since the integrity of the lipid vesicles is maintained after polyelectrolyte incorporation, we checked their ability to transport hydrophilic and hydrophobic compounds, therefore extending the applications of these fluorescent nanoparticles to those typical of liposomes.<sup>28</sup> Finally, the capacity of the nanoparticles to be used as fluorescent probes for biological imaging was demonstrated by studies performed with HaCaT cells. All these results support the potential use of these novel nanostructures as multifunctional platforms in important biomedical applications such as bioimaging and drug delivery.<sup>50–52</sup> To our knowledge this is the first time that nanoparticles composed of liposomes coated with conjugated polyelectrolytes have been made and used to fluorescently label the cell membrane of live cells as well as to carry hydrophobic and hydrophilic compounds. This work therefore represents an important step toward designing and applying conjugated polyelectrolyte based nanoparticles that function in both imaging and therapeutic applications.

## ■ ASSOCIATED CONTENT

### Supporting Information

The Supporting Information is available free of charge on the ACS Publications website at DOI: 10.1021/acsami.5b10167.

Polymer characterization made with NMR, IR, and GPC and some other fluorescence studies and TEM experiments (PDF)

## ■ AUTHOR INFORMATION

### Corresponding Author

\*E-mail: [rmateo@umh.es](mailto:rmateo@umh.es).

### Author Contributions

The manuscript was written through contributions of all authors. All authors have given approval to the final version of the manuscript.

Z.K. and R.V.-G. contributed equally.

### Notes

The authors declare no competing financial interest.

## ■ ACKNOWLEDGMENTS

We are thankful to our colleagues Amalia Mira Carrio and Alberto Falcó Gracia for their great help in the preliminary studies with HaCaT cell cultures. The authors thank the Spanish Ministerio de Economía y Competitividad and Generalitat Valenciana for financial support MAT-2014-53282-R, MAT-2011-23007, and PROMETEO/2013/018, respectively.

## ■ REFERENCES

- (1) Pu, K. Y.; Cai, L.; Liu, B. Design and Synthesis of Charge-Transfer-Based Conjugated Polyelectrolytes as Multicolor Light-Up Probes. *Macromolecules* **2009**, *42*, 5933–5940.
- (2) Jiang, H.; Taranekekar, P.; Reynolds, J. R.; Schanze, K. S. Conjugated Polyelectrolytes: Synthesis, Photophysics, and Applications. *Angew. Chem., Int. Ed.* **2009**, *48*, 4300–4316.
- (3) Zhu, C.; Yang, Q.; Liu, L.; Wang, S. A Potent Fluorescent Probe for the Detection of Cell Apoptosis. *Chem. Commun.* **2011**, *47*, 5524–5526.
- (4) Wang, L.; Li, H.; Cao, D. Conjugated Polyelectrolytes: Synthesis and Application in Biomolecule Detection. *Curr. Org. Chem.* **2012**, *16*, 1468–1484.
- (5) Liu, Y.; Ogawa, K.; Schanze, K. S. Conjugated Polyelectrolyte Based Real-Time Fluorescence Assay for Phospholipase C. *Anal. Chem.* **2008**, *80*, 150–158.
- (6) Hill, E. H.; Zhang, Y.; Evans, D. G.; Whitten, D. G. Enzyme-Specific Sensors via Aggregation of Charged p-Phenylene Ethynyls. *ACS Appl. Mater. Interfaces* **2015**, *7*, 5550–5560.
- (7) Zhan, R.; Liu, B. Benzothiadiazole-Containing Conjugated Polyelectrolytes for Biological Sensing and Imaging. *Macromol. Chem. Phys.* **2015**, *216*, 131–144.
- (8) Zhu, C.; Liu, L.; Yang, Q.; Lv, F.; Wang, S. Water-Soluble Conjugated Polymers for Imaging, Diagnosis, and Therapy. *Chem. Rev.* **2012**, *112*, 4687–4735.
- (9) Pu, K. Y.; Liu, B. Fluorescent Conjugated Polyelectrolytes for Bioimaging. *Adv. Funct. Mater.* **2011**, *21*, 3408–3423.
- (10) Lee, K.; Lee, J.; Jeong, E. J.; Kronk, A.; Elenitoba-Johnson, K. S. J.; Lim, M. S.; Kim, J. Conjugated Polyelectrolyte-Antibody Hybrid Materials for Highly Fluorescent Live Cell-Imaging. *Adv. Mater.* **2012**, *24*, 2479–2484.
- (11) Tapia, M. J.; Montserin, M.; Valente, A. J. M.; Burrows, H. D.; Mallavia, R. Binding of Polynucleotides to Conjugated Polyelectrolytes and its Applications in Sensing. *Adv. Colloid Interface Sci.* **2010**, *158*, 94–107.
- (12) Martínez-Tome, M. J.; Esquembre, R.; Mallavia, R.; Mateo, C. R. Formation of Complexes between the Conjugated Polyelectrolyte Poly{[9,9-bis(6'-N,N,N-trimethylammonium) hexyl]fluorene-phenylene} Bromide (HTMA-PFP) and Human Serum Albumin. *Bio-macromolecules* **2010**, *11*, 1494–1501.
- (13) Evans, R. C.; Macedo, A. G.; Pradhan, S.; Scherf, U.; Carlos, L. D.; Burrows, H. D. Fluorene Based Conjugated Polyelectrolyte/Silica Nanocomposites: Charge-Mediated Phase Aggregation at the Organic-Inorganic Interface. *Adv. Mater.* **2010**, *22*, 3032–3037.
- (14) Burrows, H. D.; Valente, A. J. M.; Costa, T.; Stewart, B.; Tapia, M. J.; Scherf, U. What Conjugated Polyelectrolytes Tell us about Aggregation in Polyelectrolyte/Surfactant Systems. *J. Mol. Liq.* **2015**, *210*, 82–99.
- (15) Li, K.; Liu, B. Polymer-Encapsulated Organic Nanoparticles for Fluorescence and Photoacoustic Imaging. *Chem. Soc. Rev.* **2014**, *43*, 6570–6597.
- (16) Dias, F. B.; King, S.; Monkman, A. P.; Perepichka, I. I.; Kryuchkov, M. A.; Perepichka, I. F.; Bryce, M. R. Dipolar Stabilization of Emissive Singlet Charge Transfer Excited States in Polyfluorene Copolymers. *J. Phys. Chem. B* **2008**, *112*, 6557–6566.
- (17) Shi, H.; Sun, H.; Yang, H.; Liu, S.; Jenkins, G.; Feng, W.; Li, F.; Zhao, Q.; Liu, B.; Huang, W. Cationic Polyfluorenes with Phosphorescent Iridium(III) Complexes for Time-Resolved Luminescent Biosensing and Fluorescence Lifetime Imaging. *Adv. Funct. Mater.* **2013**, *23*, 3268–3276.
- (18) Liu, B.; Bazan, G. C. Synthesis of Cationic Conjugated Polymers for Use in Label-Free DNA Microarrays. *Nat. Protoc.* **2006**, *1*, 1698–1702.
- (19) Pina, J.; Seixas De Melo, J. S.; Eckert, A.; Scherf, U. Unusual Photophysical Properties of Conjugated, Alternating Indigo-Fluorene Copolymers. *J. Mater. Chem. A* **2015**, *3*, 6373–6382.
- (20) Chen, L.; Tong, H.; Xie, Z.; Wang, L.; Jing, X.; Wang, F. Red Electroluminescent Polyfluorenes Containing Highly Efficient 2,1,3-Benzoselenadiazole- and 2,1,3-Naphthothiadiazole-Based Red Dopants in the Side Chain. *J. Mater. Chem.* **2011**, *21*, 15773–15779.
- (21) Huang, F.; Hou, L.; Wu, H.; Wang, X.; Shen, H.; Cao, W.; Yang, W.; Cao, Y. High-Efficiency, Environment-Friendly Electroluminescent Polymers with Stable High Work Function Metal as a Cathode:

Green- and Yellow-Emitting Conjugated Polyfluorene Polyelectrolytes and their Neutral Precursors. *J. Am. Chem. Soc.* **2004**, *126*, 9845–9853.

(22) Kim, S.; Lim, C. K.; Na, J.; Lee, Y. D.; Kim, K.; Choi, K.; Leary, J. F.; Kwon, I. C. Conjugated Polymer Nanoparticles for Biomedical in vivo Imaging. *Chem. Commun.* **2010**, *46*, 1617–1619.

(23) Huang, J.; Liu, Y.; Qian, C. G.; Sun, M. J.; Shen, Q. D. Multicolour Fluorescence Cell Imaging Based on Conjugated Polymers. *RSC Adv.* **2014**, *4*, 3924–3928.

(24) Liu, J.; Feng, G.; Ding, D.; Liu, B. Bright Far-Red/Near-Infrared Fluorescent Conjugated Polymer Nanoparticles for Targeted Imaging of HER2-Positive Cancer Cells. *Polym. Chem.* **2013**, *4*, 4326–4334.

(25) Lu, X.; Jiang, R.; Yang, M.; Fan, Q.; Hu, W.; Zhang, L.; Yang, Z.; Deng, W.; Shen, Q.; Huang, Y.; Liu, X.; Huang, W. Monodispersed Grafted Conjugated Polyelectrolyte-Stabilized Magnetic Nanoparticles as Multifunctional Platform for Cellular Imaging and Drug Delivery. *J. Mater. Chem. B* **2014**, *2*, 376–386.

(26) Kahveci, Z.; Martínez-Tomé, M. J.; Mallavia, R.; Mateo, C. R. Use of the Conjugated Polyelectrolyte Poly{[9,9-bis(6'-N, N, N-trimethylammonium)hexyl]fluorene-phenylene} Bromide (HTMA-PFP) as a Fluorescent Membrane Marker. *Biomacromolecules* **2013**, *14*, 1990–1998.

(27) Kahveci, Z.; Martínez-Tomé, M. J.; Esquembre, R.; Mallavia, R.; Mateo, C. R. Selective Interaction of a Cationic Polyfluorene with Model Lipid Membranes: Anionic versus Zwitterionic Lipids. *Materials* **2014**, *7*, 2120–2140.

(28) Allen, T. M.; Cullis, P. R. Liposomal Drug Delivery Systems: from Concept to Clinical Applications. *Adv. Drug Delivery Rev.* **2013**, *65*, 36–48.

(29) Yang, F.; Zhang, Y.; Liang, H. Interactive Association of Drugs Binding to Human Serum Albumin. *Int. J. Mol. Sci.* **2014**, *15*, 3580–3595.

(30) Yang, J.; Jiang, C.; Zhang, Y.; Yang, R.; Yang, W.; Hou, Q.; Cao, Y. High-Efficiency Saturated Red Emitting Polymers Derived from Fluorene and Naphthoselenadiazole. *Macromolecules* **2004**, *37*, 1211–1218.

(31) Tena, A.; Vazquez-Guilló, R.; Marcos-Fernández, A.; Hernández, A.; Mallavia, R. Polymeric Films Based on Blends of 6FDA-6FpDA Polyimide Plus Several Copolyfluorenes for CO<sub>2</sub> Separation. *RSC Adv.* **2015**, *5*, 41497–41505.

(32) Chen, J.; Dong, W. F.; Mohwald, H.; Krastev, R. Amplified Fluorescence Quenching of Self-Assembled Polyelectrolyte - Dye Nanoparticles in Aqueous Solution. *Chem. Mater.* **2008**, *20*, 1664–1666.

(33) Lakowicz, J. R. *Principles of Fluorescence Spectroscopy*; Kluwer Academic/Plenum Press: New York, 1999; Vol. 2nd.

(34) Wei, P.; Duan, L.; Zhang, D.; Qiao, J.; Wang, L.; Wang, R.; Dong, G.; Qiu, Y. A New Type of Light-Emitting Naphtho[2,3-c][1,2,5]thiadiazole Derivatives: Synthesis, Photophysical Characterization and Transporting Properties. *J. Mater. Chem.* **2008**, *18*, 806–818.

(35) Kahveci, Z.; Martínez-Tomé, M. J.; Mallavia, R.; Mateo, C. R. Use of the Conjugated Polyelectrolyte Poly{[9,9-bis(6'-N, N, N-trimethylammonium)hexyl]fluorene-phenylene} Bromide (HTMA-PFP) as a Fluorescent Membrane Marker. *Biomacromolecules* **2013**, *14*, 1990–1998.

(36) Monteserin, M.; Burrows, H. D.; Valente, A. J. M.; Mallavia, R.; Di Paolo, R. E.; Maçanita, A. L.; Tapia, M. J. Interaction between Poly(9, 9-bis(6'-N, N, N-trimethylammonium)hexyl]fluorene phenylene) Bromide and DNA as Seen by Spectroscopy, Viscosity, and Conductivity: Effect of Molecular Weights and DNA Secondary Structure. *J. Phys. Chem. B* **2009**, *113*, 1294–1302.

(37) Taboada, P.; Gutiérrez-Pichel, M.; Mosquera, V. Effects of the Molecular Structure of Two Amphiphilic Antidepressant Drugs on the Formation of Complexes with Human Serum Albumin. *Biomacromolecules* **2004**, *5*, 1116–1123.

(38) Dockal, M.; Carter, D. C.; Rüker, F. The Three Recombinant Domains of Human Serum Albumin. Structural Characterization and Ligand Binding Properties. *J. Biol. Chem.* **1999**, *274*, 29303–29310.

(39) Esquembre, R.; Pastor, I.; Mallavia, R.; Mateo, C. R. Fluorometric Detection of Nitric Oxide Using 2,3-Diaminonaphthalene Incorporated in  $\beta$ -cyclodextrin. *J. Photochem. Photobiol., A* **2005**, *173*, 384–389.

(40) Catena, G. C.; Bright, F. V. Thermodynamic Study on the Effects of  $\beta$ -cyclodextrin Inclusion with Anilidonaphthalenesulfonates. *Anal. Chem.* **1989**, *61*, 905–909.

(41) Abou-Zied, O. K.; Al-Shihi, O. I. K. Characterization of Subdomain HA Binding Site of Human Serum Albumin in its Native, Unfolded, and Refolded States Using Small Molecular Probes. *J. Am. Chem. Soc.* **2008**, *130*, 10793–10801.

(42) Litman, B. J.; Barenholz, Y. Fluorescent Probe: Diphenylhexatriene. *Methods Enzymol.* **1982**, *81*, 678–685.

(43) Coutinho, A.; Prieto, M. Self-Association of the Polyene Antibiotic Nystatin in Dipalmitoylphosphatidylcholine Vesicles: A Time-Resolved Fluorescence Study. *Biophys. J.* **1995**, *69*, 2541–2557.

(44) Davenport, L.; Dale, R. E.; Bisby, R. H.; Cundall, R. B. Transverse Location of the Fluorescent Probe 1,6-Diphenyl-1,3,5-Hexatriene in Model Lipid Bilayer Membrane Systems by Resonance Excitation Energy Transfer. *Biochemistry* **1985**, *24*, 4097–4108.

(45) Van Renswoude, J.; Hoekstra, D. Cell-Induced Leakage of Liposome Contents. *Biochemistry* **1981**, *20*, 540–546.

(46) Bandyopadhyay, P.; Bandyopadhyay, P.; Regen, S. L. An Ion Conductor that Recognizes Osmotically-Stressed Phospholipid Bilayers. *J. Am. Chem. Soc.* **2002**, *124*, 11254–11255.

(47) Chemburu, S.; Ji, E.; Casana, Y.; Wu, Y.; Buranda, T.; Schanze, K. S.; Lopez, G. P.; Whitten, D. G. Conjugated Polyelectrolyte Supported Bead Based Assays for Phospholipase A 2 Activity. *J. Phys. Chem. B* **2008**, *112*, 14492–14499.

(48) Martínez-Tomé, M. J.; Esquembre, R.; Mallavia, R.; Mateo, C. R. Formation and Characterization of Stable Fluorescent Complexes between Neutral Conjugated Polymers and Cyclodextrins. *J. Fluoresc.* **2013**, *23*, 171–180.

(49) Traiphol, R.; Sanguansat, P.; Srikhirin, T.; Kerdcharoen, T.; Osotchan, T. Spectroscopic Study of Photophysical Change in Collapsed Coils of Conjugated Polymers: Effects of Solvent and Temperature. *Macromolecules* **2006**, *39*, 1165–1172.

(50) Wen, C. J.; Sung, C. T.; Aljuffali, I. A.; Huang, Y. J.; Fang, J. Y. Nanocomposite Liposomes Containing Quantum Dots and Anticancer Drugs for Bioimaging and Therapeutic Delivery: A Comparison of Cationic, Pegylated and Deformable Liposomes. *Nanotechnology* **2013**, *24* (32), 325101.

(51) Chen, K.; Xie, J.; Chen, X. RGD-Human Serum Albumin Conjugates as Efficient Tumor Targeting Probes. *Mol. Imaging* **2009**, *8*, 65–73.

(52) Quan, Q.; Xie, J.; Gao, H.; Yang, M.; Zhang, F.; Liu, G.; Lin, X.; Wang, A.; Eden, H. S.; Lee, S.; Zhang, G.; Chen, X. HSA Coated Iron Oxide Nanoparticles as Drug Delivery Vehicles for Cancer Therapy. *Mol. Pharmaceutics* **2011**, *8*, 1669–1676.

Supporting Information

New Red-Emitting Conjugated Polyelectrolyte:  
Stabilization by Interaction with Biomolecules  
and Potential Use as Drug Carriers and  
Bioimaging Probes

*Zehra Kahveci†, Rebeca Vázquez-Guilló†, María José Martínez-Tomé, Ricardo Mallavia, C.Reyes Mateo\**

Instituto de Biología Molecular y Celular, Universidad Miguel Hernández, 03202, Elche, Alicante, Spain

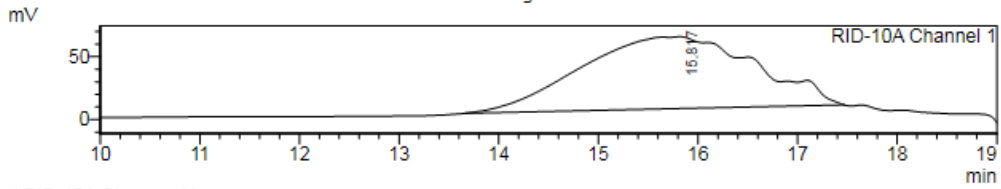
\*E-mail: [rmateo@umh.es](mailto:rmateo@umh.es)

==== Shimadzu LCsolution Analysis Report ====

Sample Information

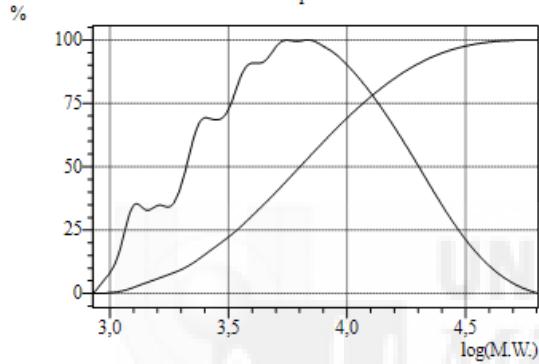
Acquired by : Admin  
Sample Name : P1  
Sample ID : 56  
Vial# : 33  
Injection Volume : 20 uL  
Method Filename : calibrado PS dos columnas.lcm  
Report Filename : Report GPC  
Date Acquired : 04/06/2014 11:18:29  
Date Processed : 04/06/2014 11:43:33

Chromatogram



1 RID-10A Channel 1/

GPC Graph



GPC Results  
Peak#:1 (RID-10A Channel 1)  
[Peak Information]

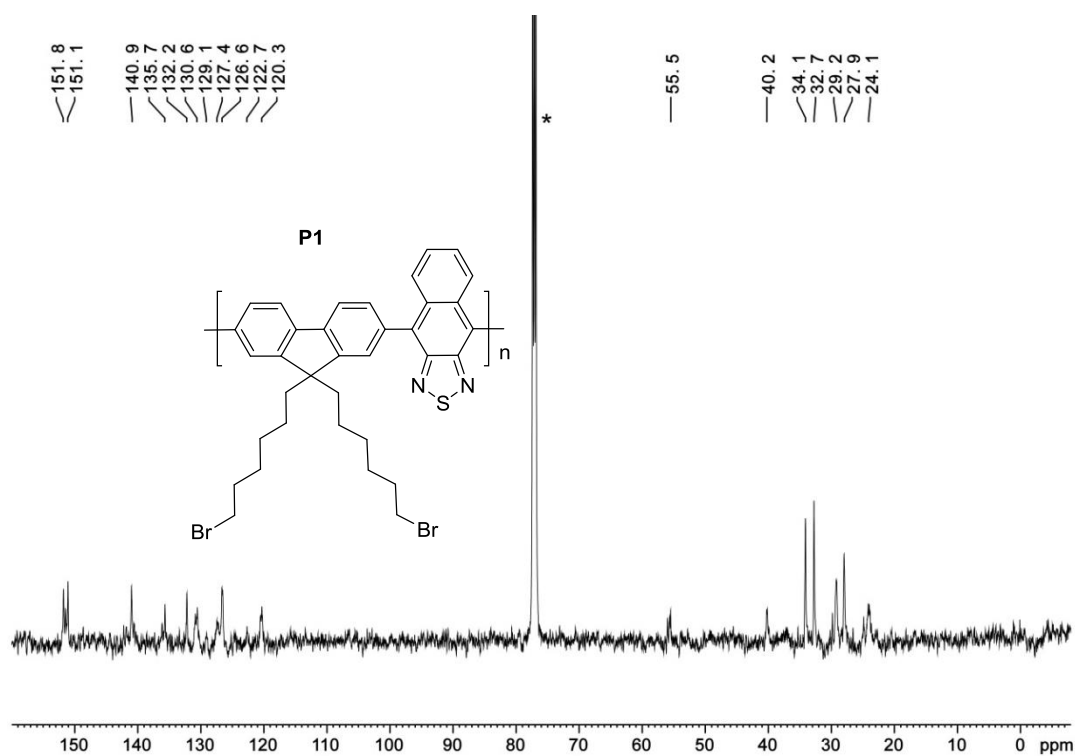
Title	Time(min)	Molecular Weight
Start	13,667	64197
Top	15,817	5530
End	17,467	844

Chromatogram Detector 1 Ch1

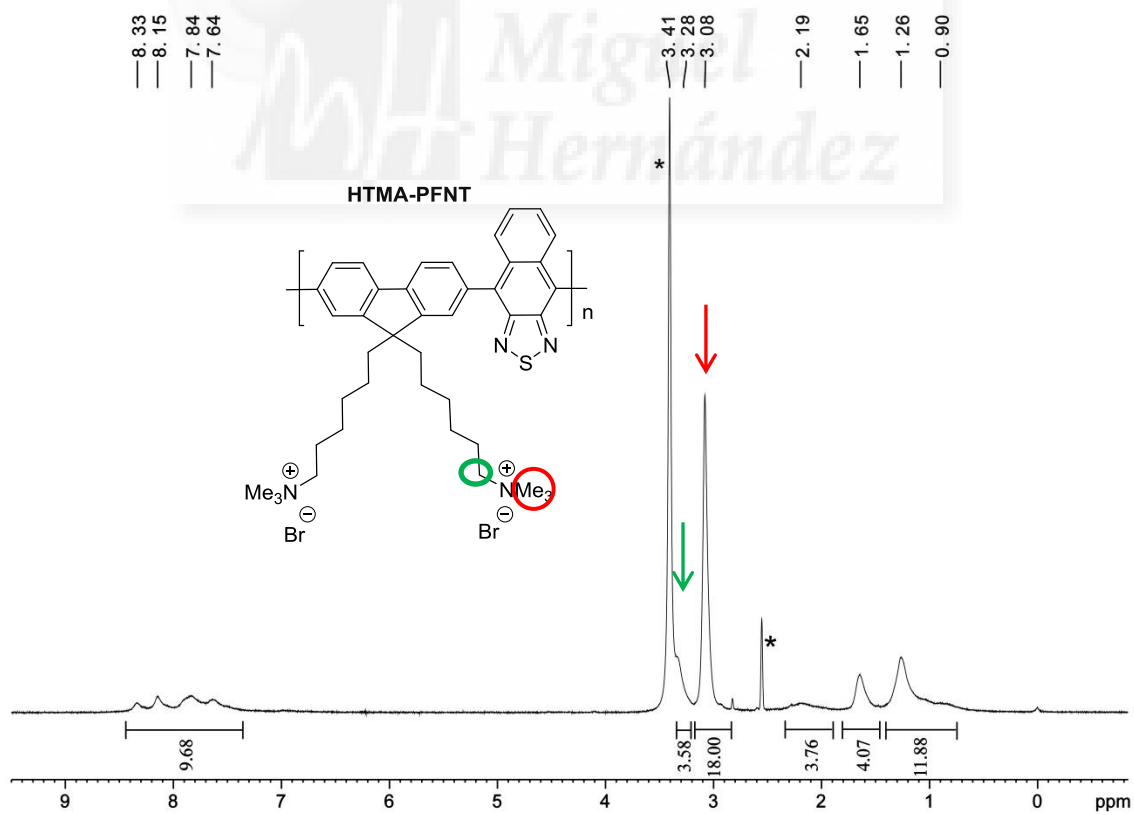
Mn	Mw	Mw/Mn
4507	8990	1,99480

Figure S1. GPC chromatogram of P1 and molecular weight distribution using RID-10A (Refraction Index Detector).





**Figure S4.**  $^{13}\text{C}$ -NMR spectra of **P1** in  $\text{CDCl}_3$ , 125 MHz. \*Solvent signals



**Figure S5.**  $^1\text{H}$ -NMR spectra of **HTMA-PFNT** in  $\text{DMSO-d}_6$ , 500MHz. \*Solvent signals

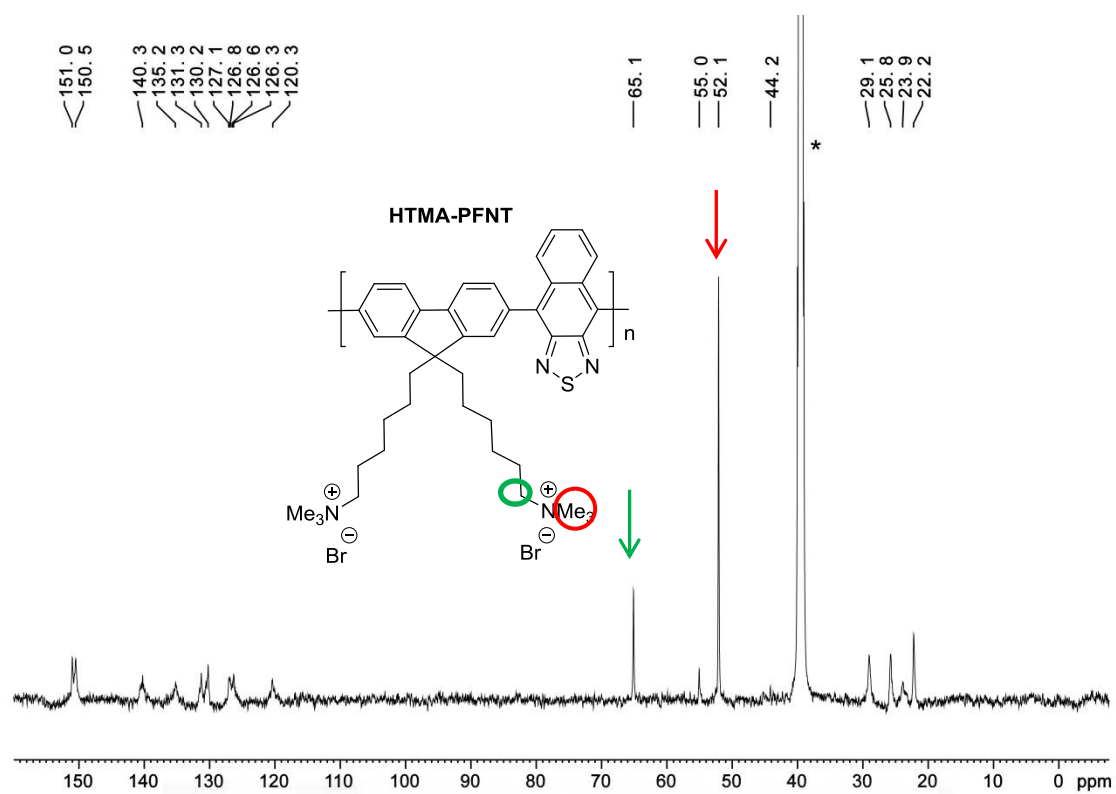


**Figure S6.**  $^{13}\text{C}$ -NMR spectra of HTMA-PFNT in DMSO- $\text{d}_6$ , 125 MHz. \*Solvent signals

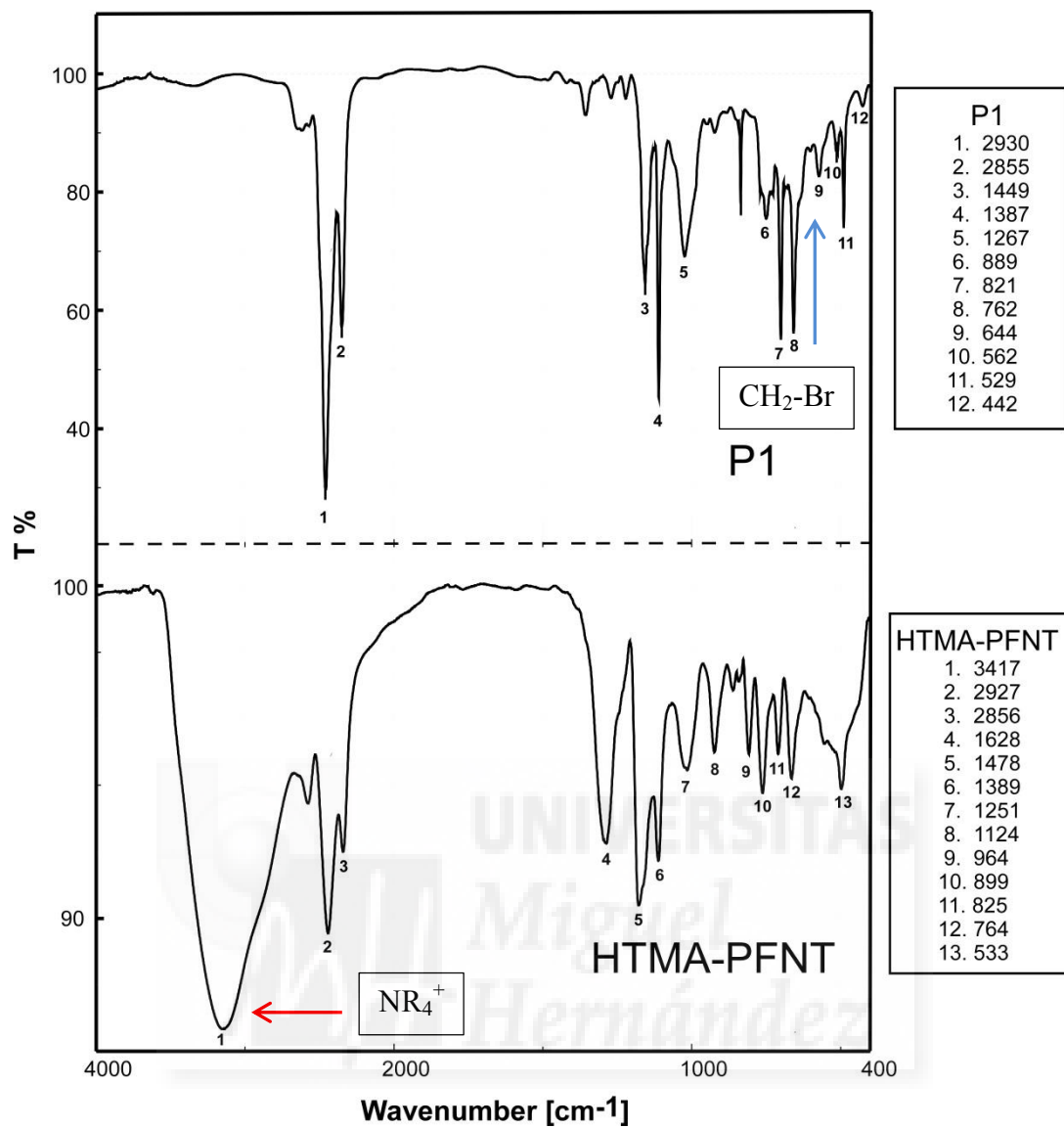


**Figure S7.** FT-IR spectra of **P1** and **HTMA-PFNT**.

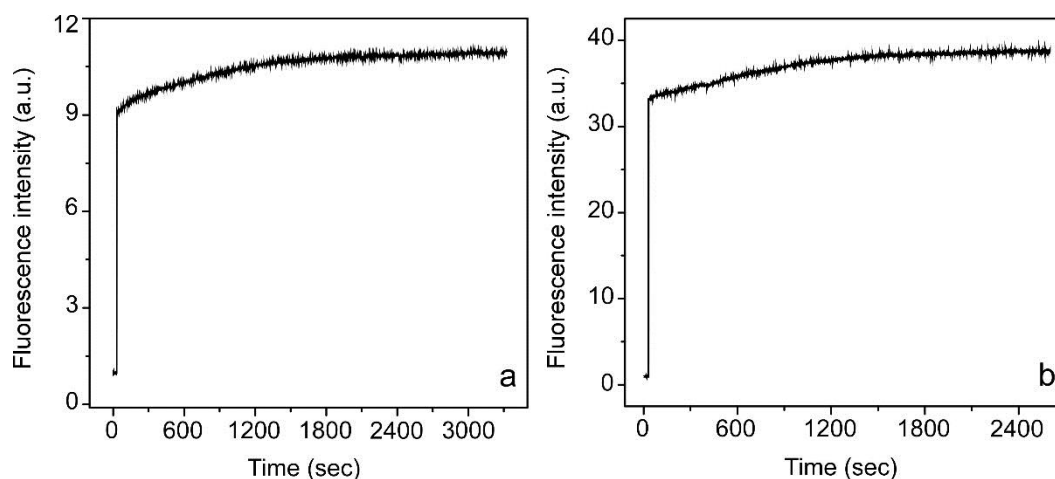


**Figure S8.** Kinetics of interaction of HTMA-PFNT (1.5  $\mu\text{M}$ ) with a) HSA (6  $\mu\text{M}$ ) and b) LUVs of DOPC (1mM).  $\lambda_{\text{exc}}=510$  nm;  $\lambda_{\text{em}}=650$  nm.

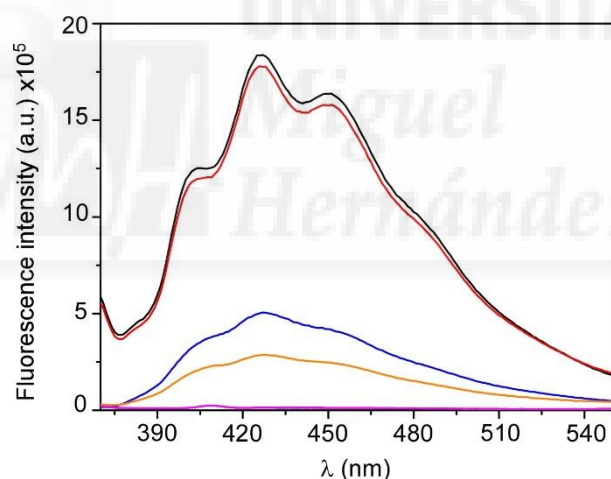


**Figure S9.** Fluorescence spectra of DPH in different samples: LUVs of DOPC (black), LUVs coated with polyelectrolyte chains (red), HSA (blue), HSA-polyelectrolyte complexes (yellow) and polyelectrolyte aggregates in buffer (pink).  $\lambda_{\text{exc}}=370$  nm

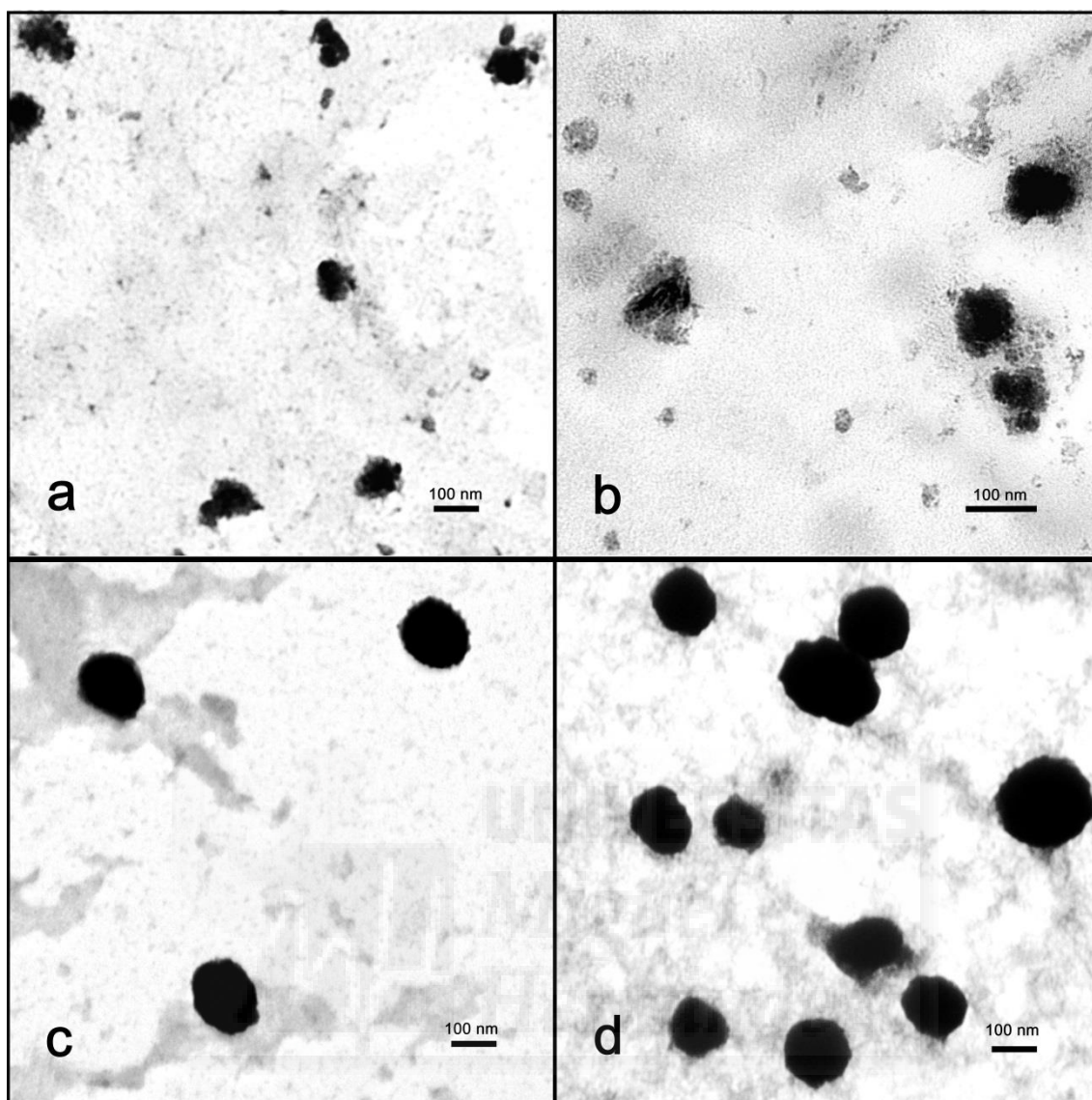


**Figure S10.** Transmission electron micrographs of negatively stained (a) HTMA-PFNT in buffer, (b) HTMA-PFNT with HSA, (c) lipid vesicles (LUVs) of DOPC and (d) lipid vesicles (LUVs) of DOPC with HTMA-PFNT.

## Publication 8.4





**Selective Recognition and Imaging of Bacterial Model  
Membranes over Mammalian Ones by Using Cationic Conjugated  
Polyelectrolytes**

**Zehra Kahveci, Rebeca Vázquez-Guilló, Amalia Mira, Lorena Martinez, Alberto Falcó,**

**Ricardo Mallavia and C. Reyes Mateo**

Instituto de Biología Molecular y Celular, Universidad Miguel Hernández, 03202

Elche, Spain

**Analyst, 2016**

**DOI:** 10.1039/c6an01427e

Impact Factor: **4.033**





Cite this: DOI: 10.1039/c6an01427e

## Selective recognition and imaging of bacterial model membranes over mammalian ones by using cationic conjugated polyelectrolytes†

Z. Kahveci,\* R. Vázquez-Guilló, A. Mira, L. Martínez, A. Falcó, R. Mallavia and C. R. Mateo\*

The development of new tools for the detection and fluorescence imaging of bacteria is of great interest in clinical diagnosis and food and environmental safety. In this work, we have explored the ability of two cationic fluorene-based conjugated polyelectrolytes, HTMA-PFP and HTMA-PFNT, emitting in the blue and red spectral regions respectively, to selectively label bacterial over mammalian cells. With this end in view, vesicles with lipid compositions mimicking those of bacterial or mammalian membranes were used as model membranes to explore the interaction of the polyelectrolytes with both systems in samples containing either a single type of vesicle or a mixture of both. Changes in the intrinsic fluorescence of HTMA-PFP and HTMA-PFNT were used to quantify the affinity of these polyelectrolytes for the model lipid membranes, while quenching experiments were employed to evaluate their selectivity to each lipid system. In addition, fluorescence microscopy experiments were performed to check the ability of polyelectrolytes to label the vesicles without affecting their integrity. Results showed that both polyelectrolytes rapidly label the model vesicles but they preferentially bind to those mimicking bacterial membranes, HTMA-PFNT being much more selective to this type of membranes than HTMA-PFP. Preliminary experiments with living bacteria and mammalian cells support this conclusion, showing that in samples with both types of cells together, HTMA-PFNT only images the bacterial cells, thus evidencing its potential use for the selective recognition and imaging of bacterial presence.

Received 22nd June 2016,  
Accepted 7th September 2016

DOI: 10.1039/c6an01427e

www.rsc.org/analyst

### Introduction

Bacteria are among the most ubiquitous of living organisms. They are extremely adaptable and able to quickly colonize and grow in a wide range of environments, even under extreme conditions.<sup>1</sup> Conventional, laboratory-based methods of bacterial detection often require specialized equipment, particular reagents, and trained users; therefore, they are costly and entail long processing times.<sup>2,3</sup> In the case of pathogenic bacteria, their rapid detection and identification in, for instance, clinical samples and food and beverages, are critical for either the prevention or early treatment of many problems related to health. As a result, there is an obvious need to develop fast and highly sensitive assays that could detect very small numbers of pathogenic bacterial cells in these types of samples.<sup>4,5</sup>

Fluorescence imaging of bacterial contamination by selectively targeting the bacterial cell membranes over the mammalian cell membranes has emerged as a powerful and fast tool in clinical diagnosis and food and environmental safety.<sup>6–9</sup> Most of the existing membrane fluorescent markers (generally, small organic fluorophores and fluorescent proteins) exhibit interesting properties; for instance, they can adapt to different experimental conditions and possess tunable optical properties. However, these fluorescent materials also show important limitations such as photobleaching, self-quenching and chemical decomposition, which restrict their applications.<sup>10,11</sup> Among them, the most known alternative is semiconductor-based quantum dots (QDs), but the potential cytotoxicity risk associated with their heavy metal components, for instance, cadmium, remains a major concern for the use of these nanoparticles in biological studies.<sup>12–14</sup> Recently, a new class of fluorescent carbon nanomaterials, *i.e.* carbon quantum dots (CQDs), has been developed. These materials, which have been used for bacterial detection recently,<sup>8</sup> possess the attractive properties shown by QDs with the added advantage of being biocompatible as well.<sup>15</sup> However, complex processes of passivation and anchoring of recognition molecules using

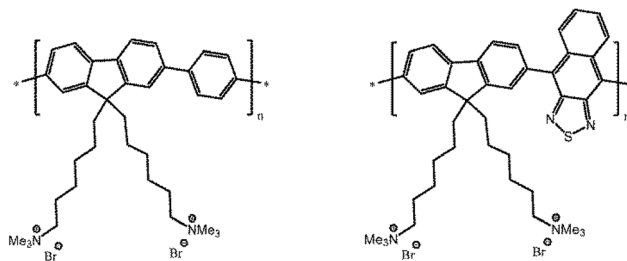
Instituto de Biología Molecular y Celular, Universidad Miguel Hernández, 03202 Elche, Alicante, Spain. E-mail: rmateo@umh.es, zkahveci@umh.es

† Electronic supplementary information (ESI) available: Additional fluorescence studies and equations. See DOI: 10.1039/c6an01427e

expensive and, in occasions, toxic coupling agents are currently indispensable in the functionalization of CQDs for selective targeting.<sup>16</sup> In addition, long incubation times are required before cell visualization using these materials.<sup>8</sup> Therefore, the improvement of synthesis methods for the biofunctionalization or development of new fluorescent markers targeting bacterial membranes continues to be a significant challenge.

Ideal membrane markers should be highly fluorescent, water-soluble, biocompatible, photostable and composed of two structural components: a group with affinity for the membrane surface and a reporter group. Recently, much interest has been generated in synthesizing novel highly-fluorescent conjugated polyelectrolytes (CPEs). These materials are photostable polymers with delocalized  $\pi$ -electron systems which show strong absorption and high fluorescent quantum yields<sup>17,18</sup> and contain ionic side groups to facilitate their water solubility and their electrostatic interaction with species of opposite charge. Electron delocalization facilitates rapid intra- and inter-chain exciton migration, conferring collective optical responses and amplified signals when compared to conventional fluorophores. Their potential biocompatible and biodegradable characteristics enable the use of CPEs *in vitro* without risking the cellular viability.<sup>19,20</sup> Moreover, another advantage is the ease of attaching reactive groups to these CPEs as side chains, which consequently allows, for instance, bioconjugation of extra recognition elements.<sup>21</sup> Given these properties, CPEs have received great attention in biomedical applications, especially as potential fluorescence sensors for small molecules, metal ions and biomolecules<sup>22–25</sup> and as promising alternatives in cell imaging as novel fluorescent probes.<sup>26–35</sup> In addition, certain CPEs have been demonstrated to exhibit antimicrobial and antitumoral activities through different mechanisms.<sup>36,37</sup>

Fluorene-based CPEs contain a rigid hydrophobic backbone with flexible charged side chains, which shows an interesting aggregation behaviour. They represent an attractive class of CPEs due to their high fluorescence quantum yield, good chemical and thermal stability and easy substitution at the fluorene C9 position enabling the grafting of different side chains. Polyfluorenes emitting at different wavelengths can be obtained, among others, by copolymerizing the fluorene monomer with appropriate aryl monomers. In this sense, our group has synthesized a blue-emitter cationic CPE, copoly- $\{[9,9\text{-bis}(6'\text{-}N,N,N\text{-trimethylammonium})\text{ hexyl}]\text{-}2,7\text{-}(\text{fluorene})\text{-alt-}1,4\text{-}(\text{phenylene})\}$  bromide (HTMA-PFP), which incorporates a phenyl group on the fluorene backbone, and a red-emitter cationic polyfluorene, copoly- $\{[9,9\text{-bis}(6'\text{-}N,N,N\text{-trimethylammonium})\text{ hexyl}]\text{-}2,7\text{-}(\text{fluorene})\text{-alt-}1,4\text{-}(\text{naphtho}[2,3c]\text{-}1,2,5\text{-thiadiazole})\}$  bromide (HTMA-PFNT), which incorporates the chromophore naphtho[2,3c][1,2,5]thiadiazole (NTD) (Scheme 1). Incorporation of the NTD group induces a long red shift in the emission spectrum, which can be due to either an extension of the conjugation length in the polymer backbone or to an extensive charge transfer between fluorene and NTD entities. Both CPEs have been characterized in aqueous solutions as



**Scheme 1** Chemical structure of HTMA-PFP (left) and HTMA-PFNT (right).

well as in the presence of biological systems such as lipid vesicles and proteins.<sup>38–41</sup> These studies show the rapid interaction of both CPEs with the biomolecules and indicate their potential use as fluorescent membrane markers. In particular, in the case of the blue polymer HTMA-PFP, an exhaustive study was carried out with anionic and zwitterionic model lipid membranes, showing that this CPE displays a higher affinity for anionic lipids than that for zwitterionic lipids, as has been also found for other cationic CPEs,<sup>42</sup> selectively labeling and imaging the anionic vesicles over zwitterionic ones.<sup>40</sup>

It is known that one of the most characteristic differences between bacterial and mammalian cells is in the composition of their cell membranes. For instance, the outer leaflet of bacterial membranes contains abundant negatively charged lipids, while it is predominantly zwitterionic for human eukaryotic cell membranes.<sup>43</sup> The different behaviour of HTMA-PFP towards anionic and zwitterionic membranes suggests that this kind of CPE could be used for the selective recognition and imaging of bacteria over mammalian cells and, therefore, as a rapid tool to detect the presence of bacteria. In the present work we have investigated this possibility by exploring, on the one hand, the interaction of HTMA-PFP with unilamellar vesicles with lipid compositions mimicking those in mammalian or bacterial membranes and, on the other hand, the capacity of the CPE to fluorescently label and differentiate bacterial cells from mammalian cells. In addition, a similar study has been performed with the red CPE HTMA-PFNT, and the abilities of both polymers to selectively bind bacterial cell membranes have been compared.

## Experimental section

### Materials

The synthetic phospholipids 1,2-dioleoyl-*sn*-glycero-3-phosphocholine (DOPC), 1,2-dioleoyl-*sn*-glycero-3-phosphoethanolamine (DOPE), 1,2-dioleoyl-*sn*-glycero-3-phospho-rac-(1-glycerol) sodium salt (DOPG), cholesterol (Chol), and cardiolipin sodium salt from bovine heart (CA) were from Sigma-Aldrich and were used as received. The cationic CPEs HTMA-PFP ( $M_n$  [g mol<sup>-1</sup>] = 4170;  $M_w$  [g mol<sup>-1</sup>] = 8340) and HTMA-PFNT ( $M_n$  [g mol<sup>-1</sup>] = 4507;  $M_w$  [g mol<sup>-1</sup>] = 8990) were obtained and characterized in our laboratory. Briefly, batches of the neutral polymers,

poly[bis(6'-bromohexyl)fluorene-phenylene] and copoly-{9,9-bis(6-bromohexyl)-2,7-fluorene-alt-1,4-(naphto[2,3c]-1,2,5-thiadiazole)}, were synthesized by Suzuki coupling reaction with Pd(II) as a catalyst and treated with gas-phase trimethylamine in order to obtain the corresponding cationic CPEs HTMA-PFP and HTMA-PFNT, respectively.<sup>41,44,45</sup> Stock solutions of HTMA-PFP and HTMA-PFNT were prepared in DMSO with a final concentration of  $3.65 \times 10^{-4}$  M (in repeat units) and stored at  $-20$  °C before use. The quencher 9,10-anthraquinone-2,6-disulfonic acid (AQS) was obtained from Sigma-Aldrich (St Louis, MO, USA) and dissolved in water (5 mM) just before use. All other solvents were of spectroscopic reagent grade (Uvasol, Merck). Sodium phosphate buffer (50 mM, 0.1 M NaCl, pH 7.4) was prepared with water which was previously double distilled in all-glass apparatus and deionized using Milli-Q equipment (Millipore, Madrid, Spain).

### Preparation of large unilamellar vesicles (LUVs)

Chloroform/methanol solutions containing 3 mg of lipid mixtures for each model membrane (for the bacterial model membrane: DOPE : DOPG : CA (67 : 23.2 : 9.8, molar ratio) and for the mammalian model membrane: DOPC : Chol (70 : 30, molar ratio)) were first dried by evaporation under a dry nitrogen gas stream and subsequently under vacuum for 3 h. Multilamellar vesicles (MLVs) were formed on resuspending the dried mixture of lipids in a certain volume of buffer to reach the required final concentrations. The vesicle suspension was then vortexed several times. Large unilamellar vesicles (LUVs) of the model membranes were prepared from these MLVs by pressure extrusion through 0.1  $\mu$ m polycarbonate filters (Nucleopore, Cambridge, MA, USA). All samples were used on the same day they were prepared.

### Preparation of giant unilamellar vesicles (GUVs)

Giant unilamellar vesicles (GUVs) composed of DOPE : DOPG : CA and DOPC : Chol were prepared with the gentle hydration method instead of the most widely used electroformation method because the presence of charged lipids or cholesterol is a limitation to the electroformation of vesicles.<sup>46</sup> Briefly, lipids were dissolved in chloroform/methanol at a final lipid concentration of 5 mM. Then, 10  $\mu$ L of this solution was dropped on a microscope slide which was previously washed with alcohol and dried. This sample was left to dry at room temperature for a few seconds and subsequently under vacuum for 2 h. Afterwards, the lipid film was hydrated with 15  $\mu$ L of a sucrose solution (0.2 M) in a humid chamber overnight. To better observe the synthesized GUVs under the microscope, 400  $\mu$ L of a 0.2 M glucose solution were previously added to the wells in order to settle 50  $\mu$ L of GUVs to the bottom of the chamber. Samples were preserved for 2 h at 10 °C before microscopy visualization.

### Preparation of CPE/lipid samples

Aliquots of HTMA-PFP and HTMA-PFNT in DMSO were externally added to the lipid vesicle suspension. In all cases, the proportion of DMSO in the aqueous samples was always lower

than 1% (v/v). In the fluorescence studies, the final concentration of the CPEs was 1.5  $\mu$ M (in terms of repeat units). Previous studies by our group have reported that at this concentration, these CPEs do not perturb the membrane integrity.<sup>39-41</sup>

### Fluorescence measurements

Fluorescence spectra and fluorescence intensity measurements were performed using a QuantaMaster spectrofluorometer (PTI, Birmingham, NJ, USA). The experimental samples were placed in 10 mm  $\times$  10 mm path length quartz cuvettes. Samples were excited at 380 nm (HTMA-PFP) and 510 nm (HTMA-PFNT). Background intensities were always checked and subtracted from the sample when necessary. All fluorescence spectra were corrected for the variations in photo-multiplier response over wavelength.

### Partition coefficient measurements

Changes in the fluorescence intensity of HTMA-PFP and HTMA-PFNT as a function of lipid concentration were used to estimate the partition coefficient of the CPE between the lipid membrane and the aqueous phase ( $K_p$ ), which is defined in terms of molar concentrations as:

$$K_p = \frac{n_L/V_L}{n_W/V_W} \quad (1)$$

where  $n_i$  represents the moles of the compound in phase  $i$  and  $V_i$  represents the volume of phase  $i$ . The phase is either aqueous ( $i = W$ ) or lipidic ( $i = L$ ). The quantitation of  $K_p$  was done according to:<sup>47</sup>

$$\Delta I = \frac{\Delta I_{\max}[L]}{1/(K_p\gamma) + [L]} \quad (2)$$

where  $\Delta I$  ( $\Delta I = I - I_0$ ) represents the difference between the fluorescence intensities (or emission spectrum areas) of the CPEs measured in the presence ( $I$ ) and absence ( $I_0$ ) of lipid vesicles,  $\Delta I_{\max} = I_{\infty} - I_0$  is the maximum value of this difference once the limiting value is reached ( $I_{\infty}$ ) upon increasing the lipid concentration  $[L]$ , and  $\gamma$  is the phospholipid molar volume, which is  $0.763 \text{ M}^{-1}$  for fluid phases.<sup>48</sup>

### Fluorescence quenching experiments

Fluorescence emissions of the CPEs HTMA-PFP and HTMA-PFNT in buffer and incorporated in model membrane LUVs were studied in the absence and presence of different concentrations of AQS. This molecule is an electron acceptor and acts as a quencher of cationic CPEs, forming static quenching complexes *via* attractive electrostatic interactions.<sup>49,50</sup> Stern-Volmer analysis was applied to the fluorescence quenching data according to eqn (3):

$$\frac{I_0}{I} = 1 + K_{sv}[Q] \quad (3)$$

where  $I_0$  and  $I$  represent the steady-state fluorescence intensities in the absence and presence of the quencher, respec-

tively,  $[Q]$  is the quencher concentration and  $K_{SV}$  is the Stern-Volmer constant, which represents the association constant for complex formation in the case of static quenching.<sup>49</sup> The percentage of quenching efficiency was calculated as  $(1 - I/I_0) \times 100$ . In samples containing LUVs of bacterial and mammalian lipid compositions at different proportions, the expected intensity was obtained taking into account the fluorescence intensity ratio of the CPE in both systems as well as the fraction of each system (see ESI†).

### Microscopy experiments

Fluorescence microscopy images were recorded using a Leica DMI 3000B inverted microscope equipped with a Leica EL6000 compact light source and a Leica DFC3000G digital camera. The imaging was performed using 63 $\times$  magnification with 0.7 objective and the filter DAPI (Ex: BP 350/50, Em: BP 460/50) or DsRed (Ex: BP 555/25, Em: BP 620/60). Data acquisition was monitored by manually formatting and processing with Leica Application Suite AF6000 Module Systems.

### Bacterial and mammalian cell imaging

The bacterial strain used in this study was *Escherichia coli* Top 10 F'. A culture of this strain that was grown in LB medium at 37 °C overnight was used to make 20% glycerol stock aliquots, which were then stored at -80 °C until use. The concentration of bacteria was determined as the number of colony forming units per ml (CFUs per ml) from one of these stock aliquots.

The human cell line HeLa was cultured in high glucose DMEM (Sigma Aldrich) supplemented with 2 mM L-glutamine, 10% FBS, penicillin-streptomycin (100 units penicillin per mL and 0.1 mg streptomycin per mL; Sigma Aldrich) at 37 °C in a humidified incubator under a 5% CO<sub>2</sub> atmosphere. For microscopy images, HeLa cells were previously trypsinized, harvested and resuspended in phosphate-buffered saline (PBS).

For the fluorescence microscopy assays, 8-well plates were used. The final concentrations were 10<sup>6</sup> *E. Coli* Top 10 F'

bacteria per mL, 10<sup>5</sup> HeLa cells per mL and 0.2  $\mu$ M of either HTMA-PFP or HTMA-PFNT, in a total volume of 300  $\mu$ L final volume per mL in PBS. Microscopy images were taken in the absence and presence of the CPEs separately or combining both bacteria and cells.

## Results and discussion

### HTMA-PFP in model membranes

As was already mentioned above, the cationic conjugated CPE HTMA-PFP (Scheme 1) interacts with lipid vesicles displaying higher affinity for anionic lipid membranes than that for zwitterionic lipid membranes, *i.e.* selectively labeling and imaging the anionic vesicles over the zwitterionic ones.<sup>51</sup> This result suggests that this CPE could be used for the selective recognition and imaging of bacterial cell membranes rich in anionic lipids. To test this possibility, as a first step, we have explored the interaction of the CPE with bacterial and mammalian membrane models. In order to mimic the different membranes, the mixture of phospholipids of DOPE (% 67), DOPG (% 23.2) and CA (% 9.8) was selected as the component of the bacterial model membrane, which corresponds with the composition of the outer membrane of the bacteria *E. coli*, while the mixture of DOPC (% 70) and cholesterol (% 30) was used for the mammalian model membrane.<sup>52-54</sup> The affinity of HTMA-PFP to both membranes was studied by recording its fluorescence emission spectrum after addition (1.5  $\mu$ M final concentration) to samples containing increasing amounts of the corresponding lipid vesicles, from 0 to 1 mM (Fig. 1a and b). Note that changes in absorbance spectra were not used to determine the affinity because of their being not very pronounced and due to the high scattering induced by liposomes (Fig. S2†). For the bacterial model, a strong enhancement of the fluorescence intensity was observed as a function of lipid concentration a few seconds after CPE addition, together with a blue shift of the emission spectrum. Higher concentrations

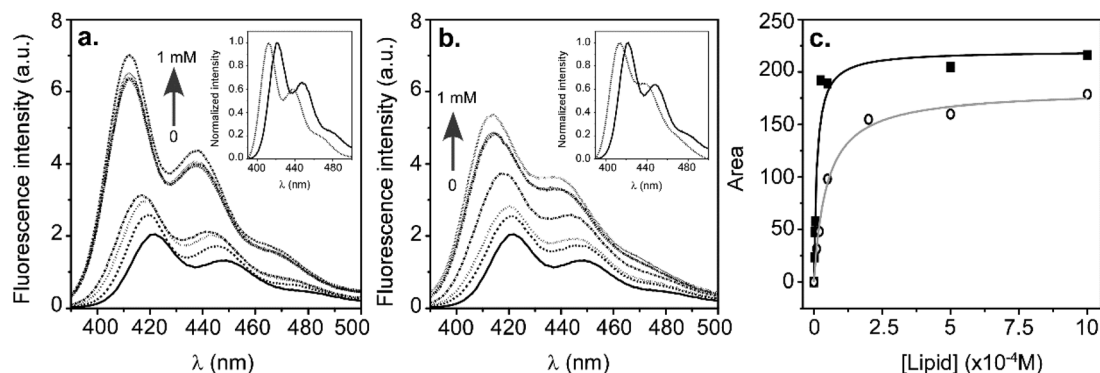


**Fig. 1** Fluorescence emission spectra, recorded upon excitation at 380 nm, for HTMA-PFP (1.5  $\mu$ M) in buffer and at increasing concentrations (up to 1 mM) of (a) the bacterial model membrane and (b) the mammalian model membrane. (c) Area of the emission spectrum of HTMA-PFP at different concentrations of bacterial (squares) and mammalian (circles) model membranes. Insets in (a) and (b) represent the normalized emission spectra recorder in buffer (black) and in the presence of 1 mM of lipid (grey).

of lipid, above 0.125 mM, practically did not modify the fluorescence signal. This behaviour, which was also observed for the CPE in the presence of LUVs of pure DMPG,<sup>39</sup> indicates that HTMA-PFP interacts with high affinity with the lipid bilayer. As a consequence of this interaction, the polymer chains become more extended than in buffer, where it forms metastable aggregates, and the probability of polymer–polymer interaction, and therefore the self-quenching efficiency, is reduced, increasing the fluorescence quantum yield. For the mammalian model, a blue-shift was also observed in the emission spectrum of the polymer, supporting the existence of interaction, but it was slightly lower than that observed for the bacterial lipids (Fig. 1b). In addition, the increase in fluorescence intensity was slower and clearly lower, reaching its maximum value at higher lipid concentrations (about 0.3 mM). This result indicates a lower affinity of the poly-electrolyte for the mammalian membrane model as well as a different mechanism of interaction, and suggests that aggregates of HTMA-PFP are better solubilized in the bacterial membrane model than in the mammalian membrane model.

The partition coefficient of the CPE between the lipid and the aqueous phase ( $K_p$ ) was determined plotting the area of each spectrum as a function of lipid concentrations (Fig. 1c) using eqn. (2). This value was obtained from a two-parameter ( $\Delta I_{\max}$  and  $K_p$ ) fitting procedure. Results are shown in Table 1 and compared with those obtained in lipid vesicles of pure zwitterionic (PC) and anionic (PG) lipid vesicles.<sup>39–41</sup> The different obtained  $K_p$  values are indicative of a preference of HTMA-PFP for bacterial over mammalian membranes, but this preference is lower than that observed for pure anionic over zwitterionic membranes. The value obtained for the bacterial model is slightly lower than that determined for pure anionic vesicles, probably due to the presence of zwitterionic lipids in its composition. However, both values are in the same scale, suggesting that the mechanism of interaction between the CPE and the bacterial membranes is mainly based on electrostatic interactions between the quaternary amine groups of the CPE (Scheme 1) and the anionic surface of the bacterial membrane.

The fact that the  $K_p$  for the mammalian system is about 4 times lower than that for the bacterial one, but still high despite the absence of negative surface charge on the vesicles, indicates that the hydrophobic effect and van der Waals forces that dominate the partition to the neutral systems can also account for an important part of the polymer–membrane interaction.<sup>48</sup>

To gain more insight into the membrane–CPE interactions, we took advantage of the fact that the fluorescence of HTMA-PFP can be quenched by anionic electron acceptors such as AQS, which is soluble in water but not in lipid membranes.<sup>40,49,50</sup> When the AQS concentration was increased in bacterial and mammalian model membrane suspensions containing HTMA-PFP, different behaviours were observed. In the bacterial model, only a slight decrease in the fluorescence signals of the CPE was detected, while the quenching effect was much more pronounced in the mammalian model. Fig. 2a shows the Stern–Volmer plots corresponding to these experiments. Using eqn (3),  $K_{SV}$  values of  $1.3 \pm 0.3 \times 10^3 \text{ M}^{-1}$  and  $2.2 \pm 0.3 \times 10^4$  were obtained from the slope of the plots for bacterial and mammalian models, respectively (Table 1). This result was used to estimate the most probable location of the CPE in the different systems. A lower quenching and thus a lower  $K_{SV}$  for HTMA-PFP in the presence of vesicles would indicate its protection from the quencher and hence its insertion into the lipid bilayer. In the buffer, in the absence of lipid vesicles, the  $K_{SV}$  value is  $1.6 \times 10^7 \text{ M}^{-1}$ ;<sup>39</sup> therefore, the lower values determined for HTMA-PFP in the presence of both model membranes confirm its interaction. However, the fact that  $K_{SV}$  in the mammalian model is about 17 times higher than that in the bacterial model indicates that the CPE

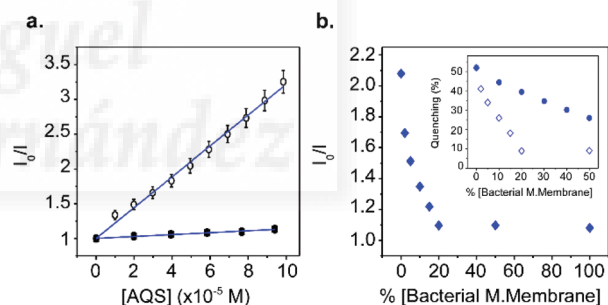


**Fig. 2** (a) Stern–Volmer plots for the quenching of HTMA-PFP (1.5  $\mu\text{M}$ ) by AQS in model bacterial (squares) and mammalian (circles) membranes. (b) Quenching induced by [AQS] = 50  $\mu\text{M}$  in the fluorescence intensity of HTMA-PFP (1.5  $\mu\text{M}$ ) in samples containing mammalian LUVs coexisting with increasing concentrations of bacterial LUVs. Inset: Quenching efficiency versus increased bacterial vesicle percentage (blue diamonds) compared with the theoretical quenching efficiency obtained if the CPE had the same preference for both model membranes (blue circles).

**Table 1** Partition coefficient,  $K_p$ , values obtained from the fit of eqn (2), and Stern–Volmer constants,  $K_{SV}$ , determined for HTMA-PFP and HTMA-PFNT in different lipid membrane models in the presence of the quencher, AQS

System	$K_p$		$K_{SV} (\text{M}^{-1})$	
	HTMA-PFP	HTMA-PFNT	HTMA-PFP	HTMA-PFNT
Mammalian	$2.9 \pm 0.1 \times 10^4$	$2.2 \pm 0.4 \times 10^4$	$2.2 \pm 0.3 \times 10^4$	$5.1 \pm 0.1 \times 10^3$
Bacterial	$1.2 \pm 0.3 \times 10^5$	$4.7 \pm 0.6 \times 10^5$	$1.3 \pm 0.3 \times 10^3$	$4.0 \pm 0.3 \times 10^2$
PC	$1.3 \pm 0.8 \times 10^4$	$1.1 \pm 0.1 \times 10^4$	$1.4 \pm 0.2 \times 10^5$	$5.9 \pm 0.2 \times 10^4$
PG	$2.9 \pm 1.3 \times 10^5$	$1.1 \pm 0.1 \times 10^6$	0	0

remains located close to the membrane surface in the mammalian model, while it penetrates more deeply into the lipid bilayer of the bacterial membrane. Comparing these  $K_{SV}$  values with those determined in lipid vesicles of PC and PG (Table 1<sup>39–41</sup>), we can conclude that HTMA-PFP in the bacterial model is effectively embedded in the bilayer but it resides less close to the hydrophobic core than for pure anionic lipids, where no quenching is observed. This effect could be due to the lipid composition of the bacterial membrane, containing 67% of zwitterionic phospholipids (DOPE), which reduces the anionic net charge of the membrane surface and thus decreases the level of penetration of the CPE into the bilayer.

The above results suggest the existence of different mechanisms for the interaction of HTMA-PFP with bacterial and mammalian membrane models, which are caused by the variations in the net membrane surface charge. In this sense, although the fast and higher affinity of HTMA-PFP for the anionic membrane is mainly attributed to electrostatic interactions, the final location of the CPE indicates that hydrophobic forces also contribute to its solubilisation in the bilayer, thus reducing its aggregation and increasing the fluorescence quantum yield in bacterial membranes compared to mammalian ones. This different behaviour supports the hypothesis of HTMA-PFP being selective for bacterial over mammalian membranes and, therefore, suggests its potential use as a bacterial membrane marker. However, to confirm this selectivity it is necessary to know the behaviour of the CPE in samples containing both types of vesicles.

The fact that the extent of quenching by AQS is clearly different in bacterial and mammalian membranes can be used as a tool to monitor this behaviour. To this end, different samples containing LUVs of mammalian lipid composition were prepared, coexisting with increasing concentrations of bacterial LUVs, from 0% to 100% (the final total lipid concentration was 1 mM). A constant concentration of HTMA-PFP (1.5  $\mu\text{M}$ ) and AQS (50  $\mu\text{M}$ ) was added to each sample, the fluorescence spectra were recorded and the quenching efficiency was analysed. According to Fig. 2a, for the sample containing only mammalian vesicles, the quenching efficiency is around 50% at  $[\text{AQS}] = 50 \mu\text{M}$ , while for the sample containing only bacterial vesicles, it is  $\sim 7\text{--}8\%$ . Fig. 2b (and its inset) illustrates the experimental decrease observed in the quenching efficiency as the proportion of bacterial vesicles increases. This plot is also compared with the theoretical data expected if HTMA-PFP had the same preference for bacterial and mammalian membranes. The theoretical curve shows that, for a sample containing the same amounts of both vesicles, a quenching efficiency of around 26% would be obtained (see eqn (S1) in the ESI† and the inset in Fig. 2b). However, this result was not observed and the efficiency determined experimentally under these conditions was instead much lower. In fact, an increase in the proportion of bacterial vesicles rapidly decreased the quenching efficiency, reaching similar efficiencies in a sample still containing 80% of mammalian membranes and another one containing only bacterial LUVs. This result confirms the selectivity of

HTMA-PFP to bacterial over mammalian model membranes, as was previously suggested.

### HTMA-PFNT in model membranes

In a recent paper we have already reported the synthesis and characterization of a new fluorene-based CPE, HTMA-PFNT (Scheme 1), which emits in the red region of the visible spectrum.<sup>41</sup> This CPE is unstable in buffer, showing a low fluorescence quantum yield and a high tendency to self-aggregate. However, it shows high affinity for zwitterionic lipid vesicles, increasing its fluorescence signal and leading to stable structures. From the affinity studies, a  $K_p$  value of  $1.1 \pm 0.1 \times 10^4$  was obtained between the zwitterionic membrane and the aqueous phase, which was in a similar range as that determined for HTMA-PFP<sup>39–41</sup> (Table 1). The fact that both CPEs have similar structures, containing side chains with cationic quaternary amine groups, suggests that HTMA-PFNT could also have a preference for anionic lipid over zwitterionic ones. To explore this possibility, firstly we determined the CPE affinity for pure anionic vesicles composed of DOPG. With this aim, a fixed concentration of HTMA-PFNT (1.5  $\mu\text{M}$ ) was added to samples containing increasing concentrations of lipid and the fluorescence emission spectra were recorded and analyzed. An enhancement in fluorescence intensity, with several folds of amplification of the quantum yield, was observed in a lipid concentration-dependent manner, as well as a slight blue-shift of the emission maximum, which indicates the interaction of the CPE with the anionic membrane (ESI, Fig. S1†). From these results,  $K_p = 1.1 \times 10^6$  was determined using eqn (1) (Table 1). This value was two orders of magnitude greater than that obtained using the zwitterionic system, indicating that the preference of HTMA-PFNT for anionic lipids over zwitterionic ones is even higher than that determined for HTMA-PFP. Therefore, the CPE could be used for selective recognition of bacterial cell membranes, probably with more efficacy than HTMA-PFP. To test this possibility, we explored the interaction of the CPE with bacterial and mammalian membrane models following the same procedure as was previously shown with HTMA-PFP. Fig. 3 shows the fluorescence emission spectra of the CPE recovered at increasing concentrations of both membrane models. As was found for DOPG LUVs, an increase in the fluorescence intensity and a blue-shift were observed depending on the lipid concentration. In the case of the bacterial model, a very little amount of lipid was required to reach the maximum fluorescence signal, in contrast to that observed for the mammalian model. The partition curves were plotted for each lipid system and the  $K_p$  was extracted from these curves using eqn (1) (Fig. 3c and Table 1). Thus, the  $K_p$  recovered for the bacterial model is about one half of the value corresponding to that obtained with pure PG vesicles, but 20 times higher than with the mammalian model. Comparing the  $K_p$  values of both CPEs for the different systems, we can conclude that HTMA-PFNT would be more selective than HTMA-PFP for bacterial membranes, as was previously suggested.

The location of HTMA-PFNT in the different lipid models was explored using AQS, as previously described for the blue

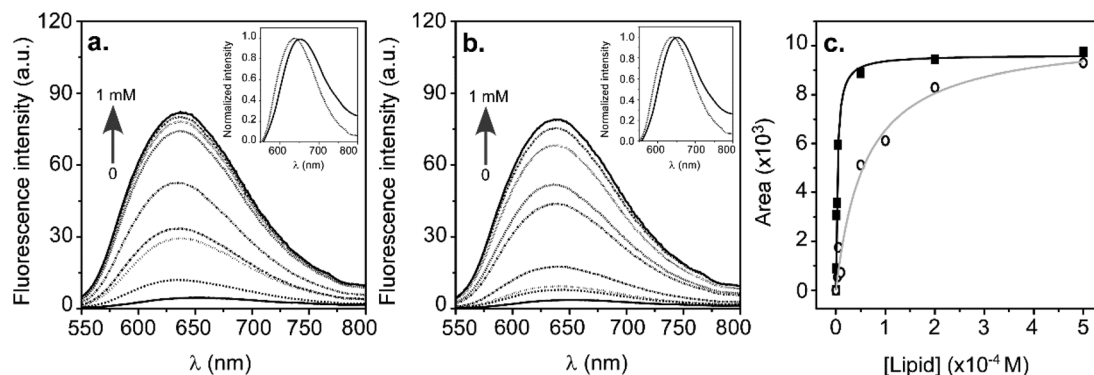


**Fig. 3** Fluorescence emission spectra, recorded upon excitation at 530 nm, for HTMA-PFNT (1.5  $\mu\text{M}$ ) in buffer and at increasing concentrations (up to 1 mM) of (a) the bacterial model membrane and (b) the mammalian model membrane. (c) Area of the emission spectrum of HTMA-PFNT at different concentrations of bacterial (squares) and mammalian (circles) model membranes. Insets in (a) and (b) represent the normalized emission spectra recorded in buffer (black) and in the presence of 1 mM of lipid (grey).

CPE. When increasing concentrations of the quencher were added to DOPG vesicles containing HTMA-PFNT, no quenching was observed, indicating that the CPE is well embedded in the lipid bilayer (Table 1). However, the addition of AQS to mammalian and bacterial vesicles induced a decrease in the fluorescence, this effect being higher in the mammalian model than in the bacterial one (Fig. 4a). The Stern–Volmer plots were linear in the range studied, with  $K_{\text{SV}} = 5.1 \times 10^3 \text{ M}^{-1}$  and  $K_{\text{SV}} = 4.0 \times 10^2 \text{ M}^{-1}$  for mammalian and bacterial models, respectively (Table 1). These values are lower than the value of  $K_{\text{SV}} = 1.1 \times 10^6 \text{ M}^{-1}$  obtained in buffer,<sup>41</sup> which confirms that in both membrane models the CPE is incorporated into the bilayer. However, the higher value determined for the mammalian model indicates that in this system the polymeric chains are inserted in the lipid bilayer close to the membrane surface, relatively accessible to the quenchers, while in the bacterial model, HTMA-PFNT is located deeper inside the lipid bilayer.

As for HTMA-PFP, we have taken advantage of the fact that the extent of quenching is different in bacterial and mamma-

lian model membranes in order to explore the selectivity of the CPE in samples with both types of vesicles together. Samples containing mixtures of bacterial and mammalian model membranes were prepared by increasing the proportion of the model bacterial membrane in the mixture from 0 to 100% (final lipid concentration 1 mM). The same concentration of CPE was added to all the samples (1.5  $\mu\text{M}$ ) and the fluorescence spectra were recorded before and after the addition of AQS (200  $\mu\text{M}$ ). Fig. 4b shows the experimental decrease observed in the quenching efficiency as the proportion of bacterial vesicles increases. The plot is compared with the theoretical data expected if the CPE had the same preference for bacterial and mammalian membranes (inset). From this plot we can conclude that a very small proportion of bacterial vesicles rapidly decreases the quenching efficiency and that when HTMA-PFNT is added to a sample containing 95% of mammalian membranes and 5% of bacterial membranes, all the polymer chains are incorporated into the bacterial LUVs and not in the mammalian ones.

This result evidences the high preference of the CPE for these vesicles, and confirms that HTMA-PFNT has higher selectivity and sensitivity for bacterial model membranes than HTMA-PFP.

#### HTMA-PFP and HTMA-PFNT as cell membrane markers

The above results suggest the possibility of using the CPEs, especially HTMA-PFNT, to detect bacterial contamination by selectively targeting bacterial membranes over mammalian cells. Before testing this possibility, firstly we explored whether the CPEs were able to label and image the two types of cells separately, preserving their integrity. The study was performed by fluorescence microscopy, initially with model membranes and later with bacterial and mammalian cells. For the study with model membranes, GUVs composed of DOPE : DOPG : CA and DOPC : Chol were prepared as described in Experimental section. Microscopy images were recorded before and after the addition of HTMA-PFP or HTMA-PFNT. In the absence of CPE, both types of vesicles were visualized by phase contrast

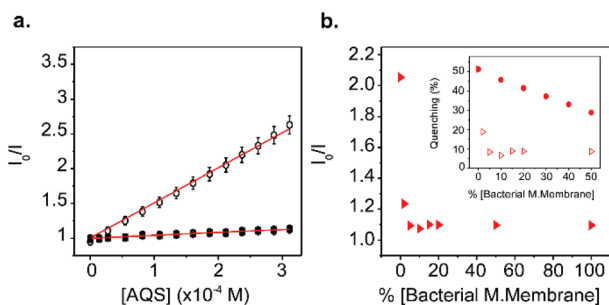


**Fig. 4** (a) Stern–Volmer plots for quenching of HTMA-PFNT (1.5  $\mu\text{M}$ ) by AQS in model bacterial (squares) and mammalian (circles) membranes. (b) Quenching induced by [AQS] = 200  $\mu\text{M}$  in the fluorescence intensity of HTMA-PFNT (1.5  $\mu\text{M}$ ) in samples containing mammalian LUVs coexisting with increasing concentrations of bacterial LUVs. Inset: Quenching efficiency versus increased bacterial vesicle percentage (red triangles) compared with the theoretical quenching efficiency obtained if the CPE had the same preference for both model membranes (red circles).

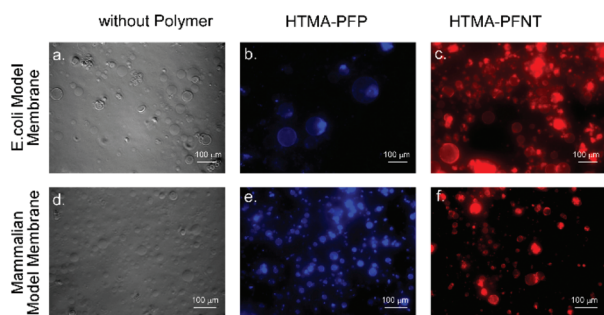


**Fig. 5** (a) Phase contrast image of GUVs of model bacterial membranes in the absence of CPEs. (b) Fluorescence microscopy images of GUVs of model bacterial membranes in the presence of HTMA-PFP and (c) HTMA-PFNT, recorded upon irradiation with UV- and visible-light, respectively. (d) Phase contrast image of GUVs of model mammalian membranes in the absence of CPEs. (e) Fluorescence microscopy images of GUVs of model mammalian membranes in the presence of HTMA-PFP and (f) HTMA-PFNT, recorded upon irradiation with UV- and visible-light, respectively.

microscopy (Fig. 5a and d), and no fluorescence was detected when the samples were excited with UV or visible light. CPEs were added to the same samples and fluorescence images were taken 5 min after addition. Samples containing HTMA-PFP were excited with UV-light (Fig. 5b and e), while those containing HTMA-PFNT were excited with visible-light (Fig. 5c and f). Results show that both CPEs rapidly interact with the two types of GUVs, labelling the membrane and allowing for their visualization, without altering their spherical morphology.

For the *in vitro* studies with bacterial and mammalian cells, *E. coli* Top 10 F' strain and human HeLa cells were used. The microscopy images were obtained before and after adding the CPEs (0.2 µM final concentration). Fig. 6a and b show the fluorescence images observed 5 min after the addition of HTMA-PFP, upon excitation with UV-light. Results show the ability of this CPE to label in blue both, bacterial and mammalian cells. In the same way, addition of HTMA-PFNT to the samples and excitation with visible-light allowed for the visualization in red color of the two types of cells (Fig. 6c and d). CPEs were photostable, preserving their fluorescence during the acquisition without suffering from photobleaching.

### Selective imaging of bacteria over mammalian cells

Once it was proven that the CPEs are able to label and image bacterial and mammalian cells separately, we explored the possibility of using them to detect bacterial contamination by carrying out a preliminary experiment where both types of cells were together in the same sample. To this end, PBS resuspended HeLa cells (100 000 cells per mL) and bacteria *E. coli* Top10 F' (1 000 000 bacteria per mL) were mixed in a total volume of 300 µL in a microscopy plate. Then, HTMA-PFP and HTMA-PFNT were added separately (0.2 µM final concentration), and phase contrast and fluorescence microscopy images were taken 5 min after addition (Fig. 7). In Fig. 7a it is possible to visualize both populations of bacteria *E. coli* and

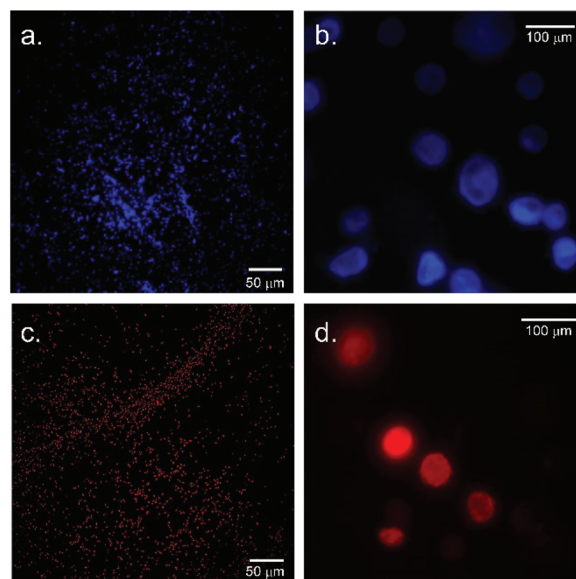


**Fig. 6** Top: Fluorescence microscopy images of bacteria *E. coli* (a) and HeLa cells (b) after the addition of HTMA-PFP and irradiation with UV-light. Bottom: Fluorescence microscopy images of bacteria *E. coli* (c) and HeLa cells (d) after the addition of HTMA-PFNT and irradiation with visible-light.

human HeLa cells coexisting in the sample. The image in Fig. 7b corresponds to the same field as Fig. 7a and was obtained after excitation with UV-light. The image shows that HTMA-PFP is able to label both types of cells without, apparently, any preference for one over the other.

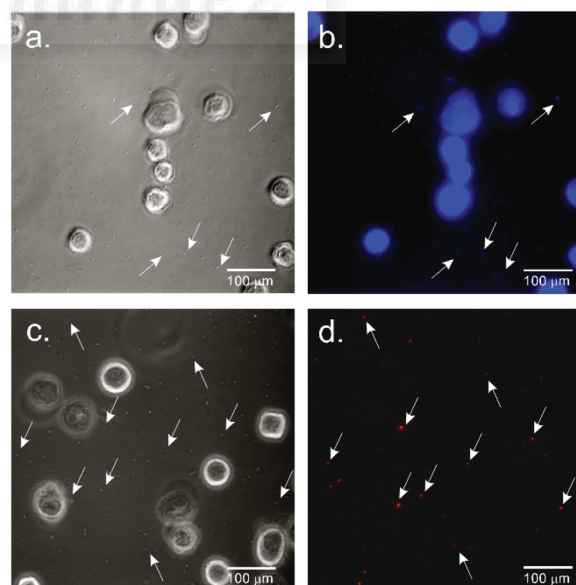


**Fig. 7** Microscopy images of human HeLa cells contaminated with bacteria *E. coli* after the addition of HTMA-PFP in phase contrast (a) and upon irradiation with UV-light (b). Microscopy images of human HeLa cells contaminated with bacteria *E. coli* after the addition of HTMA-PFNT in phase contrast (c) and upon irradiation with visible light (d). Arrows are included to better visualize the bacteria population.

It should be noted that the higher fluorescence intensity coming from the HeLa cells is due to their bigger size, and this effect masks the fluorescence from the bacteria and makes more difficult their visualization.

Therefore, in spite of the results obtained with model systems, the above experiments suggest that HTMA-PFP can be used as a fluorescent membrane marker, but it is not a good candidate to selectively recognize and image bacteria over mammalian cells, at least with the bacterial strains and cell lines used in this study. Results obtained with HTMA-PFNT were totally different (Fig. 7c and d). No HeLa cells were observed after excitation with visible light, but the bacterial population could be detected. This result indicates that the CPE was only bound to *E. coli* without apparently labelling the HeLa cells. This is a very interesting result which supports the conclusions obtained for HTMA-PFNT with model membranes and confirms the potential use of this CPE as a rapid diagnostics tool to detect bacterial contamination.

## Conclusions

In this study, the ability of the cationic CPEs HTMA-PFP and HTMA-PFNT to selectively label bacteria over mammalian cells was explored using fluorescence spectroscopy and microscopy in model membranes and cells. Experiments performed with biomimetic LUVs, representative of mammalian and bacterial membranes, indicate that both CPEs rapidly label the vesicles but preferentially interact with the bacterial biomimetic membrane model, probably due to electrostatic interactions between the quaternary amine groups of the CPEs and the anionic surface of the bacterial membrane. In spite of their similar structures, HTMA-PFNT is much more selective towards this type of membrane than HTMA-PFP, as was confirmed from quenching experiments carried out in samples containing simultaneously bacterial and mammalian LUVs. The fluorescence microscopy images obtained from *E. coli* bacteria and HeLa cells, in separate samples, reveal the ability of HTMA-PFP and HTMA-PFNT to rapidly label in blue and red, respectively, both bacterial and mammalian cells. However, in samples containing simultaneously *E. coli* bacteria and HeLa cells, a different behaviour was observed for the two CPEs: HTMA-PFP was able to label both types of cells without apparently any preference for one over the other, while HTMA-PFNT was bound only to the bacteria *E. coli*. This result indicates that CPE HTMA-PFNT is a better candidate than HTMA-PFP to selectively recognize and image bacteria over mammalian cells, and thus could be potentially used as a fast diagnosis tool for detecting bacterial contamination in different samples.

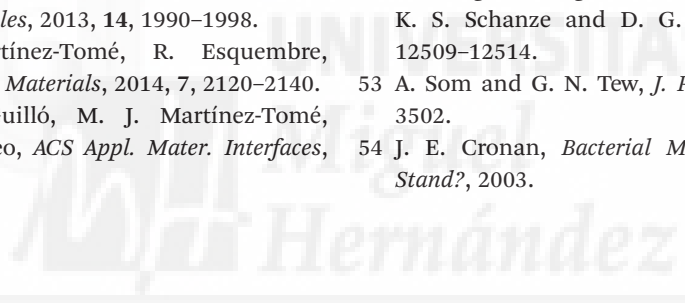
## Acknowledgements

The authors thank the Spanish Ministerio de Economía y Competitividad and Generalitat Valenciana for financial support (MAT-2014-53282-R and PROMETEO/2013/018, respectively).

## References

- 1 C. Guilini, C. Baehr, E. Schaeffer, P. Gizzi, F. Rufi, J. Haiech, E. Weiss, D. Bonnet and J. Galzi, *Anal. Chem.*, 2015, **87**, 8858–8866.
- 2 A. K. Deisingh and M. Thompson, *Analyst*, 2002, **127**, 567–581.
- 3 D. Meir, L. Silbert, R. Volinsky, S. Kolusheva, I. Weiser and R. Jelinek, *J. Appl. Microbiol.*, 2008, **104**, 787–795.
- 4 J. Heo and S. Z. Hua, *Sensors*, 2009, **9**, 4483–4502.
- 5 M. Behra, N. Azzouz, S. Schmidt, D. V. Volodkin, S. Mosca, M. Chanana, P. H. Seeberger and L. Hartmann, *Biomacromolecules*, 2013, **14**, 1927–1935.
- 6 W. M. Leevy, S. T. Gammon, H. Jiang, J. R. Johnson, D. J. Maxwell, E. N. Jackson, M. Marquez, D. Piwnica-Worms and B. D. Smith, *J. Am. Chem. Soc.*, 2006, **128**, 16476–16477.
- 7 A. G. White, N. Fu, W. M. Leevy, J. Lee, M. A. Blasco and B. D. Smith, *Bioconjugate Chem.*, 2010, **21**, 1297–1304.
- 8 S. Nandi, M. Ritenberg and R. Jelinek, *Analyst*, 2015, **140**, 4232–4237.
- 9 J. Zhou, N. Butchosa, H. S. N. Jayawardena, J. Park, Q. Zhou, M. Yan and O. Ramström, *Biomacromolecules*, 2015, **16**, 1426–1432.
- 10 F. Chen and D. Gerion, *Nano Lett.*, 2004, **4**, 1827–1832.
- 11 W. Yang, C. Pan, X. Liu and J. Wang, *Biomacromolecules*, 2011, **12**, 1523–1531.
- 12 W. M. Leevy, S. T. Gammon, J. R. Johnson, A. J. Lampkins, H. Jiang, M. Marquez, D. Piwnica-Worms, M. A. Suckow and B. D. Smith, *Bioconjugate Chem.*, 2008, **19**, 686–692.
- 13 K. M. Tsoi, Q. Dai, B. A. Alman and W. C. W. Chan, *Acc. Chem. Res.*, 2013, **46**, 662–671.
- 14 E. Oh, R. Liu, A. Nel, K. B. Gemill, M. Bilal, Y. Cohen and I. L. Medintz, *Nat. Nanotechnol.*, 2016, **14**, 479–486.
- 15 Y. Wang and A. Hu, *J. Mater. Chem. C*, 2014, **2**, 6921–6939.
- 16 I. P. Lai, S. G. Harroun, S. Chen, B. Unnikrishnan, Y. Li and C. Huang, *Sens. Actuators, B*, 2016, **228**, 465–470.
- 17 K. Y. Pu, L. Cai and B. Liu, *Macromolecules*, 2009, **42**, 5933–5940.
- 18 S. W. Thomas III, G. D. Joly and T. M. Swager, *Chem. Rev.*, 2007, **107**, 1339–1386.
- 19 S. Kim, C. K. Lim, J. Na, Y. D. Lee, K. Kim, K. Choi, J. F. Leary and I. C. Kwon, *Chem. Commun.*, 2010, **46**, 1617–1619.
- 20 B. A. Smith and B. D. Smith, *Bioconjugate Chem.*, 2012, **23**, 1989–2006.
- 21 A. Duarte, K. Y. Pu, B. Liu and G. C. Bazan, *Chem. Mater.*, 2011, **23**, 501–515.
- 22 A. T. Ngo, P. Karam and G. Cosa, *Pure Appl. Chem.*, 2011, **83**, 43–55.
- 23 Y. Liu, K. Ogawa and K. S. Schanze, *J. Photochem. Photobiol., C*, 2009, **10**, 173–190.
- 24 L. Wang, H. Li and D. Cao, *Curr. Org. Chem.*, 2012, **16**, 1468–1484.
- 25 Y. Tang, Y. Liu and A. Cao, *Anal. Chem.*, 2013, **85**, 825–830.
- 26 K. Y. Pu and B. Liu, *Adv. Funct. Mater.*, 2011, **21**, 3408–3423.

- 27 C. Zhu, L. Liu, Q. Yang, F. Lv and S. Wang, *Chem. Rev.*, 2012, **112**, 4687–4735.
- 28 K. P. R. Nilsson and P. Hammarstrom, *Adv. Mater.*, 2008, **20**, 2639–2645.
- 29 I. B. Kim, H. Shin, A. J. Garcia and U. H. F. Bunz, *Bioconjugate Chem.*, 2007, **18**, 815–820.
- 30 C. Zhu, Q. Yang, L. Liu and S. Wang, *Chem. Commun.*, 2011, **47**, 5524–5526.
- 31 G. Feng, D. Ding and B. Liu, *Nanoscale*, 2012, **4**, 6150–6165.
- 32 Q. Wen, C. Zhu, L. Liu, Q. Yang, S. Wang and D. Zhu, *Macromol. Chem. Phys.*, 2012, **213**, 2486–2491.
- 33 B. Wang, C. Zhu, L. Liu, F. Lv, Q. Yang and S. Wang, *Polym. Chem.*, 2013, **4**, 5212–5215.
- 34 Z. Chen, P. Wu, R. Cong, N. Xu, Y. Tan, C. Tan and Y. Jiang, *ACS Appl. Mater. Interfaces*, 2016, **8**, 3567–3574.
- 35 J. E. Houston, M. Kraft, U. Scherf and R. C. Evans, *Phys. Chem. Chem. Phys.*, 2016, **18**, 12423–12427.
- 36 Y. Wang, E. Y. Chi, K. S. Schanze and D. G. Whitten, *Soft Matter*, 2012, **8**, 8547–8558.
- 37 H. Yuan, B. Wang, F. Lv, L. Liu and S. Wang, *Adv. Mater.*, 2014, **26**, 6978–6982.
- 38 M. J. Martínez-Tomé, R. Esquembre, R. Mallavia and C. R. Mateo, *Biomacromolecules*, 2010, **11**, 1494–1501.
- 39 Z. Kahveci, M. J. Martínez-Tomé, R. Mallavia and C. R. Mateo, *Biomacromolecules*, 2013, **14**, 1990–1998.
- 40 Z. Kahveci, M. J. Martínez-Tomé, R. Esquembre, R. Mallavia and C. R. Mateo, *Materials*, 2014, **7**, 2120–2140.
- 41 Z. Kahveci, R. Vázquez-Guilló, M. J. Martínez-Tomé, R. Mallavia and C. R. Mateo, *ACS Appl. Mater. Interfaces*, 2016, **8**, 1958–1969.
- 42 L. Ding, E. Y. Chi, K. S. Schanze, G. P. Lopez and D. G. Whitten, *Langmuir*, 2010, **26**, 5544–5550.
- 43 K. Matsuzaki, K. Sugishita, N. Fujii and K. Miyajima, *Biochemistry*, 1995, **34**, 3423–3429.
- 44 R. Mallavia, D. Martínez-Pérez, B. F. Chmelka and G. C. Bazan, *Bol. Soc. Esp. Ceram. Vidrio*, 2004, **43**, 327–330.
- 45 R. Molina, S. Gómez-Ruiz, F. Montilla, A. Salinas-Castillo, S. Fernández-Arroyo, M. Del Mar Ramos, V. Micol and R. Mallavia, *Macromolecules*, 2009, **42**, 5471–5477.
- 46 N. Rodriguez, F. Pincet and S. Cribier, *Colloids Surf., B*, 2005, **42**, 125–130.
- 47 A. Coutinho and M. Prieto, *Biophys. J.*, 1995, **69**, 2541–2557.
- 48 M. N. Melo and M. A. R. B. Castanho, *Biochim. Biophys. Acta, Biomembr.*, 2007, **1768**, 1277–1290.
- 49 J. Chen, W. F. Dong, H. Mohwald and R. Krastev, *Chem. Mater.*, 2008, **20**, 1664–1666.
- 50 S. Chemburu, E. Ji, Y. Casana, Y. Wu, T. Buranda, K. S. Schanze, G. P. Lopez and D. G. Whitten, *J. Phys. Chem. B*, 2008, **112**, 14492–14499.
- 51 Z. Kahveci, M. J. Martínez-Tomé, R. Esquembre, R. Mallavia and C. R. Mateo, *Materials*, 2014, **7**, 2120–2140.
- 52 Y. Wang, Y. Tang, Z. Zhou, E. Ji, G. P. Lopez, E. Y. Chi, K. S. Schanze and D. G. Whitten, *Langmuir*, 2010, **26**, 12509–12514.
- 53 A. Som and G. N. Tew, *J. Phys. Chem. B*, 2008, **112**, 3495–3502.
- 54 J. E. Cronan, *Bacterial Membrane Lipids: Where Do We Stand?*, 2003.



## Supporting Information

### **SELECTIVE RECOGNITION AND IMAGING OF BACTERIAL MODEL MEMBRANES OVER MAMMALIAN ONES BY USING CATIONIC CONJUGATED POLYELECTROLYTES.**

*Zehra Kahveci\**, *Rebeca Vázquez*, *Amalia Mira*, *Lorena Martinez*, *Alberto Falcó*,  
*Ricardo Mallavia* and *C. Reyes Mateo\**

Instituto de Biología Molecular y Celular, Universidad Miguel Hernández, 03202,  
Elche, Alicante, Spain

#### **KEYWORDS:**

Conjugated polyelectrolytes, bacterial imaging, polyfluorene, polyelectrolyte-liposomes  
interaction, bioimaging probes

Theoretical curve in figure 2b and 4b (inset) were obtained by using following equation by calculating the theoretical quenching efficiency ( $\eta_{expected}$ ) :

$$\eta_{expected} = (1 - I^t / I_0^t) \times 100 \quad \text{(eq. S1)}$$

where,  $I_0^t$  and  $I^t$  stand for the CPEs fluorescence intensities in the absence and presence of the quencher, respectively. The values expected for these intensities if the CPE had the same preference for both model membranes can be estimated as:

$$I_0^t = (\chi^M I^M) + (\chi^B I^B)$$

$$I^t = (\chi^M I^M \eta^M / 100) + (\chi^B I^B \eta^B / 100)$$

$\chi^M$  and  $\chi^B$  are the lipid molar fraction of the mammalian and bacterial model systems in the mixture, respectively.

$I^M$  and  $I^B$  are the fluorescence intensities obtained experimentally from CPE either in mammalian or bacterial model membrane, respectively . For HTMA-PFP, the ratio  $I^B / I^M = 1.35$  (Figure 1c), while for HTMA-PFNT,  $I^B / I^M = 1$  (Figure 3c).

$\eta^M$  and  $\eta^B$  are the percentage of quenching efficiencies when the sample contains 100% of mammalian or bacterial membranes, respectively. These values were  $\eta^M = 50\%$  and  $\eta^B = 92\%$  for HTMA-PFP and HTMA-PFNT in the presence of 50 and 200  $\mu\text{M}$  of AQS, respectively (Figures 2a and 4a).

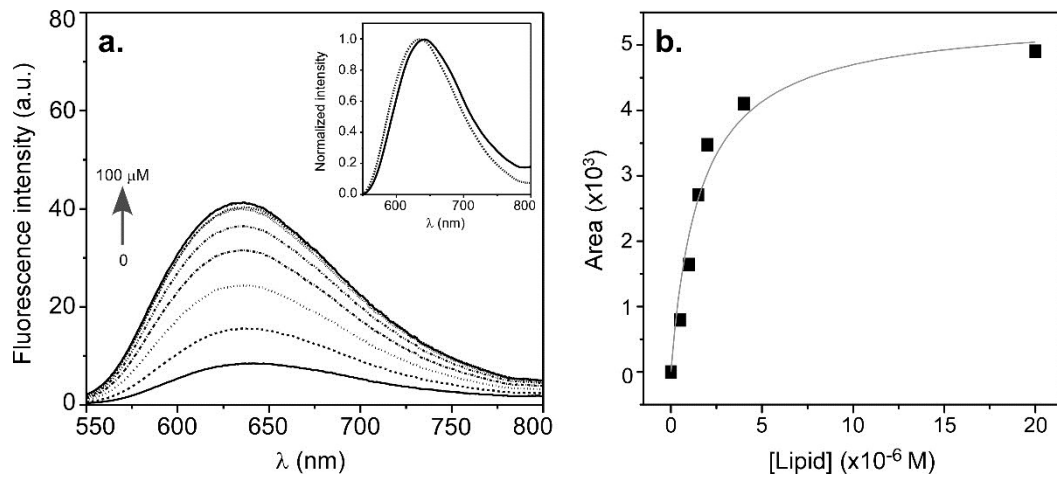


**Figure S1:** Fluorescence emission spectra of HTMA-PFNT (1.5  $\mu\text{M}$ ) in buffer with increasing concentrations of DOPG. Inset: Differences in fluorescence intensity by increasing the DOPG concentration compared to DOPC ( $\lambda_{\text{exc}}=510$  nm).

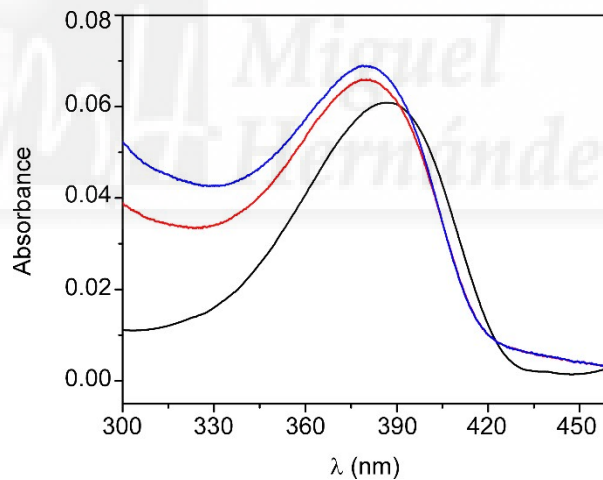


**Figure S2:** Absorption spectra of HTMA-PFP (1.5  $\mu\text{M}$ ) in buffer (black), bacterial (red) and mammalian (blue) model membranes.



## Publication 8.5





## **Fluorimetric Biosensor for Alkaline Phosphatase based on Immobilized Polyfluorene-Liposomal Nanoparticles**

**Zehra Kahveci, Maria José Martínez-Tomé, Ricardo Mallavia and C. Reyes Mateo**

Instituto de Biología Molecular y Celular, Universidad Miguel Hernández, 03202

Elche, Spain

**ACS Appl. Mater. Interfaces**

(In revision)



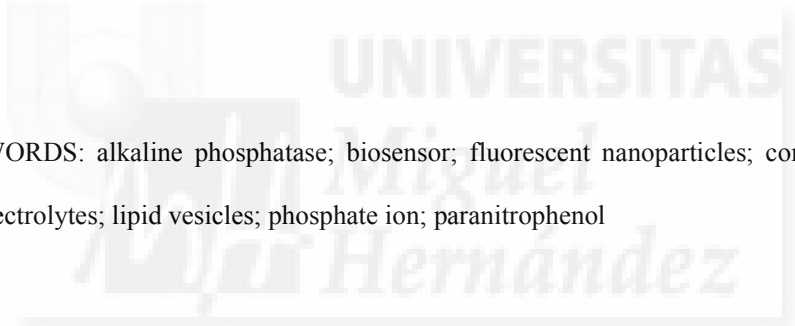
1  
2  
3  
4  
5  
6  
7  
8  
9  
10  
11  
12  
13  
14  
15  
16  
17  
18  
19  
20  
21  
22  
23  
24  
25  
26  
27  
28  
29  
30  
31  
32  
33  
34  
35  
36  
37  
38  
39  
40  
41  
42  
43  
44  
45  
46  
47  
48  
49  
50  
51  
52  
53  
54  
55  
56  
57  
58  
59  
60

# Fluorimetric Biosensor for Alkaline Phosphatase based on Immobilized Polyfluorene-Liposomal Nanoparticles.

*Zehra Kahveci, Maria José Martínez-Tomé, Ricardo Mallavia, C.Reyes Mateo\**

Instituto de Biología Molecular y Celular, Universidad Miguel Hernández, 03202,  
Elche, Alicante, Spain

KEYWORDS: alkaline phosphatase; biosensor; fluorescent nanoparticles; conjugated  
polyelectrolytes; lipid vesicles; phosphate ion; paranitrophenol



1  
2  
3 ABSTRACT  
4  
5

6 This work describes the development of a novel fluorescent biosensor based on the  
7 inhibition of alkaline phosphatase (ALP). The biosensor was composed of the enzyme  
8 ALP and the conjugated cationic polyfluorene HTMA-PFP. The working principle of  
9 the biosensor is based on the fluorescence quenching of this polyelectrolyte by  
10 paranitrophenol (PNP), a product of the hydrolysis reaction of glycerol-1-phosphate  
11 (PNPP) catalyzed by ALP. Since HTMA-PFP forms unstable aggregates in buffer, with  
12 low fluorescence efficiency, previous stabilization of the polyelectrolyte was required  
13 before the development of the biosensor. HTMA-PFP was stabilized through its  
14 interaction with lipid vesicles to obtain stable blue-emitting nanoparticles (NPs).  
15 Fluorescent NPs were characterized and the ability to be quenched by PNP was  
16 evaluated. These nanoparticles were coupled to ALP and entrapped in a sol-gel matrix  
17 to produce a biosensor that can serve as a screening platform to identify ALP inhibitors.  
18 The components of the biosensor were examined before and after sol-gel entrapment,  
19 and the biosensor was optimized to allow the determination of phosphate ion in aqueous  
20 medium.  
21  
22  
23  
24  
25  
26  
27  
28  
29  
30  
31  
32  
33  
34  
35  
36  
37  
38  
39  
40  
41  
42  
43  
44  
45  
46  
47  
48  
49  
50  
51  
52  
53  
54  
55  
56  
57  
58  
59  
60

## INTRODUCTION

The enzyme alkaline phosphatase (ALP) nonspecifically catalyzes the hydrolysis of phosphoryl esters in alkaline media. This low biocatalytic selectivity enables the use of the enzyme for a wide range of substrates in enzyme activity assays, one of which is glycerol-1-phosphate or p-nitrophenyl phosphate (PNPP). In the last years, the catalytic activity of ALP has been exploited in the design of immunosensors and biosensors, either for direct monitoring of analytes (enzymes or substrates) or for indirect monitoring of organic (i.e. pesticides) or inorganic salts (i.e. phosphate, heavy metals) which act as inhibitors<sup>1-5</sup>. Studies of ALP activity and screening of its inhibitors are required in clinical diagnosis to develop potential drug therapies for different diseases, as well as in environmental monitoring of pollutants<sup>6</sup>. The choice of the substrates for these analytical applications depends on the transduction methods, i.e. fluorescence, chemiluminescence or amperometry, and on the purpose of the analytical measurements<sup>3</sup>. Up to date, various fluorimetric assays and fluorescent biosensors based on ALP activity have been reported using organic dyes, inorganic semiconductor quantum dots (QDs) and carbon quantum dots as fluorometric indicators<sup>7-9</sup>. Many of these fluorophores suffer drawbacks such as poor stability of dyes or high toxicity of QDs which constitute important concerns for the practical application. Recently, much interest has been generated in synthesizing novel highly-fluorescent conjugated polyelectrolytes (CPEs)<sup>10-12</sup>. These materials are photostable polymers with delocalized  $\pi$ -electron systems which show strong absorption and high fluorescence quantum yields<sup>13, 14</sup>. Electron delocalization facilitates rapid intra- and inter-chain exciton migration, conferring collective optical responses and amplified signals when comparing to conventional fluorophores<sup>14, 15</sup>. Their biocompatible and biodegradable characteristics enable the use of CPEs *in vitro* without risking the cellular viability<sup>16, 17</sup>.

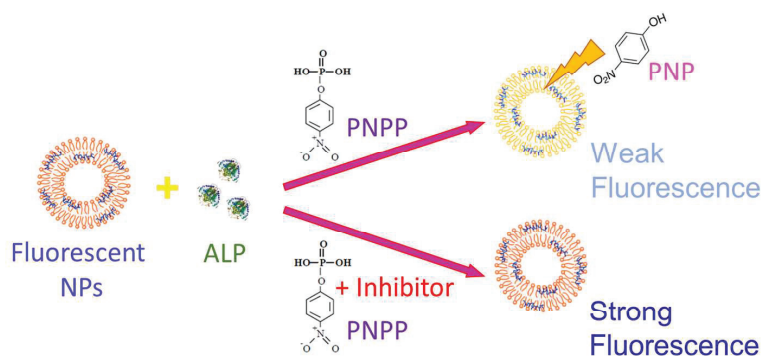
1  
2  
3 Given these properties, CPEs have received great attention in biomedical and  
4  
5 environmental applications, especially as potential fluorescent sensors for small  
6  
7 molecules, metal ions and biomolecules<sup>18-21</sup>.  
8  
9

10  
11 The amplified quenching of CPEs upon binding to an opposite charge molecule is  
12  
13 frequently used in the design of CPEs-based sensors or biosensors<sup>13, 19, 22, 23</sup>. Chen et al.  
14  
15 demonstrated that the fluorescence of the CPEs, can be very efficiently quenched via a  
16  
17 photo-induced electron transfer mechanism (PET), by electron acceptors of opposite  
18  
19 charge<sup>24</sup>. Fluorescence can also be quenched due to fluorescence resonance energy  
20  
21 transfer (FRET) between the CPEs and molecules with absorption spectra overlapping  
22  
23 the polyelectrolyte emission spectrum<sup>25-27</sup>. In a previous work, it was shown that p-  
24  
25 nitrophenol (PNP), an electron acceptor that absorbs at 400 nm in its anionic form, is  
26  
27 able to quench the fluorescence intensity of blue-emitter cationic polyfluorenes, such as  
28  
29 poly{(9,9-bis(6'-N,N,N-trimethylammonium) hexyl]fluorene-phenylene} bromide  
30  
31 (HTMA-PFP), presumably via a combination of PET and FRET mechanisms<sup>28, 29</sup>. Cao,  
32  
33 et al. used this property to develop a fluorimetric assay in buffer for the screening of  $\alpha$ -  
34  
35 glucosidase inhibitors, taking into account that this enzyme catalyzes the hydrolysis of  
36  
37 p-nitrophenyl- $\alpha$ -D-glucopyranoside to PNP. PNP is also the end product of hydrolysis of  
38  
39 PNPP, catalyzed by ALP. Therefore, a fluorescent ALP biosensor could be developed  
40  
41 by coupling of the polyelectrolyte HTMA-PFP to this enzyme. At a constant  
42  
43 concentration of PNPP, this biosensor could be capable of detecting the ALP activity in  
44  
45 absence and presence of inhibitors.  
46  
47  
48  
49

50  
51 The fluorescence quenching of HTMA-PFP and similar polyfluorenes has been also  
52  
53 used as a tool to determine DNA, metal-organic ions or proteins in water<sup>30-33</sup>. However,  
54  
55 our group recently reported that this polyelectrolyte is not stable in aqueous solvents. In  
56  
57 particular, we investigated the behaviour of HTMA-PFP in buffer, comparing the results  
58  
59  
60

1  
2  
3 with those obtained in a good solvent<sup>34</sup>. The polyelectrolyte showed a low fluorescence  
4  
5 quantum-yield and a red-shift of the emission spectrum in buffer. This result was  
6  
7 attributed to the formation of aggregates by self-assembly of the polymer hydrophobic  
8  
9 chains and to the existence of nonspecific electrostatic interactions between these  
10  
11 aggregates and anionic species contained in the buffer. The average size of aggregates  
12  
13 largely increased through the time, inducing the corresponding decrease in their  
14  
15 fluorescence intensity. This behaviour is common to other CPEs and must be taken into  
16  
17 account to define the real-world sensing applications of this class of polymers, because  
18  
19 the fluorescence decrease can be due not only to the presence of a specific analyte but  
20  
21 also to the continuous aggregation process. As a consequence, previous stabilization of  
22  
23 the CPE in buffer is usually needed before the development of quenching based-sensor  
24  
25 systems.  
26  
27  
28  
29

30 In the present work, we have incorporated HTMA-PFP in lipid vesicles to obtain stable  
31  
32 fluorescent nanoparticles (NPs). NPs were characterized and the ability to be quenched  
33  
34 by anionic PNP (at alkaline pH) was evaluated. These nanoparticles were coupled to  
35  
36 ALP and entrapped in a sol-gel matrix to develop a biosensor that can serve as a  
37  
38 screening platform to identify ALP inhibitors. The biosensor was examined before and  
39  
40 after the sol-gel entrapment of its components and was used to determine phosphate ion,  
41  
42 a competitive inhibitor of ALP. Determination of this analyte is very important in  
43  
44 clinical and environmental studies since variations in its optimal concentrations are  
45  
46 associated to different pathologies and to the quality of water<sup>35</sup>. The scheme and  
47  
48 working principle of the biosensor is shown in Scheme 1.  
49  
50  
51  
52  
53  
54  
55  
56  
57  
58  
59  
60



**Scheme 1.** Working principle of the biosensor: The PNP produced after hydrolysis of PNPP, catalyzed by ALP, quenches the fluorescence of NPs, leading to fluorescence turn-off. The presence of inhibitors inactivate the ALP and the fluorescence of the system turns on.

## MATERIALS AND METHODS

The synthetic phospholipid 1,2-Diacyl-sn-glycero-3-phospho-(1-rac-glycerol) (PG), enzyme alkaline phosphatase (ALP) (E.C. 3.1.3.1; from bovine intestinal mucosa, 2982 U/mL), substrate 4-nitrophenyl phosphate (PNPP) and the quencher p-nitrophenol (PNP) were obtained from Sigma-Aldrich (St. Louis, MO, USA) and used as received. Stock solutions of ALP, PNPP and PNP were dissolved in Tris buffer (50 mM, pH 9.2) at 40 U/mL, 1.2 mM and 5 mM respectively, just before use. Tetraethyl orthosilicate (TEOS) was obtained from Sigma-Aldrich (Spain). All other solvents were of spectroscopic reagent grade (UVASOL, Merck). Tris buffer (50 mM, pH 9.2) was prepared with water, which was twice distilled in all-glass apparatus and deionized using Milli-Q equipment (Millipore, Madrid, Spain). Enzyme inhibitor, sodium phosphate dibasic ( $\text{Na}_2\text{HPO}_4$ ) was purchased from Sigma-Aldrich (Spain). Stock solution of  $\text{Na}_2\text{HPO}_4$  was prepared with Milli-Q water at 200 mM.

### *Preparation of the Cationic Polyelectrolyte HTMA-PFP*

The cationic CPE HTMA-PFP ( $M_w = 8340$  g/mol, repeat unit molecular weight,  $M_u = 694$  g/mol;  $n = 12$  based on polifluorene calibration) was obtained and characterized in our laboratory<sup>36, 37</sup>. Briefly, a low molecular batch of the neutral polymer, poly[bis(6'-bromohexyl)fluorene-phenylene] was synthesized by the Suzuki coupling reaction with Pd(II) as catalyst and treated with gas-phase trimethylamine in order to obtain the corresponding cationic polyelectrolyte HTMA-PFP. Stock solutions of HTMA-PFP were prepared in DMSO, with final concentrations of  $3.65 \times 10^{-4}$  M (in repeat units) and stored at  $-20$  °C before use.

### *Formation of PG Liposomes*

Chloroform/methanol solutions containing 3 mg of PG was dried first by evaporation under dry nitrogen gas stream and subsequently under vacuum for 3 h. Multilamellar vesicles (MLVs) were formed by resuspending the dried phospholipid in the buffer to the required final concentrations (0.5 mM). The vesicle suspension was then vortexed several times. Large unilamellar vesicles (LUVs) of model membranes were prepared from these MLVs by pressure extrusion through  $0.1 \mu\text{m}$  polycarbonate filters (Nucleopore, Cambridge, MA, USA).

### *Preparation of Fluorescent NPs*

Aliquots of HTMA-PFP (final concentration of  $1.5 \mu\text{M}$  in terms of repeat units) in DMSO were externally added to the LUVs suspension (0.5 mM in lipid) and incubated during 2 min at room temperature. In all cases, the proportion of DMSO in the aqueous sample was always lower than 1% (V/V).

### ***Preparation of the ALP Biosensor in Solution***

The ALP biosensor was prepared from the addition of the enzyme ALP stock solution (40 U/mL) to the solution of fluorescent NPs (0.5 mM in lipid) at 2 U/mL for all the studies.

### ***Sol-Gel Immobilization of the Fluorescent NPs***

Silica stock solution was prepared using TEOS as precursor. Briefly, 4.46 mL of this product were mixed under vigorous stirring with 1.44 mL of H<sub>2</sub>O and 0.04 mL HCl (0.62 M) at 22°C in a closed vessel. After 1 hour, 1 mL of the resulting sol was mixed with 1 mL of deionised doubly distilled water, and submitted to rotaevaporation for a weight loss of 0.62 g (the alcohol mass resulting from alkoxyde hydrolysis). Immobilized fluorescent nanoparticles were prepared by adding 700 µL of fluorescent nanoparticles (PG:HTMA-PFP, 1 mM:3 µM) to 700 µL of the aqueous sol in an ice-cooled polystyrene cuvette. Gelation occurs readily after mixing. Following gelation, transparent monoliths, having a size of ~ 9 x 9 x 12 mm, were washed three times with Tris buffer solution and were wet aged in 0.5 mL of the same buffer at 4°C during 24 h. Cuvettes were covered with parafilm and stored in the dark at that temperature before use. Immobilization of PG liposomes (in the absence of HTMA-PFP) was required as a control for the dispersity of the samples.

### ***Sol-Gel Immobilization of the Enzyme ALP***

Silica stock solution was prepared using TEOS as precursor following the same protocol as described above. Immobilized ALP was prepared by adding 700 µL of buffered ALP (300 U/mL) solution to 700 µL of the sol stock solution in a disposable polystyrene cuvette. Gelation occurred readily after mixing. The freshly formed

1  
2  
3 monoliths (~ 9 x 9 x 12 mm) containing the immobilized enzyme were rinsed with Tris  
4  
5 buffer solution three times and were wet aged in 0.5 mL of the same buffer at 4°C  
6  
7 temperature in the dark before use. Note that, for fluorescence intensity measurements  
8  
9 of ALP, glass monoliths were prepared using a higher concentration of enzyme (final  
10  
11 concentration 150 U/mL).  
12  
13

#### 14 15 ***Preparation of the ALP Biosensor in Sol-Gel matrix*** 16

17  
18 Solutions containing fluorescent nanoparticles and enzyme ALP were simultaneously  
19  
20 immobilized in sol-gel matrix. In brief, 700 µL of a solution of fluorescent nanoparticles  
21  
22 (PG:HTMA-PFP, 1 mM:3 µM) and enzyme ALP (4 U/mL) in Tris buffer were mixed  
23  
24 with 700 µL of a silica sol stock solution in a disposable polystyrene cuvette. Following  
25  
26 gelation, transparent monoliths were washed three times with Tris buffer solution and  
27  
28 were sealed with parafilm and store in dark at 4°C temperature before use.  
29  
30

#### 31 32 ***Fluorescence Measurements*** 33

34  
35 Fluorescence spectra and fluorescence intensity measurements were performed on a  
36  
37 QuantaMaster spectrofluorometer (PTI, Birmingham, NJ, USA). The experimental  
38  
39 samples were placed in 10 mm × 10 mm path length quartz cuvettes. Excitation  
40  
41 wavelength at 380 nm for HTMA-PFP was used. Background intensities were always  
42  
43 checked and subtracted from the sample when necessary.  
44  
45

#### 46 47 ***Dynamic Light Scattering (DLS)*** 48

49  
50 The size of nanoparticles was explored by DLS techniques, using a Brookhaven 90  
51  
52 Plus Nanoparticle Size Analyzer instrument, equipped with a 35 mW red diode laser ( $\lambda$   
53  
54 = 640 nm) as light source, with a 90° scattering angle of lecture for size measurements.  
55  
56 All measurements were performed in disposable cuvettes, in triplicate.  
57  
58  
59  
60

## RESULTS AND DISCUSSION

*Design of Fluorescent Nanoparticles (NPs)*

As was mentioned in the Introduction, HTMA-PFP and, in general, CPEs have high tendency to aggregate in aqueous environment leading to detrimental emission quenching. Several methods are being developed to stabilize and increase the quantum yield of the CPEs by overcoming the aggregation<sup>38</sup>. In the present work stabilization of the HTMA-PFP was obtained through the incorporation of the polyelectrolyte in LUVs, using the same strategy previously reported by our group in the stabilization of other polyfluorenes<sup>39</sup>. We selected phosphatidylglycerol (PG) lipid vesicles due to the high affinity of HTMA-PFP for anionic vesicles and its insertion in the lipid bilayer<sup>34, 40</sup>. Vesicles were prepared in Tris buffer, pH 9.2, which is an adequate pH for ALP activity. The lipid concentration was fixed to 0.5 mM to limit the turbidity of samples which becomes an obstacle for fluorescence measurements. The polymer concentration was 1.5  $\mu$ M to ensure that all the polymer chains were incorporated in the vesicles, taking into account its partition coefficient between lipid and aqueous phase<sup>34</sup>. Figure 1 shows the emission spectra and the stability plot obtained at these conditions for HTMA-PFP in PG and Tris buffer. The low fluorescence intensity and its decrease as a function of time confirm the formation of aggregates of polyelectrolyte in buffer. The incorporation of the HTMA-PFP into the vesicles is evidenced from the increase in the fluorescence intensity and the blue shift of the fluorescence spectrum when compared to the buffer. This behavior is probably due to the transformation of the initially formed polymer aggregates into liposomal nanoparticles (NPs) within which polymer segments are separated by the lipid molecules. The fact that the fluorescence intensity was constant as a function of time confirms the total incorporation of the polymer chains in the vesicles.

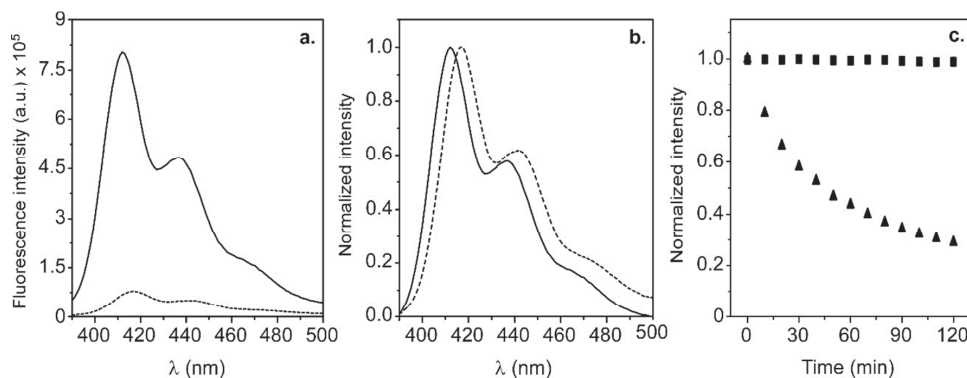


**Figure 1.** **a)** Fluorescence emission spectra and **b)** Normalized fluorescence emission spectra of HTMA-PFP in LUVs of PG (solid) and Tris buffer pH 9.2 (dash). **c)** Normalized fluorescence intensity at the maximum emission wavelength of HTMA-PFP in LUVs of PG (squares) and Tris buffer pH 9.2 (triangles) recorded as a function of time ( $\lambda_{exc}=380$ ).

The formed NPs were furtherly characterized by DLS. This technique was used to confirm their formation as well as to check their size and stability through time. The hydrodynamic radius (Rh) of the vesicles was measured before and after the addition of HTMA-PFP and was compared to that obtained for the polyelectrolyte in the Tris buffer. Results obtained in the buffer solution confirm the formation of aggregates and their instability through time (Table 1). For the vesicles, in absence of HTMA-PFP, a single distribution was observed with Rh ~ 86 nm. When the polyelectrolyte was incorporated into the vesicles to form the fluorescent NPs, a similar distribution centered at 89 nm was obtained and no additional population was detected. The DLS results support that HTMA-PFP is well inserted into the lipid membrane because the size of the vesicle practically does not change after polymer interaction. The fact that the same result was obtained 1 h after the preparation confirms, on one hand, that polymer aggregates are not found in the buffer, and therefore all the polymer chains are forming the NPs and, on the other hand, that the integrity of the lipid vesicles is retained

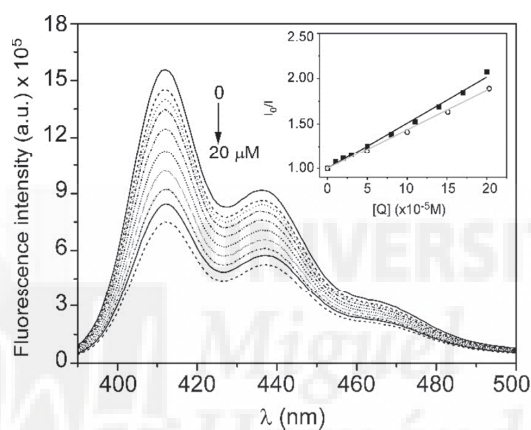
1  
2  
3 after HTMA-PFP incorporation since no vesicle fusion or decomposition into small  
4  
5 fragments was detectable. Nanoparticles remained stable even 24h after preparation as  
6  
7 can be inferred from the Rh values measured during this time period (Table 1).  
8  
9

Sample	Rh (nm)		
	$t_0$	$t = t_0 + 1h$	$t = t_0 + 24h$
PG LUVs	86	89	89
NPs	89	89	88
HTMA-PFP/Buffer	85	130	180

10  
11  
12  
13  
14  
15  
16  
17  
18  
19  
20  
21  
22  
23  
24  
25 **Table 1.** Average hydrodynamic Radii, Rh, determined by DLS measurements for  
26 different samples: PG LUVs, NPs (HTMA-PFP/PG LUVs) and HTMA-PFP in Tris  
27 buffer pH 9.2, recorded at different times after preparation.  
28  
29

30  
31  
32  
33  
34  
35  
36  
37  
38  
39  
40  
41  
42  
43  
44  
45  
46  
47  
48  
49  
50  
51  
52  
53  
54  
55  
56  
57  
58  
59  
60  
Once the stability of the fluorescent NPs was confirmed, the ability to be quenched by PNP was explored as an essential requirement for the biosensor construction. The increasing concentrations of PNP (0 to 20  $\mu\text{M}$ ) were added to a suspension of NPs and their emission spectra were recorded after each addition (Figure 2). Results indicate that, in spite of HTMA-PFP is incorporated into the vesicles, PNP is still able to quench its fluorescence. The inset of Figure 2 shows that the dependence of the fluorescence intensity on the quencher concentration is linear, being described by a Stern-Volmer plot with a value of  $K_{sv}=5.08\pm 0.07\times 10^4 \text{ M}^{-1}$ . This value is large but about 7-fold lower than the value reported for the same polyelectrolyte in buffer<sup>28</sup>. A decrease in quenching efficiency has been also reported for other CPEs in presence of surfactants<sup>41, 42</sup>, and reflects a lower association constant between quencher and polymer. In our case, this could be attributed to two factors: firstly, the lower accessibility of the PNP to the

1  
2  
3 polyelectrolyte, which is extended and intercalated between the lipid chains; secondly, a  
4  
5 reduction in the electrostatic attraction between PNP and HTMA-PFP, because the  
6  
7 polyelectrolyte cationic charge is partially neutralized by interactions with the anionic  
8  
9 lipid heads. In addition, the high quenching efficiency reported for the HTMA-PFP in  
10  
11 buffer could be also overestimated because of the continuous aggregation process,  
12  
13 previously described, which largely decreases the fluorescence intensity due to self-  
14  
15 quenching.  
16  
17  
18

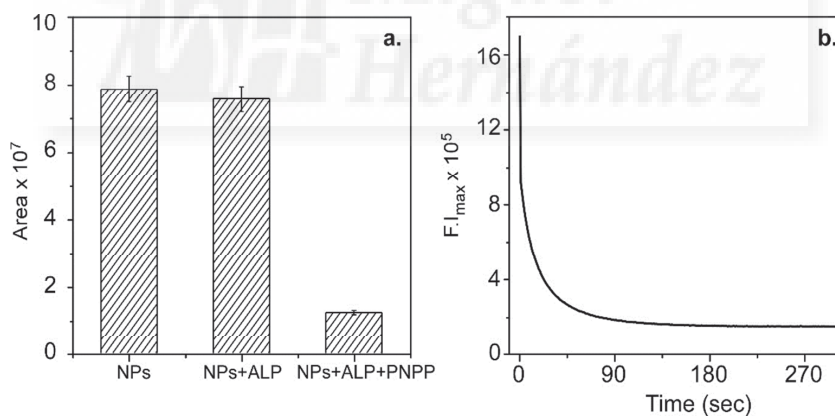


19  
20  
21  
22  
23  
24  
25  
26  
27  
28  
29  
30  
31  
32  
33  
34  
35  
36 **Figure 2. a)** Fluorescence emission spectra of NPs at increasing concentrations of PNP.  
37 Inset: Stern-Volmer plots for quenching of NPs by PNP (black squares) and after  
38 addition of PNPP (60 $\mu$ M) to NPs, in presence of ALP (2 U/mL) (circles).  
39  
40  
41  
42  
43

#### 44 *Development of the ALP Biosensor: Study in Solution*

45  
46  
47 Once proved the quenching of the fluorescent nanoparticles by PNP, we investigated  
48  
49 their ability to detect ALP activity, taking into account that this enzyme catalyses the  
50  
51 hydrolysis of PNPP to PNP. With this end, firstly we recorded the emission spectra of  
52  
53 the NPs in absence and presence of ALP (2 U/mL), and the areas under the spectra were  
54  
55 plotted in Figure 3a. The fact that this area was not affected by the presence of the  
56  
57  
58  
59  
60

1  
2  
3 enzyme suggests that no interaction is occurring between them. Addition of substrate  
4  
5 PNPP (60  $\mu\text{M}$ ) to the sample containing the enzyme induced a strong decrease in the  
6  
7 fluorescence intensity of the NPs which was monitored as a function of time (Figure  
8  
9 3b). The fluorescence intensity practically reached its minimum value ( $\sim 12\%$  of the  
10  
11 initial value) in the 2 first min after addition of substrate, reflecting the kinetics of the  
12  
13 enzymatic activity. To confirm that the fluorescence quenching was due to the PNP  
14  
15 formed from the hydrolysis of PNPP, increasing concentrations of substrate (0 to 20  
16  
17  $\mu\text{M}$ ) were added to a sample containing NPs and ALP. Fluorescence spectra were  
18  
19 recorded after 3 min of incubation for each substrate concentration. The inset of Figure  
20  
21 2 shows the SternVolmer plot corresponding to this experiment. The Stern-Volmer  
22  
23 constant extracted from the lineal plot ( $K_{\text{SV}}=4.94\pm 0.28\times 10^4 \text{ M}^{-1}$ ) was very close to that  
24  
25 obtained when PNP was directly added to the NPs suspension, evidencing the adequate  
26  
27 operation of the biosensor in solution.  
28  
29  
30  
31



32  
33  
34  
35  
36  
37  
38  
39  
40  
41  
42  
43  
44  
45  
46  
47  
48 **Figure 3. a)** Fluorescence intensities represented as integrated areas under the emission  
49  
50 spectrum, for the fluorescent NPs without and with ALP (2 U/mL) and in presence of  
51  
52 ALP and PNPP (60  $\mu\text{M}$ ), after 3 min of incubation. **b)** Fluorescence intensity kinetics of  
53  
54 NPs in presence of ALP (2 U/mL), recorded after addition of PNPP (60  $\mu\text{M}$ ). ( $\lambda_{\text{exc}}=380$   
55  
56 nm ;  $\lambda_{\text{em}}=412$  nm).  
57  
58  
59  
60

1  
2  
3 As was described in the Introduction, this biosensor could be used for ALP inhibitors  
4  
5 screening and to determine the concentration of a specific inhibitor in a sample. The  
6  
7 mechanism of sensing is shown in Scheme 1 and is based on the fluorescence turn-  
8  
9 off/turn on. The PNP produced after hydrolysis of PNPP quenches the fluorescence of  
10  
11 NPs, leading to fluorescence turn-off, but in the presence of inhibitors, the fluorescence  
12  
13 of the system turns on. This potential application was explored using phosphate ion,  
14  
15 which is a competitive inhibitor of the enzyme. To carry out this study different samples  
16  
17 containing the fluorescent NPs in presence of ALP (2 U/mL) and increasing  
18  
19 concentrations of phosphate ion (0 to 1 mM) were prepared. The same concentration of  
20  
21 PNPP (60  $\mu$ M) was added to all the samples and the quenching of fluorescence (which  
22  
23 reflects the ALP activity) was recorded as a function of time for each sample. The  
24  
25 quenching kinetics was found to be slower as the concentration of phosphate increases,  
26  
27 evidencing a significant decrement in the enzymatic activity (Figure 4a). This result  
28  
29 indicates that our method is sensitive to the presence of the phosphate ions and  
30  
31 therefore, it could be used for the determination of inhibitors. Results are shown in  
32  
33 Figure 4b in form of calibration curve. The plot represents the maximum fluorescence  
34  
35 intensity of the NPs, recorded 3 minutes after PNPP addition, *versus* phosphate ion  
36  
37 concentration. This plot was linear in the range of concentrations studied (up to 1 mM),  
38  
39 with a limit of detection (LOD) of 52  $\mu$ M, equivalent to three times the blank value<sup>43</sup>.  
40  
41 This LOD is lower than the concentration of phosphate which is normally present in  
42  
43 human blood serum (1.1-1.4 mM) and is similar to that recently reported for an ALP-  
44  
45 conductimetric biosensor<sup>44</sup>.  
46  
47  
48  
49  
50  
51  
52  
53  
54  
55  
56  
57  
58  
59  
60

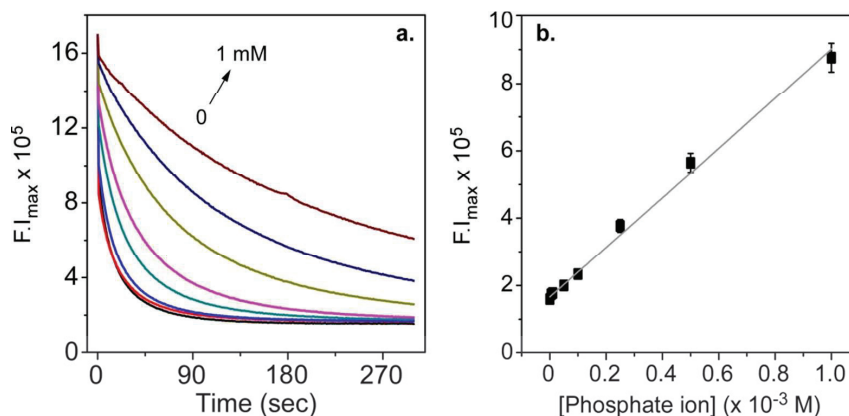


**Figure 4.** a) Time-dependent fluorescence intensity of NPs, in presence of ALP (2 U/mL) and increasing concentrations of phosphate ions, after addition of PNPP (60  $\mu\text{M}$ ). b) Phosphate ion calibration curve. The fluorescence intensities were taken 3 minutes after the addition of PNPP to each sample. ( $\lambda_{\text{exc}}=380$  nm ;  $\lambda_{\text{em}}=412$  nm).

#### *Development of the ALP Biosensor: Immobilization of Components*

The practical application of the biosensor described above requires the preparation of different samples (fluorescent NPs, fresh solutions of the enzyme, etc.) after each use, with the consequent time and economic burden. Immobilization of the biosensor components would facilitate their handling, enabling their reutilization and thus reducing the cost of the procedure. In the last two decades, the renaissance of sol-gel chemistry has provided a versatile method for immobilizing and stabilizing a wide variety of biological systems, such as enzymes and liposomes, in transparent inorganic matrices<sup>45-51</sup>. Compared to other immobilization methods the sol-gel glasses show numerous advantages, including entrapment of large amount of macromolecules, thermal and chemical stability of the matrix, enhanced stability of the encapsulated biomolecules and flexibility in controlling pore size and geometry. Furthermore, thanks to the porous nature of the matrix, the immobilized systems remain accessible to

1  
2  
3 interact with external specific analytes, with negligible biomolecule leaching. In this  
4  
5 work, we have selected the sol-gel methodology to simultaneously encapsulate the  
6  
7 biosensor components: ALP and NPs in the pores of a single matrix to obtain a stable,  
8  
9 easy-to-use and reusable device for detection of ALP inhibitors. Firstly, each  
10  
11 component of the biosensor was immobilized separately, to check the effects of the  
12  
13 immobilization process on its properties, as is described below.  
14  
15

16  
17 A preliminary analysis was done to demonstrate that the immobilization process did not  
18  
19 affect the fluorescent properties of NPs. Fluorescence spectra of the immobilized NPs  
20  
21 were directly recorded from the sol-gel monolith and are shown in the inset of Figure  
22  
23 5a. The shape and spectral position, as well as the fluorescence intensity, were very  
24  
25 similar to those observed for the spectrum of NPs in buffer, suggesting the suitability of  
26  
27 the immobilization method.  
28  
29

30  
31 To better characterize the immobilized NPs, we explored their stability as a function of  
32  
33 storage time, pH and temperature. Stability was assessed monitoring the fluorescence  
34  
35 spectra of the NPs and plotting the area of each spectrum as a function of time (days  
36  
37 after preparation), pH and temperature. Fluorescent spectra were recorded at room  
38  
39 temperature, with exception of the thermal stability experiments. Fig. 5a shows the  
40  
41 stability as a function of storage time for samples which were prepared and kept at 4°C,  
42  
43 for up to 12 days. During this period of time small fluctuations of the fluorescence  
44  
45 intensity were detected but, in general, the behaviour was stable. In addition, the shape  
46  
47 and position of the fluorescence maxima were not altered with the time (inset in Fig.  
48  
49 5a). Larger stability (up to 6 months) was also found when the monolith was stored at  
50  
51 4°C and preserved from light (data not shown). These results suggest that, at the  
52  
53 selected conditions, the immobilized NPs are physically and chemically stable and that  
54  
55  
56  
57  
58  
59  
60

1  
2  
3 the leaching of the NPs from the matrix is practically negligible during, at least, six  
4  
5 months.  
6

7  
8 Stability of the complexes as a function of pH was evaluated by immersion of the  
9  
10 monoliths containing NPs in water samples at different pHs (from pH=2.5 to pH=10.5)  
11  
12 for 30 minutes before the measurement. Fig. 5b displays the normalized fluorescence  
13  
14 intensity determined at the different pHs as well as the fluorescence spectra recovered  
15  
16 for each sample (inset in Figure 5b). Results show that the incorporation of the monolith  
17  
18 in an acid or basic solution practically does not modify the intensity, shape or spectral  
19  
20 position of the immobilized NPs, indicating that they are stable under these conditions.  
21  
22

23  
24 Finally, thermal stability was evaluated recording the emission spectrum of the  
25  
26 immobilized NPs at different temperatures (Fig. 5c). The increase of temperature from  
27  
28 15° to 55°C induced a slight decrease in the fluorescence intensity which have been also  
29  
30 reported for other conjugated polymers<sup>39, 52, 53</sup>. These changes in intensity were  
31  
32 accompanied by a barely perceptible blue shift of the emission spectrum followed by a  
33  
34 lower resolution in the vibrational structure, suggesting an increase in the degree of  
35  
36 freedom of the polymer chains within the bilayer (inset in Figure 5c). When the  
37  
38 monolith was cooled to 25°C, the initial fluorescence spectrum was recovered. This  
39  
40 result indicates that the reduction of intensity is mainly caused by the increase of  
41  
42 probability of nonradiative transitions at higher temperatures, and not by degradation of  
43  
44 NPs. The high stability of the sol-gel immobilized NPs under different conditions open  
45  
46 the possibility of using this system not only for the ALP biosensor, but also for the  
47  
48 development of many other sensing applications.  
49  
50  
51  
52  
53  
54  
55  
56  
57  
58  
59  
60

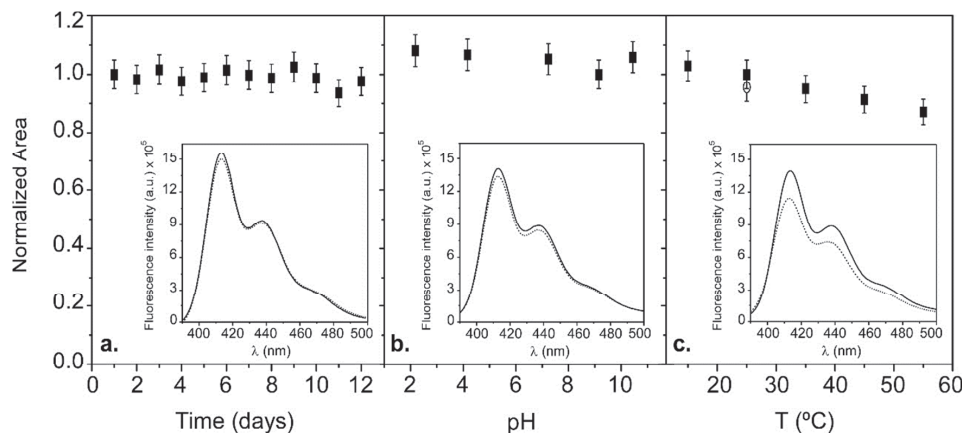
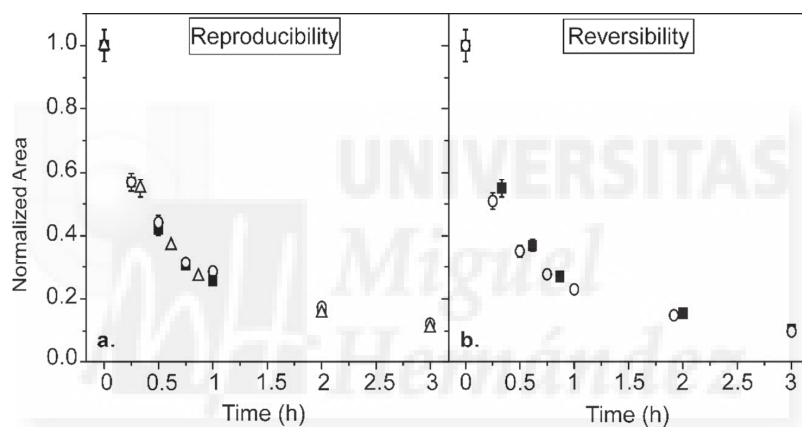


**Figure 5.** Effect of **a)** storage time **b)** pH and **c)** temperature on the stability of the immobilized NPs, measured as the area under the fluorescence spectrum. Inset: Fluorescent emission spectra of the immobilized NPs recorded as a function of **a)** storage time **b)** pH and **c)** temperature. For temperature experiments the sample was heated from 15 to 55 °C (squares) and subsequently cooled to room temperature (circle). ( $\lambda_{exc}=380\text{nm}$ ).

Once the stability of the immobilized NPs was confirmed, we explored the possibility of being quenched by PNP. With this end, a monolith containing NPs was introduced in a PNP solution (200  $\mu\text{M}$ ) and the fluorescence spectrum of the monolith was recorded as a function of time. Contrary to that found for free NPs in solution, no intensity decrease was observed in the first seconds, and longer times were necessary to quench the fluorescence of NPs (Figure 6a). This result confirms that the immobilized NPs can be still quenched by PNP but indicates that PNP diffuses much more slowly through matrix than through the buffer. This behaviour has been observed for other analytes and is attributed to the steric restrictions imposed by the sol-gel matrix<sup>45</sup>. The same experiment was carried out with other two monoliths in order to explore the reproducibility of the assay. A similar quenching kinetics was obtained for the three monoliths confirming

1  
2  
3 that the behaviour of the NPs immobilized in the sol-gel matrices is highly reproducible  
4  
5 (Figure 6a).

6  
7  
8 Once the suitability of the encapsulated NPs to be quenched by PNP was demonstrated,  
9  
10 we checked the capability of reusing the above monoliths after washing to eliminate  
11  
12 PNP. Monoliths were immersed in Tris buffer every 1 hour for 3 times. Figure 6b shows  
13  
14 the quenching kinetics recorded for a same monolith before and after washing with  
15  
16 buffer. Both curves were very similar confirming the possibility of using the same  
17  
18 monolith in more than one occasion without losing efficacy.  
19  
20  
21

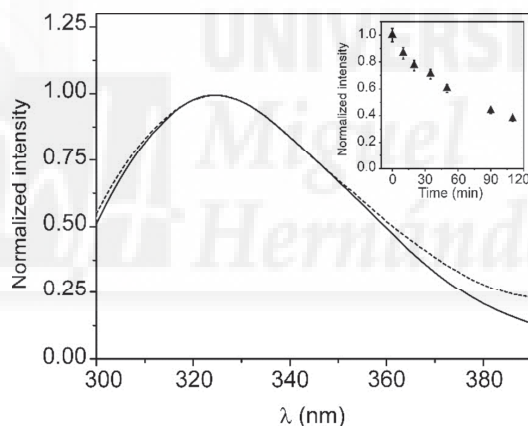


22  
23  
24  
25  
26  
27  
28  
29  
30  
31  
32  
33  
34  
35  
36  
37  
38  
39 **Figure 6.** Fluorescence quenching kinetics of immobilized NPs after addition of PNP:  
40 **a)** Reproducibility of the assay using three different monoliths; **b)** Reutilization of the  
41 monoliths: first (squares) and second (circles) use.  
42  
43  
44  
45  
46

47  
48 As for immobilized NPs, a preliminary experiment was performed to check the effects  
49  
50 of sol-gel encapsulation on the properties of ALP, by following changes in its intrinsic  
51  
52 fluorescence (mainly from tryptophan). The fluorescence of tryptophan is very sensitive  
53  
54 to the polarity of its environment, providing a convenient probe to distinguish native  
55  
56 and unfolded states of proteins. To obtain fluorescence spectra of good quality the  
57  
58 concentration of the free and immobilized protein was increased to 150 U/mL, due to its  
59  
60

1  
2  
3 low fluorescence quantum yield. Figure 7 shows the emission spectra recorded in  
4  
5 solution and after sol-gel immobilization. The fact that both spectra are almost identical  
6  
7 indicates the suitability of the immobilization method.  
8  
9

10 After ALP was successfully encapsulated in the sol-gel matrix, the kinetic properties of  
11  
12 the protein were tested by immersion of the monolith in a solution containing PNPP and  
13  
14 fluorescent NPs. Note that for this study, the protein concentration in the matrix was 2  
15  
16 U/mL, as for the assay in solution. Emission spectra, recorded from the solution, were  
17  
18 taken each 10 minutes. Inset in Figure 7 shows the decrease of the fluorescence  
19  
20 intensity as a function of the incubation time.  
21  
22  
23  
24  
25



26  
27  
28  
29  
30  
31  
32  
33  
34  
35  
36  
37  
38  
39  
40  
41  
42  
43 **Figure 7.** Fluorescence emission spectra of free (solid) and immobilized (dash) ALP  
44 (150 U/mL) ( $\lambda_{exc}=290$  nm). **Inset:** Fluorescence intensity kinetics of NPs measured in  
45 a PNPP solution (60  $\mu$ M), after immersion of the protein-containing matrix (2 U/mL).  
46  
47  
48  
49  
50

51  
52 The fluorescence decrease confirms the formation of PNP and, therefore, the  
53  
54 functioning of the enzyme. However, the kinetics was largely slower than that obtained  
55  
56 for the enzyme in solution. As was discussed for the immobilized NPs, this result  
57  
58  
59  
60

1  
2  
3 suggests that diffusion of PNP and PNPP through the matrix is restricted, limiting the  
4  
5 response time of the sol-gel biosensor. A similar result was obtained by García Sánchez  
6  
7 et al. when immobilized ALP in a sol-gel matrix to obtain a biosensor for the  
8  
9 determination of pesticides<sup>54</sup>.  
10  
11

#### 12 13 14 *Alkaline Phosphatase Biosensor in Sol-Gel Matrices.* 15

16  
17 The above results indicate the suitability of the immobilization methodology for the  
18  
19 components separately and suggest that the slow diffusion of PNPP and PNP through  
20  
21 the sol-gel matrix slows down the fluorescence quenching. The following step was the  
22  
23 co-immobilization of both NPs and ALP in the same sol-gel monolith to obtain the final  
24  
25 form of the biosensor. This monolith was immersed in a solution containing PNPP and  
26  
27 its fluorescence was measured at different incubation times. To reduce the response  
28  
29 time of the biosensor due to diffusional restrictions the concentration of substrate was  
30  
31 increased from 0.6  $\mu\text{M}$  to 0.2 and 1 mM. Figure 8a shows the results of this experiment.  
32  
33 The fluorescence decrease confirms the formation of PNP and, therefore, the suitability  
34  
35 of the co-immobilization process. Increases of the PNPP concentration resulted in a  
36  
37 clear improvement of the assay. Using 1 mM of substrate, a 90% of quenching was  
38  
39 obtained after 30 minutes of incubation (Figure 8a), which is an acceptable time of  
40  
41 response for a biosensor. These conditions were selected to check the possible  
42  
43 reutilization of the biosensor. The same monolith was used for seven consecutive assays  
44  
45 and the efficiency of the quenching was measured after 30 minutes of incubation  
46  
47 (Figure 8b). After each assay, the monolith was washed with Tris buffer for 3 h by  
48  
49 changing the buffer every hour to remove the residual PNP. The fact that the quenching  
50  
51 efficiency is similar in all the assays demonstrates that this biosensor can be used  
52  
53 repeatedly for various measurements without losing its sensitivity.  
54  
55  
56  
57  
58  
59  
60

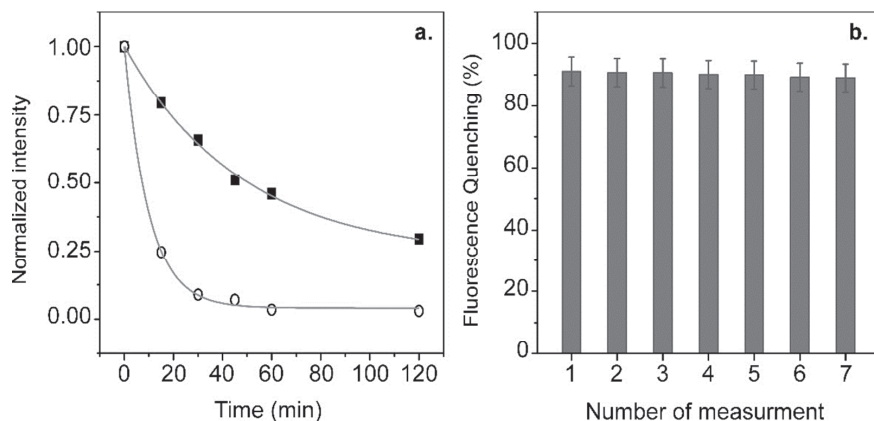
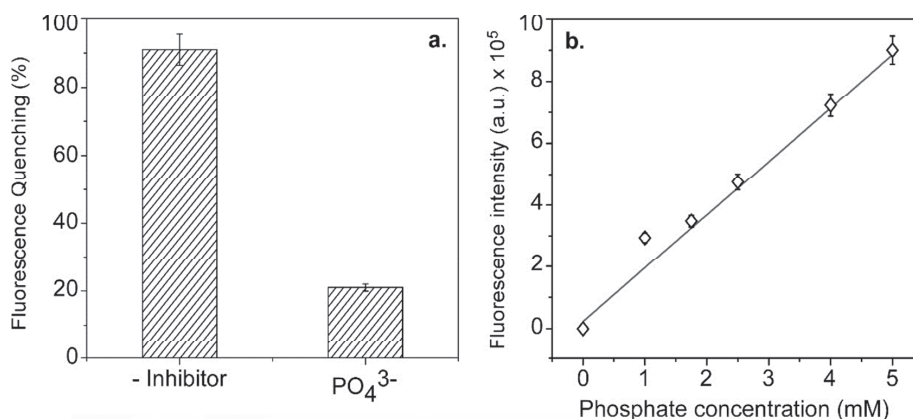


**Figure 8. a)** Fluorescence quenching kinetics measured in the immobilized biosensor after its immersion in a solution containing 200  $\mu\text{M}$  PNPP (black squares) and 1 mM PNPP (circles). **b)** Reusability study of the biosensor performed using the same monolith after washing with buffer, for seven consecutive assays, measuring the fluorescence quenching percentage after 30 minutes of incubation ( $[\text{PNPP}] = 1\text{mM}$ ).

Once the working conditions of the biosensor were optimized, we explored its ability to determine the presence of inhibitors such as phosphate ion. Figure 9a shows the fluorescence quenching percentage obtained in absence and presence of 1mM of phosphate ion, after 30 min of incubation. The drop in the quenching efficiency confirms the capacity of the biosensor to detect the inhibitor. Results are shown in Figure 9b in the form of calibration curve. To build this curve, the biosensor was immersed in buffer samples containing increasing concentrations of phosphate ion (0 to 5 mM). After the addition of 1mM PNPP, monoliths were incubated for 30 min and then their fluorescence intensity was measured and plotted as a function of phosphate concentration. This plot was linear in the range of concentrations studied (up to 5 mM), with a limit of detection (LOD) of 370  $\mu\text{M}$ , equivalent to three times the blank value. This LOD is higher than that obtained for the biosensor in solution, but is still lower

1  
2  
3 than the concentration of phosphate normally present in human blood serum (1.1-1.4  
4  
5 mM), with the advantage of being reusable.  
6  
7  
8  
9



10  
11  
12  
13  
14  
15  
16  
17  
18  
19  
20  
21  
22  
23  
24  
25  
26  
27  
28 **Figure 9. a)** Percentage of fluorescence quenching, after the addition of PNPP (1mM)  
29 to the immobilized ALP biosensor, in the absence of inhibitor compared to that obtained  
30 in the presence of inhibitor phosphate ion (5mM). **b)** Fluorescence intensities recorded  
31 for immobilized ALP biosensor in the absence and presence of different concentrations  
32 of phosphate ions.  
33  
34  
35  
36  
37  
38  
39  
40  
41  
42  
43  
44  
45  
46  
47  
48  
49  
50  
51  
52  
53  
54  
55  
56  
57  
58  
59  
60

## CONCLUSIONS

In this work we have developed a fluorescent biosensor for the detection of ion phosphate, a competitive inhibitor of the enzyme ALP. The biosensor is based on the fluorescence intensity quenching of the conjugated polyelectrolyte HTMA-PFP induced by PNP, the ALP catalysed hydrolysis product of PNPP. HTMA-PFP was previously stabilized in buffer through its interaction with lipid vesicles to obtain blue-emitting nanoparticles (NPs). These NPs were stable under pH and temperature and their fluorescence was efficiently quenched by PNP. Coupling of NPs with ALP in solution was used to develop a biosensor able to determine in three minutes the concentration of

1  
2  
3 ion phosphate in an aqueous sample, with a LOD of 52  $\mu\text{M}$ . In order to improve the  
4  
5 performance of the biosensor, its components (NPs and ALP) were immobilized in a  
6  
7 sol-gel matrix, making the biosensor reusable for, at least, seven assays. The device was  
8  
9 successfully used for the determination of ion phosphate, with a LOD higher than that  
10  
11 determined in solution, and a longer response time that reflects the slower diffusion of  
12  
13 PNPP and PNP through the matrix. This methodology could be easily extrapolated for  
14  
15 the screening of inhibitors of other enzymes, such as  $\alpha$ -glucosidase and  $\alpha$ -galactosidase,  
16  
17 which catalyze reactions yielding PNP as final product.  
18  
19  
20  
21  
22  
23

#### 24 ACKNOWLEDGMENTS

25  
26 The authors thank the Spanish Ministerio de Economía y Competitividad and  
27  
28 Generalitat Valenciana for financial support MAT-2014-53282-R, and  
29  
30 PROMETEO/2013/018, respectively.  
31  
32  
33  
34  
35  
36  
37

#### 38 REFERENCES

- 39  
40 (1) Alvarado-Gómez, A. L.; Alonso-Lomillo, M. A.; Domínguez-Renedo, O.; Arcos-  
41  
42 Martínez, M. J. A Disposable Alkaline Phosphatase-Based Biosensor for Vanadium  
43  
44 Chronoamperometric Determination. *Sensors* **2014**, *14*, 3756-3767.
- 45 (2) Miao, P.; Ning, L.; Li, X.; Shu, Y.; Li, G. An Electrochemical Alkaline Phosphatase  
46  
47 Biosensor Fabricated with Two DNA Probes Coupled with  $\Lambda$  Exonuclease.  
48  
49 *Biosens. Bioelectron.* **2011**, *27*, 178-182.
- 50 (3) Mousty, C.; Kaftan, O.; Prevot, V.; Forano, C. Alkaline Phosphatase Biosensors  
51  
52 Based on Layered Double Hydroxides Matrices: Role of LDH Composition. *Sens*  
53  
54 *Actuators, B Chem* **2008**, *133*, 442-448.
- 55 (4) Neagu, D.; Micheli, L.; Palleschi, G. Study of a Toxin-Alkaline Phosphatase  
56  
57 Conjugate for the Development of an Immunosensor for Tetrodotoxin  
58  
59 Determination. *Anal. Bioanal. Chem.* **2006**, *385*, 1068-1074.  
60

- 1  
2  
3 (5) Yin, Z.; Liu, Y.; Jiang, L. P.; Zhu, J. J. Electrochemical Immunosensor of Tumor  
4 Necrosis Factor a Based on Alkaline Phosphatase Functionalized Nanospheres.  
5 *Biosens. Bioelectron.* **2011**, *26*, 1890-1894.  
6  
7 (6) Wang, S.; Su, P.; Huang, J.; Wu, J.; Yang, Y. Magnetic Nanoparticles Coated with  
8 Immobilized Alkaline Phosphatase for Enzymolysis and Enzyme Inhibition  
9 Assays. *J. Mater. Chem. B* **2013**, *1*, 1749-1754.  
10  
11 (7) Qian, Z. S.; Chai, L. J.; Huang, Y. Y.; Tang, C.; Jia Shen, J.; Chen, J. R.; Feng, H. A  
12 Real-Time Fluorescent Assay for the Detection of Alkaline Phosphatase Activity  
13 Based on Carbon Quantum Dots. *Biosens. Bioelectron.* **2015**, *68*, 675-680.  
14  
15 (8) Liu, S.; Pang, S.; Na, W.; Su, X. Near-Infrared Fluorescence Probe for the  
16 Determination of Alkaline Phosphatase. *Biosens. Bioelectron.* **2014**, *55*, 249-254.  
17  
18 (9) Deng, J.; Yu, P.; Wang, Y.; Mao, L. Real-Time Ratiometric Fluorescent Assay for  
19 Alkaline Phosphatase Activity with Stimulus Responsive Infinite Coordination  
20 Polymer Nanoparticles. *Anal. Chem.* **2015**, *87*, 3080-3086.  
21  
22 (10) Duarte, A.; Pu, K. Y.; Liu, B.; Bazan, G. C. Recent Advances in Conjugated  
23 Polyelectrolytes for Emerging Optoelectronic Applications. *Chem. Mater.* **2011**,  
24 *23*, 501-515.  
25  
26 (11) Houston, J. E.; Kraft, M.; Scherf, U.; Evans, R. C. Sequential Detection of Multiple  
27 Phase Transitions in Model Biological Membranes using a Red-Emitting  
28 Conjugated Polyelectrolyte. *Phys. Chem. Chem. Phys.* **2016**, *18*, 12423-12427.  
29  
30 (12) Houston, J. E.; Kraft, M.; Mooney, I.; Terry, A. E.; Scherf, U.; Evans, R. C.  
31 Charge-Mediated Localization of Conjugated Polythiophenes in Zwitterionic  
32 Model Cell Membranes. *Langmuir* **2016**, *32*, 8141-8153.  
33  
34 (13) Thomas III, S. W.; Joly, G. D.; Swager, T. M. Chemical Sensors Based on  
35 Amplifying Fluorescent Conjugated Polymers. *Chem. Rev.* **2007**, *107*, 1339-1386.  
36  
37 (14) Pu, K. Y.; Cai, L.; Liu, B. Design and Synthesis of Charge-Transfer-Based  
38 Conjugated Polyelectrolytes as Multicolor Light-Up Probes. *Macromolecules* **2009**,  
39 *42*, 5933-5940.  
40  
41 (15) Jiang, H.; Taranekar, P.; Reynolds, J. R.; Schanze, K. S. Conjugated  
42 Polyelectrolytes: Synthesis, Photophysics, and Applications. *Angew. Chem. Int. Ed.*  
43 **2009**, *48*, 4300-4316.  
44  
45 (16) Kim, S.; Lim, C. K.; Na, J.; Lee, Y. D.; Kim, K.; Choi, K.; Leary, J. F.; Kwon, I. C.  
46 Conjugated Polymer Nanoparticles for Biomedical in Vivo Imaging. *Chem.*  
47 *Commun.* **2010**, *46*, 1617-1619.  
48  
49 (17) Smith, B. A.; Smith, B. D. Biomarkers and Molecular Probes for Cell Death  
50 Imaging and Targeted Therapeutics. *Bioconjugate Chem.* **2012**, *23*, 1989-2006.  
51  
52  
53  
54  
55  
56  
57  
58  
59  
60

- 1  
2  
3 (18) Ngo, A. T.; Karam, P.; Cosa, G. Conjugated Polyelectrolyte-Lipid Interactions:  
4 Opportunities in Biosensing. *Pure Appl. Chem.* **2011**, *83*, 43-55.  
5  
6 (19) Liu, Y.; Ogawa, K.; Schanze, K. S. Conjugated Polyelectrolytes as Fluorescent  
7 Sensors. *J. Photochem. Photobiol. C Photochem. Rev.* **2009**, *10*, 173-190.  
8  
9 (20) Wang, L.; Li, H.; Cao, D. Conjugated Polyelectrolytes: Synthesis and Application  
10 in Biomolecule Detection. *Curr. Org. Chem.* **2012**, *16*, 1468-1484.  
11  
12 (21) Tang, Y.; Liu, Y.; Cao, A. Strategy for Sensor Based on Fluorescence Emission  
13 Red Shift of Conjugated Polymers: Applications in pH Response and Enzyme  
14 Activity Detection. *Anal. Chem.* **2013**, *85*, 825-830.  
15  
16 (22) Cumming, C. J.; Aker, C.; Fisher, M.; Fox, M.; La Grone, M. J.; Reust, D.;  
17 Rockley, M. G.; Swager, T. M.; Towers, E.; Williams, V. Using Novel Fluorescent  
18 Polymers as Sensory Materials for Above-Ground Sensing of Chemical Signature  
19 Compounds Emanating from Buried Landmines. *IEEE Trans. Geosci. Remote*  
20 *Sens.* **2001**, *39*, 1119-1128.  
21  
22 (23) Toal, S. J.; Trogler, W. C. Polymer Sensors for Nitroaromatic Explosives  
23 Detection. *J. Mater. Chem.* **2006**, *16*, 2871-2883.  
24  
25 (24) Chen, L.; McBranch, D. W.; Wang, H. -.; Helgeson, R.; Wudl, F.; Whitten, D. G.  
26 Highly Sensitive Biological and Chemical Sensors Based on Reversible  
27 Fluorescence Quenching in a Conjugated Polymer. *Proc. Natl. Acad. Sci. U. S. A.*  
28 **1999**, *96*, 12287-12292.  
29  
30 (25) Senthilkumar, T.; Asha, S. K. Selective and Sensitive Sensing of Free Bilirubin in  
31 Human Serum using Water-Soluble Polyfluorene as Fluorescent Probe.  
32 *Macromolecules* **2015**, *48*, 3449-3461.  
33  
34 (26) Qin, C.; Cheng, Y.; Wang, L.; Jing, X.; Wang, F. Phosphonate-Functionalized  
35 Polyfluorene as a Highly Water-Soluble Iron(III) Chemosensor. *Macromolecules*  
36 **2008**, *41*, 7798-7804.  
37  
38 (27) Qin, C.; Tong, H.; Wang, L. Water-Soluble Phosphate-Functionalized Polyfluorene  
39 as Fluorescence Biosensors Toward Cytochrome C. *Sci China Ser B Chem* **2009**,  
40 *52*, 833-839.  
41  
42 (28) Cao, A.; Tang, Y.; Liu, Y. Novel Fluorescent Biosensor for  $\alpha$ -Glucosidase Inhibitor  
43 Screening Based on Cationic Conjugated Polymers. *ACS Appl. Mater. Interfaces*  
44 **2012**, *4*, 3773-3778.  
45  
46 (29) Naeem, A.; Khan, I. M.; Ahmad, A. Spectral Investigations of Multiple Charge  
47 Transfer Complex of P-Nitrophenol as an Electron Acceptor with Donor P-  
48 Dimethylaminobenzaldehyde. *Russ. J. Phys. Chem. A* **2011**, *85*, 1840-1843.  
49  
50 (30) Tapia, M. J.; Montserín, M.; Valente, A. J. M.; Burrows, H. D.; Mallavia, R.  
51 Binding of Polynucleotides to Conjugated Polyelectrolytes and its Applications in  
52 Sensing. *Adv. Colloid Interface Sci.* **2010**, *158*, 94-107.  
53  
54  
55  
56  
57  
58  
59  
60

- 1  
2  
3 (31) Martínez-Tome, M. J.; Esquembre, R.; Mallavia, R.; Mateo, C. R. Formation of  
4 Complexes between the Conjugated Polyelectrolyte Poly{[9,9-Bis(6'-  
5 N,N,N-trimethylammonium) Hexyl]Fluorene-Phenylene} Bromide (HTMA-PFP)  
6 and Human Serum Albumin. *Biomacromolecules* **2010**, *11*, 1494-1501.  
7  
8  
9 (32) Maiti, J.; Pokhrel, B.; Boruah, R.; Dolui, S. K. Polythiophene Based Fluorescence  
10 Sensors for Acids and Metal Ions. *Sens Actuators, B Chem* **2009**, *141*, 447-451.  
11  
12 (33) Fan, L. -.; Zhang, Y.; Murphy, C. B.; Angell, S. E.; Parker, M. F. L.; Flynn, B. R.;  
13 Jones Jr., W. E. Fluorescent Conjugated Polymer Molecular Wire Chemosensors  
14 for Transition Metal Ion Recognition and Signaling. *Coord. Chem. Rev.* **2009**, *253*,  
15 410-422.  
16  
17 (34) Kahveci, Z.; Martínez-Tomé, M. J.; Mallavia, R.; Mateo, C. R. Use of the  
18 Conjugated Polyelectrolyte Poly{[9,9-Bis(6'- N, N, N-  
19 Trimethylammonium)Hexyl]Fluorene-Phenylene} Bromide (HTMA-PFP) as a  
20 Fluorescent Membrane Marker. *Biomacromolecules* **2013**, *14*, 1990-1998.  
21  
22  
23 (35) Upadhyay, L. S. B.; Verma, N. Recent Advances in Phosphate Biosensors.  
24 *Biotechnol. Lett.* **2015**, *37*, 1335-1345.  
25  
26 (36) Molina, R.; Gómez-Ruiz, S.; Montilla, F.; Salinas-Castillo, A.; Fernández-Arroyo,  
27 S.; Del Mar Ramos, M.; Micol, V.; Mallavia, R. Progress in the Synthesis of  
28 Poly(2,7-Fluorene-Alt-1,4-Phenylene), PFP, Via Suzuki Coupling.  
29 *Macromolecules* **2009**, *42*, 5471-5477.  
30  
31  
32 (37) Mallavia, R.; Martínez-Peréz, D.; Chmelka, B. F.; Bazan, G. C. Blue Fluorescent  
33 Films Based on Poly-2,7-Fluorene-Phenylene Derivatives. *Bol. Soc. Esp. Ceram.*  
34 *Vidr.* **2004**, *43*, 327-330.  
35  
36  
37 (38) Al Attar, H. A.; Monkman, A. P. Effect of Surfactant on Water-Soluble Conjugated  
38 Polymer used in Biosensor. *J Phys Chem B* **2007**, *111*, 12418-12426.  
39  
40 (39) Kahveci, Z.; Vázquez-Guilló, R.; Martínez-Tomé, M. J.; Mallavia, R.; Mateo, C.  
41 R. New Red-Emitting Conjugated Polyelectrolyte: Stabilization by Interaction with  
42 Biomolecules and Potential use as Drug Carriers and Bioimaging Probes. *ACS*  
43 *Appl. Mater. Interfaces* **2016**, *8*, 1958-1969.  
44  
45 (40) Kahveci, Z.; Martínez-Tomé, M. J.; Esquembre, R.; Mallavia, R.; Mateo, C. R.  
46 Selective Interaction of a Cationic Polyfluorene with Model Lipid Membranes:  
47 Anionic Versus Zwitterionic Lipids. *Mater.* **2014**, *7*, 2120-2140.  
48  
49 (41) López-Cabarcos, E.; Retama, J. R.; Sholin, V.; Carter, S. A. Controlling the  
50 Photoluminescence of Water-Soluble Conjugated Poly[2-(3-Thienyl)Ethoxy-4-  
51 Butylsulfonate)] for Biosensor Applications. *Polym. Int.* **2007**, *56*, 588-592.  
52  
53 (42) Chen, L.; Xu, S.; McBranc, D.; Whitten, D. Tuning the Properties of Conjugated  
54 Polyelectrolytes through Surfactant Complexation [4]. *J. Am. Chem. Soc.* **2000**,  
55 *122*, 9302-9303.  
56  
57  
58  
59  
60

- 1  
2  
3 (43) Thomsen, V.; Schatzlein, D.; Mercurio, D. Limits of Detection in Spectroscopy.  
4 *Spectroscopy* **2003**, *18*, 112-114.  
5  
6 (44) Upadhyay, L. S. B.; Verma, N. Alkaline Phosphatase Inhibition Based  
7 Conductometric Biosensor for Phosphate Estimation in Biological Fluids. *Biosens.*  
8 *Bioelectron.* **2015**, *68*, 611-616.  
9  
10 (45) Pastor, I.; Esquembre, R.; Micol, V.; Mallavia, R.; Mateo, C. R. A Ready-to-use  
11 Fluorimetric Biosensor for Superoxide Radical using Superoxide Dismutase and  
12 Peroxidase Immobilized in Sol-Gel Glasses. *Anal. Biochem.* **2004**, *334*, 335-343.  
13  
14 (46) Esquembre, R.; Poveda, J. A.; Mateo, C. R. Biophysical and Functional  
15 Characterization of an Ion Channel Peptide Confined in a Sol-Gel Matrix. *J Phys*  
16 *Chem B* **2009**, *113*, 7534-7540.  
17  
18 (47) Esquembre, R.; Pinto, S. N.; Poveda, J. A.; Prieto, M.; Mateo, C. R.  
19 Immobilization and Characterization of Giant Unilamellar Vesicles (GUVs) within  
20 Porous Silica Glasses. *Soft Matter* **2012**, *8*, 408-417.  
21  
22 (48) Pastor, I.; Salinas-Castillo, A.; Esquembre, R.; Mallavia, R.; Mateo, C. R.  
23 Multienzymatic System Immobilization in Sol-Gel Slides: Fluorescent Superoxide  
24 Biosensors Development. *Biosens. Bioelectron.* **2010**, *25*, 1526-1529.  
25  
26 (49) Pastor, I.; Ferrer, M. L.; Lillo, M. P.; Gómez, J.; Mateo, C. R. Structure and  
27 Dynamics of Lysozyme Encapsulated in a Silica Sol-Gel Matrix. *J Phys Chem B*  
28 **2007**, *111*, 11603-11610.  
29  
30 (50) Avnir, D.; Lev, O.; Livage, J. Recent Bio-Applications of Sol-Gel Materials. *J.*  
31 *Mater. Chem.* **2006**, *16*, 1013-1030.  
32  
33 (51) Jin, W.; Brennan, J. D. Properties and Applications of Proteins Encapsulated within  
34 Sol-Gel Derived Materials. *Anal. Chim. Acta* **2002**, *461*, 1-36.  
35  
36 (52) Martínez-Tomé, M. J.; Esquembre, R.; Mallavia, R.; Mateo, C. R. Formation and  
37 Characterization of Stable Fluorescent Complexes between Neutral Conjugated  
38 Polymers and Cyclodextrins. *J. Fluoresc.* **2013**, *23*, 171-180.  
39  
40 (53) Traiphol, R.; Sanguansat, P.; Srihirin, T.; Kerdcharoen, T.; Osotchan, T.  
41 Spectroscopic Study of Photophysical Change in Collapsed Coils of Conjugated  
42 Polymers: Effects of Solvent and Temperature. *Macromolecules* **2006**, *39*, 1165-  
43 1172.  
44  
45 (54) García Sánchez, F.; Navas Díaz, A.; Ramos Peinado, M. C.; Belledone, C. Free and  
46 Sol-Gel Immobilized Alkaline Phosphatase-Based Biosensor for the Determination  
47 of Pesticides and Inorganic Compounds. *Anal. Chim. Acta* **2003**, *484*, 45-51.  
48  
49  
50  
51  
52  
53  
54  
55  
56  
57  
58  
59  
60

